MoO_3-based heterogeneous catalysts for the metathesis of propene

DAMIEN P. DEBECKER

MAI 2010

Thèse présentée en vue de l'obtention
du grade de docteur en sciences agronomiques
et ingénierie biologique

Faculté d'ingénierie biologique,
agronomique et environnementale

Université catholique de Louvain

ACKNOWLEDGMENTS

Je tiens à remercier le Professeur Eric Gaigneaux, promoteur de cette thèse, pour la grande confiance qu'il m'a accordée dès mon arrivée dans le laboratoire. En entretenant avec moi des interactions scientifiques enrichissantes et en m'accordant une bonne dose d'autonomie, il m'a très vite permis de m'épanouir pleinement dans le métier de chercheur.

Ma reconnaissance va également aux Professeurs M. Devillers (UCL, Belgique), P. Ruiz (UCL, Belgique) et B. Sels (KULeuven, Belgique) qui m'ont fait l'honneur de suivre régulièrement l'avancement de mes travaux. Je tiens à remercier le Professeur J. Védrine (Université Pierre et Marie Curie, France) de s'être joint au jury de cette thèse ainsi que le Professeur J. Mahillon, Doyen de la Faculté, d'avoir accepté de présider ce jury.

J'aimerais dire merci aux collègues du laboratoire qui participent chacun à la réussite de projets comme celui-ci: Pierre, Pascal, Françoise, Nathalie. Je tiens à remercier les étudiants et stagiaires qui ont travaillé avec moi sur cette thèse et sur d'autres projets. Merci à Eglantine avec qui j'ai eu la chance, depuis le début de l'aventure, de vivre les difficultés et les joies du thésard. Merci aussi à Romain, Marc, Damien, Inma avec qui j'ai partagé bureau, maison et festivités, ainsi qu'à tous les autres collègues doctorants, techniciens, mémorants, post-doctorants que j'ai eu la chance et le plaisir de côtoyer au laboratoire et en dehors.

Au gré des rencontres et des collaborations scientifiques, j'ai eu l'occasion de travailler avec d'autres personnes auxquelles je voudrais exprimer ma gratitude: messieurs M. Genet, C. Poleunis, B. Schimmöller, K. Bouchmella, les Docteurs C. Faure, U. Rodemerck, M. Stoyanova et les Professeurs G. Busca et A. Buekens. J'adresse un merci particulier au Dr. H. Mutin qui, par son enthousiasme communicatif et sa rigueur scientifique, m'a beaucoup apporté sur le plan humain et professionnel.

Je tiens ici à remercier tout spécialement mes parents, pas uniquement pour leur soutien sans faille tout au long de la réalisation de ma thèse, mais plus largement pour toute l'attention et l'affection dont ils m'ont entouré, et pour m'avoir donné les armes pour croquer la vie à pleines dents. Avec mes frères, Julien et Alexandre, cette famille de cinq constitue le socle solide sur lequel mes projets les plus fous peuvent s'appuyer résolument. Je remercie aussi mes deux grands-mères pour leur soutien.

Finalement, c'est à Melinda que je voudrais dire ma grande reconnaissance. Oreille attentive et soutien sans faille depuis bientôt quatre ans, Melinda est celle qui comprend et qui participe à mes rêves et à mes joies. Melinda est une scientifique qui s'ignore, une perpétuelle source de questions et de suggestions pertinentes. Même loin, elle a toujours été très proche de moi et de l'avancement de ce travail. Merci à toi, pour tout.

Merci à tous !

Cette thèse de doctorat a été réalisée dans le cadre d'un mandat d'Aspirant du FNRS.

Table of Contents

GENERAL INTRODUCTION

ABSTRACT

This section presents the context in which this research has been initiated and conducted. Then a detailed literature survey concerning the catalytic reaction studied and the types of catalytic formulations employed are proposed. The limitations of nowadays understanding and existing know-how are exposed in correlation with our own objectives. Finally, our strategy established in order to address these issues is depicted.

1. CONTEXT

The intensive use of petroleum both as energy and as chemical feedstock source has prompted huge progresses in our society in the past century. More recently however, growing concern has been rising concerning (i) the limited stocks of petroleum and the increasing difficulty to extract it at reasonable cost and (ii) the huge environmental impact of the anthropogenic production of CO_2 through the combustion of fossil fuel. These emissions are the main cause of the unprecedented rate of global warming we are currently experiencing. Up to now, the energy industry is still widely relying on petroleum and other fossil resources. However, intense efforts are conducted to develop alternative renewable energy sources [1]. As far as the chemical industry is concerned, efforts are conducted in two directions. Firstly, alternative production methods are developed that are relying on renewable carbon sources (e.g. vegetable fibres-derived plastics) [2-3]. Secondly, intensive efforts toward carbon and energy efficiency are realized [4-5]. This last strategy drives the (petro)chemist toward transformation and synthesis processes that are realized with low energy input (low temperature, low pressure) and with excellent selectivity. The parsimonious use of hydrocarbon is one of the strings to the bow of our society in its will to address current challenges. In that perspective, heterogeneous catalysis is recognized as a privileged tool to increase energy efficiency and fuel economy, to improve efficiency in the use of petroleum-based feedstock in chemical processes and to lower emissions of toxic or greenhouse gases in petroleum refineries [6].

Propene is an important chemical feedstock that is produced from petroleum at the refinery. The demand for propene is structurally rising as it is used in the production of wide arrays of products (Figure i). It is the monomer of polypropylene and the source of various oxygenates (acrolein, acrylic acid, propylene oxide, methacrolein, etc.) that are involved in the production of plastics, resins, surfactants and solvents. The proportion of propene that can be recovered by simple distillation of crude oil is low. This is why, propene is further produced by steam cracking (along with ethylene) or fuel catalytic cracking of higher hydrocarbon fractions (Figure ii) [7].

These two processes can be qualified as “by-products processes” since propene is only obtained as a by-product of other hydrocarbons. The selectivity towards propene is relatively low (Figure iii). Moreover, the processes of cracking involve high temperature (500-850 °C) and usually high pressure (1-50 bar) conditions. In other words, they involve high energy costs.

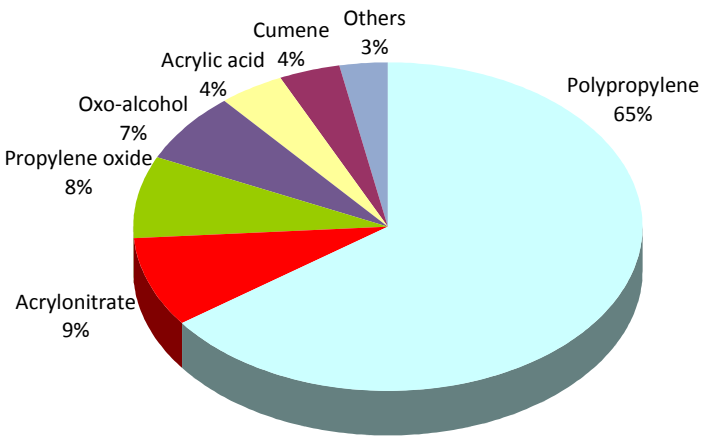

Figure i: Principal uses of propylene (data reproduced from a Lummus Technology report [8]).

In this context, alternative routes that would be more environmentally-friendly and more cost-effective are desirable for the production of propene. This is why active fundamental and applied researches are conducted on the light olefin metathesis reaction. This reaction indeed allows the on purpose catalytic production of propene from ethene and butene. It is non thermal, meaning that the energy input is very low. It can be conducted at low temperature, atmospheric pressure and with excellent selectivity (Figure iii) provided that an efficient catalyst is used. Moreover, ethene and butene, unlike propene, tend to be produced in excess at the refinery, resulting in relatively low price. It is thus particularly appealing for the petrochemical industry to master the metathesis technology since it gives the possibility to regulate the stocks of hydrocarbons as a function of the needs or as a function of the price of the market. As the metathesis reaction is equilibrated, one could use exactly the same process

(catalyst, industrial plant) to perform the reverse reaction, in case the market situation demands it. Historically in fact, the first industrial olefin metathesis process (Phillips triolefin process, operated for 6 years from 1966) was the production of high-purity ethene and but-2-ene from surplus propene [9]. More recently, the *Lummus Technology* Company has developed commercial solutions for the conversion of C2 and C4 olefins to the desired C3 alkene (propene). At the moment 26 metathesis units are either in operation or under design and construction. Their technology, called "Olefin Conversion Technology" (OCT) is claimed to be the lowest capital route for ultra-high purity propylene production [10]. The "Institut Français du Pétrole" and the Chinese Petroleum Corporation have also jointly developed a process for the production of propene from ethene and butene [11].

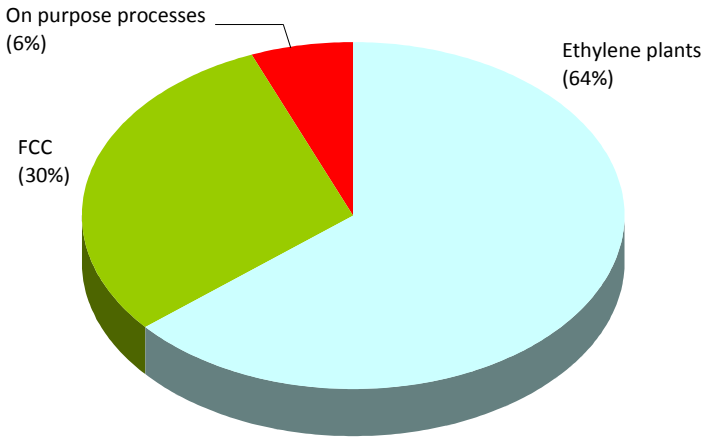

Figure ii: Modes of production of propylene. By-products processes, namely vapour cracking in ethylene plants and fluidized catalytic cracking represent the large majority of the production. Olefin metathesis and propane dehydrogenation are the two available on purpose processes but they represent only 6% of the production of propene (data reproduced from a Lummus Technology report [8]).

Molybdenum oxide, along with rhenium [12-16] and tungsten [17-19] oxides, is known to catalyze this interesting reaction. The discovery of the metathesis reaction was actually made on supported Mo oxide catalysts, more than 40 years ago [20]. However, the mechanisms that lead to the formation of active metathesis centres on MoO_3-based catalysts are far from

being elucidated. Also, the actual nature of the active metathesis site is still under debate. The achieved performances are dictated by important parameters such as the catalyst formulation, the mode of preparation of the catalyst and the procedure used for its activation. However, only few data are available from the scientific literature on these aspects. Further fundamental understanding is needed as there is evidently still room for performance improvement. This work addresses some of the essential issues in the understanding of the genesis and of the nature of the active metathesis centres in MoO_3-based catalysts and proposes innovative preparation methods to obtain efficient metathesis catalysts.

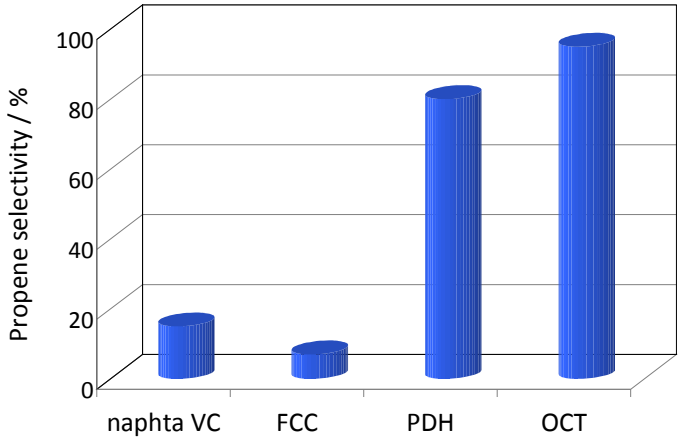

Figure iii: Propene selectivity in the existing propene production technologies. Naphta vapour cracking (VP) and fluidized catalytic cracking are "by-products technologies". Propane dehydrogenation (PDH) and olefin conversion technology (OCT) are "on-purpose technologies exhibiting good to excellent selectivities (data reproduced from a Lummus Technology report [8]).

2. LITERATURE SURVEY ON METATHESIS

2.1. Discovery

The word "metathesis" has a Greek root meaning "changing position". The metathesis of olefins can be defined as a reaction by which

the chemical groups located around the double bond of an alkene are exchanged. It can be formalised as in Scheme i.

In 1960, a first open publication mentioned particular polymerization reactions actually based on the metathesis reaction [21]. The olefin metathesis was really discovered at Phillips Petroleum Company four years later, when Banks and Bailey [20] described the "olefin disproportionation" with alumina-supported molybdenum oxide, molybdenum hexacarbonyl and tungsten hexacarbonyl. These catalysts produced ethene and butene from propene. The mechanism of this reaction (Scheme ii) was clearly established only in 1971 by Hérisson and Chauvin [22] who proposed a 4-membered metallacycle intermediate to account for this transalkylidenation reaction. The key step is a reaction between an olefin and a transition metal alkylidene complex (M=CHR ; also called carbene) to give a unstable metallacyclobutane intermediate [23].

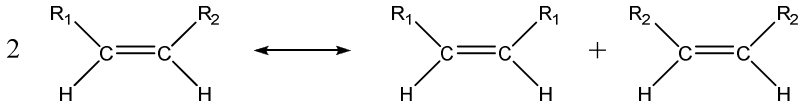

Scheme i: Schematic representation of the metathesis reaction. The chemical groups around the double bond (H, R_1 and R_2) are exchanged to give new olefins. In the case of the self-metathesis of propene, R_1 = H and R_2 = CH_3. Thus, the produced olefins are ethene and butene.

Whilst the early discovery of the metathesis reaction was made on relatively undefined catalysts, sensitive to air, moisture and very short-lived, it rapidly became evident that the development of reliable and effective metathesis catalysts would have a great importance in organic synthesis. Indeed, with the metathesis of two alkenes, a new C-C bond is catalytically created, which allows for example the closing or the opening of organic rings. The goal was thus to find catalysts that are well-defined, selective and stable and to develop means to adjust their reactivity depending on the targeted reaction. Research on the chemistry of metal carbene, also termed metal alkylidene, allowed stepping further in that direction.

Richard R. Schrock highlighted the interest of molybdenum and tungsten as the most suitable metals for achieving effective catalysts. The real breakthrough of Schrock's research was the development, in 1990 of a new type of organometallic catalysts in which the metal is surrounded by iso-propyl and phenylic groups [24]. These complexes are still being the object of intense researches [25-26].

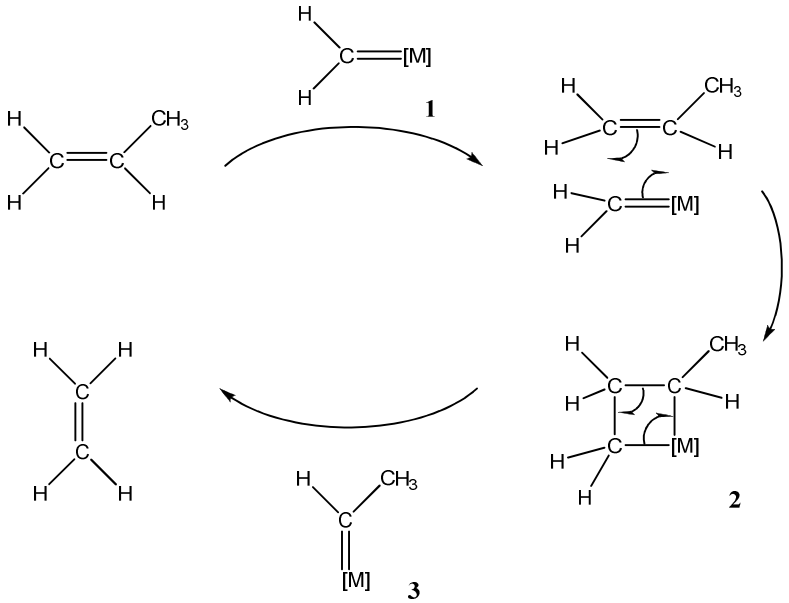

Scheme ii: Chauvin's mechanism applied to one catalytic cycle in the metathesis of propene. **1** is the starting metal carbene active centre, in which the metal with its ligands ([M]) is doubly linked to a carbon atom. When propene approaches the carbene, electrons displacements yield a four-member ring species called metallacyclobutane (**2**). A second electron rearrangement leads to the formation of a new olefin (here ethene). The remaining carbene (**3**) is different from **1**. Upon further reaction with propene, the carbene will allow the formation of butene following the same mechanism.

Robert H. Grubbs, working mainly on ruthenium-based catalysts, developed a "general catalyst" that is stable in air, highly selective (but less reactive than Schrock'catalysts) and that still works efficiently in the presence of alcohols, water and carboxylic acids [27]. Note that the stability of metathesis catalyst towards impurities is still a crucial issue that must be

carefully taken into account in the design of metathesis set-ups (see Experimental part Section 0, p. 33)

Olefin metathesis is now successfully used in a wide range of applications including drug synthesis [28-31] and polymerization reactions [32-37]. Chauvin, Grubbs and Schrock were awarded the 2005 Nobel Prize in Chemistry for their works on the development of metathesis methods in organic synthesis [38].

2.2. Homogeneous organometallic metathesis catalysts

Separately from the discoveries made on oxides in the petroleum and chemical industries, fundamental research was conducted on the chemistry of metal carbenes [39]. The group of Schrock first studied tantalum carbenes and discovered that bulky alkoxide ligands slow down the rearrangement of the tantalacyclobutane rings to olefins and promote olefin metathesis [40]. Tungsten carbenes were then investigated and it soon became clear that the ligands around the metal carbene should be sterically demanding and should create an electron deficiency to account for the stability of the complex toward bimolecular decomposition. It was early found that the activity of tungsten carbene complexes correlates roughly with the electron-withdrawing power of the ligands (e.g. hexafluoro-*tert*-butoxide ligands promoted higher activity). Imido ligands surrounded by large organic groups were then targeted in order to maximize steric protection at the metal centre and to limit the tendency of the imido group to bridge between metal centres [41].

The actual intermediate proposed by Chauvin in the metathesis reaction could be isolated by Feldman and Schrock [42]. Tungstacyclobutane intermediates were indeed characterized on a crystallographic basis. However, these stable species do not exhibit high metathesis activity. Indeed, the opening of the ring to yield an olefin is so slow that the metal is blocked in the tungstacyclobutane configuration [41]. This led Schrock and co-workers to envisage the use of Mo-analogues, since the molybdenum-ligand bonds were known to be generally weaker than tungsten-ligands bonds. Moreover, molybdenum is cheaper than tungsten. Molybdenum bisalkoxide catalysts soon became a wide class of very

efficient homogeneous metathesis catalysts (Scheme iii). $Mo(CHR')(NAr)(OR)_2$ complexes would react bimolecularly with themselves if the ligands would not prevent them from doing so because of steric hindrance [23]. The size (and thus the steric hindrance) of the alkoxide and imido groups, as well as their electronic properties were very elegantly exploited as instruments to control the metathesis activity of the complexes.

The nature of the alkylidene affects the reactivity of the complex: $Mo=CH_2$ are much more reactive than Mo=CHR' species, while $Mo=CR'_2$ are by far less reactive. The electron withdrawing effect of the alkoxide ligands determines strongly the reactivity of the alkylidene complex. The more electron withdrawing the alkoxide, the more electrophilic the metal, and the more active the catalyst.

It is important to notice that the alkylidene, in imido alkylidene complexes can exist in two stereoisomeric forms. This observation is the starting point for a huge field of research aiming at the development of stereoselective metathesis catalysts [43-50] having a crucial importance for example in the production of polymers by metathesis polymerization reactions.

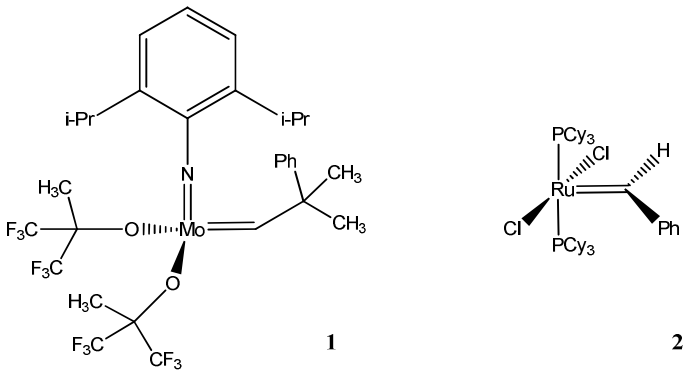

Scheme iii: Examples of Schrock's catalysts (**1**) and of Grubbs' catalysts (**2**). (i-Pr = iso-propyl, Ph = phenyl and PCy_3 = tricyclohexylphosphine)

2.3. Heterogenized organometallic catalysts: bridging the gap between homogeneous and heterogeneous catalysis

As a rule, for industrial processes, the use of heterogeneous catalysts is more convenient than the use of homogeneous catalysts. The main intrinsic advantages of heterogeneous catalysts are linked to the ease of separation from the reaction medium, the possibility to recycle them and to run continuous flow processes. As homogeneous organometallic complexes proved to be very active and selective for numerous metathesis reactions, it was tried to support them on solids. An additional key reason why supported well-defined metathesis catalysts are very desirable is that very active complexes, if well immobilized, would not have the possibility to be decomposed by bimolecular reactions [23]. The strategy consists in using silica as a solid siloxy ligand for the grafting of an organometallic complex to form immobilized and isolated alkylidene complexes (Scheme iv).

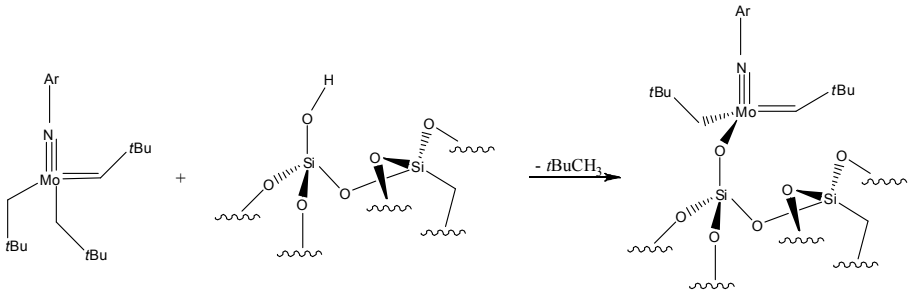

Scheme iv: Grafting of an organometallic metathesis complex precursor onto silica to give a well-defined and highly active heterogeneous metathesis catalyst. Redrawn from Blanc et al. [51]

An impressive number of excellent results have been obtained via this strategy in the past decade [52-61]. However, it should be reminded that the organometallic chemistry that leads to these interesting complexes remains heavy and expensive.

2.4. Heterogeneous catalysis with supported oxides: cheap and robust catalysts for high tonnage applications

The huge tonnages that are to be treated with high space velocities in the industrial plants dedicated to the conversion of light olefin imply large fixed bed reactors with large amounts of catalysts (in the order of the ton) [8]. Therefore, for this particular application - as opposed to fine organic synthesis and metathesis polymerization - catalysts that are robust, cheap and easy to prepare are highly regarded. This is why active research is ongoing concerning the development of Re, W or Mo oxide based catalysts [9]. Current investigations include works on new catalytic formulations [62], on new preparation methods [14, 63-64] and fundamental works on the nature and genesis of the active metathesis centres [65].

It is interesting to notice that, in a recent review [40], Schrock insisted on the definitions of (i) well-defined metathesis catalysts and (ii) metathesis catalysts precursor or "precatalysts". The distinction arises from the fact that in homogeneous organometallic catalysis it is possible to precisely characterize the species that are actually active in the metathesis reaction – e.g. by spectroscopic means or X-Ray analysis. Also when supporting well-defined organometallic complexes onto inorganic supports like silica, it is possible to predict (or even trace) its reaction with the fed olefin and the nature of the persistent new alkylidene complex derived from that reaction. In that sense, organometallic chemistry-derived catalysts are "well-defined catalysts". On the contrary, metathesis catalysts based on inorganic oxides should be classified among the group of catalyst precursors or "precatalysts". Supported oxides catalysts initially have neither a carbene nor an alkyl or allyl group that can readily generate a carbene to yield active sites. The metal carbene can only be formed by interaction of the substrate olefin itself with the transition metal centre [9]. Even if the solids can be thoroughly characterized, both the formation of the carbene active species and the nature of this active species remain very difficult to depict precisely.

Several studies were published 20-40 years ago as attempts to describe the mechanism of alkylidene sites formation on supported metal oxide catalysts on experimental basis [66-70]. These draw attention to the formation of π-alkyl complexes as key intermediates in the initiation step.

None of these works however allows describing in details a common mechanism for the formation of carbenes from supported oxides. More recently, kinetic methods [71] and poisoning experiments [72] evidenced that the number of active centres in a molybdena-alumina catalyst is only a small fraction of the Mo atoms present (ca. 1 % [71]). Spectroscopic methods can therefore be misleading since characterizing the majority sites instead of the actually active centres. The latter active centres could only be readily described with operando or in situ techniques [63] and provided that a distinction can be made between active and non active Mo atoms. Presently, the attention is often brought to computational studies which allow evaluating the viability of given mechanisms on theoretical basis (vide infra).

The present study focuses on correlations between various physico-chemical properties of the precatalysts and the catalytic activity reached with them. The description of the active sites at the molecular scale is not in the scope of this work. Remembering always that the samples are only the precursors of the actual active species, we will systematically by-pass Schrock's distinction and always talk about "catalysts" for what he would have called "precatalysts". Albeit the detailed destription of the formation of carbenes on supported oxides remains unclear, progresses are being made in the understanding of the chemistry of these systems and on their optimization. An overview of the recent developments (theoretical and experimental) in the case of MoO_3-based catalysts is presented below.

2.4.1. Theoretical investigations

Since the structure and the formation of surface alkylidene centres on supported oxide catalysts are not described unambiguously via experimental means, many studies propose to step forward in this direction by means of computational approaches [65, 73-83]. The density functional theory is applied to calculate the geometry and the location of potential Mo-alkylidene species at the surface of well-defined supports. Then, from their relative energy, the probability of existence of these species is evaluated. By analogy with the homogeneous organometallic catalysts, where the stability and the reactivity is governed by the electronic properties of the ligands, in

supported oxide catalysts, the carrier is considered as a multidentate ligand of the metal centre. The local electronic properties of the support (depending for example on the crystallographic plane on which the Mo species is grafted) and the geometry of each considered active site determine the relative stability of the molybdacyclobutane intermediate and thus the reactivity in alkene metathesis. While calculations on the chemistry of the surface alkylidene species are numerous, the issue of the actual genesis of these species from the reaction of the alkene with the pretreated oxide surface is still unresolved. In a recent publication, the goup of Bao has addressed the problem with the aid of density functional calculations [73]. These authors show that the first step of the formation of the Mo-alkylidene is the formation of the oxamolybdacyclobutane intermediate in which four single bonds constitute a "MoOCC" ring. The opening of this ring leads to the Mo-methylidene species and to formaldehyde (Scheme v).

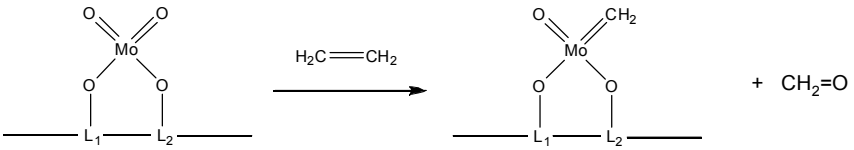

Scheme v: Schematic representation of the phenomenon that is described theoretically from DFT calculation. The stability of a hyphothetical Mo site, as well as the stability of the corresponding carbene species, are calculated, considering the support to which they are linked as ligands (e.g. L_1, L_2). Adapted from Guan et al. [73]

Recent works reported by Handzlik et al. should be mentioned as well [65]. Applying a new periodic model, on a series of potential monomeric methylidene centers on alumina they were able to demonstrate that the molybdacyclobutane species are in many cases significantly more stable than the metathesis reactants (they considered ethene). This means that in a large majority the sites are reactive with the olefin and yield the four-member ring species. However, the release of the new olefin and the restoration of the carbene site by means of metallacycle opening is the rate limiting step. In many cases, the sites are blocked at the molybdacyclobutane step. Only some of the envisaged structures were shown to be active at low temperature (room temperature) and this was linked to the role of the

support. Indeed, in some cases, the support imposes a constraint on the Al-O-Mo bonds that reduces the stability of the metallacycle by deforming the environment of Mo atoms. The deformation imposed by the surface on the coordination of Mo atoms leads to reduced stability of the molybdacyclobutane and to higher activity. The recent results of Guan et al. [73] confirm these findings. In addition, these authors have demonstrated the superior activity of the molybdenum centres in the $Mo^{(VI)}$ oxidation state as compared to $Mo^{(V)}$. In other words, $Mo^{(VI)}$ sites generate more readily the corresponding Mo-methylidene upon reaction with the olefin, than $Mo^{(V)}$.

It is clear that these approaches bring new crucial insights to the understanding of the formation mechanism of active metathesis centres. Yet, these computational methods are based on models and on simplified hypotheses. Confronting computational findings with experimental data is in any case compulsory.

2.4.2. Experimental investigations on the formulations and on the preparation methods

As seen from the previous sections, heterogeneous catalysts based on Mo oxide can not be comprehensively depicted by simple analogy with organometallic complexes. In addition, their behaviour and performances can not be completely described and predicted by theoretical calculations. Direct experimental studies on the activity of the samples and on the correlations that exist between their catalytic performances and their physico-chemical properties are thus very informative.

It is worth warning that the direct comparison of the results found in the literature is generally delicate. The activation procedures and the reaction conditions are very often different when the results arise from different research groups and these have marked impacts on the observed catalytic behaviour. Moreover, activity data are frequently expressed in variable terms. As a consequence, the ranking of different catalytic formulations must always be made with much care. Only results obtained in very similar conditions can be compared directly. The following sections summarize the recent findings keeping in mind this precaution.

2.4.2.1. Effect of the support

Various refractory materials have been used as supports, in particular Si, Al, Zr, Ti oxides; SiO_2 and Al_2O_3 being the most commonly tested [9]. In their comprehensive review, Ivin and Mol insist on the importance of the chemical interactions between the support and the transition metal [9]. One interesting study was published recently by Handzlik et al. [84] in which one silica, one alumina and one silica-alumina were used as supports for the preparation MoO_3-based metathesis catalysts. They identified the silica-alumina-supported catalyst as the best support. The alumina supported catalyst was only interesting at high Mo loading. The silica-supported catalyst was only active after activation under the olefin flow at relatively high temperature. These results were tentatively correlated to the presence of acidic sites at the surface of silica-alumina which would have a beneficial electron withdrawer effect on the Mo centres. However, only one support of each type was used and even if the superiority of the samples containing both silica and alumina was assessed, the actual role of Al and the optimum support composition was not determined.

The group of Bao et al. mainly reported on HBeta zeolite-supported MoO_3 metathesis catalysts [85]. Interestingly they also reported dramatic improvement when Al_2O_3 was added to this silicic support in the preparation of their metathesis catalyst [86-87].

Other authors claim that ordered mesoporous supports induce enhanced catalytic activity as compared to their amorphous analogues [14, 88-90]. It is not clear whether the geometry of the support has a direct impact on the reactivity of the Mo species deposited on it or if the positive effect is merely linked to an improved accessibility of the active centres. Another interesting attempt concerned pillared clays Mo-based catalysts and gave moderately active catalysts [91].

From the literature, it appears obvious that the nature of the support impacts on the catalytic behaviour of the catalyst. However, few systematic comparative studies have been reported. More importantly, no convincing explanation of the role of the support in real catalysts has been proposed up to now. One striking example is the case of silica-alumina support, which is

often chosen but for which the choice was only justified by isolated attempts [92].

2.4.2.2. Effect of the MoO_3 loading

The MoO_3 loading is obviously an important parameter that is very often screened in the reported studies. Mo oxide is the active phase so it can be expected that the introduction of higher amount of Mo in the catalyst would lead to higher number of active sites and to better performances. It is however well-known that such simple relationship between the loading in active phase and the catalytic activity is rare. In the case of MoO_3-based metathesis catalysts, studies show that there is no direct relationship between catalytic activity and MoO_3 loading [93]. Very often, the activity increases with the increase in the MoO_3 only up to a given loading. Then the performances level off or decrease sharply [84, 86, 93-95].

This behaviour is usually discussed in relationship with the spreading of Mo oxide on the available support surface. It is commonly accepted that MoO_3 crystals are inactive [96]. Overloading of the catalyst is thus generally seen as deleterious since the production of inactive crystals is favoured when the surface density of Mo increases.

However, it has to be recalled that, even in low-loaded catalysts where the dispersion is excellent, only a small fraction of Mo atoms yields active metathesis centres [71]. This is why efforts should be made, not only towards formulations that keep high dispersion of the Mo phase, but also on trying to identify the nature of the well-spread species that actually yield active sites and on increasing their proportion.

2.4.2.3. Effect of the mode of preparation

The most convenient way to prepare a MoO_3-based catalyst is to impregnate a Mo precursor on the dedicated support and to decompose this precursor by thermal treatment to the Mo oxide phase. Wet impregnation of ammonium heptamolybdate (AHM) is commonly used for that purpose [97-100]. However, as inferred from the previous paragraphs, the morphology of the MoO_3 deposit, the nature and proportion of Mo oxide species and the interaction of Mo atoms with the support are crucial parameters that dictate the performance of the catalyst. In that perspective, it is important to work

on the improvement of existing preparation procedures and to explore alternative preparation routes.

Balcar and co-workers have proposed a very convenient method for the transfer of Mo oxide onto a support by simple "thermal spreading" [93]. The direct spreading of MoO_3 on an inorganic support was already used in the preparation of catalysts dedicated to other reactions [101]. The occurrence of gas-phase transport governing this phenomenon was demonstrated by other authors as well [102]. This method allows the use of fragile ordered mesoporous support whose structure would be partially destroyed upon impregnation with aqueous solution of AHM. This easy, cheap and environmentally attractive technique yielded active metathesis catalysts, exhibiting predominantly isolated surface molybdenum oxide species and dispersed polymolybdates (at low MoO_3 loading) [88]. Thermal spreading of Bis(acetylacetonato)dioxomolybdenum (VI) ($MoO_2(C_5H_7O_2)_2$) on alumina was also proposed by Handzlik et al. [103] who also put forward a positive influence of the better spreading reached through this technique as compared to classically prepared MoO_3/Al_2O_3 catalysts. The sublimation of $Mo(CO)_6$ is another very effective dry process for the formation of dispersed Mo species at the surface of silica or alumina [104-105].

The Balcar group recently reported on the preparation of metathesis catalysts by immobilization of bis(acetylacetonato)dioxomolybdenum and bis(glycolato)dioxomolybdenum on mesoporous molecular sieve SBA-15 [63]. Tested in the liquid phase metathesis of 1-dodecene, these catalysts outperformed classical MoO_3/SiO_2 and MoO_3/SBA prepared by a classical route. This effect is interpreted in terms of a better dispersion achieved with the new precursors proposed in the study, as supported by Raman spectroscopy.

Catalysts prepared by wet impregnation of AHM must be calcined to decompose the salt and form the MoO_3 phase. A molybdena-alumina catalyst was either calcined under air at 550 °C or evacuated under reduced pressure at 250 °C [106]. Both were activated under Ar at 600 °C prior to the propene metathesis test reaction. It was shown that the preliminary treatment influences the final reactivity toward propene. The authors link the better

performances of the evacuated sample to the increased reducibility and improved spreading of the Mo oxide phase.

From these studies, it appears that progresses are still possible based on the development on new alternative preparation methods.

2.4.3. Experimental investigations on the activation and on the genesis of active sites

MoO_3-based catalysts are always activated prior to reaction with the olefin(s). Usually, the pre-treatment is carried out in a flow of inert gas at a temperature ranging from 500 °C to 800 °C or at lower temperature under vacuum [107]. This step is dedicated to the complete removal of residual adsorbed water and oxygen. Additionally, a partial reduction of Mo atoms is sometimes claimed to be the condition to generate active species [96]. Photoreduction of MoO_3/SiO_2 catalysts was used to produce unsaturated $Mo^{(IV)}$ species that react effectively with the olefin to generate the active molybdenum carbenes [66, 108-111]. Nevertheless, more recent results indicate that $Mo^{(VI)}$ centres are the precursors to active metathesis centres [73] and prove the inactivity of some reduced species [112]. In any case, performing such thermal or photo pre-treatment is essential in the subsequent genesis of active metathesis centres. However, it is clear that the creation of active sites occurs at the first stage of the reaction with the olefin. The activation merely allows creating the adequate conditions for the formation of the carbenes. No systematic study was reported that unambiguously elucidates the role of this activation step in the genesis of active metathesis centres. Several papers highlight the importance of the procedure used, e.g. the strong influence of activation temperature [113], while other reports support the idea that the details of the activation procedure do not decisively dictate the final performances reached. For example, treatment of a molybdena-alumina catalyst in inert or in air (followed by flushing in inert) resulted in similar metathesis performances [114]. In practice, different inert gases, different activation temperatures and durations are used in an apparent arbitrary way. The most common activation procedure is a treatment under inert atmosphere around 550 °C [9].

It should be mentioned also that an important field of research concerns the treatment of the catalysts with co-catalysts. This strategy relies of the use of compounds (e.g. Me_4Sn) that promote the formation of metal carbenes on the catalyst surface [103, 115-117].

3. TOWARDS THE OBJECTIVE OF THE THESIS

As exposed in the previous sections, remaining questions persist in the route to mastering the performances of MoO_3-based heterogeneous metathesis catalysts. This study proposes to address some of these remaining issues on systematic experimental bases. Original strategies that are proposed in the literature regularly yield improvements in the performance of these systems. This study will thus also investigate alternative routes to the production of MoO_3-based metathesis catalysts in the perspective of further progress in that field.

Even if Mo oxide is the active phase of the catalyst, actually accomplishing the catalytic role, it is clear that the inorganic carrier on which it is supported plays a key role. Silica and silica-alumina supports are the most often proposed supports. Recent results indicate the superior activity of silica-alumina-supported Mo oxide as compared to silica-supported catalysts. The actual impact of the presence of Al in silica-rich supports is not yet understood and will be investigated systematically here.

The intricate relationship between the MoO_3 loading and the metathesis activity is the next issue that will be addressed. Because this question is linked to the spreading of the Mo oxide phase and since the calcination step most probably influences this parameter too, the impact of the calcination temperature will also be assessed. Depending on the Mo loading and on the thermal treatment, different Mo species can be expected. The pragmatic conclusions concerning the optimum loading and optimum calcination temperature will expectantly be accompanied by a better fundamental understanding on the nature of the most active species.

Keeping in mind the preliminary identification of relevant physico-chemical properties that dictate positively the performances of the catalysts, the next objective will be to explore alternative methods for the preparation

of MoO_3-based metathesis catalysts. The purpose will be to propose ways to amplify these properties and to look for improved catalytic performances. The mode of deposition or the mode of incorporation of Mo oxide in the catalyst can indeed impact the final properties of the catalysts as well as their performances.

Overall, the aim of this study is to develop further understanding of the genesis and nature of the active metathesis centres on MoO_3-based heterogeneous catalysts. In the context of actual challenges, this study is prompted to offer new guidelines for progressing towards improved catalytic processes that would allow regulating the stocks of light hydrocarbons in a more efficient way.

4. STRATEGY

The strategy that was used in this research to answer the questions raised in the previous sections can be articulated around three parts, as outlined below. It is based on the dedicated preparation of catalytic formulations, on their extensive physico-chemical characterization and on a standard activity measurement procedure. The details of the latter procedure were chosen as to fit closely the experimental conditions of major works reported previously in the literature – mainly by the group of Handzlik [71, 84, 103, 106, 115, 118] – and thus to allow proper comparisons.

In the first part, a classical approach for the preparation of MoO_3-based metathesis catalysts will be used to highlight the most adapted composition and some of the decisive physico-chemical properties that dictate the activity of the catalysts. In this perspective the first strategy is to prepare a set of model catalysts with different silica-alumina supports in order to identify the best support composition and to elucidate the effect of Al in MoO_3/SiO_2-Al_2O_3 catalysts. Then, starting from a given catalytic formulation which proved to be successful in the targeted reaction, the loading of active phase and the calcination temperature will be varied systematically. The results obtained in this first part will be used as a starting point for the following axes of research.

The second part will focus on alternative procedures to produce a molybdena phase at the surface of a silica-alumina support. The approach relies on the fact that several parameters of the classical preparation method can be varied on purpose in order to exacerbate one given property. More precisely, two strategies will be evaluated. In the first one the nature of the precursor used in the wet impregnation will be changed, aiming at the formation of a highly dispersed Mo oxide phase. The two alternative precursors chosen will hopefully either allow the production of smaller molybdate clusters in solution (leading to a better spreading of the active phase) or be more readily converted to Mo oxide upon moderate calcination (leading to a reduced tendency of MoO_3 to sinter). The second strategy will rely on a very simple preparation method reported recently: the direct thermal spreading of MoO_3 onto the desired support. This technique was chosen for its simplicity – which makes it very attractive for industrial applications, but also because it is thought to yield well-spread molybdate species.

In the third and last part of this document, a non-conventional preparation route will be investigated. The strategy relies on the non-hydrolytic sol-gel chemistry that is thought to lead to a very different kind of MoO_3-based catalysts. Indeed, this technique consists in the one step preparation of a mixed oxide through the condensation of chloride and/or alkoxide precursors in the absence of water [119]. Instead of depositing the active phase on a preformed support, Mo species will be incorporated directly with the other components of the catalyst. Very likely, the nature of the Mo species created will be different from the species found in catalysts prepared in two steps starting from preformed supports. The technique is recognized as yielding very homogeneous mixed oxides with each metal statistically dispersed in the solid [120-122]. Therefore, the approach could allow us studying the potential of monomeric molybdate species in the metathesis reaction. One challenge however will be to efficiently involve Mo atoms in the reaction, since it is supposed that part of it will be "lost" in the bulk of the material and thus not accessible at the surface for catalytic reactions. This technique has never been used to prepare catalysts based on Si, Al and Mo oxide and was only scarcely used in the preparation of heterogeneous catalysts [123-131]. This technique additionally presents

competitive advantages with respect to the more conventional hydrolytic sol-gel technique (cost of the precursors, control on the kinetics of the synthesis) [121].

It must here be recalled that the current industrial interest for the metathesis of light olefins is linked to the possibility to produce propene from the cross-metathesis of ethene and butene. In fact, historically, the reverse reaction was important because the industry was facing surplus of propene [9]. The self-metathesis of propene has frequently been used and is still used as a probe reaction to measure the catalyst metathesis activity. This reaction is equilibrated and non-thermal, meaning that the potentialities of catalytic formulations can actually be measured in both directions. At the laboratory scale, it is more convenient to run the reaction in the propene to ethene/butene direction because only one gaseous reactant has to be fed. The whole strategy of this project was thus centred on the measurement of the activity of the studied catalysts in the self-metathesis of propene to ethene and butene. A catalyst that would be highlighted as excellent in the self-metathesis of propene should also perform well in the cross-metathesis of ethene and butene.

EXPERIMENTAL

ABSTRACT

This section describes the experimental set-ups used to (i) prepare the catalysts, (ii) characterize their physico-chemical properties and (iii) evaluate their performances in the metathesis of propene. Mainly the techniques employed systematically in most chapters are described in details here. Techniques that are only specifically used in given chapters are described in specific experimental sections. Some important parameters of catalyst preparation and characterisation will occasionally be repeated in each chapter for the sake of clarity.

1. CATALYST PREPARATION

Two types of catalysts were investigated in this study: supported Mo oxide catalysts and Si-Al-Mo mixed oxides. The details of their preparation are outlined below.

1.1. Supported molybdenum oxide

Catalysts were prepared by the addition of molybdenum oxide onto preformed silica or silica-alumina supports. The supports used are described below. Different methods were used to transfer MoO_3 or its precursor onto the support.

1.1.1. Preparation of the supports

All supports used in this study were calcined at 500 °C under static air for 15h. The supports used in this study can be classified in two categories:

- One commercial silica-alumina catalyst support purchased from Aldrich, Grade 135 (denoted A). This support contains 13 wt. % of alumina and has a specific surface area of 490 $m^2 g^{-1}$.
- One set of silica-alumina prepared by co-precipitation (sol-gel), through hydrolysis of ethyl orthosilicate and aluminium isopropoxyde, as described by Rouxhet et al. [132-133]. The procedure involved a purification of the reagents and their hydrolysis at controlled pH. The products were heated at 500 °C in air before storage. These samples are denoted SAx where x stands for the silica weight content in %.

1.1.2. Wet impregnation

A wet impregnation method was used to prepare supported molybdenum oxide catalysts. Different precursors were used.

1.1.2.1. Ammonium heptamolybdate (AHM)

12.2682 g of ammonium heptamolybdate was dissolved in 1 l of distilled water to obtain the precursor solution (6.66 g of Mo per liter). $(NH_4)_6Mo_7O_{24}.4H_2O$ was purchased from Aldrich and had a purity of 99.98 %. For each impregnation the desired volume of the precursor solution (depending on the targeted nominal MoO_3 loading) was diluted with distilled water to 200 ml. 4g of calcined support was the mixed with this impregnation solution for 2 hours. Water was then evaporated under reduced pressure in a rotavapor at 40 °C. The recovered solid was dried at 110 °C for one night and calcined at the desired temperature (300 °C, 400 °C or 500 °C) for 2 hours in a muffle furnace under static air.

1.1.2.2. Oxalic acid additive

The preparation of the precursor solution is similar to the one described above. Here, oxalic acid (Aldrich, 98 %) is added during the preparation of the precursor solution via dissolution of AHM (6.66 g of Mo per liter). The amount of oxalic acid is calculated in order to reach three moles of acid for one mole of Mo. This solution was then used for the wet impregnation in a procedure identical to the one described in Section 1.1.2.1. The drying and calcination steps were also identical.

1.1.2.3. Molybdenum oxide hydrates

A solution of molybdenum oxide hydrates was prepared from metallic molybdenum (99.95 %, Alfa Aesar) and a 15 % w/w solution of hydrogen peroxide (obtained from the dilution of a 30 % w/w solution from Aldrich, semiconductor grade). 2 g of metallic molybdenum powder was added progressively to 30 ml of the hydrogen peroxide solution. The mixture was kept at 0 °C in an ice bath. After effervescence had ended a platinum grid was placed into the solution in order to catalyse the decomposition of excess hydrogen peroxide. The solution was finally filtered and diluted to the desired concentration and used as impregnation solution as described in Section 1.1.2.1. The drying and calcination steps were also identical.

1.1.3. Thermal spreading

An appropriate amount of molybdenum oxide powder (Aldrich 99,5 %) was mixed with the calcined support. The mechanical mixture was hand-ground in an agate mortar for 5-10 minutes and was then placed in a muffle furnace and heated at 500 °C for 8 hours under static air.

1.2. Non-hydrolytic sol-gel catalysts

A non-conventional method for the preparation of MoO_3-SiO_2-Al_2O_3 catalysts and based on the non aqueous sol-gel route [121] was investigated. This part of the work was realized in collaboration with the group of Dr. Mutin, in the *Institut Charles Gerhardt, Université de Montpellier 2* in Montepellier, France.

The non-hydrolytic sol-gel syntheses were performed under an argon atmosphere using a glovebox. $SiCl_4$ (Alfa Aesar 99.9%), $AlCl_3$ (Alfa Aesar 99.9%), and $MoCl_5$ (Alfa Aesar 99.6%) were used as received. Diisopropyl ether ($^iPr_2O$) was purchased from Aldrich with 99% purity and was further dried by distillation over sodium wire. The chloride precursors were introduced first in a 50 ml Pyrex glass tube, and then the stoichiometric amount of $^iPr_2O$ was added. More precisely, as each O atoms in the oxide must orginate from $^iPr_2O$, the number of moles of $^iPr_2O$ is calculated as the number of O atoms needed to convert each mole of $MoCl_5$, $AlCl_3$ and $SiCl_4$ into MoO_3, Al_2O_3 and SiO_2 respectively (3 x number of moles of $MoCl_5$ + 1.5 x number of moles of $AlCl_3$ + 2 x number of moles of $SiCl_4$). In the end the solvent – CH_2Cl_2 – was introduced. The solution obtained was frozen in liquid nitrogen under vacuum and the tube was sealed. The tube was heated in an oven at 110 °C for 4 days under autogeneous pressure (ca. 0.7 MPa). After cooling to room temperature, the tube was opened and the gel was crushed in a mortar, and then dried at 20 °C under vacuum (0.00001 MPa) for 12 h. The xerogel was then calcined for 5 hours at 500 °C in flowing air (50 ml min^{-1}) leading to white to pale yellowish powders.

2. CATALYST CHARACTERIZATION

2.1. Chemical analysis

The weight percentages of Mo, Si and Al were measured by Inductively Coupled Plasma-Atomic Emission Spectroscopy (ICP-AES) on an Iris Advantage apparatus from Jarrell Ash Corporation. The materials were dried at 105 °C prior to measurements. In Chapter 2, the ICP-AES technique will be applied on liquid samples. Details on these experiments will be given in a dedicated section (p. 59).

2.2. Textural analysis

N_2 physisorption experiments were performed at -196 °C on a Micromeritics Tristar. The samples were outgassed at 150 °C under vacuum (2 Pa). The specific surface area was determined from the BET method in the 0.05 – 0.30 P/P_0 range. The pore size distribution was derived from the desorption branch using the BJH method. The average pore diameter is calculated as (4 * Pore Volume / BET specific surface area). The micropore volume was estimated using *t*-plot analysis in the 0.35-0.05 nm range.

2.3. X-Ray Diffraction

X-ray diffraction (XRD) measurements were performed with a Siemens D5000 diffractometer using the Kα radiation of Cu (λ = 1.5418 Å). The 2θ range was recorded between 5 ° and 75 ° at a rate of 0.02 ° s^{-1}. The ICDD-JCPDS database was used to identify the crystalline phases. In Chapter 4, in-situ XRD experiments are presented (experimental details are provided in p. 125)

2.4. Raman spectroscopy

2.4.1. Confocal Raman spectroscopy

Raman characterization was done on the InVia Raman microscope (Renishaw) equipped with a diode light (785 nm). Resolution was set to 4 cm^{-1}. Acquisition time was 10 s and 10 scans were recorded and averaged for

each sample. The laser power was set to 10 mW and the 50x objective was used.

2.4.2. Fourier Transform Raman spectroscopy

Some precursor solutions were analysed in by Raman spectroscopy, using the Bruker RFS 100/S apparatus. About 1 ml of the solution was introduced in a dedicated quartz cell. A coherent Nd-YAG laser of 1064 nm wavelength was used and its power was set to 450 mW. The resolution was 4 cm^{-1} and the frequency was analyzed in the 1600-100 cm^{-1} range. For each reported spectra 720 scans were recorded and averaged.

2.5. X-Ray photoelectron spectroscopy

X-ray photoelectron spectroscopy (XPS) was performed on a Kratos Axis Ultra spectrometer (Kratos Analytical – Manchester – UK) equipped with a monochromatized aluminium X-ray source (powered at 10 mA and 15 kV). The pressure in the analysis chamber was about 10^{-6} Pa. The analyzed area was 700 µm x 300 µm. The pass energy of the hemispherical analyzer was set at 160 eV for the wide scan and 40 eV for narrow scans. Charge stabilization was achieved by using the Kratos Axis device. The electron source was operated at 1.8 A filament current and a bias of –1.1 eV. The charge balance plate was set at –2.8 V. The sample powders were pressed into small stainless steel troughs mounted on a multi specimen holder. The following sequence of spectra was recorded: survey spectrum, C1s, O1s, Si 2p, Al 2p (when needed), Mo 3d, Mo 3p + N 1s (when needed), Cl 2p (when needed) and C1s again to check for charge stability as a function of time and for the absence of degradation of the sample during the analyses. The binding energy (BE) values were referred to the C-(C, H) contribution of the C1s peak fixed at 284.8 eV. Molar fractions (%) were calculated using peak areas normalized on the basis of acquisition parameters after a linear background subtraction, with experimental sensitivity factors and transmission factors provided by the manufacturer. Spectra were decomposed with the CasaXPS program (Casa Software Ltd. UK) with a Gaussian/Lorentzian (70/30) product function.

2.6. Magic-angle spinning nuclear magnetic resonance

These experiments were realized in collaboration with the *Laboratoire de Chimie des Matériaux Inorganiques (CMI), I.S.I.S, Facultés Universitaires Notre-Dame de la Paix (FUNDP)*, in Namur, Belgium.

The environment of Si and Al atoms has been studied by measuring the magic-angle spinning nuclear magnetic resonance (MAS-NMR) of the ^{29}Si and ^{27}Al isotopes. NMR spectra of solids have usually very broad bands, due to dipolar interactions between nuclear spins. Because of such interactions, and because each dipole has a fixed orientation in the solid, a multitude of peaks are generated for each dipole. These interactions are actually cancelled if the sample is tilted to the "magic angle" (54°44 with respect to the direction of the magnetic field). In addition, a spinning is imposed to the sample in order to reduce field inhomogeneities in the solid sample. The technique allows differentiating Si or Al atoms coordinated in different environment.

The Bruker Avance 500 apparatus was used to record the Al resonance, using a flip of 10 ° (with respect to the vertical) and recording 5000 scans for each sample at intervals of 0.1 s. The sample rotation speed was 15000 rpm. To record the Si resonance the Varian 400 apparatus was used with a flip of 30°. Between 20000 and 40000 scans were recorded for each sample at intervals of 6 s. The sample rotation speed was 7000 rpm. In Chapter 4, special experiments were realized on "fresh" sampes (directly after the preparation and without ageing or storage). Details about these analyses are given in a dedicated section (p. 125).

2.7. Transmission electron microscopy

Transmission electron microscopy (TEM) analyses were performed using a LEO922 electron microscope operating at 200 keV. The powdered samples, dispersed in 2-butanol, were deposited on copper grids coated with a porous carbon film and the solvent was then evaporated.

2.8. Acidity measurements

Acididy data will be presented in Chapter 1 and 5 as obtained via NH_3-chemisorption and NH_3-Temperature Programmed Desorption respectively. The results obtained by these two distinct sets of experiments are not directly comparable. The first one measures the amount of chemisorbed ammonia at a given temperature and under vacuum. The second one follows ammonia desorption during a progremmed temperature increase. The detailed experimental details are thus provided directly in the chapters (see p. 41 and p. 152).

2.9. Time-of-flight secondary ion mass spectroscopy

This surface characterization will only be used in Chapter 5 with the aim to finely characterize the outermost surface of the non-hydrolytic sol-gel catalysts. Details are given directly in the chapter (p. 152).

3. CATALYTIC ACTIVITY MEASUREMENTS

The evaluation of the metathesis activity of the catalysts was performed in collaboration with the group of Dr. Rodemerck at the *Leibniz-Institut für Katalyse e.V. an der Universität Rostock*, in Rostock, Germany.

3.1. Apparatus

All experiments were carried out in a multi-channel apparatus with a capacity of treating of up to 15 samples under identical conditions (Figure E-1) and equipped with one by-pass line [16, 134]. The whole design allows fully automated control of gas flows via mass flow controllers. To divide the common flow equally between the 15 ports, capillary feeding lines are used and their length (which determines the drops of pressure) is adjusted if needed. Three temperature zones (gas pre-heating, reactor, and post reactor lines with 16-port valve) are automatically controlled along with reactor switching and product sampling (Scheme E-1).

Figure E-1: 15-channel reactor used for carrying the metathesis reaction.

All catalysts were sieved and selected in the 200-315 μm granulometric size range. The catalysts (200 mg except in Chapter 5 were 100 mg were used) were introduced in straight quartz reactors (5 mm i.d.). In each experiment, several samples were pre-treated in parallel by heating up to 550 °C (temperature ramp of 5 °C min^{-1}) in N_2 (Air Liquide, 99.999 % purity) of 14 ml min^{-1} flow in each reactor and keeping this temperature for 2 h. Afterwards the system was cooled down to the reaction temperature (40 °C) under the same N_2 flow. A propene (Air Liquide, 99.95 % purity) flow of 8 ml min^{-1} was admitted for one hour sequentially in each reactor in order to measure the initial metathesis activity of each sample. During activity

measurement, the other reactors are kept under the same N_2 flow. Propene and nitrogen were purified over Molsieve 3A (Roth) filters. N_2 was also purified by an oxygen filter (Oxysorb-glass, Linde). The composition of the reaction gas was analyzed by an Agilent 6890 GC. Product analysis took about 6.5 min for each injection. The separation of hydrocarbons was performed on a HP-AL/M column (30 m length, 0.53 mm i.d., 0.15 µm film thickness) applying a temperature ramp between 90 and 140 °C and FID detection. The experiments were carried out at atmospheric pressure.

3.2. Expression of the catalytic performances

The selectivity to metathesis products was always found to be very close to 100% (typically 99%). Only traces of secondary metathesis products (1-butene, pentenes, hexenes) and isomerisation products (isobutene) were detected. The activity is calculated on the basis of metathesis products (ethene and *trans*- and *cis*-butene) formation. It will be expressed either in "average turn-over frequency" (TOF) or in specific activity. The TOF is defined as the number of propene molecules converted to metathesis products per atom of Mo introduced in the reactor and per second.[1] The specific activity is defined as the number of moles of propene converted per gram of catalyst and per hour.

[1] It must be stressed that this value is an average for all Mo atoms present in the catalyst and not a real turn over frequency for each active site. As a reminder, only a small fraction of the Mo atoms are thought to exhibit a catalytic activity. It is however not possible – in the framework of this study – to determine this proportion in each case. Therefore, the total amount of Mo atoms (active and inactive) is taken into account in the calculation of this average turn-over frequency and the actual turn over frequency of a given active site is of course underestimated.

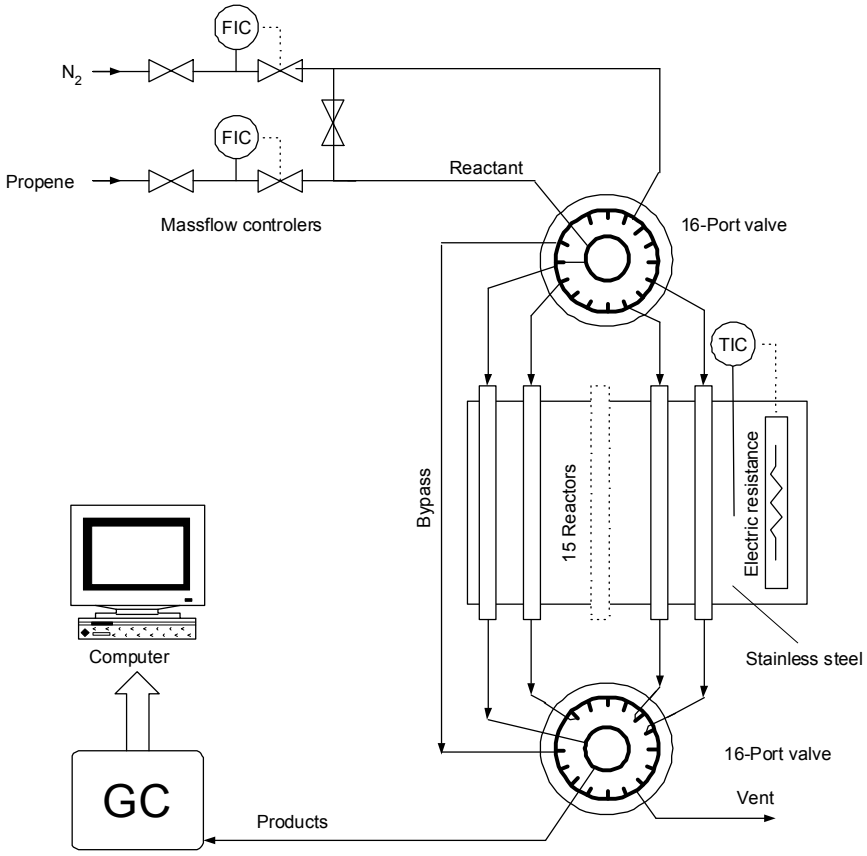

Scheme E-1: Schematic representation of the 15-channel reactor apparatus.

Blank experiments showed no activity at all. One reference catalyst was tested three times in the same experiment to evaluate the repeatability of the measurement. There was no difference between catalysts tested just after activation (as soon as the reaction temperature was reached) and the catalysts that were kept in the N_2 flow for several hours after activation and before reaction. The repeatability of the measurements appeared excellent, with a standard deviation lower than 1 % in relative. The same catalyst was again tested during two other experiments to evaluate the reproducibility of the measurements (independent sampling, independent activation and reaction procedures). The reproducibility of the activity measurement was satisfactory as well since the standard deviation was ~ 3 % in relative.

3.3. Precautions regarding metathesis activity measurements

The experimental setp-up described above takes into account many practical precautions that must be taken to run the metathesis reaction in a reliable way. Some of them are listed below.

3.3.1. Impurities

Metathesis catalysts are very sensitive to water and oxygen (and also to organic oxygenates). It is crucial to purify both the activation and the reaction gases via dedicated filters. When the filters are saturated, a progressive drop in the metathesis activity is observed in the experiments.

3.3.2. Hydrocarbon traces

The activation step is designed to remove all traces of adsorbed water and oxygen. It is performed at relatively high temperature (here 550 °C). It is crucial that this step is performed in a pure inert gas. At high temperature, traces of hydrocarbons in the flow can presumably alter the properties of the catalyst (the organic is oxidized by Mo oxide which is thus reduced). Traces of hydrocarbons may arise from the adsorption of the reactants (here propene) on the inox lines during the previous catalytic test. In the following experiment, when the furnace is heated for activation, propene may desorb from the lines, join the pretreatment flow and react with the hot catalyst. This problem is solved by using a hot box that heats the whole system at 120 °C and allows the flushing of adsorbed hydrocarbons from the lines before the samples reach a high temperature.

3.3.3. Temperature increase rate

Water is a poison for the active metathesis centres, but should also not be present during the activation step. In the case of porous samples that are not stored under totally dry conditions, the intrinsic humidity of the materials should not be underestimated. As a note, after outgassing for N_2-textural measurements, a weight loss of ca. 10 % was classically observed with the samples used in this study. Upon heating the samples to the activation temperature, this water evaporates. It appeared crucial to increase

the temperature at a moderate rate (here 10 °C min^{-1}) to allow the departure of water before the high activation temperature is reached. In fact experiments carried out with very rapid temperature increase led to lower metathesis activity and to an important lack of reproducibility.

3.3.4. Control of the temperature

The metathesis reaction is run at relatively low temperature, close to ambient. The regulation of the temperature is thus delicate. Marked differences were observed when the reaction was run at slightly lower or high temperatures. Here the circular multi-channel furnace was checked to be thermally very homogeneous and the temperature controllers were accurate enough to keep a reaction temperature of 40 °C ± 1.

Part I

On the catalytic formulation

ABSTRACT

In this first part, typical MoO_3-based catalysts prepared by the wet impregnation of ammonium heptamolybdate onto silica and silica-alumina supports are evaluated in the metathesis of propene. The first aim (Chapter 1) is to determine the most appropriate support for preparing such catalytic formulation. The second chapter presents the results obtained with a set of MoO_3/SiO_2-Al_2O_3 catalysts. In that section, the effect of the MoO_3 loading and the effect of the calcination temperature are screened. The results presented in Part 1 will be used as reference data throughout the following parts of this document.

CHAPTER 1: EFFECT OF AL ON THE PERFORMANCES OF MoO_3/SiO_2-AL_2O_3 IN THE METATHESIS OF PROPENE

ABSTRACT

This chapter highlights the essential effect of alumina on the catalytic behaviour of silica and silica-alumina supported molybdenum oxide catalysts in the metathesis of propene. MoO_3/SiO_2-Al_2O_3 catalysts with ~6 % MoO_3 weight are prepared via wet impregnation of ammonium heptamolybdate on a set of amorphous mesoporous silica-alumina with silica weight content comprised between 100 and 75 %. The addition of aluminim oxide into silicon oxide increases the acidity of the catalyst. It also affects the mode of deposition and the dispersion of Mo. Overall, the presence of Al is crucial for the metathesis reaction. It appears that the acidity, created by the introduction of alumina in silica, is beneficial for the metathesis reaction at low temperature. An optimum of activity is however found for the catalyst supported on the silica-alumina containing 15 weight % of Al_2O_3.

1. INTRODUCTION

As far as the catalytic upgrading of light alkenes is concerned, different kinds of chemical transformations may be envisaged. An important and widely studied catalytic process is the selective oxidation of light hydrocarbons which is often performed with Mo-based heterogeneous catalysts [135]. Classically, the catalysts are prepared by depositing Mo oxide onto an inorganic support: silica [136-137], magnesium oxide [138], alumina [139], etc. It is of common conception that acidic supports should be avoided because acidic sites provoke coke formation and C-C bond cleavage which lead to catalyst deactivation and/or to poor selectivity [140]. In silica-based materials, the introduction of Al that substitutes Si atoms brings significant additional acidity [133, 141-142]. Therefore, in selective oxidation reactions, pure silica supports are usually preferred to silica-alumina supports [143].

The situation is less clear for the metathesis of light alkenes. Classically, Mo oxide is deposited onto a support (silica [90, 144], silica-alumina [84, 86, 145], alumina [103, 146], titania [147-148], magnesia [149], zirconia [150] and even synthetic clays [91]) by impregnation, grafting or sublimation. It is commonly accepted that the nature of the support can have a major impact on the performance of the active phase. Silica-alumina and silica supported catalysts are more frequently proposed as best supports for MoO_3-based metathesis catalysts. The rare comparative studies concerning the effect of the support seem to indicate the better performances of molybdenum oxide when deposited onto silica-alumina [84, 92, 115, 145, 151]. However, the actual effect of alumina on the activity of Mo is not fully identified. As the metathesis of light alkenes is conducted at relatively low temperature and under anaerobic condition, coke formation and C-C bond cleavage would presumably not occur. On the other hand the process might demand reactive surface species that would allow activation and breaking of the C=C double bond. In that sense, unlike the case of the partial oxidation reaction, the presence of alumina could be advantageous and it is of primary interest to investigate its effect in a systematic way.

As stated in the Introduction, the role of the support is sometimes interpreted in comparison with the situation encountered in the metathesis with organometallic catalysts complexes for which the effect of each ligand surrounding the metal active centre is more straightforward. Indeed, one can compare the interactions (chemical bonds) between the Mo species and its support to the interaction between the metal centre of a homogeneous catalyst and its ligands. In that way, the superior activity of silica-alumina supported Mo oxide catalysts was tentatively attributed to the electron withdrawing effect created by acid centres found at Si-O-Al bridges [84]. Also, attempts are made to describe the nature of the molybdenum active species by theoretical calculations [65, 73]. These computational works show that the role of the support is to impose a constraint on the M_s-O-Mo bonds (where M_s is the metal of the support), that deforms the Mo environment and reduces the stability of the metallacyclobutane intermediate, leading to facilitated metallacycle opening and enhanced turnover frequencies [65]. Such approaches however need to start from simplified systems (for example isolated Mo species deposited on silica or alumina but not polymolybdates on silica-alumina) and omit parameters like surface irregularities, etc. So, experimental investigations on the effect of Al are still needed.

In this work, model catalysts are prepared by the wet impregnation of a molybdenum salt onto a series of preformed silica and silica-alumina supports. They mainly differ by the composition of the support since the MoO_3 loading was kept approximately constant, around 6 wt. %. The catalysts and the supports are characterized in terms of texture, bulk and surface composition, crystallinity and acidity. The purpose of this study is to identify the most suited support for Mo oxide as metathesis catalyst. In addition, characterization data will be correlated to activity measurements in order to elucidate the effect of Al on the catalytic behaviour of the catalysts.

2. SUMMED UP EXPERIMENTAL

The samples are prepared by wet impregnation of ammonium heptamolybdate on a set of silica-alumina, denoted SAx, where x is the silica wt. %. The catalysts, denoted SAxMo have a nominal MoO_3 weight loading

of 6 %. Details of the preparation are given in the Experimental section, paragraph 1.1, p.24.

ICP-AES (p. 27), N_2-physisorption (p. 27), XPS (p. 28) and XRD (p. 27) measurements are described in the Experimental section. The metathesis activity of the samples was measured at 40 °C after activation under N_2 as depicted in the Experimental section, p. 30.

The acidity of the samples was measured by NH_3-chemisorption. It was performed on the Micromeritics ASAP2010Chemi apparatus. The U-shaped sample tube containing 150 - 200 mg of catalyst was first flushed under a He flow at 300 °C for 2h and then evacuated at 50 °C for 2 h down to a residual pressure of <6.6 10^{-7} MPa (5 μmHg). A first NH_3 adsorption isotherm was measured at 50 °C. Then the sample was evacuated at the same temperature and down to 6.6 10^{-7} MPa. After that a second NH_3 adsorption isotherm was taken. The difference between the two isotherms represents the amount of NH_3 still chemisorbed on the sample at 50 °C (and under vacuum). The intercept of a linear interpolation built on the difference points measured between 0.026 and 0.091 MPa is taken as a measurement of the acidity of the sample, expressed in terms of ml of chemisorbed NH_3 per gram of catalyst (Figure I-1). This value is then normalized by the specific surface area of the sample, to give its “total surface acidity”. The same experiment is carried out a second time (on a fresh sample), also taking the two consecutive isotherms at 50 °C but running the intermediate evacuation step at 150 °C. The difference between the two isotherms gives the amount of NH_3 still chemisorbed at 150 °C and under vacuum (6.6 10^{-7} MPa), which is also normalized by the specific surface area to give the “strong surface acidity” of the sample. The standard deviation for each reported value is lower than 10 % in relative. A representative example is given in Figure I-1 for the SA90Mo catalyst.

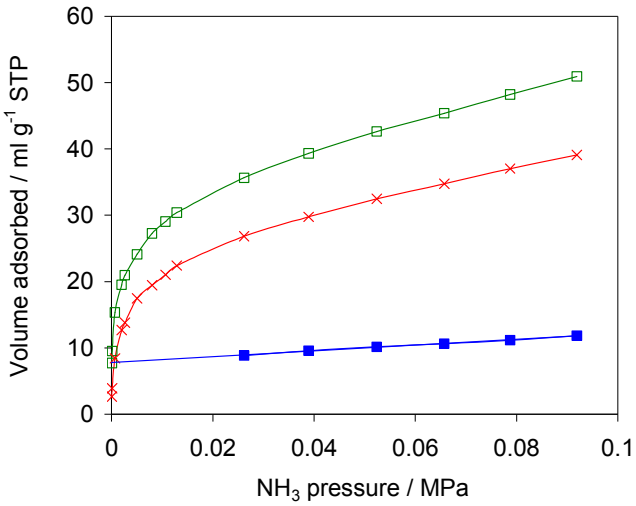

Figure I-1: Example of chemisorption measurement on the SA90Mo catalyst. All isotherms are measured at 50 °C. (□) First isotherm, (×) second isotherm after evacuation at 50 °C and down to a pressure of 6.6 10^{-7} MPa. (■) Difference (measuring the amount of NH_3 chemisorbed on the catalyst as the intercept of the linear interpolation line with the y-axis). This first experiment is used to determine the total number of acid sites. The second experiment (not shown) is designed to determine the number of strong sites: the same first isotherm is obtained; then after evacuation at 150 °C, only strongly chemisorbed NH_3 remain on the sample after evacuation and the second isotherm is thus closer to the first one and the difference is smaller.

3. RESULTS

3.1. Catalyst characterization

The nominal composition of the supports has been verified by ICP-AES and the surface of these supports was also studied by XPS (Figure I-2). The proportion of SiO_2 both in the bulk of the materials and at its surface corresponds well to the ratio calculated from their nominal compositions. It is important to note that the texture of the supports varied along the range of composition investigated (Table I-1). The specific surface area (SSA) decreases when the proportion of alumina increases. This is inherent to the preparation method and has to be taken into account in the discussion of other results. After impregnation of MoO_3, the SSA decreased slightly with

respect to the SSA of the corresponding supports. The MoO_3 loading is in the same order for each catalyst (around 6 wt. %). A non-negligible variability has however to be noticed.

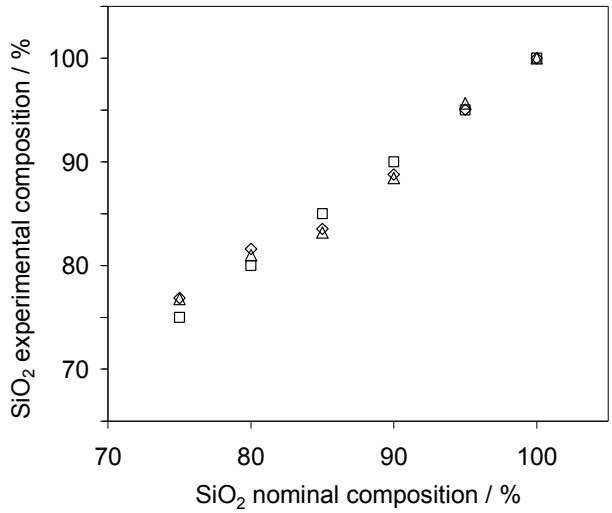

Figure I-2: SiO_2 content in the support as determined (□) from the nominal composition of the support, (Δ) from ICP-AES and (◊) from XPS measurements.

Table I-1: Specific surface area of the catalysts and supports (N_2-physisorption) and MoO_3 loading (ICP-AES).

	$SSA_{support}$ ($m^2\ g^{-1}$)	$SSA_{catalyst}$ ($m^2\ g^{-1}$)	MoO_3 loading (wt. %)
SA100Mo	481	413	7.3
SA95Mo	397	341	5.8
SA90Mo	263	246	5.5
SA85Mo	171	155	4.3
SA80Mo	169	164	4.3
SA75Mo	152	141	7.6

In XRD experiments all samples were characterized by a broad band around 20-25 °, typical of amorphous solids (Figure I-3). In addition, traces of crystalline orthorhombic MoO_3 were sometimes found as evidenced by the small diffraction lines mainly found around 27.3° and 23.3° (JCPDS 05-0508). The tendency to form MoO_3 crystals is slightly more pronounced on silica (SA100Mo) as compared to silica-alumina. The catalyst with the

highest alumina content (SA75Mo) is the only sample which does not exhibit diffraction lines at all.

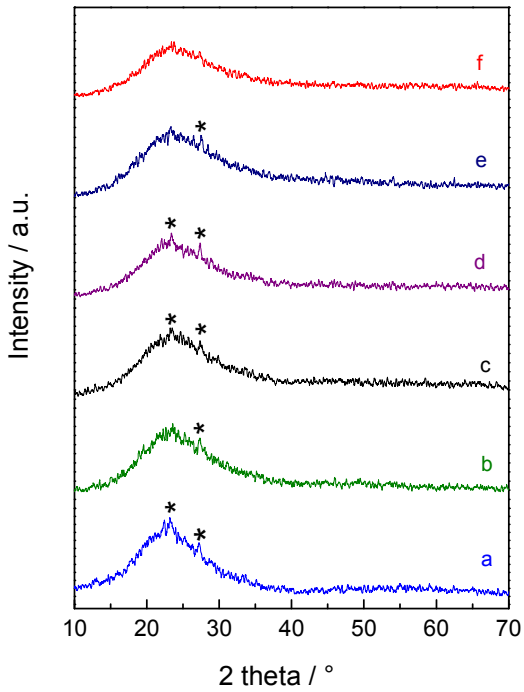

Figure I-3: XRD patterns obtained with (a) SA100Mo, (b) SA95Mo, (c) SA90Mo, (d) SA85Mo, (e) SA80Mo and (f) SA75Mo. Following JCPDS 05-0508, the peaks at 27.3 ° and 23.3 ° correspond respectively to the (021) and to the (110) crystallographic planes of orthorhombic MoO_3.

The amount of ammonia chemisorbed per gram of sample was normalized by the specific surface area of each sample (Figure I-4). For the set of support compositions investigated here, and with the exception the SA75 sample, the higher the Al content, the higher the total acidity. On the basis of Infra Red spectroscopy coupled with pyridine adsorption, a similar trend was found by Rouxhet and co-workers on the bare SAx supports [132]. In the latter study, the total acidity was shown to increase when the alumina content was increased from 0 to 25 and to start to decrease smoothly when the Al_2O_3 content was further increased (up to ~75 wt. %). The total acidity of SA80 was however not measured in that study, so that the maximum

measured here could not be observed. It is a well-known fact that silica-alumina materials are more acidic than silica powders [132-133, 141]. From NH_3-chemisorption measurements, it appears clearly that the silica support is virtually not acidic. Only a very small amount of weak acidic sites is detected, while the strong acidity equals zero for the silica support. As soon as a small amount of Al is introduced (5 wt.% of Al_2O_3 in SA95), the total acidity increases significantly and a relatively important proportion of strong acid sites is present. This strong acidity is even more pronounced when the alumina content is raised up to 10 wt. % and then remains approximately constant in the supports with a higher Al_2O_3 content.

The total surface acidity of the SA*x*Mo catalysts is clearly dependent on the support composition (Figure I-4b). The same trend is found as for the supports: the total acidity increases with the amount of Al_2O_3 (except for SA75Mo). For most catalysts, the amount of strong acid sites does not seem to be affected by the impregnation of MoO_3 (SA100Mo, SA90Mo, SA85Mo) or only increases slightly (SA95Mo, SA80Mo). The only notable exception is SA75Mo which exhibits an unexpected high proportion of strong acid sites. As it will be discussed later, the particularity of the support of this catalyst seems to affect the properties of the deposited Mo oxide phase. From the comparison between the supports and the catalysts, three important observations can be made: (i) in SAxMo and for x comprised between 100 and 80, the impregnation of MoO_3 mainly generates additional weak acid sites, (ii) in the SA75Mo sample in contrast, the impregnation generates strong acidity and (iii) the silica-based catalysts (SA100Mo) exhibits only weak acid sites.

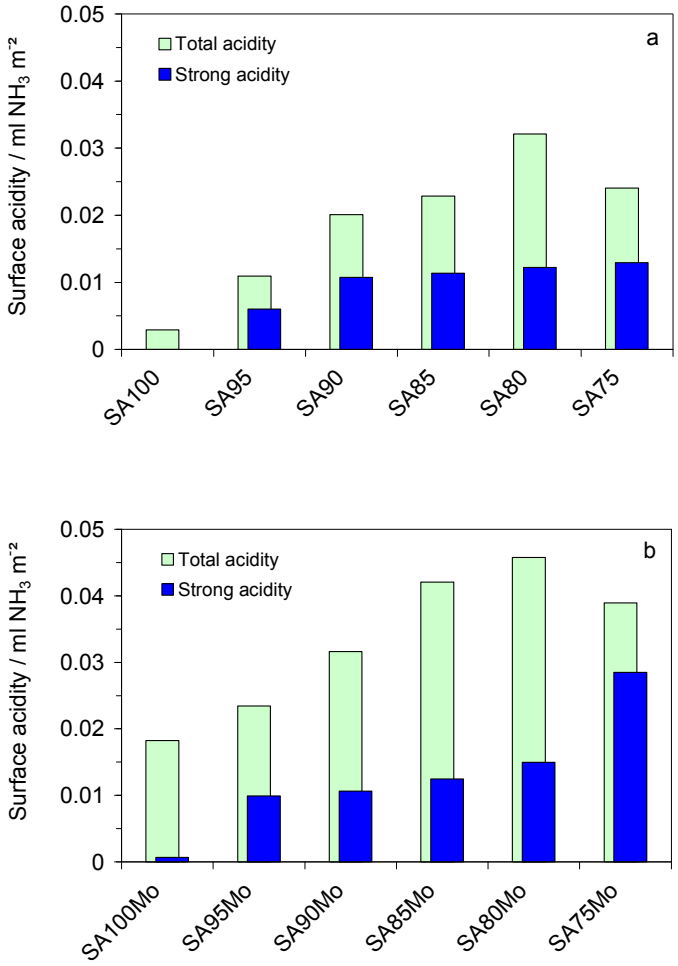

Figure I-4: Surface acidity of (a) the SA*x* supports and (b) of the SA*x*Mo catalysts probed by NH_3-chemisorption. The total acidity (amount of chemisorbed NH_3 per square meter of sample at 50 °C) is represented by the light grey columns and the strong acidity (amount of chemisorbed NH_3 per square meter of sample at 150 °C) is given in the dark grey columns. The weak acidity can be visualized as the difference between both values.

3.2. Catalytic activity

The catalysts were tested in the self metathesis of propene at low temperature (40 °C). In these conditions, primary metathesis products (ethene, *cis*- and *trans*-butene) were produced with selectivity close to 100%. The supports were all checked to be totally inactive. The evolution of

the activity with time-on-stream is showed in Figure I-5. All catalysts are active in the metathesis reaction but the silica-based catalyst is clearly weaker than the catalysts based on silica-alumina. Moreover, fast deactivation takes place with SA100Mo during the first 20 min of the reaction. Al-containing catalysts deactivate slower. It appears that increasing the Al_2O_3 content results in higher stability of the catalyst. For SA85Mo, SA80Mo and SA75Mo a maximum in activity is even noticed after about 14 min time-on-stream. Note also that the level of activity (in TOF) compares well with reports of the literature for similar systems and similar experimental conditions [64, 84, 87, 94, 106, 152].

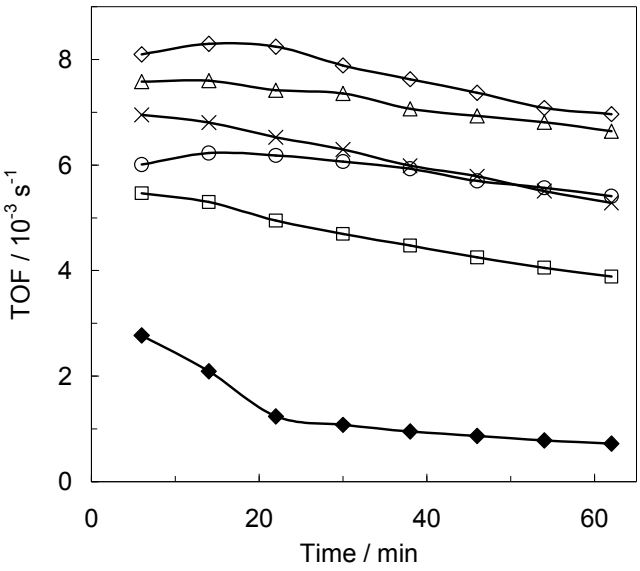

Figure I-5: Evolution of the metathesis activity with time on stream with (♦) SA100Mo, (□) SA95Mo, (×) SA90Mo, (◊) SA85Mo, (Δ) SA80Mo and (○) SA75Mo.

4. DISCUSSION

Silica-alumina prepared both industrially or at the laboratory scale usually can not be seen as a homogeneously mixed oxide materials as they exhibit heterogeneities at the nanoscale [153]. However, both surface and bulk characterizations showed that the composition of the support is close to

the nominal composition indicating that the composition of the support was well controlled during the preparation and that alumina is not preferentially located in the bulk or segregated at the surface.

The strategy was to systematically vary the composition of the support while keeping the MoO_3 loading constant. Nevertheless a significant variability was noticed from ICP-AES measurements. These discrepancies – that are attributed to errors in the preparation procedure – were noticed at a late stage of this research and could not be corrected. It might be argued that the undesired variability in the loading is superimposed to the intended variation in the composition of the support, thereby introducing a bias in the study. The next paragraph shows that this bias was probably not so impacting and explains how it was tried to take it into account.

Textural analysis shows that the specific surface area (SSA) of the silica-alumina systems tends to decrease with the increase in Al-content. As expected, further decrease is resulting from the impregnation of Mo oxide. The variation of the SSA with respect to the composition of the support affects the Mo surface density. In turn, this might affect the morphology of the MoO_3 layer that is deposited on the support (e.g.: formation of crystals). So, this important parameter would vary, even if the loading was kept precisely constant. However, considering the loadings and the SSAs encountered here, all catalysts are in the sub-monolayer range (as a guideline, a loading of 10 % would spread as a monolayer of Mo oxide on a surface of about 110 m^2). Additionally, XRD results show that the tendency to form MoO_3 crystallites is not correlated to the decrease in SSA in the set of catalysts investigated here. The Mo oxide deposit appears totally amorphous in the SA75Mo catalyst and only small diffraction lines appear in the other formulations, revealing traces of MoO_3 crystallites. SA100Mo is the catalyst in which the presence of small crystallites is slightly more marked, even though it has the highest SSA. This must be correlated to the well-known poor interaction between silica and MoO_3 that tends to favour the agglomeration of Mo oxide during calcination. Overall, the properties of the Mo oxide phase seem to be more influenced by the composition of the support, that by the small changes in loading or by the available surface

offered by the support. As the activity are discussed in terms of TOF the performance of the catalysts are normalized on the basis of the loading.

The results reported in Figure I-4a unambiguously show the effect of Al on the acidity of the supports. While silica only exhibits a small amount of weak acid sites, all silica-aluminas exhibit higher total acidity and a significant proportion of strong acid sites. In fact, the range of composition of the silica-alumina supports studied here was selected on purpose. The superior acidity of silica-alumina is indeed reported to be particularly marked when the proportion of Al_2O_3 is comprised between 5 and 25 wt. % [132]. A mixed $SiAlO_x$ phase is mainly formed in that case. The $SiAlO_x$ phase bears acidic Si-(OH)-Al bridging hydroxyl groups created by the substitution of Al^{3+} for Si^{4+} in a tetrahedral arrangement [133]. In contrast, in silica-alumina having 25 wt. % alumina or more, a highly dispersed alumina phase builds up at the expense of the mixed $SiAlO_x$ phase and this was associated to the appearance of Lewis acidity as confirmed by Rajagopal et al. [141]. SA75 is thus situated at the border of the two zones described above. The fact that the continuous and linear tendency found in Figure I-4 is broken at the level of this catalyst is not surprising. It should thus be considered that the nature of the acidic site may be different in SA75 and in the other silica-alumina supports studied. Finally, correlating our acidity measurements with previous investigations, it can be stated that (i) the acidity of the silica support is very low, (ii) the acidity of the SAx support increases when the SiO_2 content decreases from 95 to 80, as the mixed $SiAlO_x$ phases builds up, thereby creating bridging OH acidic groups and (iii) the SA75 sample seems to already exhibit a particular character, most probably due to the appearance of an alumina phase at the expense of the mixed $SiAlO_x$ phase which results in a lower weak acidity.

In the catalysts (Figure I-4b), even if Mo oxide partially covers the support surface, the same trend is noticed as in the SAx series. In other words, the nature of the support determines strongly the acidic properties of the catalyst. The impregnated MoO_3 phase appears to bring additional weak acidity to the SAxMo catalysts with x comprised between 100 and 80. The extent of this increase in weak acidity is roughly the same for all catalysts. Such increase in acidity provoked by the impregnation of Mo oxide is a

classical observation, also noticed in the case of titania-supported catalysts [154]. The peculiar acidity of the SA75 support translates into peculiar acidity of the SA75Mo catalyst. Here, the impregnation of Mo oxide provokes an increase in the strong acidity. Reports indicate that the spreading of MoO_3 is more effective on a support exhibiting higher number of Lewis sites [155]. XRD results (Figure I-3) also suggested that the spreading was better in SA75Mo. The model of Rouxhet et al. [132] implies that an alumina phase starts to develop in the SA75 support, which decreases the proportion of Si-Al bridging hydroxyl groups and creates additional Lewis acidity. Like described by Rajagopal et al. the heterogeneity of such support gives rise to a variety of Mo oxide species which results in different acidic characteristics [141]. These additional acidic sites found in SA75 may be responsible for a particular mode of deposition of the MoO_3 phase which would tend to develop a stronger acidity.

The depicted evolution of the metathesis activity with time (Figure I-5) is commonly observed in the metathesis of propene with Mo oxide-based catalysts [64, 84]. The latency stage sometimes observed corresponds to the formation of surface carbene species by reaction of propene with activated Mo sites. The nature of these activated sites is still under debate as results indicate that isolated [9, 74, 88, 108, 156], dimeric [74] or well-spread polymeric [88, 157] MoO_x species are the actual active sites. It is however known that a thermal activation is needed to remove traces of molecular oxygen and water [118]. Surface carbenes, produced from the reaction of Mo sites with the olefin at the very beginning of the reaction, then act as the catalytic active sites. It is thought that deactivation occurs when an oxidation reaction occurs instead of the metathesis reaction, leaving a reduced Mo site [110, 118, 152] or when the fragile carbene active centre reacts with trace impurities (O_2 or H_2O) [158].

In our experimental conditions only alumina-containing catalysts exhibit high activity in the metathesis of propene. The activity of the molybdena-silica catalyst is comparatively very low. Other studies focussing on MoO_3/SiO_2 metathesis catalysts were published and the results are not in contradiction with ours since (i) the activity was low [84], (ii) a special activation procedure based on UV or gamma irradiation had to be used [109,

144, 159] or (iii) the reaction temperature was much higher (leading to important decrease in selectivity, since oxidation and isomerization reactions also take place) [84]. In order to better visualize the role of Al, it was chosen to compare the catalysts on the basis of the activity reached after 14 min time-on-stream (Figure I-6). The catalysts can be ranked as follows: SA100Mo< SA95Mo < SA75Mo < SA90Mo < SA80Mo < SA85Mo. Thus, 15 wt. % content of alumina in silica-alumina is identified as the best support composition for preparing Mo-based metathesis catalysts, even though the supports with 10- and 20 wt. % of alumina yield similar results.

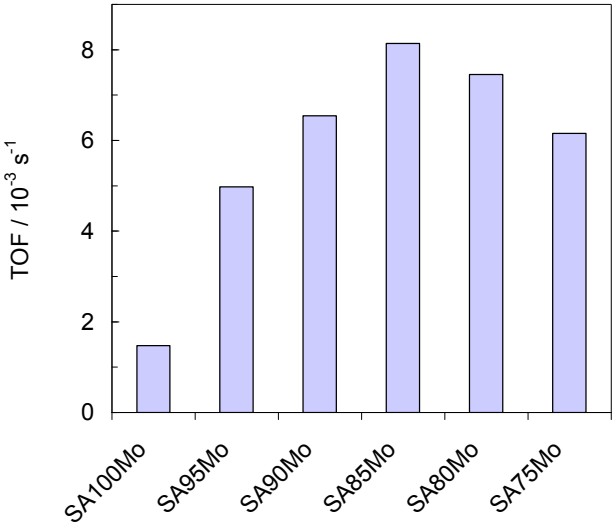

Figure I-6: Metathesis activity (TOF measured after 14 minutes time-on-stream) obtained with SA*x*Mo10 catalysts. The standard deviation for metathesis activity measurement was about 3 % in relative (see Experimental section p. 30).

The activity results discussed here should be understood in the light of acidity measurements (NH_3-chemisorption in Figure I-4). The presence of Al in the formulation provides a marked acidic character. On the one hand, it is known that the presence of Al "switches off" the ability of the catalyst to perform well in selective oxidation reactions. This tendency can be understood as follows: stronger acidity results in a stronger adsorption of the hydrocarbon, which, under high reaction temperatures and in the presence of

O_2, leads to the over-oxidation of the hydrocarbon to CO and CO_2. On the other hand, it is shown here that the presence of Al "switches on" the ability of the catalyst to perform well in the metathesis reaction. The presence of strong acidic sites can be regarded as a key factor dictating the activity of the systems. Indeed the activity of the catalysts exhibiting virtually no strong acidity is very low. However, the total amount of acidic sites follows better the trend observed in the activity. Figure I-7 indicates clearly the reasonable correlation between the total acidity and the activity developed by the catalysts.

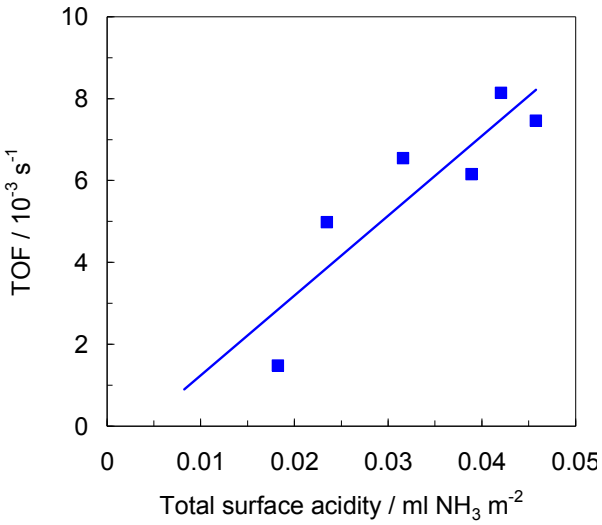

Figure I-7: Correlation between the activity (expressed in TOF) and the total surface acidity as measured via NH_3 chemisorption.

In the set of catalysts investigated here, the maximum in total acidity (SA80Mo; see Figure I-4) almost fits the maximum observed in activity (SA85Mo; see Figure I-6). This rough correspondence indicates the existence of an optimum in the alumina content (15-20 %) which translates in an optimum in terms of surface density of acidic sites and in terms of activity. Following Handzlik et al.[84], our interpretation is that the acidic sites present in silica-alumina play the role of electron withdrawer on the Mo species deposited on them. It appears that the presence of a mixed $SiAlO_x$ phase exhibiting Si-(OH)-Al species is beneficial for the genesis of active

metathesis centres. This interesting mixed phase builds up when the alumina content increases from 5 to 20 wt. %. A MoO_x species located on such acidic site displays a certain electron deficiency which, exactly like in the case of homogeneous catalysts where the electron deficiency on the Mo centre is provoked by electron withdrawer groups (e.g.: imido alkylidene), favours the completion of the metathesis reaction mechanism [23]. The catalyst based on the support containing 25 wt. % of alumina exhibited a higher proportion of strong acidic sites and this was tentatively attributed to the appearance of a new alumina phase that governs a different mode of deposition of MoO_3. These strong sites appear less appropriate for the metathesis reaction. This is coherent with a recent report showing that excessive acidity is deleterious for the metathesis reaction: in MoO_3/HBetal-Al_2O_3 catalysts the addition of Mg resulted in the tempering of the support acidity and in increased the catalytic performances [62]. Let us finally note that further studies should be conducted concerning the nature of the acidic sites (BrØnsted vs. Lewis) in order to go further in the understanding of the nature of the acidic sites that dictate the performances of MoO_3/SiO_2-Al_2O_3 metathesis catalysts.

5. CONCLUSION

MoO_3 supported on silica-alumina with low Al_2O_3 content (between 0 and 25 wt. %) has been studied as catalyst for the metathesis of propene. The main conclusion of this work is very pragmatic: MoO_3/SiO_2-Al_2O_3 catalysts should be used for the metathesis reaction. The marked acidic character of Al-containing materials as compared to Al-free samples seems to be decisive. The nature of the support strongly determines the acidic properties of the catalyst. While this acidity is commonly accepted to be deleterious for performing partial oxidation reactions of such hydrocarbons, it is identified as beneficial for the metathesis reaction. All silica-alumina supported catalysts were significantly active in the metathesis of propene while the activity of the silica-based catalyst was very low. However, an optimal Al_2O_3 content in the support was found around 15 wt. %.

Considering the crucial impact of the chemical composition of the support on the performances of the Mo oxide phase, improvement of

catalytic formulations could be obtained through strategies based on the development of a more intimate interaction of the active phase with the support.

CHAPTER 2: MoO_3/SiO_2-Al_2O_3 METATHESIS CATALYSTS PREPARED BY THE CLASSICAL WET IMPREGNATION TECHNIQUE: EFFECT OF MoO_3 LOADING AND OF CALCINATION TEMPERATURE

ABSTRACT

The classical wet impregnation of ammonium heptamolybdate onto a commercial silica-alumina support has been used to prepare MoO_3/SiO_2-Al_2O_3 catalysts. The effect of the Mo loading and the effect of the calcination temperature are studied. The samples are characterized by N_2-physisorption, XRD, Raman spectroscopy, MAS-NMR spectroscopy, TEM and X-ray photoelectron spectroscopy and evaluated in the metathesis of propene. It is shown that the temperature of calcination influences the performances of the catalyst. High temperature treatments are necessary to efficiently decompose the Mo salt precursor. The performances are levelling off when the MoO_3 loading is increased above ~8 wt. %. This effect is correlated to the appearance of MoO_3 crystals an $Al_2(MoO_4)_3$ at relatively high loading.

1. INTRODUCTION

It is shown in the first chapter of this thesis that the nature of the support for the active MoO_3 phase is crucial for the production of active metathesis sites. More precisely, the crucial role of Al for obtaining MoO_3-based catalysts that are active in the metathesis of light olefins at low temperature is clearly highlighted. Our systematic investigation confirmed previous reports [84, 115] that indicated silica-alumina as the privileged support for MoO_3-based metathesis catalysts and correlated this effect with the generation of higher acidity. In the present chapter, a commercial silica-alumina support is used as a support. Its composition (ca. 13 wt. % of Al_2O_3) is very close to the optimum composition determined in Chapter 1, namely ca. 15 % of alumina.

Supported MoO_3-based catalysts are conventionally prepared by the wet impregnation of ammonium heptamolybdate (AHM) on an appropriate support [100, 160]. The preparation involves (i) the dissolution of the Mo salt in water to obtain an impregnation solution, (ii) the impregnation of the support by stirring a suspension of it in the impregnation solution (iii) the evaporation of water, (iv) the drying of the recovered solid and (v) the calcination of the sample. Even if this standard methodology is indeed widespread, many experimental parameters can decisively affect the properties of the catalytic material that is produced. It is crucial to determine precisely the experimental conditions in which each step is conducted. The specific description of the method is given in the experimental part (p. 25). Most parameters (volume of impregnation solution, amount of support, impregnation, drying and calcination times, etc.) are fixed.

In the framework of this study, it was decided to look at two important parameters of the preparation: the molybdenum loading and the calcination temperature. These parameters were chosen because of their potential impact on the final performance of the yielded metathesis catalysts.

Molybdenum oxide being the active component of the catalyst, its loading is evidently crucial. In principle, the amount of active centres could be partially linked to the amount of Mo introduced in the formulation.

Changing the targeted MoO_3 loading induces a change in the AHM concentration in the fixed impregnation solution volume. Also, as the available surface area of the support remains constant, the Mo surface density in the resulting catalyst varies. In turn, the mode of dispersion of Mo oxide can be affected as well as the nature of the Mo species stabilized on the support.

The calcination of the catalyst leads to the decomposition of the ammonium salt and to the formation of a MoO_x phase. Changing the calcination temperature may affect the efficiency of this step (well-formed Mo oxide phase vs. partially decomposed molybdenum salt). Also, the strength of the thermal treatment may affect the dispersion of the Mo phase. Indeed, high temperature treatments are known to favour sintering phenomena, potentially leading to catalysts bearing higher proportions of MoO_3 crystals, for example. On the other hand, MoO_3 is known to be quite volatile and harsh thermal treatment might conversely promote better Mo dispersion on the support, or provoke Mo losses.

In this chapter, MoO_3/SiO_2-Al_2O_3 catalysts are prepared by the wet impregnation of ammonium heptamolybdate on a commercial silica-alumina. The samples are calcined either at 300 °C, 400 °C or 500 °C. Then, the MoO_3 loading is systematically varied. The catalysts are characterized by N_2-physisorption, ICP-AES, XRD, XPS, MAS-NMR and Raman spectroscopy and evaluated in the self metathesis of propene.

2. SUMMED UP EXPERIMENTAL

The catalysts are prepared by wet impregnation of ammonium heptamolybdate (AHM) on a commercial silica-alumina purchased from Aldrich (~13 wt. % of Al_2O_3). The samples are denoted AAxY, where the first ‘A’ is the Aldrich support, the second ‘A’ stands for the AHM precursor, x is the nominal MoO_3 weight loading (%) and Y is the calcination temperature (°C). Both the loading and the calcination temperature are screened. First, the loading (x) is fixed at 8 wt. % (following typical loading proposed in the literature [88, 93, 145] and the effect of calcination is followed (Y = 300, 400 and 500 °C). Then, the best calcination

is selected and the loading is screened in a lager range (from 4 to 15 wt. % of MoO_3).

The samples are characterized by ICP-AES, N_2-physisorption, XRD, XPS, TEM and ^{27}Al MAS-NMR as described in the Experimental section, paragraph 2. The impregnation solution was also studied by FT-Raman spectroscopy.

3. RESULTS

3.1. Catalysts preparation and characterization

The initial precursor solution (6.66 g of Mo per litre) was obtained by dissolution of ammonium heptamolybdate in distilled water. In Raman spectroscopy (Figure II-1), this solution exhibited two main bands at 942 cm^{-1} and 895 cm^{-1} that are attributed to the presence of the heptamolybdate ions (respectively the ν_s MoO_{2t} and the ν_{as} MoO_{2t} vibrations) [98, 161-162]. The pH of this precursor solution was 5.4. The desired volume of this solution (depending on the targeted MoO_3 loading) was diluted in water and used for the impregnation of the support (see Experimental section, p. 24).

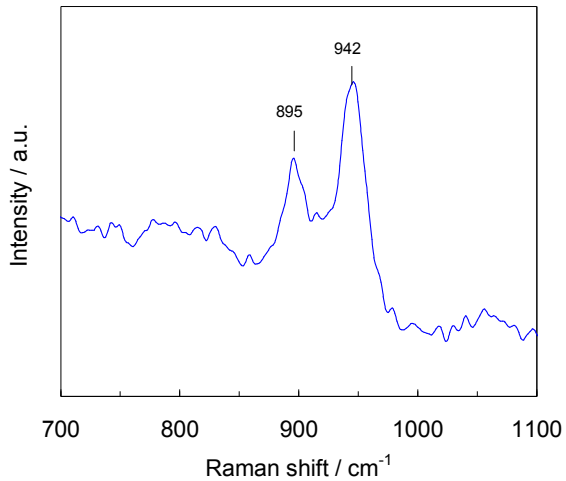

Figure II-1: FT Raman spectrum of the initial AHM precursor solution used for the preparation of the catalysts.

Table II-1: Experimental MoO_3 weight loading (ICP-AES) and textural properties (N_2-physisorption).

Catalyst name	MoO_3 loading (wt. %)	SSA ($m^2\ g^{-1}$)	Pore volume ($ml\ g^{-1}$)	Pore diameter (nm)
A	-	490	0.71	5.8
AA4500	3.8	440	0.63	5.7
AA8300	7.9	420	0.60	5.7
AA8400	8.3	400	0.57	5.7
AA8500	8.1	420	0.60	5.7
AA11500	10.9	380	0.55	5.8
AA15500	15.2	350	0.52	5.9

The experimental MoO_3 weight loading and the textural properties of the catalysts are given in Table II-1. The experimental loading fits with the nominal composition of the samples. All samples were mesoporous, with N_2 adsorption-desorption isotherms of type IV according to the BDDT classification. Such isotherms are shown in Figure II-2 in the case of the bare support taken as a representative example for all investigated catalysts. The calcination temperature has no significant effect on the specific surface area of the 8 % loaded samples. When the calcination temperature is fixed at 500 °C, the specific area and the pore volume clearly tend to decrease with increasing MoO_3 loading. On the other hand, the mean pore diameter tends to remain constant or to increase slightly after impregnation.

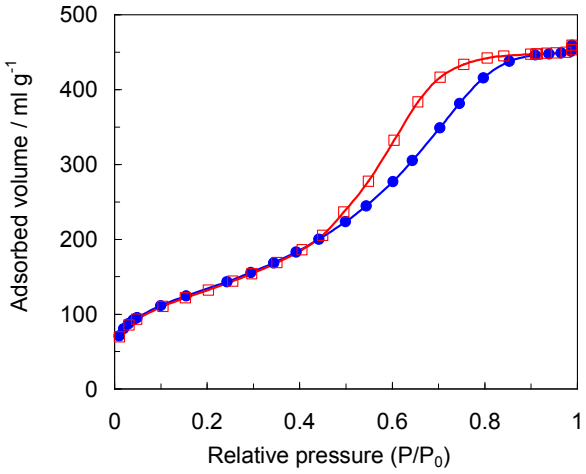

Figure II-2: N_2 adsorption (●) and desorption (□) isotherms at -196°C for the silica-alumina support ("A").

Figure II-3 and Figure II-4 were drawn in order to better visualize the effect of the MoO_3 loading and of the calcination temperature on the porosity developed by the support. Increasing the loading does not affect significantly the pore size distribution (Figure II-3). In the same way, for AA8 catalysts calcined at different temperature, no obvious alteration of the pore size distribution curve is obtained (Figure II-4).

XRD patterns of the catalysts reveal the presence of a very broad band (15 – 30 °) typical of amorphous samples. In addition, diffraction lines related to the presence of MoO_3 crystals are detected in some cases. At 8% nominal weight loading, MoO_3 crystals tend to form if the calcination temperature is high (Figure II-5). More precisely, after calcination at 300 °C no crystallites are detected in XRD (JCPDS 05-0508); small diffraction lines corresponding to traces of crystalline MoO_3 are distinguished on the catalyst calcined at 400 °C; these lines are much more pronounced after calcination at 500 °C. In the catalysts calcined at 500 °C (Figure II-6), the diffraction lines related to orthorhombic MoO_3 grow in intensity as the loading increases. Only the AA4500 sample appears amorphous. The average size of the crystals detected in samples AA8500, AA11500 and AA15500 was estimated via the Debye-Scherrer law to always fall in the 35-40 nm range.[2]

[2] The Debye-Scherrer equation is : $D = \frac{K \times \lambda}{\beta \times \cos\theta}$

In which
- D is the average size of the diffracting domain
- K is a constant used to take the morphology of the crystal into account (here the crystals are approximated to be spherical and K is set to 1)
- λ is the wave length of the R-ray source (here 0.1541 nm)
- β is the corrected peak full width at half maximum (in radian)
- θ is the Bragg angle

The measured peak full width at half maximum (β_{peak}, in °) is corrected taking into consideration the width obtained with a reference large quartz crystal (β_{quartz} here measured to be 0.1°) :

$$\beta = \sqrt{\beta_{peak}^2 - \beta_{quartz}^2}$$

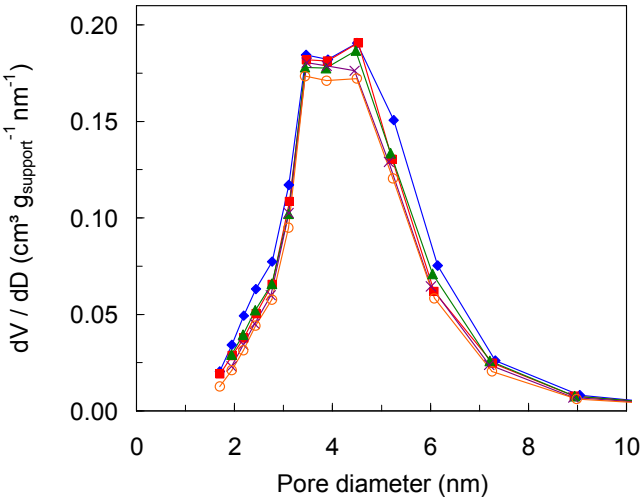

Figure II-3: Pore size distribution of (♦) the support (■) AA4500, (▲) AA8500, (×) AA11500 and (○) AA15500.[3]

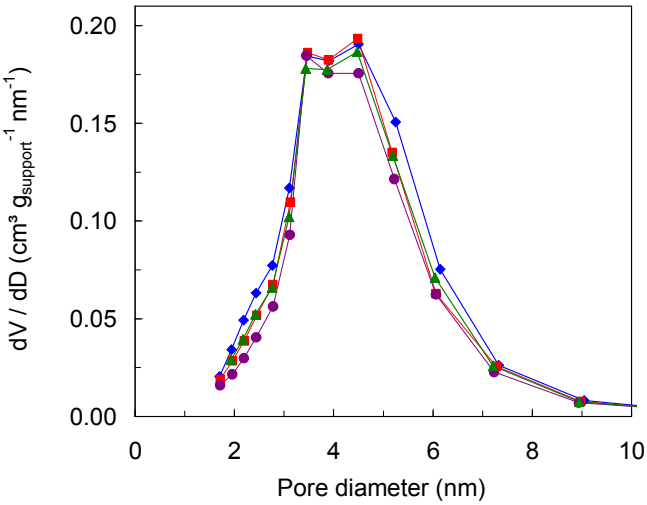

Figure II-4: Pore size distribution of (♦) the support (■) AA8300, (●) AA8400 and (▲) AA8500.

[3] If the classical pore size distribution curves are drawn (adsorption data normalized by the total mass of the sample analyzed), a systematic downward shift of the curve (following the ordinate axis) is observed for each loading increment. Actually, this shift is simply due to the addition of an increasing mass of MoO_3 which is not porous. As the porosity of the sample originates solely from the support, adsorption data have here been normalized by the mass of support.

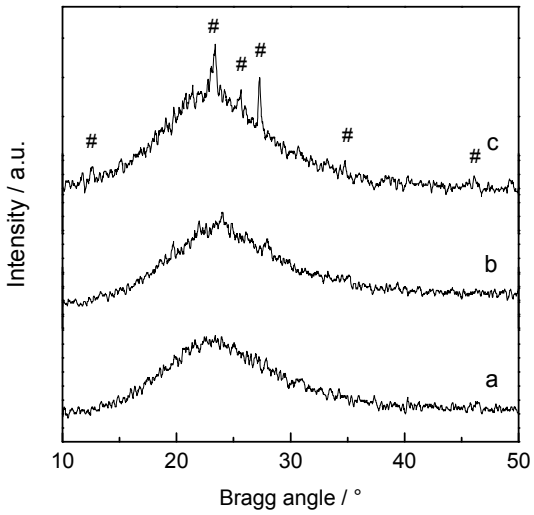

Figure II-5: XRD patterns of 8% MoO_3/SiO_2-Al_2O_3 catalysts prepared by wet impregnation of an ammonium heptamolybdate and calcined at (a) 300 °C, (b) 400 °C and (c) 500 °C. The crystallographic planes of orthorhombic MoO_3 are detected at 12.8 ° (020), 23.3 ° (110), 25.7 ° (040), 27.3 ° (021), 33.7 ° (111) and 46.3 ° (210) and are marked with # symbols (JCPDS 05-0508).

Transmission electron microscopy confirms the presence of bulky MoO_3 crystals in the samples with high loading and calcined at high temperature. The most evident case of AA15500 is presented in Figure II-7 and compared to the bare support. The support is made of irregular porous particles (Figure II-7a). In the catalyst, the same type of particles is detected along with aggregates of crystalline particles in some places (Figure II-7b, c and d). The size of these particles is in the order of 20-60 nm, thus consistent with the XRD evaluation.

Raman spectroscopy was also tentatively used to identify the nature of Mo oxide species present in the catalysts. It was found that the support itself gives a strong background signal, most probably due to fluorescence created by defects and impurities in the support (Figure II-8).

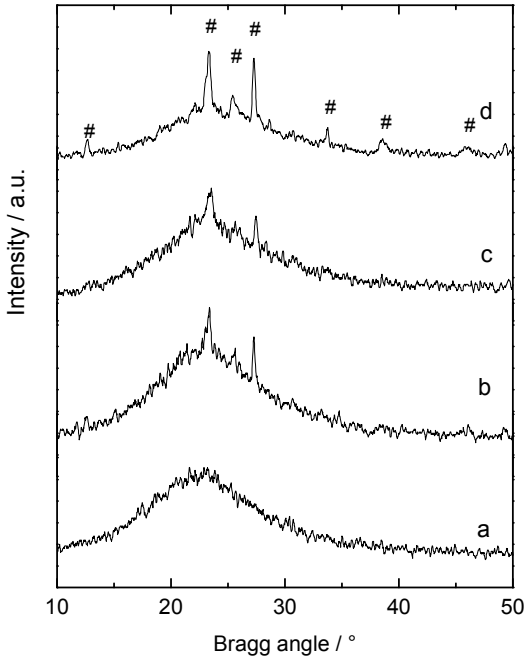

Figure II-6: XRD patterns of MoO_3/SiO_2-Al_2O_3 catalysts prepared by wet impregnation of an ammonium heptamolybdate solution and calcined at 500 °C: (a) AA4500, (b) AA8500, (c) AA11500 and (d) AA15500. # symbols indicate the diffraction lines of orthorhombic MoO_3 (JCPDS 05-0508).

In some spectra, only a broad band is found around ca. 950 cm^{-1}. This signal is attributed to surface polymolybdates [162]. In other spectra, sharper lines at 995 and 819 cm^{-1} were also detected, as clear evidence of the presence of MoO_3 crystals [162]. AAxY samples were thus found to be quite heterogeneous in terms of Mo species detected by Raman spectroscopy (Figure II-8). This must be correlated to the fact that the MoO_3 crystals form aggregates and are not homogeneously dispersed in the solid, while the area analyzed by the confocal tool is small. In fact, the signals of crystalline Mo oxide were only detected on samples that yielded MoO_3 diffraction patterns in XRD. Despite many attempts, it was not possible to establish a reproducible method for analyzing AAxY samples by Raman spectroscopy. The main conclusion that can be drawn from these experiments however, is that Raman spectroscopy confirms XRD analysis: signals related to the presence of MoO_3 crystals were detected on the catalysts that were calcined

at relatively high temperature (AA8400 and AA8500) and on catalysts with relatively high loading (AA11500 and AA15500), but never on the other samples.

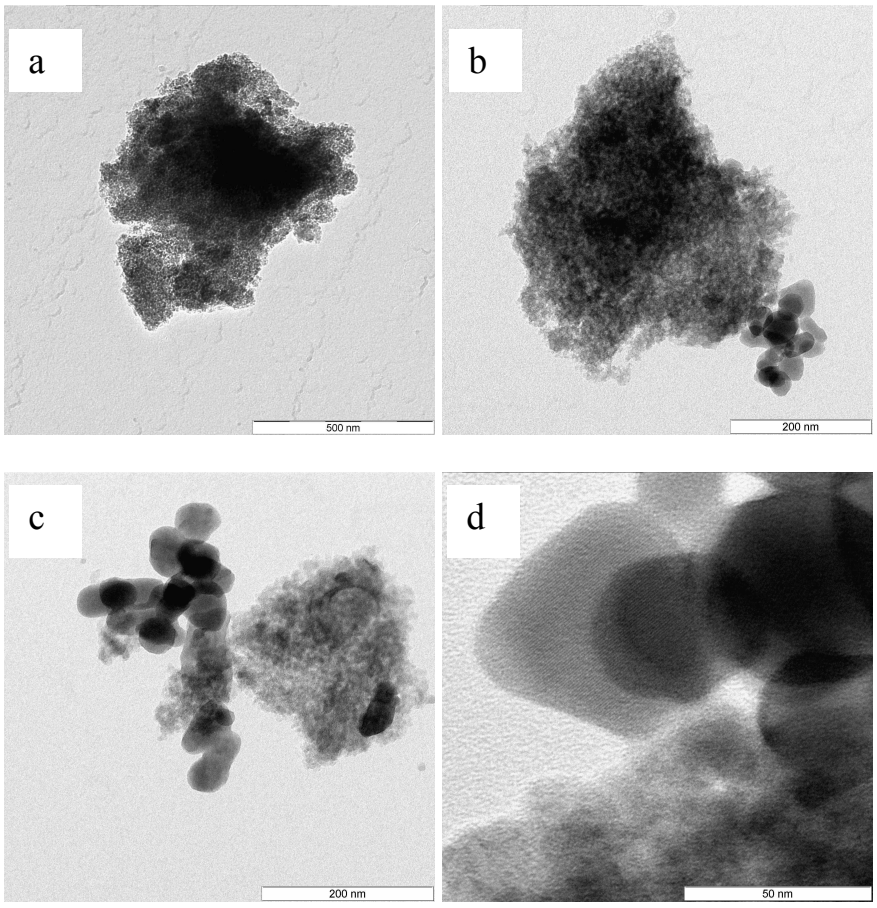

Figure II-7: TEM micrographs of the support (a) and of the AA15500 sample (b, c and d).

The ^{27}Al MAS-NMR spectrum of the bare support is composed of three bands around 2, 30 and 54 ppm (Figure II-9). This spectrum closely resembles the one reported by May et al. [163] concerning a silica-alumina prepared by the sol-gel method with aluminium isopropoxide and tetraethoxysilane as precursors (13 wt. % Al_2O_3). The signal around 54 ppm is attributed to tetrahedrally coordinated framework Al atoms (Al_{TET})

typically found in silico-aluminic materials [164]. This coordination corresponds to Al atoms isomorphously substituting Si^{4+} in silica [165-167] or to a "transition alumina phase" that may form following segregation of phases during the preparation (and singularly during calcination) [168-169]. It is often referred to as the "framework tetrahedral species" [170]. The signal at about 2 ppm corresponds to Al octahedrally coordinated (Al_{OCT}). It is attributed either to γ-Al_2O_3 [168-169] or to an amorphous polymeric aluminium oxide phase [171]. The intermediate band at 30 ppm is often contradictorily attributed to distorted tetrahedral Al shifted by a strong quadrupolar interaction [172-173] or to five-fold coordinated Al species (Al_{PEN}) [174-176]. Recent studies on amorphous silica-alumina systems and based on multiple quantum MAS-NMR measurements (that can distinguish between these two coordination states by separating the quadrupolar and chemical effects on the chemical shifts) unambiguously showed that this signal is attributable to five-coordinated Al atoms [164, 170]. In silica-aluminas, this coordination was assigned to the interface between an alumina-type phase and a truly mixed silica-alumina phase [177].

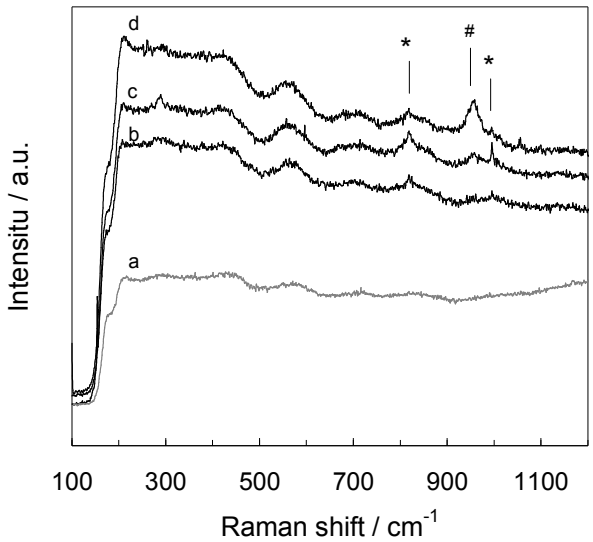

Figure II-8: Raman spectra of (a) the support and of the AA8500 sample at three different positions (noted b, c and d) on the sample. The "*" marks indicate the Raman signals of MoO_3 crystals and the "#" mark indicate the broad band related o polymolybdates .

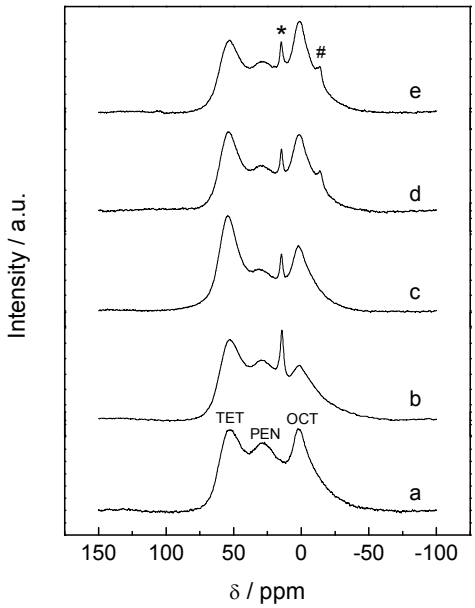

Figure II-9: ^{27}Al MAS-NMR spectra of (a) the support, (b) AA8 uncalcined (c) AA8300, (d) AA8400 and (e) AA8500. The Al_{TET}, Al_{PEN} and Al_{OCT} broad signals are indicated on the first spectrum. [$AlMo_6$] and $Al_2(MoO_4)_3$ are marked with "*" and "#"respectively.

The introduction of Mo by wet impregnation of AHM modifies the ^{27}Al MAS-NMR fingerprint of the fresh support. In the uncalcined catalyst the Al_{OCT} component is significantly reduced. The Al_{PEN} signal also decreases slightly in intensity. Additionally, one sharp signal arises at 15 ppm. Several authors attribute this band to a hydrated form of $Al_2(MoO_4)_3$ [85, 178] while others attribute it to the Anderson-type heteropolyanion $[Al(OH)_6Mo_6O_{18}]^{3-}$ [179-180]. The calcination step again perturbs the ^{27}Al MAS-NMR spectra of the samples. The signal at 15 ppm decreases and, when the calcination temperature is 400 °C or higher, a peak at - 14 ppm appears, which is broadly accepted to account for $Al_2(MoO_4)_3$ (non-hydrated) [85, 178]. The Al_{OCT} contribution (at ca. 2 ppm) increases back after calcination. The intensity of this signal increases with the calcination temperature. Finally, let us note that the intensity of the signal at 15 ppm does not depend on the calcination temperature changes.

When the calcination temperature is kept at 500 °C and the MoO_3 loading is varied (Figure II-10), the proportions of Al_{TET}, Al_{OCT} and Al_{PEN} do

not change noticeably. On the other hand, the intensity of the signals due to the aluminium molybdate (at -14 ppm) phase increases obviously. This phase is barely detected at 4 % wt. loading but clearly increases at higher loading. The peak at 15 ppm is always present.

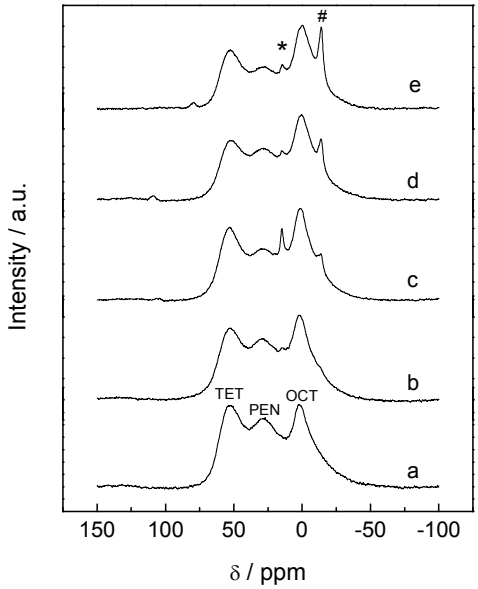

Figure II-10: ^{27}Al MAS-NMR spectra of (a) the support, (b) AA4500, (c) AA8500, (d) AA11500 and (e) AA15500. The Al_{TET}, Al_{PEN} and Al_{OCT} broad signals are indicated on the first spectrum. [$AlMo_6$] and $Al_2(MoO_4)_3$ are marked with "*" and "#"respectively.

The amount of Mo detected at the surface of the catalyst in XPS is obviously dependent on the loading: for the series of catalysts calcined at 500 °C a linear relationship is observed between the bulk and the surface Mo / (Si+Al) atomic ratios. Interestingly, the calcination temperature also has a drastic effect (Figure II-11). In particular, catalysts calcined at higher temperature exhibit a superficial Mo signal more intense than what would be expected in the case of a totally homogeneous solid.

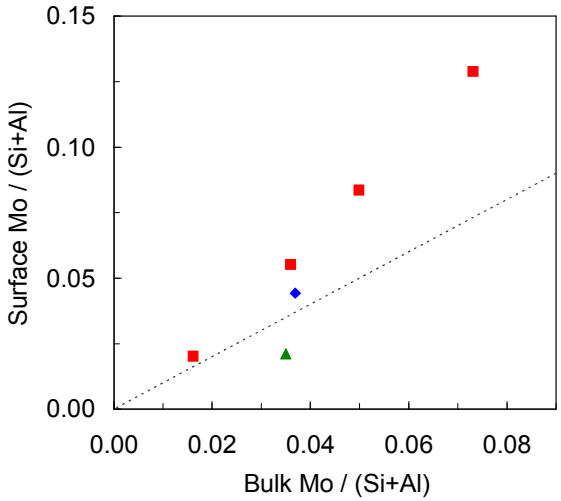

Figure II-11: Mo / (Si+Al) atomic ratio determined from XPS as a function of the bulk Mo / (Si+Al) ratio for (▲) AA8300 (♦) AA8400 and (■) AAx500. The dotted line represents the value expected for totally homogeneous samples (same amount of Mo at the surface and in the bulk). Note: the bulk ratios are calculated from the experimental compostion determined by ICP-AES.

For the series of samples with 8 % MoO_3 weight loading and calcined at different temperatures a window of the XPS spectra around 400 eV has been recorded specifically to track the presence of nitrogen (Figure II-12). In this range of binding energies, the N 1s peak falls close to the Mo $3p_{3/2}$ peak. It was found that nitrogen – originating from the ammonium heptamolybdate precursor – is still detected on these calcined catalysts. This is particularly true for the catalyst calcined at lower temperature. Visibly, the intensity of the N 1s peaks decreases with increasing temperature. In ammonium heptamolybdate ($(NH_4)_6Mo_7O_{24}.4H_2O$) there are 6 atoms of nitrogen for 7 atoms of Mo, meaning that the expected N / Mo atomic ratio is 0.86. Experimentally, a ratio of 0.82 was found by analysing pure AHM in XPS. The same ratio calculated from the quantification of N and Mo in the AA8 samples equals 1.24, 0.79 and 0.25 respectively for AA8300, AA8400 and AA8500. For a sample that was prepared by impregnation and then dried but not calcined, this ratio was measured to be 1.79. In other words, the wet impregnation clearly tends to provoke a relative increase in the proportion of

N at the surface of the catalyst and the calcination temperature has a marked impact on the removal of the ammonium species.

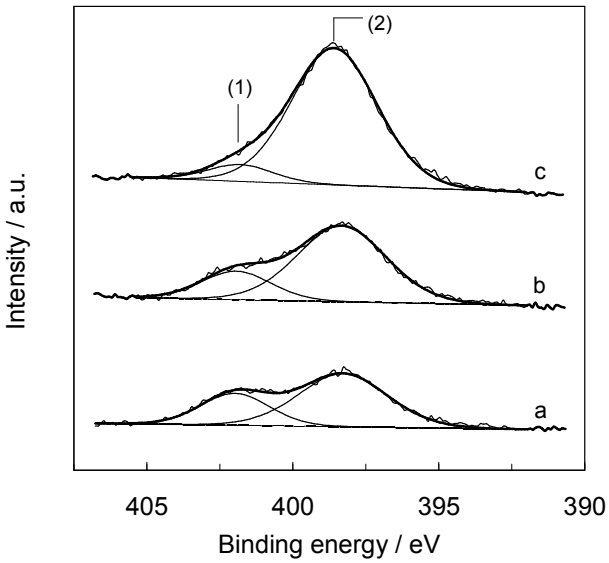

Figure II-12: Part of the XPS spectra of (a) AA8300, (b) AA8400 and (c) AA8500. The mark (1) indicates the N 1s contribution and the mark (2) indicates the Mo $3p_{3/2}$ contribution.

3.2. Activity measurements

The evolution of the specific activity for propene metathesis of the catalysts with time-on-stream is shown in Figure II-13. All catalysts exhibited a short latency stage followed by a maximum of activity after about 20 minutes. Then a slow deactivation takes place. As all catalysts follow approximately the same trend (except AA4500 which deactivates slightly slower) it was decided to compare the catalysts in terms of "maximum specific activity". This parameter was arbitrarily defined as the average of activity measured at 14, 22 and 30 minutes. This is the period where the activity of the catalysts is the most stable. It is plotted in Figure II-14 to allow the direct comparison of the catalysts.

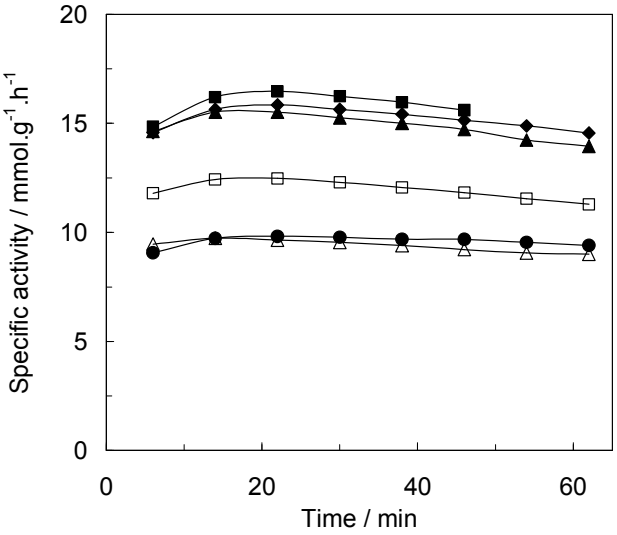

Figure II-13: Evolution of the specific activity with time-on-stream during one hour of catalytic test with (●) AA4500, (Δ) AA8300, (□) AA8400, (♦) AA8500, (▲) AA11500 and (■) AA15500 (Note: a technical problem interrupted the experiment after 46 minutes for the AA15500 sample). Specific activity is expressed in terms of mmol of propene converted to metathesis products per gram of catalyst and per hour.

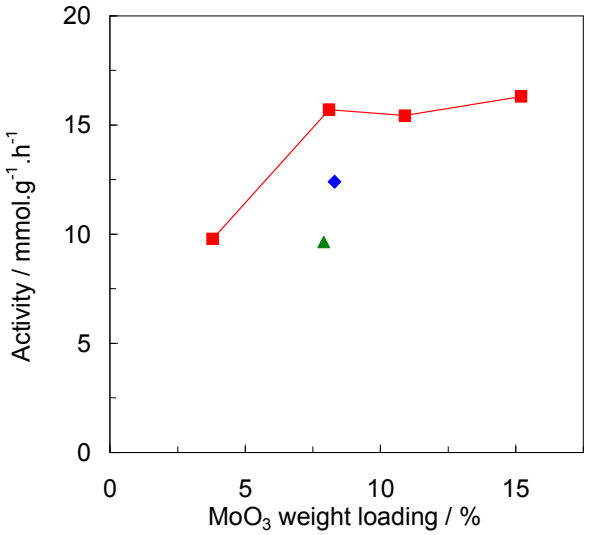

Figure II-14: Maximum specific activity obtained with (▲) AA8300 (♦) AA8400 and (■) AAx500 as a function of the MoO_3 weight loading.

It appears clearly that increasing the calcination temperature leads to increased catalytic performances, even though MoO_3 crystals form. Comparing the catalysts calcined at 500 °C, Figure II-14 shows that the activity first increases significantly when the loading is raised from 4 to 8 %. Further increase in the MoO_3 loading does not provoke any significant increase in the performances.

4. DISCUSSION

4.1. Interaction of Mo with the support

The interaction between Mo species and the support during the impregnation step deserves being addressed, before discussing the two parameters that were systematically studied in this chapter. Indeed, the inorganic support onto which the active phase is deposited is sometimes visualized as an inert component of the catalyst having mainly a physical role of carrier of the active phase. Nevertheless, several works (for example from the groups of Weckhuysen [98, 181], Che [179, 182], etc.) have demonstrated that oxomolybdenum species interact strongly with an alumina support. It was explained for example that the electrostatic interaction between the heptamolybdate anions in solution and the surface of the support favours a preferential adsorption of Mo at the external surface of the particles of the support [98]. Such uneven distribution of the Mo phase could be observed here also, even if the support is a silica-alumina with high proportion of silica. Chapter 1 showed that the composition of the support has a marked impact on the catalytic behaviour of the active component. More precisely, the presence of alumina in the support was decisive. Here, some results indicate that the support is actually reacting chemically with the Mo precursor and interacts strongly with the active phase of the catalyst. Such interaction should thus be considered.

The ^{27}Al MAS-NMR investigations showed that the environment of Al atoms changed after impregnation with ammonium heptamolybdate. As mentioned in the result part, the attribution of the peak at 15 ppm is a matter of debate. In fact many researchers attribute this signal to a “hydrated form of aluminium molybdate”. It is indeed usually detected along with the peak

at -14 ppm (related to the $Al_2(MoO_4)_3$ phase) in proportions that depend on the hydration of the sample. Bao et al. have extensively reported the occurrence of this signal in Mo/HBeta-Al_2O_3 metathesis catalysts and have even correlated the build up of the aluminium molybdate (hydrated and non-hydrated forms) with a decrease in the metathesis activity of their catalysts [86-87]. Their attribution relies on the work of Edwards and Decanio [183] who provided the tentative formula $[Al(OH)_n(H_2O)_{6-n}]_n(MoO_4)$ with n= 1 or 2.

In the late 1990 however, Carrier et al. described the interaction of AHM with alumina during the preparation of MoO_3/Al_2O_3 catalysts and proposed a more precise attribution of the peak at 15 ppm [179]. This work demonstrated the formation of an Anderson-type heteropolymolybdate $[Al(OH)_6Mo_6O_{18}]^{3-}$ during the impregnation step. This species (abbreviated to $[AlMo_6]$) forms during the impregnation step by complexation of dissolved Al^{3+} cations with oxomolybdenum species in solution. $[AlMo_6]$ gives a sharp NMR signal at 15 ppm. It was also observed by Plazenet et al. in the preparation of zeolite-supported MoO_3 catalysts [184]. A debate followed, because the result implied that many reported works had to be re-interpreted in some ways [185-187]. In fact the calcination of $[AlMo_6]$ yields both MoO_3 and $Al_2(MoO_4)_3$ following the decomposition reaction (1) and the rehydration of such calcined catalyst can lead to the partial reconversion of $Al_2(MoO_4)_3$ to $[Al(OH)_6Mo_6O_{18}]^{3-}$ following equation (2) [187]. Nowadays, such Al NMR peak at ca. 15 ppm is more frequently attributed to the presence of the $[AlMo_6]$ species [180, 188-189] even though some groups continue to consider simply a “hydrated form of aluminium molybdate” [190].

$$2\ H_3[Al(OH)_6Mo_6O_{18}] \rightarrow 9\ MoO_3 + Al_2(MoO_4)_3 + 9\ H_2O \qquad (1)$$

$$2\ Al_2(MoO_4)_3 + 24\ H_2O \rightarrow [Al(OH)_6Mo_6O_{18}]^{3-} + 3\ [Al(H_2O)_6]^{3+} + 6\ OH^- \qquad (2)$$

In any case, NMR results show that the impregnation of the silica-alumina support with ammonium heptamolybdate implies strong interactions between Mo species and Al atoms from the support. The interaction is strong enough to extract Al atoms from their initial environment, to form a new compound. Calcination then affects again the nature and proportions of Mo species at the surface of the catalyst.

4.2. Effect of the calcination temperature

4.2.1. Nature of Mo species

The thermal treatment influenced markedly the crystallinity of the 8 % loaded catalysts. Higher calcination temperature obviously favoured sintering of the MoO_3 phase to form crystals. Note that the small diffraction lines on the 8 % loaded catalyst calcined at 400 °C correspond well to those detected on similar samples – prepared on non-commercial supports of similar composition – in Chapter 1. As far as Raman measurements are concerned, the formation of MoO_3 crystals is also confirmed for the catalysts calcined at higher temperature. It must be stressed that the relative band intensities for MoO_3 and for polymolybdates do not reflect the relative amount of each species. The high Raman cross-section of MoO_3 makes this species a strong Raman scatterer [191], so the concomitant presence of the broad signal at ca. 950 cm^{-1} and at 819 and 995 cm^{-1} probably reveals a small proportion of crystals as compared to the amorphous polymeric species. Finally, TEM micrographs unambiguously evidence the formation of MoO_3 crystals aggregates at the outer surface of the support particles.

The main observation made from ^{27}Al MAS-NMR measurements is that an aluminium polymolybdate phase ($[AlMo_6]$ or hexamolybdoaluminate) appears after impregnation of AHM. Calcination provokes the partial conversion of this phase to an aluminium molybdate phase ($Al_2(MoO_4)_3$) (detected in NMR at -14 ppm) and to crystalline MoO_3 (detected in XRD, Raman and TEM). At first sight, XRD diffractograms do not totally rule out the presence of crystalline $Al_2(MoO_4)_3$ since the main diffraction line of this phase (23.4° following JCPDS 20-0034) falls very close to one of the main diffraction line of MoO_3 (23.3°). However, the other

smaller peaks of $Al_2(MoO_4)_3$ are not detected (26.3 °, 22.2 °, 21.0 °, 28.1 °, etc.). In addition, the presence of the other minor diffraction lines related to MoO_3 (12.7 °, 33.7 °, 39.0 °, etc.) and their relative intensities attest that only MoO_3 is detected. Accordingly, the aluminium molybdate phase is either amorphous or present in the form of very small crystallites. The [$AlMo_6$] phase is not detected in XRD on calcined catalysts either (a reference spectra is published in ref [191]).

4.2.2. Location of the Mo phase

The Mo / (Si+Al) atomic ratio is sometimes used as an indication of the spreading of Mo onto a silica-alumina surface. Indeed, when Mo atoms are dispersed over the support and cover Si and Al atoms, the ratio is supposed to increase. Conversely, if Mo atoms are poorly dispersed, Si and Al atoms are detected with a high intensity and the ratio should remain low. Here, the Mo / (Si+Al) ratio was appreciably higher as the catalysts were treated at higher temperature. At first glance, this observation is not in line with the detection of MoO_3 crystals that build up as the calcination temperature increases. Indeed, in the presence of bulky crystals, part of the Mo atoms are presumably not detected by XPS and the support is supposed to be covered to a lesser extend. As a result, the Mo / (Si+Al) ratio might be expected to be lower for the samples that contain crystals.

However, one should not forget that the support used in this study is highly porous. In fact, the high Mo / (Si+Al) ratio can simply be explained by the fact that the Mo phase builds up at the outer surface of the support particles. Indeed, the textural properties of the support are not significantly affected by the impregnation. Only a limited decrease in the raw pore volume is observed for the AA8 catalysts as compared to the bare support (Table II-1). The pore size distributions (Figure II-4) and the mean pore diameters (Table II-1) are not affected. These observations indicate that the MoO_3 deposit is rather located at the external surface of the support particles and does not fill the interior of the pores. In addition, in the samples that contain MoO_3 crystals, the estimation of their size via the Debye-Scherrer equation supports the idea that the MoO_3 crystals are located at the outer surface of the support particles. Indeed, the average crystal size (35-40 nm)

is much higher than the average pore size (ca. 5 nm), implying that such crystals could not be accommodated inside the porosity of the support. So, as MoO_3 crystals form at the outer surface of the support particles and not inside the pores, the Mo surface concentration detected by XPS is high.

It is well-known that the wetting of the support by Mo oxide is promoted by high temperature treatments. So two opposite phenomena take place during calcination: (i) Sintering to bulky MoO_3 crystals at the outer surface of the particles (when the temperature, the Mo surface density and the number of nucleation points are high) and (ii) Spreading of Mo atoms on the whole available support surface (potentially including the interior of the pores). The Mo deposit that forms on the support after evaporation of water is likely poorly dispersed; due to the interaction of heptamolybdate ions with the external surface of the support (see section 4.1.). This agglomerated but amorphous phase – formed by adsorbed heptamolybdate species and $[AlMo_6]$ – appears to be only weakly perturbed by calcination at 300 °C. Treatments at higher temperature on the other hand change the morphology of the deposit. During that process, part of the Mo atoms would crystallize into bulk MoO_3 or convert into $Al_2(MoO_4)_3$. The other Mo atoms (presumably those that are not included in $[AlMo_6]$ or those that are not enough agglomerated to nucleate and sinter into MoO_3 crystals) could be dispersed at the surface of the support under the effect of temperature.

4.2.3. Correlation with metathesis activity

Overall, increasing the calcination temperature led to a marked increase in catalytic activity. This crucial effect of calcination temperature may appear surprising considering the activation step at 550 °C under nitrogen that all catalysts undergo before being tested. While this activation could have been expected to level off the properties of similar catalysts, our results show that the "preparation history" of the catalysts is crucial.

As discussed above, higher calcination temperature led to higher proportion of crystalline MoO_3. The higher activity of the catalysts treated at higher temperature thus appears in contradiction with reports that indicate the inactivity of crystalline MoO_3 in the metathesis reaction [88, 96]. However, only crystalline MoO_3 is detected in XRD. With this technique,

the quantitative description of amorphous species (which presumably yield active centres) is impossible unlike the study of crystals (which are supposed to be inactive). Also, it should be recalled that only a very small fraction of the Mo atoms present in the catalyst are thought to turn into active centres [71]. So, even if the tendency of Mo atoms to form crystals clearly increases when the calcination temperature is raised, it may be put forward that the nature and proportion of remaining amorphous species are also affected by the calcination temperature, thereby influencing also the activity of the catalysts.

Another impact that the calcination temperature might have on the amorphous Mo species is linked to the chemical environment of the Mo atoms. The environment of Al atoms as studied by MAS-NMR indirectly gives indications on the interaction of these atoms with Mo atoms. It seems that mainly Al_{OCT} and Al_{PEN} atoms are extracted from their natural position in the silica-alumina and participate in the interaction with Mo. However, the calcination step decreases the interaction between Al and Mo species. The calcination at 300 °C provoked the quasi-restoration of each species. In other words, the environment of most Al atoms in the calcined catalysts is not very different from their environment in the fresh support. Nevertheless, some Al atoms are involved in aluminium-molybdenum phases. Calcining the catalyst at higher temperature provokes the conversion of part of the $[AlMo_6]$ phase into aluminium molybdate. Note that even if this correlation between the calcination temperature and the extent of the conversion from $[AlMo_6]$ to $Al_2(MoO_4)_3$ appears logical, conclusions about the hydrated to non-hydrated forms of aluminium-molybdenum phases should be drawn with much care. Indeed, the catalysts were mostly stored in a desiccator but also frequently manipulated under ambient condition. No particular treatment was applied on the catalysts before MAS-NMR analysis to control their humidity content. Such aluminium molybdate phases were reported to be inactive for the metathesis reaction [85-87].

It was shown (Figure II-12) that the removal of ammonium moieties is not completed after the two hours of calcination. At low calcination temperature the amount of remaining N is high. On the 300 °C-treated sample, the N / Mo atomic ratio is even higher than for pure AHM. This can

be explained by the strong interaction between the $Mo_7O_{24}^{6-}$ species and surface of the support [98]: during the impregnation, the Mo clusters are first fixed on the support, while the counter cations are still in the impregnation solution. Ammonium ions are subsequently deposited on top of the Mo deposit at the end of the evaporation step. This coverage might be the cause of the lower activity of the samples calcined at low temperature. In addition, if the cation of the precursor salt was preserved after calcination, part of the Mo introduced in the preparation is likely preserved in its initial cluster form as well ($Mo_7O_{24}^{6-}$). Mo atoms included in heptamolybdate clusters are most probably inactive. From Chapter 1, it is known indeed that the interaction of the Mo moieties with the support is crucial. Very likely, an intimate interaction (maybe chemical bonds) between Mo and Si and Al atoms is necessary. Mo atoms included in the heptamolybdate cluster and not in direct contact with the support do not fulfil this condition.

4.3. Effect of the MoO_3 loading

4.3.1. Nature of Mo species

When the thermal treatment was kept constant, a clear increase in the intensity of the crystalline MoO_3 diffraction lines was observed with increasing loading. This suggests that the proportion Mo atoms involved in crystals is rising when the MoO_3 loading increases. In parallel, the proportion of Mo detected in XPS increases in a linear fashion (Figure II-11). Also, regardless of the Mo loading, the porosity of the support was not significantly affected. These observations indicate that the MoO_3 crystals build up at the outer surface of the support. The environment of Al atoms appears only slightly affected by changes in the MoO_3 loading. The main modification concerns the signal of the aluminium molybdate phase which increases with increasing loading.

4.3.2. Correlation with metathesis activity

A levelling off in the performances of the catalysts was observed above 8 wt. % MoO_3 loading (Figure II-14). This loading corresponds to the appearance of MoO_3 crystals in XRD (Figure II-6). The $Al_2(MoO_4)_3$ phase

also builds up noticeably when the loading is increased above 8 wt. % of MoO_3 (Figure II-10). Such plateau in the relationship between loading and activity is classically observed with supported MoO_3 catalysts [9, 113, 192]. Also, in a preliminary phase of the present study, AAx400 catalysts with loading between 4 and 18 wt. % have been tested in the metathesis of propene at 40 °C (Figure II-15). The activity of the AA8400 sample is very close to the result presented above (Figure II-14). As the catalytic installation and some details of the activation procedure were different, direct comparison of these results with the results presented throughout the present document is delicate. Nevertheless, as published in reference [64], exactly the same kind of loading-activity relationship was found. The activity first increased when the loading increases from 4 to 8 wt. % MoO_3 loading and then a plateau is reached.

Our interpretation is that the number of dispersed – potentially active – species does not increase when the loading is increased above 8 % because most additional Mo atoms join either the inactive MoO_3 crystals or aluminium molybdate phase. At this stage it is not possible to discriminate which of these species has the most decisive responsibility in limiting the performances of the MoO_3/SiO_2-Al_2O_3 catalysts.

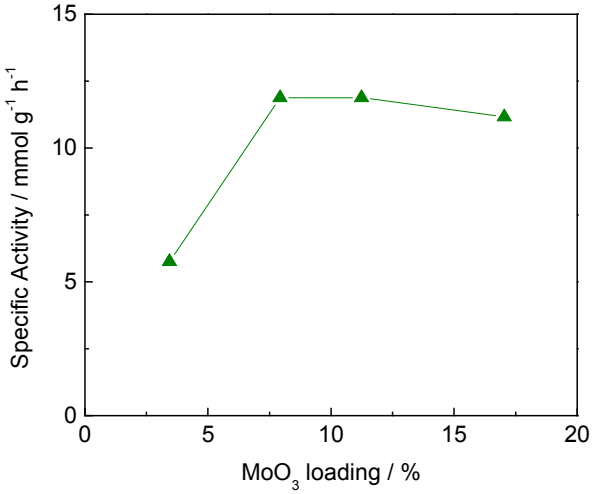

Figure II-15: Maximum pecific activity of AAx400 samples in the self-metathesis of propene at 40 °C, after activation under He at 550 °C. Data reproduced from [64].

5. CONCLUSION

This chapter highlighted the impact of two important parameters in the preparation of a MoO_3/SiO_2-Al_2O_3 catalyst by wet impregnation of ammonium heptamolybdate: the calcination temperature and the loading. These two parameters influence markedly the proportions of the different Mo species detected in the catalysts, as depicted in Scheme II-1. This study also showed that the support interacts with Mo species in solution during the impregnation step. In fact a hexamolybdoaluminate phase is formed after impregnation. This species is partially converted upon calcination to MoO_3 crystals and $Al_2(MoO_4)_3$. Raman spectroscopy shows also that part of the Mo phase is preserved as amorphous surface polymolybdate.

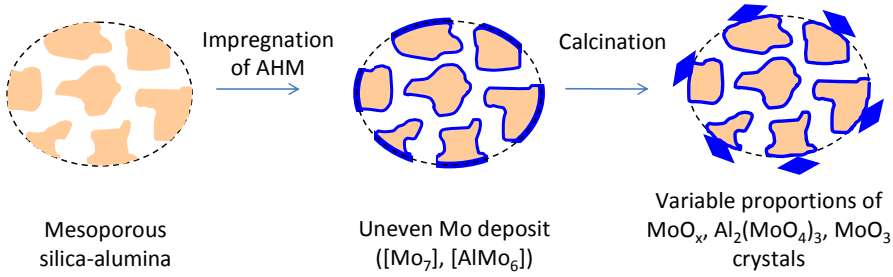

Scheme II-1: Schematic representation of the preparation of MoO_3/SiO_2-Al_2O_3 catalysts via the wet impregnation of AHM and subsequent calcination.

It was shown that the calcination temperature has a marked impact on the activity of the catalysts: samples treated at 500 °C perform better than catalysts treated at 400 °C, themselves being more active than those treated at 300 °C. After calcination at higher temperatures, the amount of Mo oxide at the surface of the support appeared higher (XPS), which is correlated to the build up of MoO_3 crystals at the outer surface of the support. It is suggested that the dispersion of the remaining amorphous species is affected (beneficially) by high calcination temperature. The decomposition of the precursor salt is also more readily achieved. One interesting strategy that might be investigated in a future project is to increase the duration of the thermal treatment. If the complete conversion of the ammonium

heptamolybdate deposit into molybdenum oxide in strong interaction with the support is important, then increasing the duration of the calcination might have a positive impact.

Increasing the MoO_3 loading from 4 to 8 wt. % increases the metathesis activity of the catalyst. Above 8 % however, inactive MoO_3 crystals and an $Al_2(MoO_4)_3$ phase build up preferentially and the performance of the catalyst levels off. As a conclusion, for this kind of systems prepared through the most classical approach of wet impregnation with ammonium heptamolybdate, overloading should be avoided. Ca. 8 % is identified as a limit above which further increase in the loading is useless. Strategies for improving the performances of MoO_3/SiO_2-Al_2O_3 catalysts should be based on the search for better spreading of the active phase on the whole available support surface (including the pores). Impeding the formation of the $[AlMo_6]$ heteropolyanion during impregnation also appears to be a relevant approach because this species was shown to convert into inactive MoO_3 crystals and aluminium molybdate.

INTERMEDIATE CONCLUSION FOR PART I

This first part has investigated the effect of the composition of the metathesis catalysts, and several parameters of their preparation. A first systematic investigation on the effect of Al in MoO_3/SiO_2-Al_2O_3 was presented in Chapter 1. It highlighted the crucial role of Al in creating acidity in the support. This acidity dictates the acidity of the catalysts obtained after deposition of MoO_3 by wet impregnation of the support. Finally, the metathesis activity correlates well with the acidic properties of the catalysts. Comparing the performances of the catalysts in the metathesis of propene and in its selective oxidation, it was explained that the substitution of Al for Si atoms in the support has opposite effects in these two different reactions. The presence of Al induces a stronger interaction between the olefin and the catalyst. This is deleterious for the partial oxidation reaction but crucial for activating the metathesis reaction. Overall, it is evident from this first part that catalysts based on silica-alumina should be preferred to silica-based formulations for the metathesis of light alkenes.

The second chapter examined the classical wet impregnation of ammonium heptamolybdate on a commercial silica-alumina. After having identified the importance of the calcination step, and the better performances of 500 °C-treated samples as compared to samples treated at lower temperature, the effect of the MoO_3 loading was investigated. It appeared clearly that overloading should be avoided since above ~8 wt. % in MoO_3 the performances of the catalysts level off. This limitation can be correlated with the appearance of significant amounts of crystalline MoO_3 and of $Al_2(MoO_4)_3$. Overall the performances of such classical catalysts seem to be restricted to about ~16 $mmol.g^{1}.h^{-1}$. This threshold is in the same order as the best activities reported in previous studies. The value will be considered as a reference mark for further attempts presented in the following parts of the present work to improve the performances of MoO_3-based metathesis

catalysts. Two relevant strategies for increasing the activity of MoO_3-based metathesis catalysts can be suggested from the results of Chapter 2: improving the dispersion of Mo oxide and avoiding the formation of hexamolybdoaluminate during the impregnation.

Part II

On the modes of deposition of MoO_3 onto SiO_2-Al_2O_3

ABSTRACT

In Part I, the most classical wet impregnation with ammonium heptamolybdate was used as preparation method to assess the superior activity of silica-alumina-supported Mo oxide catalysts and to probe the impact of the MoO_3 loading and of the calcination temperature. In this part, alternative methods are used to deposit Mo oxide onto silica-alumina. In Chapter 3, two different Mo precursors are used in the wet impregnation of the support: a polyoxomolybdenum solution with oxalic acid and a molybdenum oxide hydrates solution. Using these alternative precursors, the formation of MoO_3 crystals and $Al_2(MoO_4)_3$ can be avoided which can result in improved metathesis activity. The effect of the loading and of the calcination temperature is also screened for these systems. In Chapter 4, a very easy preparation process is proposed: the simple thermal spreading of molybdenum oxide onto the support is shown to yield good metathesis catalysts.

CHAPTER 3:
PREPARING METATHESIS CATALYSTS VIA THE WET IMPREGNATION OF SILICA-ALUMINA WITH ALTERNATIVE PRECURSORS

ABSTRACT

This chapter explores the properties and metathesis activity of MoO_3/SiO_2-Al_2O_3 catalysts prepared by wet impregnation of a commercial silica-alumina with two Mo precursors that were chosen as alternatives to the classical ammonium heptamolybdate precursor. Using ammonium heptamolybdate with oxalic acid as an additive or starting from molybdenum oxide hydrates as precursors yield MoO_3 phases exhibiting particular properties and catalytic behaviours as compared to the reference catalysts presented in Chapter 2. The present chapter shows that this strategy can be relevant for reaching higher activity. When improved performances are reached, correlations can be established with (i) the better spreading of the Mo oxide phase and/or (ii) the low amount of aluminium molybdate formed.

1. INTRODUCTION

The first part, and more precisely Chapter 2, highlighted the intrinsic limitation of the catalysts prepared by wet impregnation of ammonium heptamolybdate on a commercial silica-alumina support. Namely, overloading should be avoided because above a given loading (ca. 8 wt. % MoO_3), additional Mo atoms tend to join inactive MoO_3 crystals or $Al_2(MoO_4)_3$ and the number of well-spread – potentially active – species does not increase. Bearing in mind this limitation, one relevant strategy is to try to improve the dispersion of the Mo oxide phase that forms at the surface of the support. This can be done in two ways: (i) changing the nature of the molybdate species that are transferred to the support during the impregnation and (ii) changing the nature of the chemical groups that must be removed during calcination in order to allow lower temperature treatment.

The dissolution of the ammonium heptamolybdate salt in water to form the impregnation solution leads to $Mo_7O_{24}^{6-}$ species in solution, in complex equilibrium with other species [98]. Once deposited onto the surface of the support, these 7-Mo atom clusters could be seen as potential nucleation points for the growth of MoO_3 crystals. In other words, it can be put forward that breaking the heptamolybdate cluster to form monomeric or at least smaller molybdate species in solution would lead to a better spreading of the MoO_3 phase created at the surface of the support. This better spreading could in turn inhibit the tendency of Mo atoms to agglomerate (sinter) and form MoO_3 crystals. This hypothesis led us to add oxalic acid in the heptamolybdate impregnation solution. Beltràn et al. indeed reported that molybdenum oxalate forms stable dimeric and monomeric complex species in aqueous solution [193]. Our strategy is also supported by earlier studies that showed how the addition of oxalic acid had a marked impact on the morphology of a MoO_3 phase formed at the surface of a silica powder [160] or at the surface of Si wafers [194]. It was suggested that the heptamolybdate cluster is broken and that oxalate ions stabilize smaller Mo complexes, which leads to a better spreading of the Mo species at the surface of the support. However, no evidence of the influence of oxalic acid on the Mo speciation was given. Also, the concept of tailoring the

morphology of the MoO_3 deposit was not valorised in catalytic reactions in these cases. Using complexing agents like oxalic acid, but also like citric acid, is often used to prepare Mo-based catalysts [154-155, 160, 181, 195-197]. In addition to a potential effect on the Mo speciation in the solution, such organic ligands will probably alter significantly the interaction between the support and the oxomolybdenum species. For example, while the heptamolybdate anion tends to interact strongly with the external surface of alumina extrudates, Weckhuysen et al. have successfully used citric acid as a complexing agent to decrease such strong interaction and ensure homogeneous distribution of the Mo phase inside the porosity of the carrier [98].

With the same aim of improving the dispersion of the Mo active phase, a second strategy was imagined. The idea is to use a Mo precursor which could presumably be decomposed at lower calcination temperature. Lower temperature treatment might satisfactorily reduce the tendency of the Mo oxide phase to sinter. The preparation of a "peroxopolymolybdate" solution was performed following the method of Kudo. This method involves the use of hydrogen peroxide to oxidize metallic Mo [198-199]. The species formed in solution can be described by the following general formula: $MoO_3.nH_2O.mH_2O_2$. Upon catalytic removal of the excess of peroxide species, the yellow solution is composed of molybdenum hydrates [200]. It was used for the impregnation of the silica-alumina support. The Mo speciation in solution is not clearly established but could of course be different from the situation encountered in AHM or AHM-oxalate solution. The group of Brégault highlighted the quality of this kind of precursors for the production of highly dispersed MoO_x by impregnation on silica [97, 201-202]. It is noteworthy that only water and possibley hydrogen peroxide moieties must be removed from the catalyst to obtain the desired MoO_3 phase. No ammonium moieties or organic ligands need to be thermally decomposed.

2. SUMMED UP EXPERIMENTAL

The catalysts were prepared by wet impregnation of ammonium heptamolybdate in the presence of oxalic acid ('Ox') or of molybdenum

oxide hydrates ('P'). They are denoted AOx*x* and AP*x*Y, where 'A' stands for the Aldrich commercial silica-alumina support, 'Ox' and 'P' are the precursor solution used, *x* is the MoO_3 weight loading (%) and Y is the calcination temperature. AOx*x* catalysts were all calcined at 400 °C, so the calcination temperature is not mentioned in the name of the samples. Details on the preparation are given in Experimental section, p. 25.

The catalysts were characterized by N_2-physisorption, XRD, XPS, Raman spectroscopy, ICP-AES and MAS-NMR, as described in the Experimental section (from p. 27).

In this chapter, an additional experiment was carried out on the impregnation juice. The latter is abbreviated "IJ" and defined as the impregnation solution at the end of the impregnation procedure. In this test, the wet impregnation procedures were repeated as described in p. 24 as to prepare one AA10, one AOx10 and one AP10 catalyst. At the end of the 2 h stirring step, the suspension was allowed to rest for exactly 10 min during which sedimentation of the solid at the bottom of the flask occurred. Then 1 ml of the liquid phase (IJ) was collected with a pipette and the amount of Mo, Si and Al in solution was analysed by ICP-AES. Also one blank impregnation was realized using water as impregnation solution and the impregnation juice was also analyzed after 2h stirring and 10 min rest.

3. AHM WITH OXALIC ACID

3.1. Results

3.1.1. Catalysts characterization

The initial precursor solution ("Ox") was obtained by dissolving AHM into water and adding oxalic acid as to have three moles of acid for one mole of Mo. The pH of this solution was 1.8. Figure III-1 shows the Raman spectrum of this impregnation solution. Two bands are detected, close to the usual signals of heptamolybdate, at 950 and 911 cm^{-1}.

Table III-1 includes the experimental MoO_3 weight loading and the textural properties of the AOx catalysts. The effect of the MoO_3 loading was studied for these catalysts in the 5-19 wt. % range. In general, the

experimental weight loading corresponds well to the nominal loading. These samples were all calcined at 400 °C. Analysis of their texture shows that the specific surface area roughly tends to decrease with increasing loading (Table III-1). So does the pore volume. The average pore diameter is significantly lower than in the support.

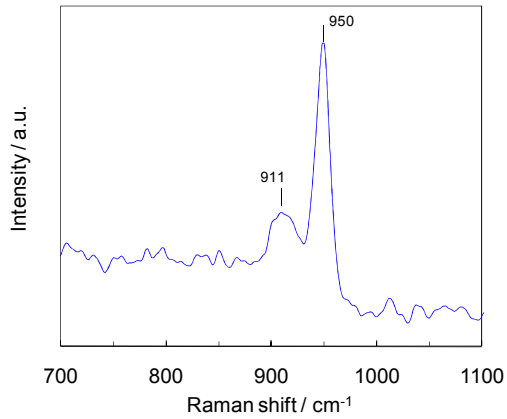

Figure III-1: FT Raman spectra of the "Ox" precursor solution (6.66 g of Mo.l^{-1}).

Table III-1: Textural properties (N_2-physisorption) and experimental MoO_3 weight loading (ICP-AES) of the AOx catalysts.

Name	Calcination temperature (°C)	MoO_3 loading (wt. %)	SSA (m^2 g^{-1})	Pore volume (ml g^{-1})	Pore diameter (nm)
A		-	490	0.71	5.8
AOx5	400	4.5	440	0.56	5.1
AOx10	400	9.6	470	0.51	4.3
AOx13	400	13.3	410	0.44	4.3
AOx19	400	19.2	310	0.37	4.7

Figure III-2 shows how the impregnation of the support with growing amount of MoO_3 using the AHM-oxalate precursor solution has affected the pore size distribution of the support. For all catalysts, the pore size distribution curve is significantly affected. A clear downward shift (with respect to the Y axis) is observed. This correlates with the marked decrease in the pore volume (Table III-1). Additionnaly, at high Mo loading, the

shape of the curve is affected. The amount of large mesopores decreases, while small pores around 2-3 nm come up.

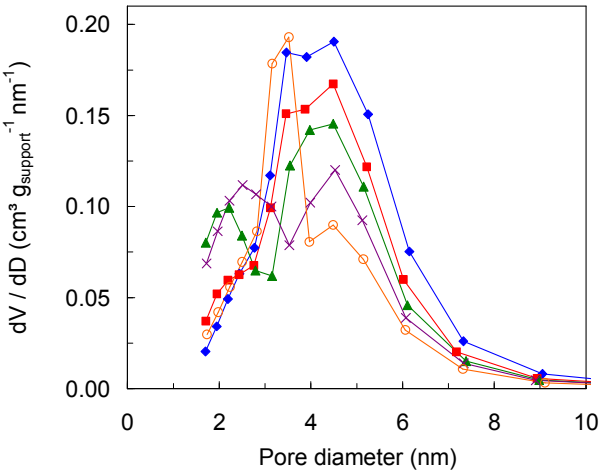

Figure III-2: Pore size distribution as measured by the BJH method on the desorption isotherms of (♦) the support, (■) AOx5, (▲) AOx10, (×) AOx13 and (○) AOx19.

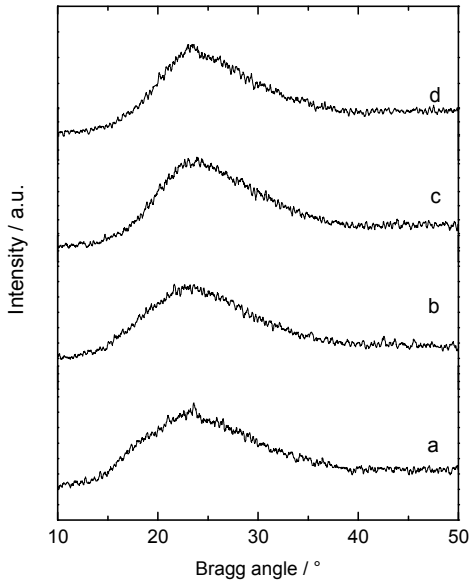

Figure III-3: XRD patterns of MoO_3/SiO_2-Al_2O_3 catalysts prepared by wet impregnation of a oxalate complex of Mo solution and calcined at 400 °C: (a) AOx5 (b) AOx10, (c) AOx13 and (d) AOx19.

X-ray diffraction analysis of the AOx samples reveals only the broad band related to the amorphous support (Figure III-3). Even at the highest MoO_3 loading, no crystals are detected.

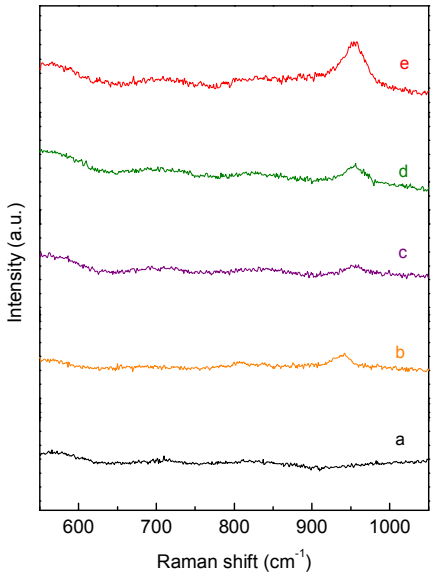

Figure III-4: Raman spectra of (a) the SiO_2-Al_2O_3 support, (b) AOx5, (c) AOx10, (d) AOx14 and (e) AOx19.

The detection limit of XRD for MoO_3 crystals lays around 5 nm-sized crystallites [99, 203]. Thus the fact that no diffraction line is detected only shows that bulk crystals, bigger than 5 nm are absent. In order to go further in the description of the MoO_x deposit in these catalysts, Raman spectroscopy was carried out (Figure III-4). As outlined in Chapter 2 (in link with Figure II-8), such analysis is delicate because of the intense background of the support. Here also, the signals related to MoO_x species were not recorded on each spectrum and the reported results are those for which the signal of interest was the most visible. No bands related to crystalline MoO_3 were detected, even though the sensitivity of Raman spectroscopy for crystalline MoO_3 species is very high. This confirms XRD analysis concerning the absence of MoO_3 crystals and goes further by demonstrating the absence of even small MoO_3 crystallites. Only one large band is detected around 950 cm^{-1}, attributed to the terminal ν(Mo=O) vibration of surface

polymolybdates [99, 162, 204-205]. This band increases with increasing MoO_3 loading. It is relatively broad, which can be taken as an indication of the good interaction between molybdenum oxide species and the support [99].

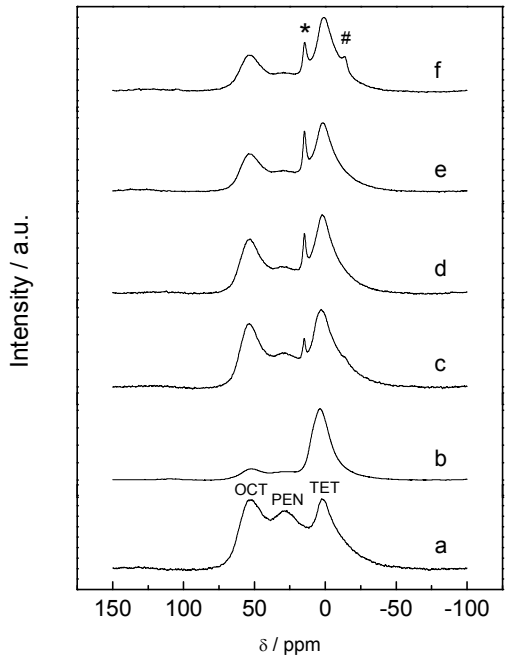

Figure III-5: ^{27}Al MAS-NMR spectra of (a) the support, (b) AOx10 dried but not calcined, (c) AOx5, (d) AOx10, (e) AOx13 and (f) AOx19. The Al_{TET}, Al_{PEN} and Al_{OCT} broad signals are indicated on the first spectrum. [$AlMo_6$] and $Al_2(MoO_4)_3$ are marked with "*" and "#"respectively.

The environment of the Al atoms present in the silica-alumina support is drastically affected by the impregnation with the 'Ox" solution (Figure III-5). In the 10 %-loaded sample, analysed by MAS-NMR after drying (uncalcined), the Al_{TET} and Al_{PEN} species disappear almost completely. Surprisingly, no band directly attributable to the interaction of extracted Al atoms with Mo is detected, unlike in the uncalcined AA8 catalyst for which [$AlMo_6$] was detected (Chapter 2, Figure II-9). After calcination at 400 °C, the Al_{TET} (ca. 54 ppm) signal is almost restored while

the Al_{PEN} (ca. 30 ppm) increases but remains lower than in the fresh support. [$AlMo_6$] is detected on calcined catalysts (15 ppm). In the catalyst with the highest loading (AOx19), a small peak at -14 ppm reveals also the presence of $Al_2(MoO_4)_3$.

At the surface of AOx catalysts, the amount of Mo tends to be lower than expected for a totally homogeneous solid (Figure III-6). The relationship between the surface and the bulk Mo / (Si+Al) ratios is not really linear.

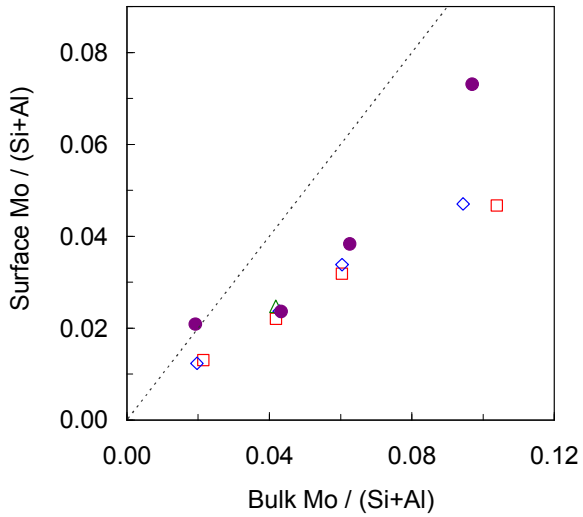

Figure III-6: Mo / (Si+Al) atomic ratio determined via XPS as a function of the bulk Mo / (Si+Al) ratio for (●) AOx, (Δ) AP10300, (□) APx400 and (◊) APx500. The dotted line represents the value expected for totally homogeneous samples (same amount of Mo at the surface and in the bulk). Note: the bulk ratios are calculated from the experimental compostion determined by ICP-AES.

To gain further insight on the phenomena that occur during the impregnation step, an ICP-AES analysis was conducted on the impregnation juice (see experimental section, p. 89). First, the Al/Si ratio was determined for the fresh support (solid sample). Then the blank impregnation juice was analyzed. As small particles of support remained in suspension when the liquid was sampled, Si and Al were detected in the liquid sample. As expected, the Al/Si ratio is close to the one of the solid (Figure III-7). In

contrast, stirring the silica-alumina support in the "Ox" impregnation solution provoked a marked increase in the Al/Si ratio found in the liquid phase. In other words, during impregnation, Al atoms are preferentially dissolved from the solid. Al atoms leach and join the liquid phase. For the purpose of comparison, the same experiment was realized on the impregnation juice obtained after impregnation with AHM. It is noticeable that such Al-enrichment of the liquid phase is also detected, although in a much lower extend.

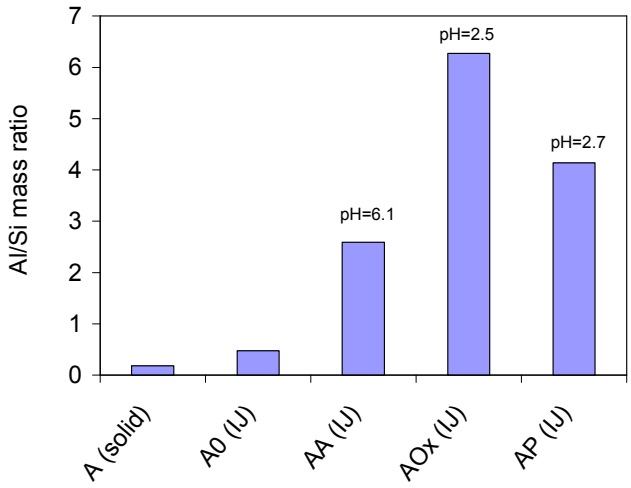

Figure III-7: Al/Si mass ratio determined by ICP-AES on the solid fresh support, A (solid) and on the impregnation juices (IJ) sampled after 2 h of impregnation of the support and 10 min rest with water (A0), AHM (AA), AHM-oxalate (AOx) and molybdenum oxide hydrates (AP). The pH of the impregnation solutions was calculated from the pH measured in the precursor solutions and taking the dilution factors into account.

Figure III-8 shows the C 1s XPS peak of the 10 %-loaded catalysts before calcination (after drying). The AA10 and AP10 catalysts present a typical C peak related to classical C contamination, with mainly one intense component at 284.8 eV corresponding to the carbon atoms linked to other C atoms or to H atoms (C-(C,H)). The AOx10 catalyst is different and exhibits an intense component at 289.6 eV corresponding to C atoms doubly linked to oxygen (C=O and O-C-O). This signal must be correlated with the

presence of the oxalate moieties. Note that after calcination at 400 °C, all samples exhibited a C 1s XPS peak with the classical shape of usual C contamination (not shown), indicating that the oxalate moieties were effectively removed after calcination at 400 °C.

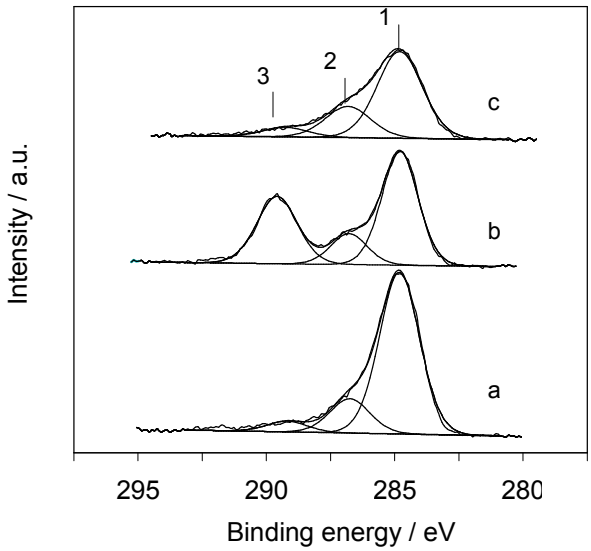

Figure III-8: XPS C 1s peak of the dried (uncalcined) catalysts (a) AA10, (b) AOx10 and (c) AP10. The marks indicate the three components of the peak: (1) C-(C,H), (2) C-O and (3) C=O and O-C-O.

The same samples were analyzed by Raman spectroscopy (Figure III-9). Both AA and AOx dried samples exhibit a main Raman band at ca. 945 cm^{-1}, attributable to polymolybdate species like heptamolybdate. In the AA catalyst, the second band appears at 896 cm^{-1}, exactly like in heptamolybdate (ν_{as} MoO_{2t} vibration). This band is not clearly visible in the AOx sample. As expected, the bands are rather broad for these solid samples and a precise identification of impregnated species is delicate.

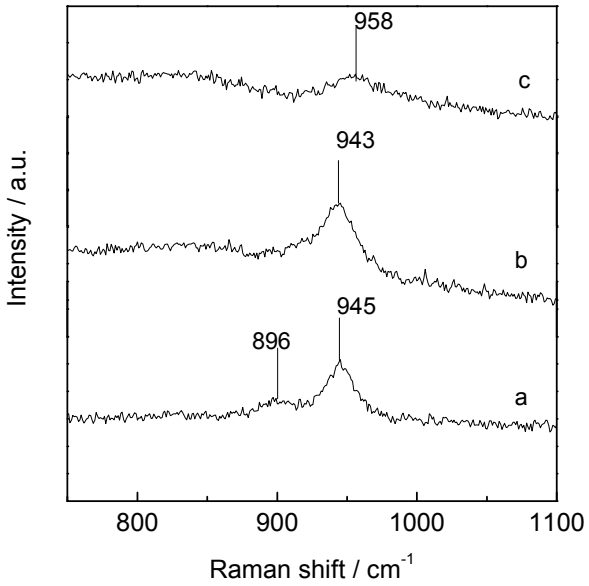

Figure III-9: Raman spectra of dried (not calcined) catalysts: (a) AA10, (b) AOx10 and (c) AP10.

3.1.2. Metathesis activity

The evolution of the metathesis activity within one hour of catalytic test was always similar to the trends depicted in Chapter 2, namely a maximum in activity is observed after about 20 minutes time-on-stream followed by slow deactivation (Figure II-13). In the same way, the specific activity measured between 14 and 26 min time-on-stream was averaged for each sample and these values are discussed here. Figure III-10 shows the metathesis specific activity of AOx*x* catalysts, along with some of the results presented in Chapter 2, for the purpose of comparison. It is remarkable that the curve of activity as a function of the loading is increasing in a linear fashion. This is different from the situation encountered with AA*x* catalysts, for which a plateau was observed from a MoO_3 loading of about 8 wt. %. From the results of Chapter 2 indeed, a horizontal line at ca. 16 mmol h^{-1} g^{-1} appeared as a limit of activity that can be reached with the catalysts prepared with AHM as precursor and calcined at 500 °C (AAx500). The AAx samples calcined at 400 °C behaved similarly (Figure II-15) and it is reasonable to imagine a horizontal limit in Figure III-10 corresponding approximately to a

specific activity of 12 mmol h^{-1} g^{-1} [64]. These two limits are broken by the curve of AOx*x* catalysts at relatively high loading. However, at relatively low loading the activity of AOx*x* catalysts is modest and lower than the AA*x*500 catalysts with similar loading.

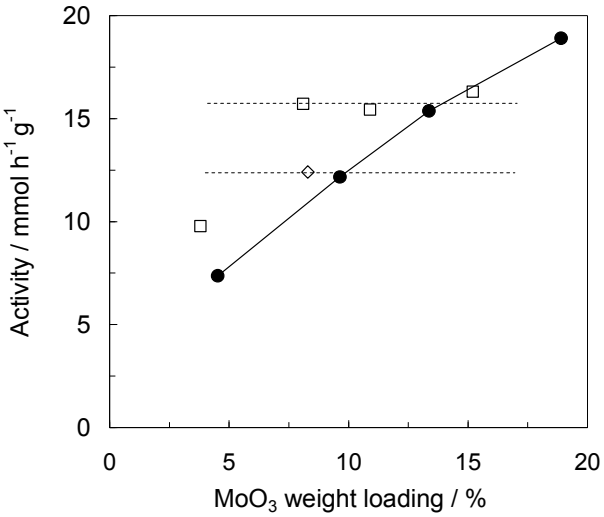

Figure III-10: Specific activity of (●) AOx*x* catalysts and comparison with (□) AA*x*500 and (◊) AA8400 catalysts (Chapter 2).

3.2. Discussion

3.2.1. Effect of oxalic acid on the Mo speciation

Unlike in the case of the impregnation with AHM (pH = 5.4), the pH of the "Ox" impregnation solution was very low. Depending on the targeted loading, an appropriate volume of the precursor solution (pH = 1.8) was diluted in water to reach the 200 ml of impregnation solution. The support was thus suspended in an impregnation solution whose pH ranged from 2.1 to 2.8 when the nominal loading was respectively 19 and 5 wt. %.

Oxalic acid was added in the impregnation solution with the hope that it would break the heptamolybdate clusters and stabilize – by complexation – different Mo species with lower nuclearity. It is difficult to state firmly whether this effect was obtained or not. Following Himeno et al. [206], the sharp band at 950 cm^{-1} could be interpreted as the major Raman

line of $Mo_3O_{10}^{2-}$ species. However, in this case, other bands at 918 and 901 cm^{-1} should be present (which is not the case here). As expected, the mononuclear MoO_4^{2-} species was not formed (one band expected at 896 cm^{-1} but only under alkaline condtions). In the present case, oxalic acid lowers the pH of the solution and does not stabilize mononuclear species by complexation. To our best knowledge, only one publication related to the preparation of MoO_3-based catalyst reports Raman characterization of molybdenum oxalate in solution. In their paper, Ng et al. [207] show spectra of molybdenum oxalate in solution as a function of the pH. At pH = 2 the two most intense peaks are found at 938 cm^{-1} and at 901 cm^{-1}, while at higher pH, the frequency of the Mo=O stretch decreases, indicating a decrease in the polymerization degree. They claim that monomeric molybdodioxalate (pH > 4.25) and dimeric molybdooxalate (1.25 < pH < 4.25) species are present in the solution but simply relied on the work of Beltran et al. [193] for this assertion. It appears consistent to consider that a peak found higher than 938 cm^{-1} indicates species with higher degree of polymerization. Indeed, under very acidic conditions species with higher nuclearity are observed [206]. Here, $Mo_8O_{26}^{4-}$ species (971 and 963 cm^{-1}) are not detected. Ng et al. prepared their solution from molybdenum oxalate salts and not from AHM, so it is possible that different equilibrium were reached in their study and in ours. Finally, as the main peak in Figure III-1 is relatively high (950 cm^{-1}) it appears more likely that the heptamolybdate cluster is conserved in the "Ox" solution used here. Indeed the two Raman bands that are detected are very close to the typical bands related to AHM. The small shifts that are noticed might tentatively be explained by a complexing effect of oxalate ions on the preserved heptamolybdate cluster. Note also that the band at 911 cm^{-1} is relatively broad and could be an overlap of two distinct bands.

After impregnation, the bands observed in the liquid state can still be distinguished, although much less resolved. In view of the large width of the bands observed for solid-state measurement, it is difficult to discriminate between different supported polyoxomolybdate species. Most of the species indeed consist in edge-sharing octahedra with distorted geometry that give rise to Mo-O vibrations in the same region [191]. In any case, a polymeric

species, close to heptamolybdate is deposited on the support, as attested by the main Raman signal at ca. 945 cm^{-1}.

3.2.2. Effect of oxalic acid on the support

Characterization results strongly indicate that a partial dissolution of the support occurred during impregnation in the presence of oxalic acid. Firstly, the Al/Si ratio measured in the liquid phase after the 2 h of stirring is strikingly high. This observation, related to the low pH of the solution, is consistent with the dissolution of aluminic domains of the support. It is well-known that silica is very resistant against acidic media while alumina already dissolves around pH 4 [208]. In several cases it was demonstrated that the dissolution of alumina support must be taken into account in the study of catalyst preparation [208-209]. In addition to the simple effect of the acidity of the impregnation medium, the effect of the oxalate ions must be envisaged here. Carrier et al. [179] have highlighted the works of geochemists and specialists of soil science who reported that oxalate ions can enhance the dissolution rate of alumina [210]. This effect has been reported in the case of aluminosilicate clays, for example [211]. It proceeds via the modification of the thermodynamic equilibrium between species in solution. The solubility of aluminium oxide is enhanced because oxalate-aluminium complexes form, thereby shifting the dissolution equilibrium to the right. Such ligand-promoted dissolution of alumina-based material is exemplified in Figure III-11 for the case of halloysite and can be called in the present study to account for some of our observations.

Secondly, the texture of the support has been strongly affected by the impregnation procedure, as revealed by the modified pore size distribution of these samples. This also supports the idea of a partial dissolution of the support. The pore volume and the mean pore size diameter both decreased drastically in the case of the impregnation in the presence of oxalic acid, as compared to the case of the impregnation with pure AHM (see Chapter 2). It seems that large pore collapsed, while a population of new very small pores was created during the impregnation. These small pores may either really be formed from the partial dissolution of the support or originate from the partial plugging of bigger pores.

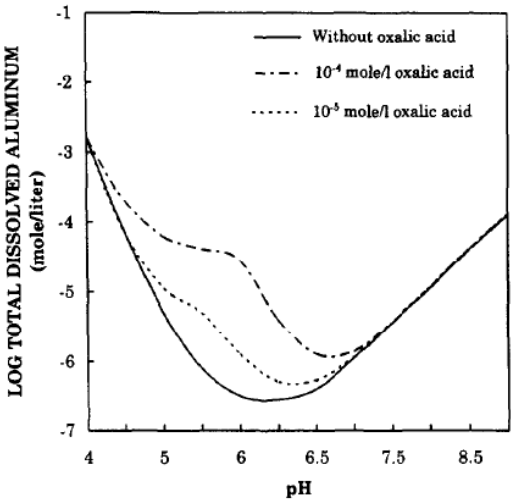

Figure III-11: Effects of oxalate complexes on the equilibrium solubility of aluminium in the presence of synthetic halloysite (from reference [211] and reference therein).

Evidently, the environment of Al atoms has changed drastically after impregnation. As MAS-NMR spectra indicate, in the silica-alumina support used here, it is the Al_{TET} species that are prone to leach during the impregnation. These species – described as framework tetrahedrally coordinated Al atoms in a mixed silica-alumina phase – were almost totally consumed after impregnation. In the present case, where oxomolybdate complexes are present in relatively acidic conditions, it could have been expected that the dissolution of the alumina-containing support is promoted by the complexation of Al^{3+} ions by oxomolybdate complexes [179]. Indeed Bergwerff et al. [181] have observed this effect during the preparation of MoO_3/Al_2O_3 extrudates and described it as a chain reaction: Al^{3+} ions generated by the dissolution of the support are consumed in the formation of $Al(OH)_6Mo_6O_{18}^{3-}$, which can precipitate in the form of $(NH_4)_3Al(OH)_6Mo_6O_{18}$. As the Al^{3+} concentration is kept low, increasing amounts of aluminium oxide are dissolved. This phenomenon was called to explain the formation of $[AlMo_6]$ in the previous chapter, even if the impregnation solution was not so acidic (the pH of the precursor solution was 5.4). It was thus reasonable to expect the occurrence of such process during impregnation with the "Ox" solution. However, no $[AlMo_6]$ was

detected on the catalyst after impregnation (before calcination) by ^{27}Al MAS-NMR. So the partial dissolution of the support can not be linked to the complexing effect of oxomolybdates in the present case. Instead, it has to be correlated to the combination of two parameters: (i) the low pH, (ii) the presence of oxalate ligands. Actually, the affinity of dissolved Al^{3+} cations for oxalate ligands is stronger than their affinity for oxomolybdenum species.

3.2.3. Catalysts properties

After the wet step, no hexamolybdoaluminate ($[AlMo_6]$) was detected by ^{27}Al MAS-NMR. However, $[AlMo_6]$ is present in the calcined catalysts (Figure III-5). Thus in the present case, the formation of such aluminium polymolybdate does not take place during the wet step, as observed in Chapter 2 and from other published studies [98, 179] but after the drying and calcination steps, when the oxalate ligands are removed by total oxidation. Actually, it is more reasonable to consider that $[AlMo_6]$ forms after the preparation is completed (after calcination), during long-term storage or during manipulation of the calcined samples under ambient conditions. Such formation of $[AlMo_6]$ via hydration of MoO_3/SiO_2-Al_2O_3 catalyst under ambient humid condition at room temperature was demonstrated experimentally [191].

Comparing AA and AOx catalyst, another important difference concerns the aluminium molybdate phase. $Al_2(MoO_4)_3$ was clearly detected on the AA8400 sample and its formation was shown to increase with increasing loading. In the case of the catalysts prepared from the "Ox" solution, $Al_2(MoO_4)_3$ is not detected except as a small signal on the catalyst with the highest loading. So in the absence of $[AlMo_6]$ after impregnation, the formation of $Al_2(MoO_4)_3$ during calcination is hampered.

The impregnation with AHM in the presence of oxalic acid followed by calcination at 400 °C finally led to a totally amorphous Mo oxide deposit, as confirmed both by Raman and XRD (Figure III-3 and Figure III-4). Once again, $[AlMo_6]$ (and $Al_2(MoO_4)_3$ in the case of AOx19) are not detected in XRD, showing that these species are either totally amorphous, or present as very small crystallites or in very low amount. The fact that no MoO_3 crystals

are found in such MoO_3/SiO_2-Al_2O_3 catalysts is a major difference with respect to the more classical preparation method based on AHM. This effect can be explained as follows. As demonstrated by Bergwerff et al. [98], the organic ligands (here oxalate) increase the solubility of Mo, thereby preventing its fast precipitation at the external surface of the support particles. This results in a homogeneous Mo deposit on the available support surface. As Mo species are well dispersed they are less prone to sinter. An additional reason for the absence of MoO_3 is the fact that the formation of $Al(OH)_6Mo_6O_{18}^{3-}$ was avoided during the wet impregnation in the presence of oxalic acid whereas it is known that [$AlMo_6$] yield MoO_3 upon calcination [98, 187]. It could be claimed also that the oxalate ligands indirectly impede the agglomeration of Mo species by acting as steric spacers during the adsorption on the support. Mo clusters surrounded by oxalate ligands would not adsorb on the support in the direct vicinity of each other. The organic ligands that are removed progressively during calcination would thus hinder agglomeration and sintering. Finally, another possible factor explaining the absence of MoO_3 crystals concerns the dissolution of the support. Dissolved Al^{3+} ions, possibly complexed by oxalate ligands, will return to the solid state during water evaporation. These species also might play the role of "spacers" or "diluting agents" during the formation of the Mo phase. In other words, this would limit the possibility for pure oxomolybdenum species to agglomerate close to each other and to sinter under the effect of calcination.

3.2.4. Correlation with metathesis activity

In the end, AOx catalysts have a metathesis activity in the same order as AA catalysts (Figure III-10). At low MoO_3 loading, they are less active than the catalysts prepared by impregnation with the classical AHM solution and calcined at 500 °C. The modest performances of AOx catalysts can be interpreted in relationship with the phenomenon of support dissolution. The specific surface area of the final catalyst is negatively affected by the impregnation with the "Ox" solution. Also, one can imagine that parts of the Mo species deposited on the support are subsequently covered by oxalate-aluminium complexes from the solution. Remarkably however, the metathesis activity rises continuously when the loading

increases. As a consequence the curves meet and AOx catalysts perform better than AAx500 catalysts at high loading.

It was shown in Chapter 2 that the calcination temperature had a marked impact on the metathesis performances of AA catalysts. Namely, higher calcination temperature led to higher metathesis activity. Here, AOx catalysts were calcined at 400 °C because this temperature is high enough to remove oxalate moieties. Comparing the activity of AOx catalysts with the activity of AA8400 is thus more relevant. Taking also into account previous results on AAx400 catalysts [64], it seems reasonable to consider that AOx catalyst perform better than AAx400 catalysts from a loading of 8-10 wt. % already.

In the previous chapter, MoO_3 crystals (XRD and Raman) and $Al_2(MoO_4)_3$ (NMR) were shown to build up when the activity was levelling-off. [$AlMo_6$] was always present in variable amount. In the present case, the metathesis activity keeps increasing when neither MoO_3 nor $Al_2(MoO_4)_3$ appear in detectable amounts. In other words, the absence of MoO_3 crystals and of aluminium molybdate in the whole range of loading can be correlated with the continuous increase in activity. To be accurate, traces of $Al_2(MoO_4)_3$ are observed on AOx19. At this level the slope of the activity-loading curve indeed gets slightly smaller. The $[Al(OH)_6Mo_6O_{18}]^{3-}$ species on the other hand form in growing amount in parallel with the increasing loading and increasing activity. Let us remember that such species can also form during storage and handling of the sample, as result of hydration of supported Mo oxide [191]. In any case the presence of this species can not be correlated with any deleterious effect on the metathesis activity.

In the end, the strategy consisting in the use of oxalic acid as an organic complexing is relevant to some extent. The control of the nature of the Mo species in solution at the molecular scale was not achieved and the beneficial effects of the addition of oxalic acid in terms of metathesis activity are rather modest. Nevertheless, the use of oxalic acid was shown to prevent the formation of MoO_3 crystals and of aluminium molybdate, which led to a linear relationship between the specific activity and the MoO_3 loading.

4. MOLYBDENUM OXIDE HYDRATES

4.1. Results

4.1.1. Catalyst characterization

The initial molybdenum oxide hydrates solution was obtained by reaction of metallic Mo with an aqueous solution of hydrogen peroxide followed by catalytic removal of the peroxide in excess (the solution is denoted "P" for peroxide; see Experimental Section, p. 25). The pH of this yellow solution was 2.0. Figure III-12 shows the Raman spectrum of this precursor solution. Two bands are detected at 949 and 967 cm^{-1}. These bands may be attributed to $Mo_3O_{10}^{2-}$ and $Mo_8O_{26}^{4-}$ species respectively [206]. Noticeably, no band was detected in the 848-856 cm^{-1} range, where the vibration modes of side-bonded peroxo ligands are usually expected [212-213] which indicates that the peroxide species have efficiently been removed catalytically by the treatment with the platinum grid.

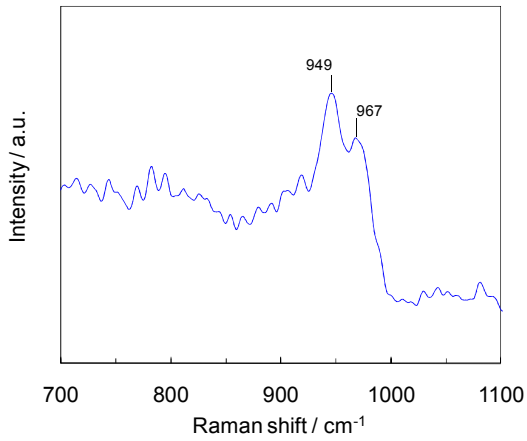

Figure III-12: FT Raman spectrum of the "P" precursor solution (8 g of $Mo.l^{-1}$)

For these catalysts the effect of the temperature (300 °C, 400 °C and 500 °C) has been investigated. Also, the loading has been varied in the 5-20 wt. % range for the 400 °C and 500 °C-calcined samples. The experimental MoO_3 loading mostly fits the targeted one or is slightly lower than expected

(Table III-2). Such discrepancies are attributed to the incomplete recuperation of the Mo that is projected on the walls of the flask during the reaction of metallic Mo and the H_2O_2 solution (these droplets are tentatively recovered during the preparation but some are lost). The filtration is another step of the preparation that can cause losses of Mo (partly remains adsorbed on the filter even after multiple washing).

Table III-2: Textural properties (N_2-physisorption) and experimental MoO_3 weight loading (ICP-AES) of the AP catalysts

Name	Calcination temperature (°C)	MoO_3 loading (wt. %)	SSA ($m^2\ g^{-1}$)	Pore volume ($ml\ g^{-1}$)	Pore diameter (nm)
A		-	490	0.71	5.8
AP10300	300	9.3	380	0.51	5.4
AP5400	400	5.0	430	0.59	5.5
AP10400	400	9.3	390	0.54	5.6
AP14400	400	12.9	370	0.52	5.6
AP20400	400	20.3	330	0.46	5.6
AP5500	500	4.6	390	0.57	5.8
AP10500	500	9.5	370	0.51	5.5
AP14500	500	12.9	320	0.47	5.9
AP20500	500	18.8	290	0.43	6.0

Catalysts having similar loading and calcined at different temperature have very similar texture as shown by similar SSA, pore volume and average pore diameter (Table III-2). This is further confirmed by the overlaid pore size distribution curves shown in Figure III-13 for the case of the 10 %-loaded samples. Catalysts having different MoO_3 loading mainly differ in terms of specific surface area and pore volume: both decrease with increasing loading. The mean pore size remains quite stable or decreases slightly. The shapes of the pore size distribution profiles are only slightly affected (Figure III-14). Unlike in the case of AA catalysts, the porse size distribution curves of AP catalysts are clearly shifted downwards (with respect to the Y axis) upon the addition of Mo oxide.

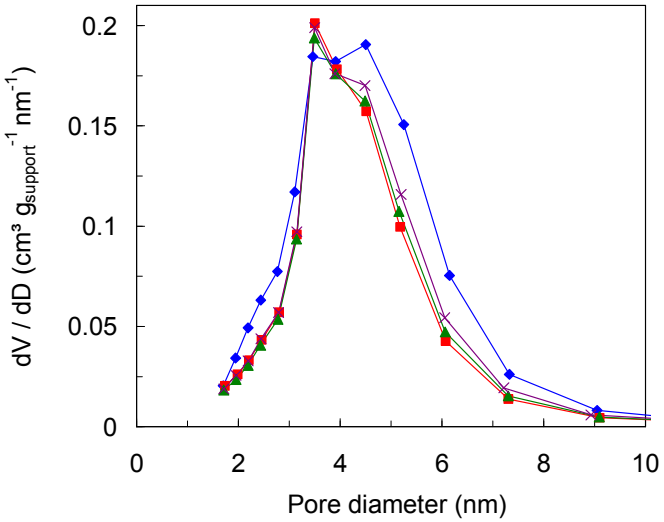

Figure III-13: Pore size distribution determined by the BJH method applied on the desorption isotherms of (♦) the support, (■) AP10300, (×) AP10400 and (▲) AP10500.

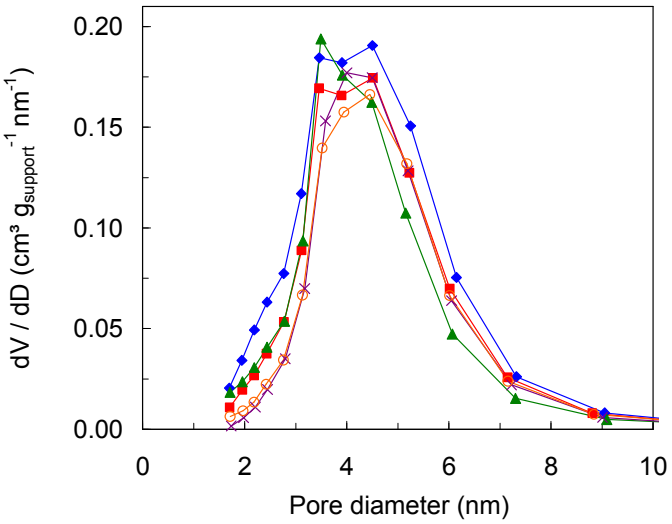

Figure III-14: Pore size distribution determined by the BJH method applied on the desorption isotherms of (♦) the support, (■) AP5500, (▲) AP10500, (×) AP14500 and (○) AP20500.

In line with the previous section on the preparation of MoO_3/SiO_2-Al_2O_3 catalysts via impregnation in the presence of oxalic acid, investigations were conducted on the impregnation juice and on the dried

(but not calcined) catalysts after impregnation with the molybdenum oxide hydrate solution. Figure III-7 shows that in this case also the liquid phase in contact with the support during 2 hours of wet impregnation is enriched in Al. The effect is more marked than in the case of impregnation with AHM but less marked than in the case of the "Ox" solution.

Unlike AOx and AA catalysts, no nitrogen peak is observed at the surface of the uncalcined catalysts (not shown) since no ammonium salt was used in the preparation of the precursor solution. The carbon peak simply reveals usual carbon contamination, as no organic compound was used in the preparation either (Figure III-8).

The Raman spectra of the uncalcined catalysts barely reveal a broad and poorly resolved peak around 958 cm^{-1} (Figure III-9). This frequency can correspond to polyoxomolybdenum species with higher nuclearity than heptamolybdate, e.g. $Mo_8O_{26}^{4-}$.

XRD investigations showed without ambiguity that all AP samples are amorphous. No MoO_3 crystallites were detected even for the catalysts with the highest loading and calcined at the highest temperature (Figure III-15 and Figure III-16).

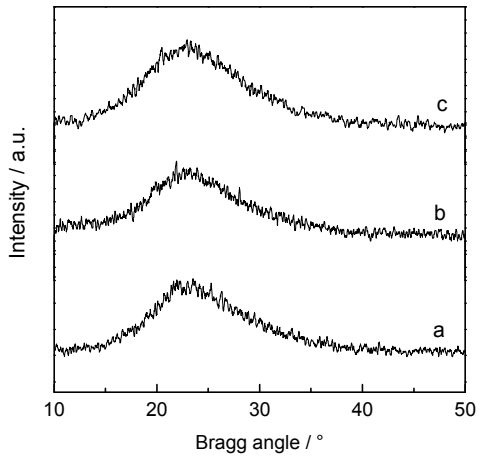

Figure III-15: XRD patterns of MoO_3/SiO_2-Al_2O_3 catalysts prepared by wet impregnation of a molybdenum oxide hydrates solution (~9 wt. % MoO_3) and calcined at different temperature: (a) AP10300, (b) AP10400 and (c) AP10500.

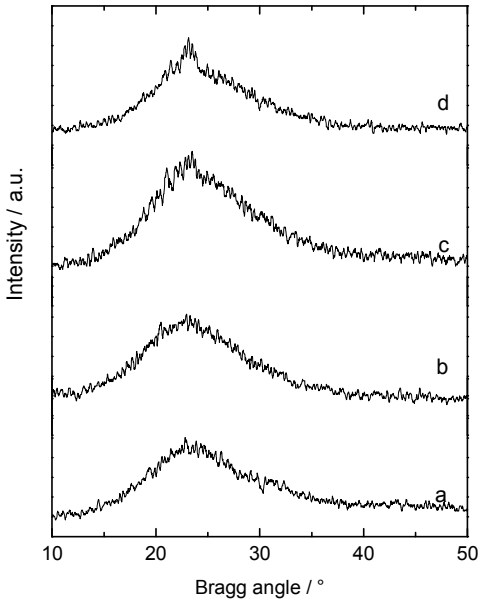

Figure III-16: XRD patterns of MoO_3/SiO_2-Al_2O_3 catalysts prepared by wet impregnation of a molybden oxide hydrates solution and calcined at 500 °C: (a) AP5500 (b) AP10500, (c) AP14500 and (d) AP20500.

In the same way, Raman spectra never showed bands related to the presence of MoO_3 crystals (Figure III-17). Instead a broad band around 950 cm^1 is always detected. It is attributed to surface polymolybdates. In some cases (like AP14400) a shoulder at ~990 cm^{-1} was detected. Consistently, Hinokuma et al., reported that the condensation of such peroxopolyanions gives large chain-shaped polyanions based corner-sharing $[MoO_5OH]$ octahedral which were characterized by Raman bands at 950 and 980 cm^{-1} [198]. The shoulder at 990 cm^{-1} is too high to account for $Mo_8O_{26}^{4-}$ species. Watson et al. proposed that the bands associated with isolated terminal Mo=O stretching are visible in the 970-1005 cm^{-1} region [214-215]. However, working with TiO_2-SiO_2 supports, they observed several better resolved bands in this region, making that such monomeric molybdate are improbable. Bearing in mind that Raman measurements were very delicate (in line with the fluorescence of the support and with the low response of amorphous species) and considering the large width of the Raman bands discussed, it will be considered that the band at 950 cm^{-1} sometimes

accompanied by a shoulder at 990 cm^{-1} is associated to an stoichiometrically ill-defined amorphous surface polymolybdates.

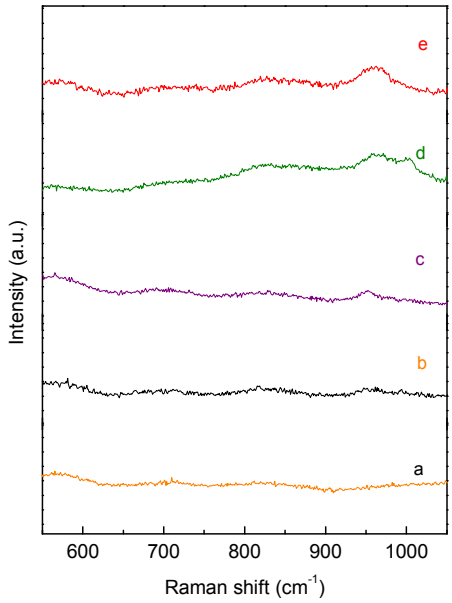

Figure III-17: Raman spectra of (a) the SiO_2-Al_2O_3 support, (b) AP5400, (c) AP10400, (d) AP14400 and (e) AP20400.

The Mo surface concentration measured in XPS increases linearly with increasing MoO_3 loading (Figure III-6). Unlike in AAxY catalysts, the surface Mo / (Si+Al) atomic ratio is always lower than expected for a totally homogeneous solid. In addition, in AP catalysts, the calcination temperature has no marked effect on the Mo / (Si+Al) atomic ratio.

After impregnation of the support with the "P" solution, the environment of Al atoms is affected (Figure III-18). Mainly the Al_{PEN} (ca. 30 ppm) and Al_{TET} (ca. 54 ppm) components of the ^{27}Al MAS-NMR spectra decrease suggesting again that these species are sensitive to the low pH. In AP10 catalysts, a small amount of [$AlMo_6$] (15 ppm) is detected after impregnation (Figure III-18). After calcination at 300 °C, 400 °C or 500 °C, the Al_{TET} signal tends to be restored and the signal of [$AlMo_6$] increases slightly. After calcination at 500 °C, traces of $Al_2(MoO_4)_3$ are detected at -14 ppm.

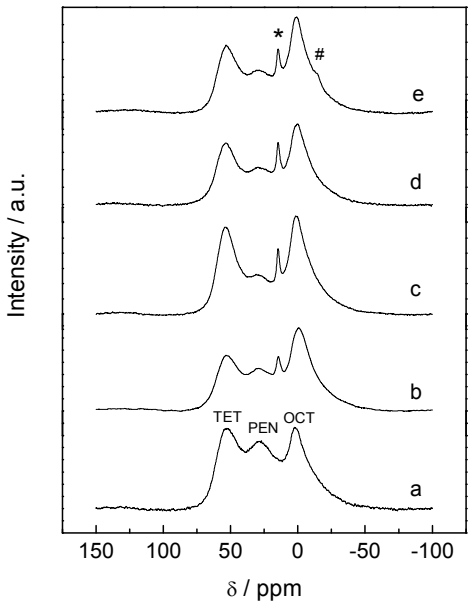

Figure III-18: ^{29}Al MAS-NMR spectra of (a) the support, (b) AP10 dried but not calcined, (c) AP10300, (d) AP10400 and (e) AP10500. The Al_{TET}, Al_{PEN} and Al_{OCT} signals are indicated on the first spectrum. [$AlMo_6$] and $Al_2(MoO_4)_3$ are marked with "*" and "#"respectively.

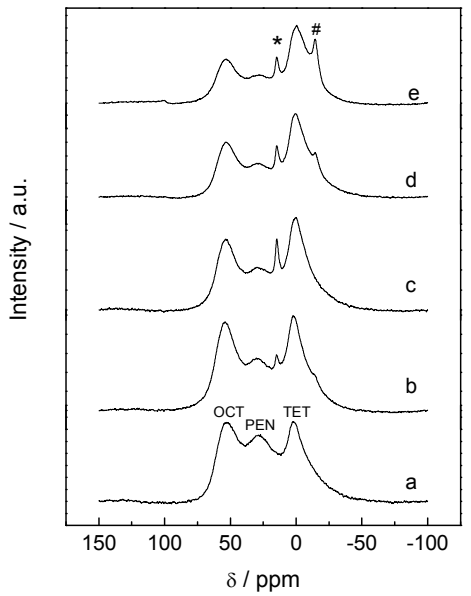

Figure III-19: ^{29}Al MAS-NMR spectra of (a) the support, (b) AP5400, (c) AP10400, (d) AP14400 and (e) AP20400. The Al_{TET}, Al_{PEN} and Al_{OCT} signals are indicated on the first spectrum. [$AlMo_6$] and $Al_2(MoO_4)_3$ are marked with "*" and "#"respectively.

In the catalysts calcined at 400 °C, the [$AlMo_6$] species (15 ppm) is always present (Figure III-19). Its intensity does not increase proportionally with increasing loading. Instead, it decreases as the loading get higher than 10 wt. %. $Al_2(MoO_4)_3$ (-14 ppm) appears only above this loading and its signal is very intense only in the AP20400 catalyst. Similarly, in the catalysts with MoO_3 loading in the same range and calcined at 500 °C, the [$AlMo_6$] species is always present (Figure III-20). Its intensity does not vary in parallel with the MoO_3 loading; instead the proportion of this species decreases at high loading. Traces of $Al_2(MoO_4)_3$ already appear at relatively low loading even if it remains low up to 14 wt. % in MoO_3. Here also the intensity of this peak at -14 ppm increases with increasing loading. In AP20500 the aluminium molybdate phase is more abundant than in AP20400.

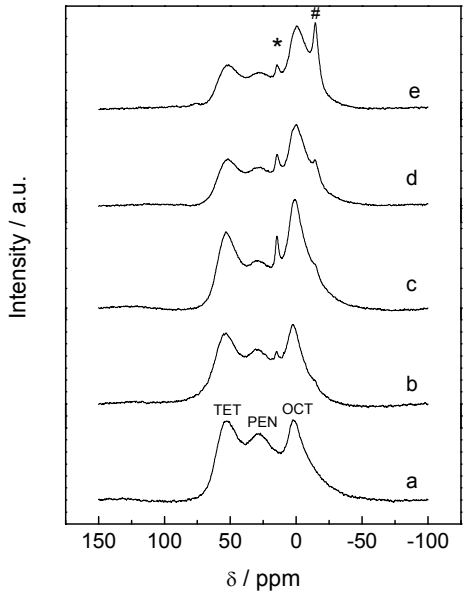

Figure III-20: ^{29}Al MAS-NMR spectra of (a) the support, (b) AP5500, (c) AP10500, (d) AP14500 and (e) AP20500. The Al_{TET}, Al_{PEN} and Al_{OCT} signals are indicated on the first spectrum. [$AlMo_6$] and $Al_2(MoO_4)_3$ are marked with "*" and "#"respectively.

4.1.2. Metathesis activity

The activity of AP catalysts develops with time on stream in a similar way as already depicted for AA catalysts. Here also, the performances of AP catalysts will be discussed on the basis their maximum specific activity obtained by averaging the activity measured after 14, 20 and 26 min (Figure III-21). Also reminded on the Figure are the results obtained with AA catalysts (Chapter 2, Figure II-14). The activity of the 10 wt. % loaded catalysts was slightly dependent on the calcination temperature. The 400 °C-treated sample that is the most active, followed by the catalysts calcined at 500 °C and finally the one calcined at 300 °C. The effect of the loading was screened for the catalysts calcined at 400 °C (apparently the best calcination temperature) and at 500 °C (for the purpose of comparison with AAx500 catalysts).

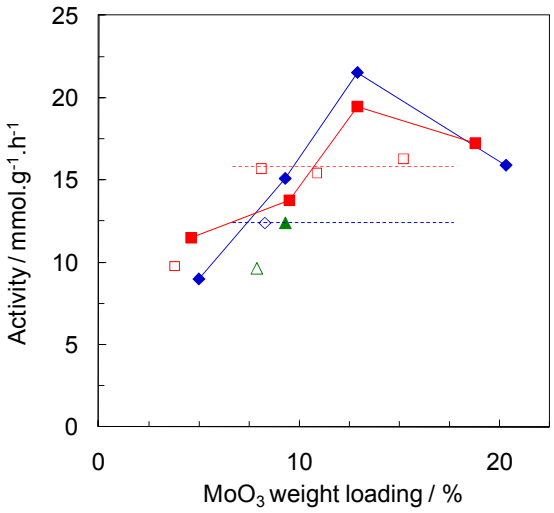

Figure III-21: Specific activity of APx catalysts. (▲) AP9300, (♦) APx400 and (■) APx500. For comparison, the activity is also given for AAxY catalysts: (Δ) AA8300, (◊) AA8400 and (□) AAx500. Horizontal dotted lines are guide to the eyes indicating the plateau observed in the activity of AA catalysts as described in Chapter 2.

The superiority of APx400 catalysts as compared to APx500 catalysts is confirmed at 14 wt. % MoO_3 loading. The highest activity is

reached with AP14400. Overall, the relationship between the metathesis activity and the MoO_3 loading is different from the trends depicted in the case of AA or AOx catalysts. Here, the activity first increases steeply when the loading is increased up to 14 wt. %. Then a marked decrease is observed. While AP14400 and AP14500 catalysts are much more active than AA catalysts with corresponding loading and calcination temperature, the activity of the 20 wt. % loaded catalysts falls down around the plateau of activity described earlier for AAx500 catalysts.

4.2. Discussion

4.2.1. Mo speciation in the molybdenum oxide hydrates solution

It is clear that the molybdenum species in the "P" impregnation solution are different from those found in the AHM or "Ox" ones. Here, the most intense signals are found at higher frequencies (Figure III-12), suggesting more condensed polymeric species. The peak at 950 cm^{-1} could be attributed to the trimolybdate anion ($Mo_3O_{10}^{2-}$) following Himeno et al. [206]. However, the peak at 967 cm^{-1} should be attributed to $Mo_8O_{26}^{4-}$ which also generates a peak around close 950 cm^{-1} [162, 206]. The presence of the trimolybdate species is not demonstrated. The presence of species with nuclearity even higher than eight, like $Mo_{36}O_{112}^{8-}$ (main Raman signal expected at 983 cm^{-1}) can not be ruled out since it may be comprised in the high frequency shoulder of the 967 cm^{-1} peak.

4.2.2. Effect on the support

As the solution is very acidic (almost as acidic as the "Ox" solution), partial dissolution of the support was expected. Indeed, the Al/Si ratio measured by ICP-AES in the impregnation juice was relatively high (Figure III-7). In addition to the effect of the pH, a ligand-promoted dissolution can be envisaged under the effect of oxomolybdenum species, that would lead to the formation of the [$AlMo_6$] species, as observed in the case of MoO_3/Al_2O_3 catalysts preparation [179]. Indeed, this species is observed in MAS-NMR after the impregnation (Figure III-18). However, even if the pH of the

impregnation solution is close to the pH of the "Ox" solution discussed previously, the extent of the dissolution of the support is clearly smaller.

Here, the porosity of the support is moderately affected by the preparation. The specific surface area and the pore volume decrease more than in the case of impregnation with AHM (Table III-2). The mean pore size diameter tends to decrease slightly after impregnation. In addition, Figure III-13 and Figure III-14 show that this is not a simple effect of the addition of non porous MoO_3 but that the porosity of the support itself is clearly affected. Overall, it must be concluded that the MoO_x phase enters the pores. In parallel, the Al_{TET} and Al_{PEN} signals are only slightly reduced after impregnation, unlike in the case of impregnation with the Mo-oxalate solution. This confirms that the drastic alteration of the support described in the previous section was promoted by oxalic acid, while here the sole effect of the the acidity of the solution is not enough to provoke a considerable dissolution of the support.

4.2.3. Catalysts properties

4.2.3.1. Absence of MoO_3 crystals

All AP catalysts were totally amorphous. The calcination temperature has no effect on the crystallinity of the catalysts, unlike in the case of AA catalysts. In the latter case indeed, calcination at 400 °C and 500 °C provoked the appearance of MoO_3 crystals. Here, the strategy was to use a precursor which decomposes at lower temperature, so that smoother treatment would be enough to obtain a MoO_3 phase at the surface of the support. In the end, it appears that no MoO_3 crystals form even after calcination at high temperature. This can appear surprising because the species found in the impregnation solution are also polymeric species and could thus also act as potential nucleation points for Mo oxide sintering. However, rational explanations can be put forward to explain such result.

Firstly, as discussed above, the Mo species are thought to enter the pores of the support instead of precipitating mainly at the outer surface of the particles, like in the case of AA catalysts. This is suggested both by textural analysis and by the determination of the Mo surface concentration by XPS. Comparing Figure III-6 with Figure II-1, the Mo concentration detected by

XPS at the surface of AP catalysts is indeed low, which is coherent with the idea that Mo atoms actually cover the walls of the pores. In this case Mo atoms that are located inside the porosity of the particles will not be detected by XPS. It should be remembered that the tentative formula of the species formed in solution via the oxidation of Mo by the hydrogen peroxide solution is $MoO_3.nH_2O.mH_2O_2$ (with m presumably close to 0 after the treatment with the Pt grid). It is reasonable to put forward that such species interact less with the positively charged support surface than the heptamolybdate anions. Indeed if present as anionic species in a very acidic solution, the Mo entities should be more protonated than the heptamolybdate cluster under moderate pH. So during the impregnation with the 'P' solution, the Mo species have a better opportunity to be transported on the whole available surface, including the interior of the porosity, instead of precipitating mostly at the outer surface of the particles, like in the case of AA catalysts. Mo species (even polymeric species with high nuclearity) that are well dispersed on the whole available surface have a lower probability to agglomerate and to form nucleation point for sintering.

The second plausible explanation to account for the absence of MoO_3 crystals concerns $[AlMo_6]$. This species is detected in the dried catalyst (Figure III-18) but in lower quantities than in AA catalysts. It is known that hexamolybdoaluminium yields crystalline MoO_3 (and aluminium molybdate) upon calcination [98, 187]. The lower amount of $[AlMo_6]$ formed during impregnation may account for the lower tendency to form crystalline molybdenum trioxide during calcination. However, this interpretation must be handled with care. It is considered that $[AlMo_6]$ forms by complexation of dissolved Al^{3+} cations during impregnation. Yet MAS-NMR spectra of calcined samples show that the intensity of this signal at 15 ppm increases after calcination. This shows that such aluminium polymolybdate forms not only during the wet step. In fact it must be remembered that $[AlMo_6]$ can also form after catalyst preparation, during storage and manipulation under ambient conditions, via hydration of supported Mo oxide [191]. So it is not ruled out that the observed (small) peak of $[AlMo_6]$ is (partly) due to humid ambient conditions during sample handling on the bench. In this case, the correlation between the low amount of $[AlMo_6]$ after impregnation and the absence MoO_3 crystals would be even

more evident. MAS-NMR investigations should be conducted on the samples immediately after impregnation or immediately after calcination and in dehydrated conditions to ascertain this link.

4.2.3.2. Limited formation of $Al_2(MoO_4)_3$

Whatever the calcination temperature, the MAS-NMR peak of [$AlMo_6$] has approximately the same intensity after calcination. On the other hand the calcination temperature determines whether $Al_2(MoO_4)_3$ forms or not. In fact among the 10 wt. % loaded samples, only the catalyst treated at 500 °C exhibits traces of this aluminium molybdate phase.

When the calcination temperature is kept constant and the MoO_3 loading is varied the proportions of alumimiun molybdate and of aluminium polymolybdate change. Formation of $Al_2(MoO_4)_3$ is favoured when the loading increases. It seems that, above a certain limit in terms of MoO_3 loading, the formation of high amounts of aluminium molybdate can not be avoided. This transition occurs clearly when the MoO_3 loading increases from 14 to 20 wt. %. In fact, when the loading is 14 wt. % the $Al_2(MoO_4)_3$ peak is very small and at lower loading, only traces of $Al_2(MoO_4)_3$ are sometimes detected. If APx400 and APx500 samples are compared to AAx500 catalysts (see Chapter 2, Figure II-10) the following observations can be made about the -14 ppm peak: (i) at 4-5 wt. % loading, traces of $Al_2(MoO_4)_3$ (if any) are detected regardless of the preparation method (ii) at 8-10 and 11-14 wt. % loading a real peak is detected for AA catalysts, while only traces are detected in AP samples and (iii) at high loading (17-20 wt. %) all catalysts exhibit a significant amount of $Al_2(MoO_4)_3$. This shows that the preparation of MoO_3/SiO_2-Al_2O_3 catalysts via the impregnation of molybdenum oxide hydrates solution impedes the formation of $Al_2(MoO_4)_3$ at intermediate loading.

4.2.4. Correlation with metathesis activity

Increasing the calcination temperature of AA8 catalysts resulted in a marked increase of activity. Here, the calcination temperature of the AP10 catalysts has a smaller impact. Interestingly however, the 400 °C-treated sample is the most active. No discrimination can be made between the three AP10 catalysts on the basis of their texture, their surface composition (XPS)

or their crystallinity (XRD, Raman). In MAS-NMR, the intensity of the [$AlMo_6$] species is similar in both catalysts. A small difference between AP10400 and AP10500 can however be noticed in MAS-NMR spectroscopy: traces of $Al_2(MoO_4)_3$ are detected in the catalyst calcined at 500 °C, while this species is not detected at all in the catalyst calcined at 400 °C. So aluminium molybdate can tentatively be pointed out as responsible for the lower activity of the AP10500 catalyst. The lower activity of the AP10300 catalyst can not be explained at this stage.

The dependence of the metathesis activity of AP catalysts as a function of the MoO_3 loading is different from the relationship established in Chapter 2 and 3 for AA and AOx catalysts respectively. In the present case, a marked increase in activity is observed when the loading rises up to ca. 14 wt. %. The superior activity of AP catalysts in the range of intermediate loading (8-14 wt. %) can be interpreted in relationship with physico-chemical characterization data. Firstly, AP10 and AP14 catalysts are totally amorphous even when the calcination is carried out at high temperature while AA8500 and AA11500 exhibit MoO_3 crystallites (Figure II-6). Exactly like in the case of AOx catalysts, the activity increases linearly with the loading as long as no MoO_3 crystals form. This tends to confirm the deleterious effect of MoO_3 crystals. Secondly, in addition to MoO_3 crystals, $Al_2(MoO_4)_3$ is also clearly present in AA8500 and AA11500, as witnessed by a noticeable peak at -14 ppm (Figure II-10). In the case of AP10 and AP14 catalysts, whether calcined at 400 or 500 °C, this peak is either absent or barely detectable (Figure III-19 and Figure III-20). Again, the presence of aluminium molybdate appears detrimental.

Similar interpretation can be developed to explain why the activity of AP catalysts suddenly drops when the MoO_3 loading is set to 20 wt. % (AP20400 and AP20500). This loading corresponds to the sudden increase in the intensity of the peak at -14 ppm. In fact the amount of $Al_2(MoO_4)_3$ in AP20400 and AP20500 appears similar to the amount detected in AA15500 which itself is a bad metathesis performer.

5. CONCLUSION

The use of alternative precursors for the formation of a MoO_3 active metathesis phase at the surface of a silica-alumina support has been investigated (Scheme III-1). In the first case, oxalic acid was added to a solution of ammonium heptamolybdate. The second precursor solution was obtained by oxidation of metallic Mo with a hydrogen peroxide solution. It is shown that the nature of the precursor can have marked impacts on (i) the transformation of the support and on its reactivity towards Mo species, (ii) on the final catalyst properties and (iii) on the metathesis activity that can be reached.

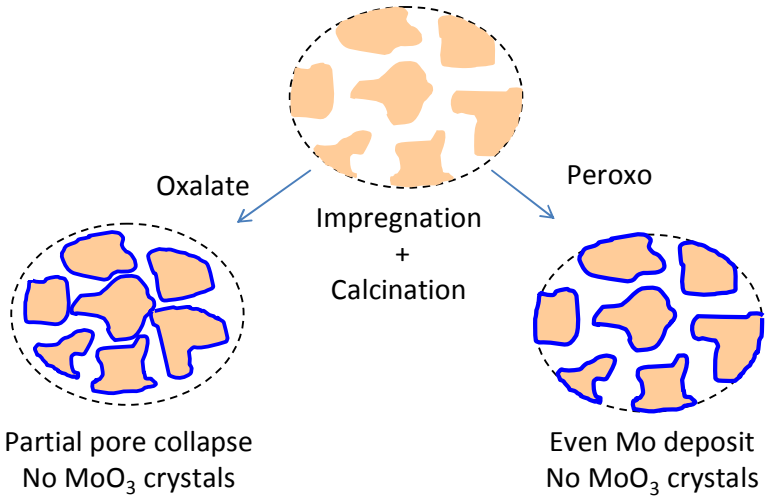

Scheme III-1: Scematic representation of the preparation of MoO_3/SiO_2-Al_2O_3 catalysts via wet impregnation of AHM in the presence of oxalic acid (left) and with a molybdenum oxide hydrates solution obtained for the H_2O_2-assisted oxidation of metallic Mo (right).

The presence of oxalic acid apparently did not lead to the stabilization of oxomolybdenum species with low nuclearity. Instead, the heptamolybdate cluster appears to be preserved. The solution of molybdenum oxide hydrates contains polymeric species like $Mo_8O_{26}^{4-}$ and the presence of species with even higher nuclearity is not ruled out.

Both investigated precursor solutions are very acidic, which has an impact on the support. Indeed, as alumina is known to be prone to dissolution under acidic conditions, partial dissolution of the support during the impregnation step has been evidenced. In the presence of oxalate ligands, the dissolution is more pronounced because the formation of Al-oxalate complexes promotes the dissolution process. As a result, the texture of the samples obtained via impregnation in the presence of oxalic acid is significantly affected.

Unlike catalysts prepared via the impregnation of AHM, the samples obtained via the alternative precursors are totally amorphous whatever their loading and calcination temperature. In the presence of oxalate ligands stable complexes are formed which prevent the formation of [$AlMo_6$] and the rapid precipitation of Mo anions at the outer surface of the support particles. In the case of the impregnation with the molybdenum oxide hydrates solution, Mo atoms appear to be better dispersed down to the bottom of the pores (as compared to impregnation with AHM). In parallel, the formation of [$AlMo_6$] is low. In both cases, the improved dispersion of Mo species on the whole available surface of the support hampers their sintering to MoO_3 crystals.

Aluminium molybdate was also formed to a lesser extent in the catalysts prepared via the alternative precursors. This is explained by the fact that lower amount (if any) of [$AlMo_6$] is formed during impregnation with the ‘Ox’ or the ‘P’ solutions as compared to the case of AHM.

In the end, AOx catalysts do not perform significantly better than AAx500 catalysts. This is tentatively linked to the dissolution of the support which alters the textural properties of the samples and probably causes partial coverage of Mo sites by re-adsorbed Al atoms. However, the activity reached with AOx catalysts is generally higher than what would be expected for catalysts prepared via impregnation of AHM and calcined at the same temperature (AAx400). In addition, the important result obtained with these catalysts is the linear relationship between the MoO_3 loading and the specific activity. This finding is in line with the absence of crystalline MoO_3 and $Al_2(MoO_4)_3$, which further recognizes these species as detrimental for the development of a high metathesis activity.

AP catalysts with intermediate loading are significantly more active than AA catalysts. Here, the limit reached in Chapter 2 is clearly broken. These best catalysts present the combination of favourable factors: the texture of the support is not strongly affected, there is no MoO_3 and only traces of $Al_2(MoO_4)_3$ (if any) are detected. At 20 wt. % loading, the specific activity drops and this phenomenon is correlated with the abrupt production of aluminium molybdate.

CHAPTER 4: FACILE PREPARATION OF MoO_3/SiO_2-Al_2O_3 METATHESIS CATALYST BY THERMAL SPREADING OF MOLYBDENUM OXIDE

ABSTRACT

This chapter reports a very straightforward preparation method to produce active metathesis catalysts. The simple physical mixing of molybdenum oxide with a silica-alumina support followed by an adapted thermal treatment leads to the spreading of Mo oxide species at the surface of the support. Characterization (XRD, in situ XRD, Raman spectroscopy, XPS) shows that the spreading is particularly efficient at low loading. Bulky MoO_3 crystals are converted partly to well-spread MoO_x species in close interaction with the support and partly to very small MoO_3 crystallites. The metathesis activity of these catalysts is in the same order but slightly lower than the activity reached with samples prepared by classical wet impregnation. This study confirms the superior activity of well-spread Mo oxide species as compared to MoO_3 crystallites.

1. INTRODUCTION

In the classical preparation of MoO_3-based metathesis catalysts by impregnation of a support with a Mo precursor – usually ammonium heptamolybdate (AHM) – followed by calcination, the dispersion of the active phase is not really controlled (see Chapter 2). Mastering the nature of Mo surface species that form on the support is not easy. That is, there is no guarantee to obtain a homogeneous deposit at the surface of the support. Two main reasons for this can be cited. Firstly, strong interactions between the species in solution and the support can prevent the species to reach the bottom of pores [98]. In consequence, the Mo deposit is not dispersed on the whole available surface. Agglomerated Mo deposit may be more readily converted to MoO_3 crystals upon calcination. Secondly, the drying step (e.g.: in a rotavapor) implies that part of the support is already dry, sticking on the edge of the flask, while another portion is still in contact with the remaining solution. In these cases the amount of Mo that is actually deposited on different particles of support can be different, which results in different surface densities and uneven distribution of dispersed and agglomerated species. Very often for example, increasing the Mo loading or the calcination temperature unavoidably leads to the formation of MoO_3 crystallites, even though the theoretical monolayer coverage is not reached. In our targeted reaction, such MoO_3 crystals are undesired [64, 88, 96]. This was identified as a limitation for the MoO_3/SiO_2-Al_2O_3 metathesis catalysts presented in Chapter 2. Even if some improvements were reported in Chapter 3, it still appears attractive to search for alternative methods to deposit a Mo oxide phase at the surface of the support.

Several reports from the literature showed that molybdenum trioxide can be transported in the gas phase and spread at the surface of another solid if an appropriate thermal treatment is applied [102, 216]. Recently, such direct thermal spreading (TS) of MoO_3 has been proposed for the preparation of metathesis catalysts [88, 93]. The technique allows getting rid of the wet state step, which is inherently one cause of the lack of homogeneity of catalysts prepared by wet impregnation. An interesting justification for using this technique is the fact that the nuclearity of the transported species is low. Günther et al. proposed that $(MoO_3)_3$ molecules desorb from bulk MoO_3 and

are transported during thermal spreading [217-218]. Indeed, MoO_3 trimers are the major species found in MoO_3 vapour under the range of temperature used for thermal spreading. This is an important difference with the situation encountered in the liquid phase where dissolved polyoxomolybdenum species with high nuclearity may lead to aggregated Mo deposit and may constitute nucleation points for the sintering to MoO_3.

Interestingly, the technique is very easy and cheap: only one step, no waste water and no energy spent for vacuum drying. For the conversion of large amounts of light alkenes in a refinery, such cheap preparation of heterogeneous metathesis catalysts would be highly regarded. In addition, the thermal spreading of MoO_3 could presumably result in catalysts having new physico-chemical properties. By comparison with the catalysts described in previous chapters, one could possibly obtain valuable information on the nature of active (or inactive) Mo species.

In this chapter, catalysts obtained by the thermal spreading of molybdenum oxide on a silica-alumina support are described in detail. The process is also followed by means of in situ X-ray diffraction experiment and its efficiency is assessed by various characterization tools (XPS, TEM, Raman, XRD, MAS-NMR). The catalysts are evaluated in the metathesis of propene and compared with classical catalysts (Chapters 1 and 2).

2. SUMMED UP EXPERIMENTAL

Catalysts were obtained by direct thermal spreading of MoO_3 on the Aldrich silica-alumina support, following the technique proposed by Topka et al. [88]. The desired proportions of Mo trioxide and support are mechanically mixed and ground and then heated at 500 °C for 8 h in static air. Samples are denoted ATS*x* where "A" stands for the Aldrich silica-alumina support, "TS" stands for thermal spreading and where "*x*" is the MoO_3 nominal weight loading (in %).

Raman, XRD, ICP-AES, N_2-physisorption, TEM and XPS characterization have been described earlier (Experimental section, p. 27).

Like in previous chapters, most ^{27}Al MAS-NMR spectra were recorded on samples that were previously stored for several months in a

desicator and often manipulated under ambient condition. No particular care was taken regarding the degree of hydration of the sample. Here, some dedicated experiments were carried out in order to evaluate the impact of the degree of hydration of the sample and of its ageing. A freshly calcined support and a freshly prepared ATS10 catalyst were analyzed rapidly after preparation (after the last thermal treatment, the samples were stored for one night in an oven at 110 °C and then analysed; the only contact with ambient conditions was during ca. 10 min needed for sampling and analysis). The same samples were then also analyzed after a 2-week ageing period under ambient conditions.

For in situ XRD experiments, a HTK10 furnace from Anton Parr was interfaced to the goniometer. The thermal spreading conditions were reproduced in that chamber. The crushed mechanical mixture (about 50 mg) was deposited on a Pt plate and heated to 500 °C under static air. Diffractograms were recorded every hour and also at room temperature before and after that thermal treatment. In addition, the Debye–Scherrer equation was used to estimate the size of the molybdenum trioxide crystals from the width of the peak at 25.7 ° and 27.3 °. The crystallites were considered to be spherical and the peak width for a reference quartz crystal was 0.1 °.

3. RESULTS

3.1. Catalyst characterization

Table IV-1: MoO_3 weight loading (ICP-AES) and textural properties (N_2-physisorption).

Name	MoO_3 loading (wt. %)	SSA ($m^2\ g^{-1}$)	Pore volume ($ml\ g^{-1}$)	Pore diameter (nm)
A	-	490	0.71	5.8
ATS5	4.2	430	0.61	5.6
ATS10	8.9	380	0.56	6.0
ATS14	11.5	350	0.54	6.1
ATS20	16.5	340	0.52	6.0

The MoO_3 weight loading was always found to be fairly lower than the nominal one (Table IV-1). Textural properties of the solids evolve as follows with increasing MoO_3 loading: specific surface area and pore volume decrease steadily while mean pore size diameter is barely affected (slight tendency to increase). These trends are confirmed by the very similar shapes of the pore size distribution curves and by the fact that the curves tend to be lower for each MoO_3 loading increment (Figure IV-1).

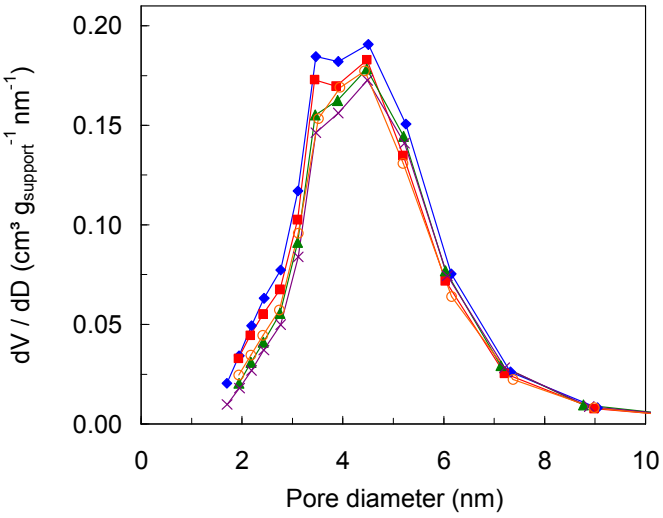

Figure IV-1: Pore size distribution obtained from the BJH method applied on the desorption isotherm on (♦) the support, (■) ATS5, (▲) ATS10, (×) ATS14 and (○) AT20.

An in situ XRD experiment was conducted in order to follow the phenomenon described in the literature as "thermal spreading". This experiment evidenced the progressive disappearance of the MoO_3 crystals provoked by the thermal treatment. In Figure IV-2 the evolution of two main diffraction lines of MoO_3 is followed as a function of time during the thermal treatment conditions. At room temperature, the orthorhombic MoO_3 phase (25.7 ° and 27.3 °, following JCPDS 05-0508) is detected for this 10 / 90 (wt. %) mechanical mixture of MoO_3 and silica-alumina. Increasing the temperature to 500 °C first provokes the conversion of this phase to its monoclinic form (the peak at 25.7 ° shifts to 25.0 ° as per JCPDS 47-1081).

It is obvious that the diffraction lines then disappear progressively with time. The thermal spreading is actually completed after about 10 hours.

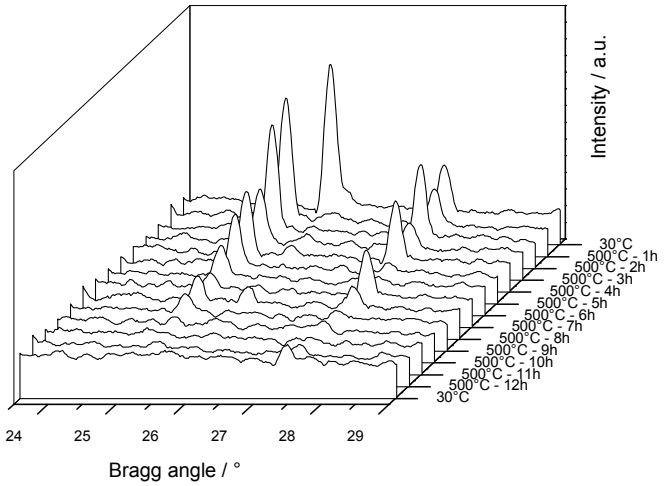

Figure IV-2: In situ XRD investigation of the effect of the thermal treatment at 500 °C of the MoO_3 : SiO_2-Al_2O_3 mechanical mixture (10 % - 90 % in weight).

Consistently with in situ XRD, no MoO_3 crystals were detected in classical XRD surveys (Figure IV-3), even in the catalysts with higher MoO_3 loading. Only a very small diffraction line appears at 27.3°, suggesting the presence of traces of crystalline molybdenum oxide in the catalyst with the highest loading. For the sake of understanding, the complete XRD diffractograms of the 10 : 90 (wt. %) mechanical mixture of MoO_3 and silica-alumina before and after the thermal treatment are compared in Figure IV-4. The Debye-Scherrer equation was applied on the peaks at 25.7° and 27.3° to estimate the average size of the crystals in the commercial MoO_3. The calculation yields a size of ca. 140 nm. It is commonly accepted that the Debye-Scherrer law applies in a range from a few nm to 100 nm. As a consequence, the value determined here is imprecise and should simply be seen as an indication that the crystals are in any case relatively big, with a size clearly higher than 100 nm.

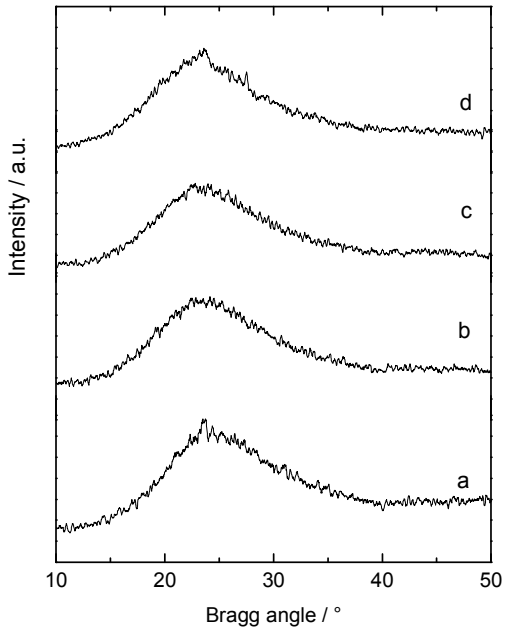

Figure IV-3: XRD patterns of MoO_3/SiO_2-Al_2O_3 catalysts prepared by thermal spreading of MoO_3 at 500 °C: (a) ATS5, (b) ATS10, (c) ATS14 and (d) ATS20.

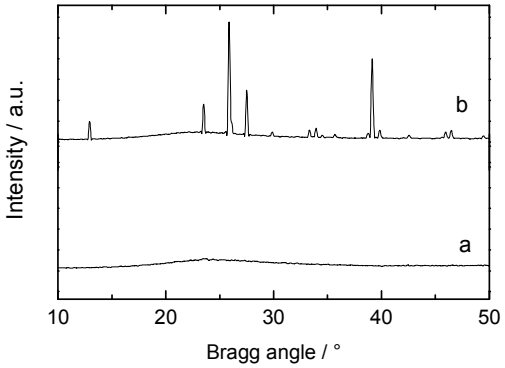

Figure IV-4: Comparison between the XRD patterns of the MoO_3 : SiO_2-Al_2O_3 mechanical mixture (10 % - 90 % in weight) and (b) the catalyst obtained from it after thermal spreading (ATS10).

The mechanical mixture and the corresponding ATS10 catalysts were investigated in transmission electron microscopy (Figure V-5). In the mechanical mixture, irregular particles (presumably consisting in the

agglomeration of smaller particles) are detected with a size in the 100 nm range. These correspond to the support particles. In addition, some big and regular crystals of MoO_3 are observed. Their size is comprised between 100 and 1000 nm. In the ATS10 sample, only irregular particles similar to those observed in the mechanical mixture are distinguished. The particles in Figure IV- 5c appear however slightly different from the ones observed in the fresh mechanical mixture (Figure IV- 5a). It seems that a kind of coating occurred around the particle, like a cement surrounding the irregularities of the particles. In the same time, the bulky regular structures attributed to MoO_3 crystals are not detected anymore in the sample after thermal spreading.

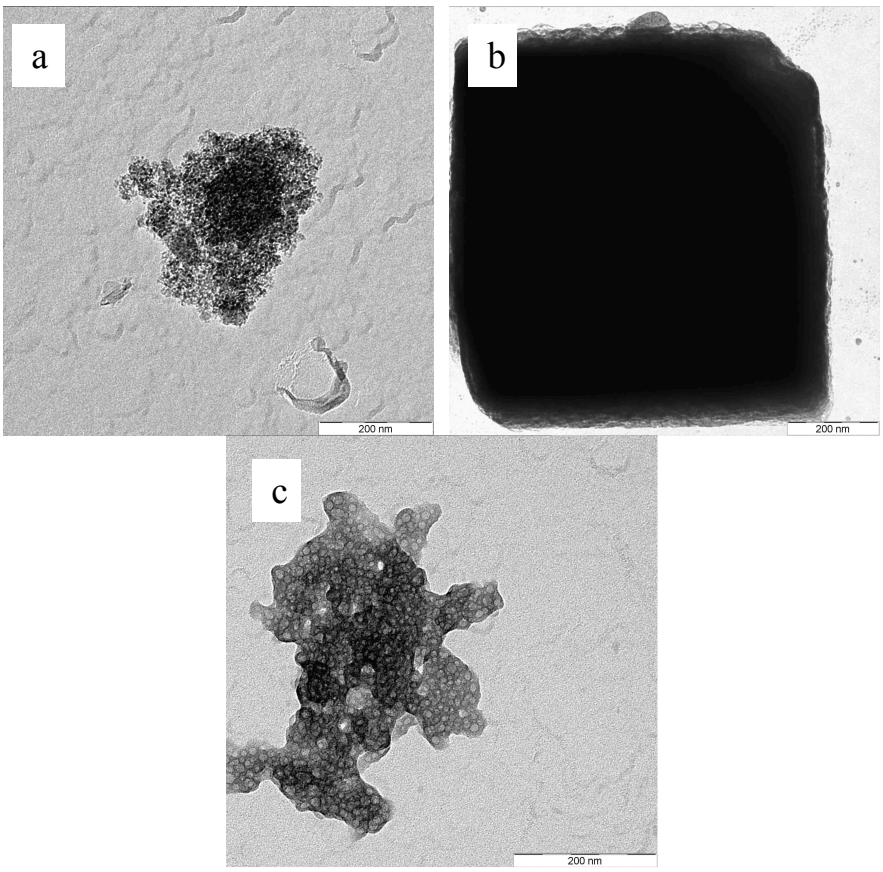

Figure IV- 5: TEM micrographs of (a) a particle of the silica-alumina support found in the 10 : 90 wt. % MoO_3 : SiO_2-Al_2O_3 mechanical mixture, (b) a bulk MoO_3 crystal found in the same mixture and (c) a particle of the ATS catalyst after thermal spreading. Each scale bars represent 200 nm.

In XPS, the proportion of Mo detected at the surface of the 10 : 90 wt. % MoO_3 : SiO_2-Al_2O_3 mechanical mixture is very low. It increases drastically after thermal spreading (Figure IV-6). This evidences unambiguously the spreading of Mo oxide at the surface of the silica-alumina support. When the MoO_3 loading is varied, the Mo / (Si+Al) ratio evolves linearly. The proportion of Mo at the surface is very close to or slightly higher than the proportion of Mo in the bulk composition of the samples. It is noteworthy that this ratio remains lower than in the case of the reference AAx500 catalysts. At 8-10 wt. % loading, the surface of the ATS catalyst exhibits a similar proportion of Mo as in AA8400 and significantly more Mo than in AA8300. In the same way, ATS catalysts exhibit a higher Mo / (Si+Al) atomic ratio than APx catalysts.

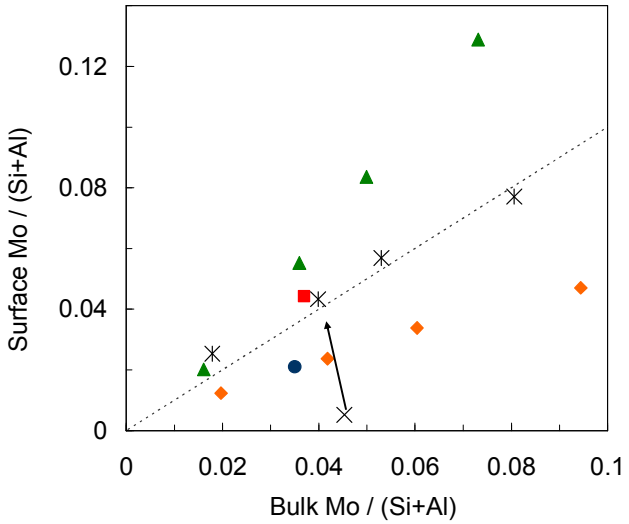

Figure IV-6: Surface Mo / (Si+Al) atomic ratio measured by XPS as a function of the bulk Mo / (Si+Al) ratio for (*) ATSx catalysts and (×) the 10 : 90 (wt. %) mechanical mixture of MoO_3 with the support (before thermal treatment). The arrow indicates the evolution of the Mo / (Si+Al) ratio after thermal spreading. For comparison, the data obtained with (▲) AAx500, (■) AA8400, (●) AA8300 and (♦) APx500 catalysts (Chapters 2 and 3) are also given. The dotted line represents the value expected for totally homogeneous samples (same amount of Mo at the surface and in the bulk). Note: the bulk ratios are calculated from the experimental compostion determined by ICP-AES.

Raman spectroscopy revealed the band attributed to 2D polymolybdates (around 950 cm^{-1}). This indicates that MoO_3 crystals are partly converted into amorphous Mo species during the thermal treatment (Figure IV-7). This band is growing as the MoO_3 loading is increased. However, in contradiction with XRD and from ~8 wt. % loading (ATS10), Raman spectroscopy enlightens the presence of growing amount of crystalline Mo oxide (main sharp bands at 666, 819 and 995 cm^{-1}). Only the ATS5 sample shows absolutely no peak related to MoO_3 crystallites.

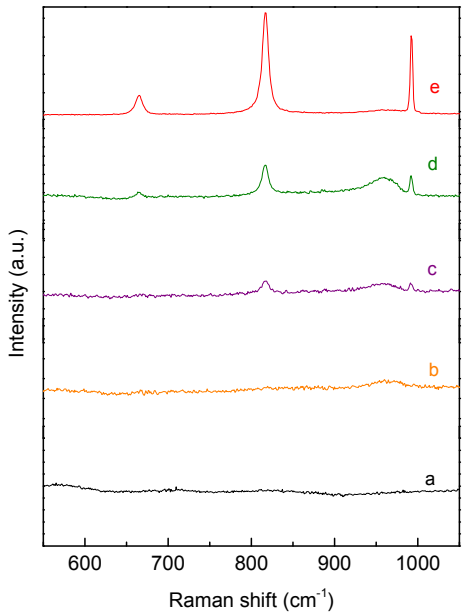

Figure IV-7: Raman spectra obtained on the MoO_3/SiO_2-Al_2O_3 catalysts prepared by thermal spreading of MoO_3 at 500 °C: (a) support, (b) ATS5, (c) ATS10, (d) ATS14 and (e) ATS20. Note: the diffractogram of ATS20 has been attenuated (signal divided by 3) to fit in the artwork. As a result, the noise and the band at 950 cm^{-1} are also graphically attenuated.

The ^{27}Al MAS-NMR spectra of these samples have been recorded (Figure IV-8). The Al_{TET} (54 ppm), Al_{PEN} (30 ppm) and Al_{OCT} (2 ppm) components of the signal are not significantly perturbed by the thermal spreading of MoO_3. On the other hand, a signal appears at ca. 15 ppm,

attributed to [$AlMo_6$]. Its intensity does not seem to increase in line with the MoO_3 loading.

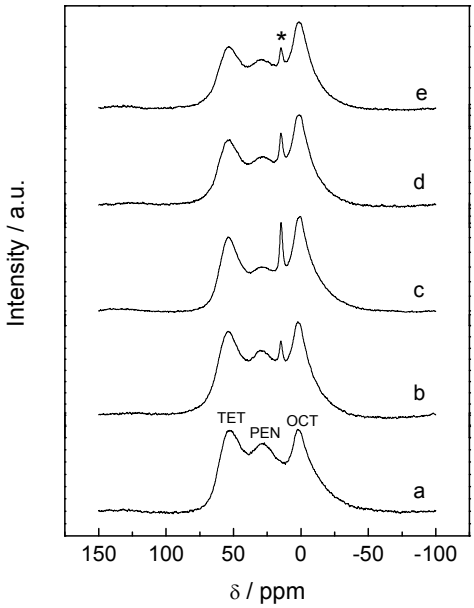

Figure IV-8: ^{27}Al MAS-NMR spectra of (a) the support, (b) AT5, (c) ATS10, (d) ATS14 and (e) AT20. The Al_{TET}, Al_{PEN} and Al_{OCT} broad signals are indicated on the first spectrum. [$AlMo_6$] is marked with "*".

In order to verify the possible effect of ageing on the formation of [$AlMo_6$], one spectrum was recorded directly after the preparation of TS10 (Figure IV-9). No [$AlMo_6$] is detected in this "fresh" TS sample. Leaving the newly prepared TS10 sample on the bench under ambient conditions for two weeks led to the re-appearance of the peak at 15 ppm. This demonstrates that the [$AlMO_6$] species also form upon ageing and not only during the wet step of an impregnation. It was observed also that the proportions of Al_{TET}, Al_{PEN} and Al_{OCT} in the "fresh TS10 catalysts (Figure IV-9) are different from those found classically with aged samples (Figure IV-8). For a comparison purpose the same procedure was applied on the freshly calcined support and on a two-week aged support sample. The same changes in the Al_{TET}, Al_{PEN} and Al_{OCT} proportions were observed and ageing provoked the restoration of

the initially obtained spectra. This shows that such modifications are simply due to the extent of the hydration of the support.

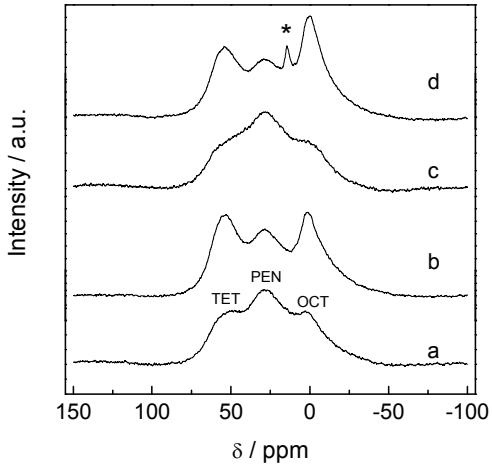

Figure IV-9: ^{27}Al MAS-NMR spectra of (a) the freshly calcined support, (b) the same sample after 2 weeks ageing under ambient conditions, (c) the "fresh" TS10 catalysts, (d) the same TS10 catalyst after 2 weeks ageing under ambient conditions. The Al_{TET}, Al_{PEN} and Al_{OCT} broad signals are indicated on the first spectrum. [$AlMo_6$] is marked with "*".

3.2. Metathesis activity

ATS catalysts were active in the metathesis of propene and their specific activity followed the same evolution with time as previously described for MoO_3/SiO_2-Al_2O_3 catalysts. Figure IV-10 shows that the maximum activity remains quite stable on the whole range of MoO_3 loading investigated. Actually, the activity increases smoothly when the loading increases up to 11.5 wt. % (ATS14). Then the performances level off (plateau or slightly decreasing curve). Figure IV-10 also reports the activity of AAx (Chapter 2) and SA85Mo (Chapter 1) catalysts for the purpose of comparison. At the lowest loading, the ATS catalyst compares very well to catalysts prepared by classical wet impregnation. When the loading increased, ATS catalysts are always fairly less active.

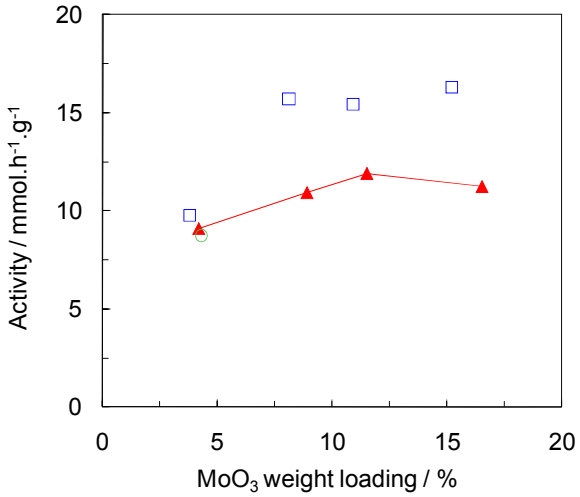

Figure IV-10: Specific activity of (▲) ATSx catalysts, (□) AAx500 catalysts (see Chapter 2) and (○) SA85Mo (see Chapter 1) in the self-metathesis of propene at 40 °C.

4. DISCUSSION

4.1. Feasibility of thermal spreading to prepare metathesis catalysts

The thermal spreading method appears as an attractive route because it is very straightforward. However, as observed from chemical analysis (Table IV-1) part of the MoO_3 introduced in the preparation (typically ca. 15% of the introduced MoO_3) was lost during the preparation, presumably as a result of sublimation. This issue would of course need to be addressed in the perspective of scaled up preparation.

4.2. Conversion of bulk MoO_3 to amorphous surface species

The thermal spreading seems to efficiently convert pure MoO_3 crystals into amorphous molybdenum oxide spread over the surface of the support. Indeed, XRD (ex situ and in situ), XPS and Raman characterizations converge to indicate such conversion. Characterization shows the effects of the thermal treatment: (i) MoO_3 diffraction lines

disappeared entirely (Figure IV-2 and Figure IV-3), (ii) the surface concentration of Mo detected in XPS increased significantly (Figure IV-6), and (iii) a Raman band attributed to amorphous surface polymolybdates appeared (Figure IV-7). MAS-NMR investigations show that intimate interaction is created after thermal spreading between Mo and Al atoms (at least part of them) since an aluminium polymolybdate phase is detected, exactly like in the case of impregnated catalysts (Figure IV-8). This result is further analyzed later in this discussion. The effect of the thermal treatment is also demonstrated in TEM. A first indication that MoO_3 has indeed covered the silica-alumina particles was found via the comparison of the support particles before and after the thermal treatment: it seemed that the particles after thermal spreading are embedded in a MoO_3 film. Note that artefacts are frequent in TEM analysis and this visual effect can not be taken as an irrefutable proof of the thermal spreading of MoO_3. On the other hand the absence of big MoO_3 crystals in the treated samples – while these structures were clearly observed in the fresh mechanical mixture – demonstrates the conversion of MoO_3 crystals upon thermal treatment.

The very low Mo / (Si+Al) atomic ratio determined via XPS at the surface of the mechanical mixture reveals the heterogeneity of the mixture. Would the mixture be really homogeneous (like in a reference compound in which the Mo / (Si+Al) ratio would be fixed by stoichiometry), the ratio would reach the expected value of 0.045 (calculated for a 10 : 90 wt. % mixture of MoO_3 : SiO_2-Al_2O_3). In fact, in the mechanical mixture, MoO_3 is present as bulky 3-dimentional crystals surrounded by smaller silica-alumina particles. When pressed together in the sample holder, only the surface of MoO_3 crystals that reach the 10 nm external surface of the sample will be probed by XPS. Considering the large size of these MoO_3 crystals (as estimated via the Debye-Scherrer equation in XRD and as observed in TEM), a large proportion of Mo atoms will not be detected. This situation is depicted schematically in the upper part of Scheme IV-1. The steep increase in the Mo / (Si+Al) atomic ratio after thermal treatment is unambiguous evidence that the Mo dispersion increases in the sample. If the MoO_x phase is dispersed over the surface of the silica-alumina material (but also if very small crystallites persist), the distribution of Mo atoms in the samples will be more homogeneous. The divergence between surface composition (obtained

via XPS) and bulk composition (nominal composition or experimental composition determined via ICP-AES) will be reduced. The fact that the Mo / (Si+Al) ratio reaches ca. 0.043 in ATS10 shows that a very homogeneous distribution of Mo in the sample is reached (lower part of Scheme IV-1).

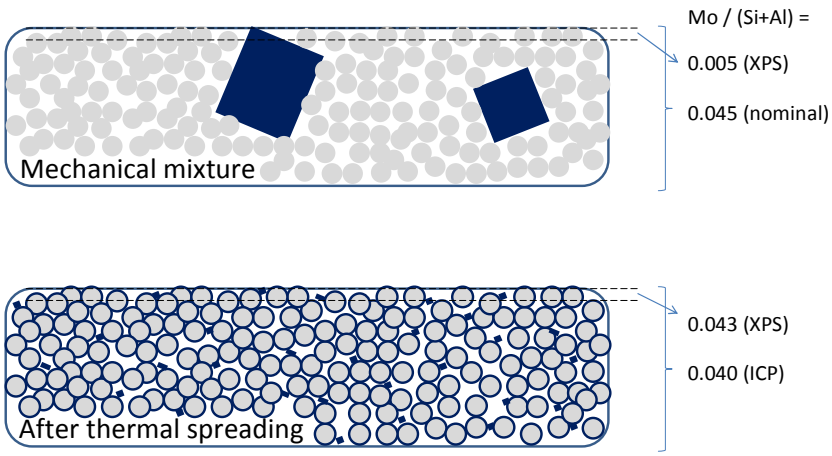

Scheme IV-1: Schematic representation of the mechanical mixture and of the ATS catalysts. In the mechanical mixture, grey balls represent support particles and dark blue squares represent bulky MoO_3 crystals. In the catalyst, after thermal spreading, grey balls surrounded by a blue line represent support particle covered by an amorphous MoO_x phase and small dark blue squares represent persistent MoO_3 crystallites. Dotted horizontal lines schematize the depth explored in XPS (ca. 10 nm). Note: this illustration is drawn as a guide to the eye only; relative proportions in size are not respected.

What is not depicted in Scheme IV-1 is that silica-alumina particles are actually highly porous. Textural analysis showed that the decrease in specific surface area and in pore volume after thermal spreading is relatively important. Figure IV-1 showed unambiguously that the porosity of the support is affected. In parallel, the mean pore diameter remains relatively stable or tends to increase slightly. Results from Chapters 2 and 3 indicated that most Mo atoms were located at the outer surface of the silica-alumina particles in the AAx500 catalysts, while Mo entered the pores of the support in the case of AP catalysts. If the XPS Mo / Si +Al atomic ratio of ATS samples is compared to the same ratio obtained on the catalysts prepared

with impregnation methods (Figure IV-6, Figure II-11 and Figure III-6), it appears that ATS catalysts exhibit more Mo at their surface than APx500 but less than AAx500. Consequently, it can be concluded that Mo oxide indeed gets partly dispersed inside the pores of the support under the effect of the thermal spreading. The transport of Mo thus seems to operate upon relatively large distances and down to confined spaces.

4.3. Incomplete conversion of MoO_3

Raman spectroscopy, in contradiction with XRD, revealed the presence of crystalline MoO_3 species. The fact that these species are detected in Raman spectroscopy but not via X-ray diffraction indicates that crystallites smaller than the XRD detection limit (~5 nm [203]) actually remained in the mixture after thermal spreading. In other words, the spreading was not complete. It should be reminded that the procedure consisted in 8 h of thermal spreading – following the method proposed by Topka et al. [88], while Figure IV-2 indicates that the complete thermal spreading (on XRD analysis basis) is only reached after about 10 h for the 10 : 90 wt. % mixture. A relevant strategy would be to investigate the impact of prolonged thermal spreading time. This effect should in any case be tracked below the XRD detection limit, by means of Raman analysis.

Only in the sample with the lowest MoO_3 loading was the thermal conversion of crystalline MoO_3 to amorphous well-spread MoO_x species complete. At higher loading, the Raman signals related to crystalline MoO_3 increased steeply. In other words, the proportion of Mo atoms that remained in the form of small MoO_3 crystallites was rising.

^{27}Al MAS-NMR results evidenced the presence of [$AlMo_6$] in ATS catalysts. This appeared surprising, since the formation of such compound was discovered – and is very often discussed – for the case of preparation steps involving a solid-liquid interface. It must be remembered however that [$AlMo_6$] can actually form independently from any wet step. Indeed, we showed previously (Chapter 3) that the signal at 15 ppm can appear or increase in calcined catalysts while it is either absent or small in the dried sample (e.g. AOx, AP catalysts). In addition, unambiguous evidence of the conversion of silica-alumina supported MoO_3 crystallites into [$AlMo_6$] under

humid atmosphere was provided by in situ Raman spectroscopy [191]. These results explained the appearance of [$AlMo_6$] in aged samples stored in ambient conditions [185-187]. Our tests on freshly prepared and 2-week aged samples confirm that [$AlMo_6$] was formed during storage and manipulation of the sample under ambient atmosphere.

In previous chapters, a clear link was established between the presence of [$AlMo_6$] in the dried catalyst before calcination, and the subsequent formation of both $Al_2(MoO_4)_3$ and MoO_3. The formation of important amounts of [$AlMo_6$] during impregnation led to increased tendency to form $Al_2(MoO_4)_3$ and MoO_3 upon calcination. Here, only the support and bulk MoO_3 crystals are present when the thermal treatment is carried out. The latter yields catalysts with no trace of $Al_2(MoO_4)_3$. This observation supports the idea that such compound, when present in wet-made catalysts, indeed originated from the transformation of [$AlMo_6$]. It also confirms that [$AlMo_6$] is formed after the thermal treatment. As far as crystalline MoO_3 is concerned, ATS and wet-made catalysts differ also significantly. The small crystallites present in ATS samples clearly originate from the incomplete conversion of MoO_3 crystals, as supported by in situ XRD. On the other hand, bigger crystals (detectable in XRD) were formed in AA catalysts by sintering of an amorphous deposit of polymolybdates, with a probable role of [$AlMo_6$] decomposition. So the origin and size of the crystalline MoO_3 species in both systems are different. It should be noted that the formation of bulk MoO_3 crystals upon calcination of AA catalysts occurred during the 2 hours of thermal treatment at 500 °C. Such crystals could in principle also be subjected to thermal spreading (also carried out in static air at 500 °C). The in situ XRD experiment reported in the present chapter however shows that the thermal spreading of MoO_3 onto the support is slow. It is thus not excluded that better dispersion of MoO_3 in AA catalyst could be obtained provided that longer calcination durations are applied.

4.4. Correlation with metathesis activity

A distinction can be made between ATS5 and the other ATS samples with higher loading in terms of characterization of the Mo oxide deposit. All characterization techniques show that ATS5 is very close to

AA4500 (Chapter 2). In the case of ATS5, the complete conversion of MoO_3 was achieved and this translates into good catalytic performances. The specific activity of ATS5 is perfectly comparable to those of similar samples prepared by classical wet impregnation.

On the other hand, ATS catalysts with higher loading are systematically less active than the reference AAx500 samples. The increase in loading only leads to a very limited increase in activity. Finally, the performances of ATS catalysts level off around 12 mol g^{-1} h^{-1}. The following paragraph is an attempt to correlate the catalytic behaviour of these catalysts with characterization data, in conjunction with previous discussions about wet made catalysts.

As discussed above, in ATS catalysts Mo oxide is partly located at the external surface of the support particles and partly inside the pores. No direct correlation can be made between specific activity and XPS atomic Mo / (Si+Al) ratio. This appeared already from Chapter 3, where AP catalysts performed better than AA catalysts even if less Mo was detected at their surface. The absence of bulk MoO_3 crystals and of $Al_2(MoO_4)_3$ – which have been pointed as inactive in previous chapters – appears encouraging but is not translated into outstanding performances or steep activity increase upon increasing loading. The band detected in Raman spectroscopy at ca. 950 cm^{-1} represents dispersed polymolybdate species which are sometimes proposed to yield the active centres [88]. Even if its intensity tends to increase with increasing loading, the increase in activity does not develop in parallel. In the same time, very small crystallites are detected in Raman spectroscopy. These Raman lines increase steeply when the MoO_3 loading increases. The occurrence of such small MoO_3 crystallites is the only observed characteristic of ATS catalysts that can account for their modest performances. In consequence, not only the bulky MoO_3 crystals detected via XRD or the significant amount of $Al_2(MoO_4)_3$ found on the reference WI samples are responsible for imposing a limit in the activity of MoO_3/SiO_2-Al_2O_3 catalysts. Also the very small (< 5 nm) crystallites left after thermal spreading are identified as inactive in the metathesis reaction.

5. CONCLUSION

The direct thermal spreading of MoO_3 on silica-alumina is a suitable and very convenient method for the preparation of active metathesis catalysts. It avoids the wet state step of classical impregnation methods. As the process is entirely dry, no [$AlMo_6$] is present in the mixture when the thermal treatment is carried out. Thus no conversion into bulk MoO_3 crystals or $Al_2(MoO_4)_3$ occurs under the effect of the treatment at 500 °C. Bulk MoO_3 crystals are partly converted to well-spread amorphous MoO_x surface species via thermal treatment in air. This transformation is especially effective at relatively low loading (ca. 5 wt. % of MoO_3). At higher loading however, MoO_3 crystallites smaller than 5 nm survive the thermal treatment.

Such incomplete spreading of Mo oxide is believed to be the reason for the modest performances of the catalysts obtained via thermal spreading. Indeed, when the spreading is complete (low loading), the activity is comparable to the activity of wet made catalysts, while in the case of incomplete spreading (high loading), the catalysts are less active.

INTERMEDIATE CONCLUSION FOR PART II

This second part investigated alternative modes of deposition of a Mo oxide phase onto a silica-alumina support, with light olefin metathesis as the application for the obtained MoO_3/SiO_2-Al_2O_3 catalysts. In Chapter 3, the wet impregnation method was carried out, in which alternative Mo precursors were used. In Chapter 4, a totally dry route was investigated to disperse directly MoO_3 on the support. The performances of the new materials are compared to the reference samples from Part I.

The addition of oxalic acid in an AHM impregnation solution had marked impacts on the support. Partial dissolution of the aluminic domains of the silica-alumina was promoted by the low pH of the solution and by the complexing effect of oxalate on dissolved Al^{3+} ions. The texture of the solids was significantly affected. The catalysts with relatively high Mo loading exhibited improved metathesis activity.

In the molybdenum oxide hydrates impregnation solution, the Mo speciation is different from the classical heptamolybdate cluster encountered with AHM-based solutions. Upon impregnation of such precursor, the Mo species are dispersed also inside the pores of the support. Improved metathesis activities were reached with catalysts with intermediate MoO_3 loading.

Dispersing MoO_3 directly on the support by means of a simple thermal treatment at 500 °C is a very straightforward method to obtain MoO_3/SiO_2-Al_2O_3 catalysts. These are active in the metathesis of propene. However, the technique is adapted only to the preparation of catalysts with low MoO_3 loading.

In all preparation methods used, the interaction of Mo atoms with Al atoms was tracked via MAS-NMR spectroscopy. The latter revealed a clear link between the presence of [$AlMo_6$] in the sample that is subjected to calcination with the formation of bulk MoO_3 crystals and of significant

amounts of $Al_2(MoO_4)_3$. In AA samples, the amount of [$AlMo_6$] formed during the wet step was high and the production of $Al_2(MoO_4)_3$ and bulk MoO_3 crystals was important. In AOx samples, no [$AlMo_6$] was present after impregnation and only traces of $Al_2(MoO_4)_3$ were formed in the catalyst having the highest loading. Not even traces of MoO_3 crystals were detected. In AP catalyst, small amount of [$AlMo_6$] in the dried catalyst led to a small amount of $Al_2(MoO_4)_3$ (depending also on the loading and calcination temperature) in the calcined samples. It appears that $Al_2(MoO_4)_3$ is the first species to be formed upon calcination of a sample which contains significant amounts of [$AlMo_6$]. Bulk MoO_3 crystals are only formed when the amount of [$AlMo_6$] is higher. In link with activity evaluations it can be concluded that $Al_2(MoO_4)_3$ and crystalline MoO_3 do not yield active metathesis sites. Indeed, when MoO_3 builds up, the metathesis activity is levelling off. In this case, $Al_2(MoO_4)_3$ is also present. When crystalline MoO_3 is not present, the amount of $Al_2(MoO_4)_3$ is inversely correlated with the metathesis activity.

In the case of the dry preparation step (thermal spreading), bulk MoO_3 crystals and $Al_2(MoO_4)_3$ are not formed, which has to be correlated to the absence of [$AlMo_6$] in the treated mechanical mixture (only MoO_3 and the support). This advantage however does not translate into high metathesis activity. The reason for that is the incomplete conversion of MoO_3 into dispersed surface molybdate. Presumably, the proportion of Mo atoms that remain in small MoO_3 crystallites is high and these species are not active in the metathesis either.

Likely, the presence of [$AlMo_6$] at the moment of the calcination has a negative impact for the above-mentioned reasons. However, it seems probable also that the intimacy between Al and Mo atoms in the final catalyst is a positive parameter for the development of active metathesis centres. Two general observations support this idea. Firstly, the conclusions of Chapter 1 stress the importance of Al atoms. Secondly, a rough classification of the catalysts indicates that the systems in which an intimate contact between Al and Mo atoms was favored perform better: AP (intermediate loading) ≈ AOx (high loading) > AA > ATS. This intimacy between Mo and Al atoms should however not take the form of $Al_2(MoO_4)_3$.

Finally, it should be stressed that in the case of such metathesis systems, the species which are difficult to characterize by means of physico-chemical characterization are actually those species which are thought to yield the active metathesis centres. Mo atoms which are not included in MoO_3 crystallites or $Al_2(MoO_4)_3$ but are converted into dispersed Mo surface species are indeed not described precisely. Only the broad band at ca. 950 cm^{-1} detected in Raman is an indication of the stabilisation of amorphous species, probably prone to generate active sites. However, it is not excluded that the very small proportion of Mo atoms that actually turn out to be active after activation are not detected at all by the set of characterization tools employed here. For example, the presence of a limited amount of isolated – or monomeric – molybdates at the surface of the support would be difficult to evidence via Raman (broad and potentially overlapping Raman bands, strong background, etc.) or via another characterization tool. So the precise identification of the nature of the active metathesis centres is still unclear.

Part III

On an innovative one step preparation of metathesis catalysts

ABSTRACT

The previous parts of this document have enlightened the good performances of MoO_3/SiO_2-Al_2O_3 catalysts in the metathesis of propene and the superior activity of highly dispersed Mo species. These findings have oriented our attention to an interesting mode of preparation of oxides: the non-hydrolytic sol-gel chemistry. This technique proved to be effective in designing solids with tailored composition, texture and homogeneity.

In this part, MoO_3-SiO_2-Al_2O_3 mixed oxides are prepared via non-hydrolytic sol-gel and characterized extensively. The location of the Mo species in such solids is investigated particularly with the help of surface and bulk characterization tools. The impact of the composition, in terms of MoO_3 loading and of Si/Al ratio on the properties of the solids is evaluated. The astonishing metathesis activity of these new materials is then interpreted in the light of an intensive survey on their solid state chemistry.

CHAPTER 5: PREPARATION OF MoO_3-SiO_2-Al_2O_3 METATHESIS CATALYSTS BY A ONE-STEP NON-HYDROLYTIC SOL-GEL ROUTE

ABSTRACT

MoO_3-based catalysts prepared by the dispersion of Mo-oxide on preformed supports perform well in the light olefin metathesis. An original alternative approach for the elaboration of Mo-based catalysts is presented in this chapter. Mesoporous ternary Si-Al-Mo mixed oxides are prepared in one step, via non-hydrolytic condensation of chloride precursors. After calcination, effective catalysts with very good textures and highly dispersed surface Mo species are stabilized. Upon optimization of the composition, these new materials markedly outcompete the catalysts prepared by the wet impregnation of SiO_2-Al_2O_3 supports with Mo precursors. The stabilization of isolated Mo species is evidenced and these species are proposed to be the main active species in the metathesis of propene.

1. INTRODUCTION

From the previous chapters of this thesis, it is known that MoO_3/SiO_2-Al_2O_3 catalysts perform well in the metathesis of propene. Our results and several other works indicate the superior activity of highly dispersed Mo species. Also the intimate interaction of Mo species with the support seems to be crucial. Classical catalyst preparation methods systematically consist in two-step procedures in which the support – prepared or bought in the first step – is covered by the active phase in the second step. This strategy implies limitations such as the lack of homogeneity of the active phase deposit (e.g.: formation of crystals in Chapter 2), the loss of interesting textural properties of the support (e.g. pore collapse in Chapter 3) or the lack of interaction between the active phase and the support (incomplete spreading of MoO_3 in Chapter 4). It appears that, even with elaborate impregnation methods, obtaining a molecular-scale dispersion of Mo species at the surface of a pre-existing support remains difficult.

In this context, sol-gel processes leading to MoO_3-SiO_2-Al_2O_3 mixed oxides appear interesting. Mixed oxides have a tremendous importance as catalysts and catalyst supports and sol-gel processes provide versatile routes for their synthesis [219-221]. However, in most cases a large part of the active species are not accessible to the reactants, and the direct sol-gel preparation of elaborate catalysts involving an active oxide phase dispersed at the surface of a mixed oxide support remains a challenge. This difficulty explains why such catalysts are usually prepared indirectly, for instance by grafting or impregnation of preformed supports [222-223]. Conventional sol-gel routes are based on the hydrolysis and condensation of molecular precursors, usually alkoxides. In particular, for SiO_2-based materials, the very different reaction rates of metal and silicon precursors make the simultaneous control of the structure and texture of mixed oxide gels difficult. Thus, even for relatively simple binary oxides such as SiO_2-TiO_2, complicated experimental procedures are required to prepare homogeneous mesoporous materials, including prehydrolysis of the less reactive precursors or modification with chelating agents of the more reactive ones, and low-temperature extraction with supercritical CO_2 (aerogels) [224].

Conversely, non-hydrolytic routes [119] based on the reaction of chloride precursors with alkoxide precursors or diisopropyl ether were shown to provide an excellent control over the stoichiometry and the homogeneity of mixed oxide gels [121]. Furthermore, owing to the generally high degree of condensation of non-hydrolytic gels, mesoporous xerogels with high surface area and pore volumes can be obtained by simple evaporative drying, thus avoiding the supercritical drying step. Accordingly, these non-hydrolytic routes are attracting increasing attention for the preparation of mixed oxide catalysts [64, 120, 122, 124-126, 128-131, 225-233]. Nevertheless, most of these studies concern binary mixed oxides and reports on the preparation of materials based on three different oxides are rare [64, 124, 128, 131].

In the framework of our study, non-hydrolytic sol-gel chemistry appears as a promising tool for the controlled preparation of MoO_3-based metathesis catalysts. From a fundamental point of view, the physico-chemical properties of the new solids might differ notably from those of more classical catalysts, which could bring new insights on the nature of active metathesis centres. Particularly, the nature of the Mo surface species will tentatively be described in more details. For that purpose, time-of-flight secondary ion mass spectroscopy will be used to gain further insights on the surface chemistry of these new systems.

This chapter reports the first direct non-hydrolytic sol-gel synthesis of SiO_2-Al_2O_3-MoO_3 olefin metathesis catalysts with well-controlled textures and composition. The materials are obtained in one step by reaction of low-cost[4] chloride precursors and diisopropyl ether. The strategy was to explore catalysts with compositions similar to classical impregnated catalysts. Two parameters of the preparation are screened: the SiO_2/Al_2O_3 ratio and the MoO_3 loading. In addition, dedicated experiments were carried out to track the possible mobility of Mo atoms in the xerogel under the effect of thermal treatment. Such migration was indeed anticipated considering the low Tammann temperature of molybdenum oxide. The structure and the catalytic activity in the self-metathesis of propene of these sol-gel materials are systematically compared to those of catalysts prepared by wet

[4] As compared to the corresponding alkoxide precursors.

impregnation of a commercial silica-alumina support with ammonium heptamolybdate (AAx500, Chapter 2).

2. SUMMED-UP EXPERIMENTAL SECTION

The samples were prepared by a one-step non-hydrolytic sol-gel route, involving the reaction at 110 °C under autogeneous pressure of $SiCl_4$, $AlCl_3$ and $MoCl_5$ precursors with diisopropyl ether ($^iPr_2O$) in CH_2Cl_2 as described in the Experimental section, p. 26. The amounts of precursors and reactants involved in the preparation of each non-hydrolytic sol-gel catalysts are reported in Table V-1. These samples are labelled NH_Y_X, where NH stands for "non-hydrolytic sol-gel", where Y represents the Al_2O_3 weight content (in %) and where X represents the MoO_3 weight loading (in %). Actually, in the NH_5_X samples (when the MoO_3 loading is screened), the nominal Al_2O_3 content is only approximately 5 wt. %, because it was chosen to keep the SiO_2/Al_2O_3 ratio constant (and equal to 17, as in NH_5_10). The precise nominal Al_2O_3 content is 5.3, 5.0, 4.7 and 4.4 wt. % for NH_5_5, NH_5_10, NH_5_15 and NH_5_20 respectively. The preparation of NH_5_10 was done twice and independently to check the reproducibility of the preparation route (samples noted NH_5_10a and NH_5_10b). All samples were calcined at 500 °C for 5 hours in flowing air (50 ml min^{-1}).

Table V-1: Amount of reactants involved in each preparation

	$SiCl_4$ (g)	$AlCl_3$ (g)	$MoCl_5$ (g)	$^iPr_2O$ (g)	CH_2Cl_2 (ml)
NH_0_10	7.733	-	0.572	8.258	14
NH_5_10a	7.196	0.394	0.570	8.400	14
NH_10_10	7.027	0.773	0.567	8.248	14
NH_15_10	6.309	1.178	0.572	8.258	14
NH_20_10	5.885	1.563	0.568	8.145	14
NH_5_0	8.042	0.470	-	8.790	14
NH_5_5	5.858	0.278	0.188	6.677	14
NH_5_10b	4.499	0.263	0.384	6.347	14
NH_5_15	4.793	0.245	0.568	5.885	14
NH_5_20	4.280	0.230	0.751	5.719	14

N_2-physisorption, ICP-AES, XRD, TEM and XPS techniques were conducted as depicted in the Experimental section, p. 26.

Positive and negative time-of-flight – secondary ion mass spectrometry (TOF-SIMS) measurements were performed with a Charles Evans & Associates spectrometer [234]. In the TOF-SIMS experiments, the sample was bombarded with pulsed Ga^+ ions (15 keV). The secondary ions were accelerated to ± 3 keV by applying a bias on the sample. The spreading of the initial energies of the secondary ions is compensated by deflection in three electrostatic analysers. In order to increase the detection efficiency of high mass ions, a post-acceleration of 15 keV was applied at the detector entry. The analyzed area used in this work was a square of 120 µm x 120 µm. With a data acquisition time of 5 min, the total dose was about 10^{12} ions cm^{-2}, which ensured static conditions. Charge effects were compensated by means of a pulsed electron flood gun (E_k = 24 eV). For the powders analyzed in this work, a stainless steel grid (non magnetic) with openings of 2 mm was placed onto the sample surface in order to prevent variations of the surface potential. The data acquisition and treatment were made using the software developed by Charles Evans & Associates. The best mass resolution obtained with this TOF-SIMS spectrometer is $M/\Delta M \approx 11000$ at m/z = 28 on a Si wafer. The mass resolution was about 3000 at m/z = 29. This highly facilitated the assignment of ions having the same nominal mass but different compositions. The powders were pressed on a double-face silver tape. The amount of powder was adjusted to keep the layer thickness as small as possible (in order to facilitate the surface potential control during the analysis) but large enough to prevent detection of the substrate by TOF-SIMS. Relative intensities of Mo^+ ion were calculated by dividing the sum of the contribution of the three main isotopes of Mo (m/z = 92, 98 and 100) by the sum of all significant contributions. The ions taken into consideration in this sum are H^+, CH_3^+, NH_4^+, Al^+, Si^+, $SiOH^+$, $^{92}Mo^+$, $^{98}Mo^+$, $^{100}Mo^+$, $^{92}MoO^+$, $^{98}MoO^+$ and $^{100}MoO^+$.

The acidity of selected samples was evaluated by NH_3-temperature programmed desorption (NH_3-TPD) on a Micromeritics AutoChem 2910 apparatus with a thermal conductivity detector (TCD). A 500 mg sample was preheated in air flow at 500 °C for 30 min (ramp 10 °C min^{-1}). Adsorption of NH_3 (5 vol. % in helium; flow rate 30 ml min^{-1}) was done at 100 °C for 45 min. Physisorbed NH_3 was removed by purging with helium at 100 °C for 1

hour (flow rate 30 ml min^{-1}). The TPD measurement was conducted by heating the sample from 100 to 600 °C at a 10 °C min^{-1} rate.

3. EFFECT OF Si/Al RATIO IN SiO_2-Al_2O_3-MoO_3 CATALYSTS

3.1. Results

3.1.1. Catalysts characterization

In the first set of samples (Table V-2), the Si/Al ratio was varied and the nominal MoO_3 wt. loading was kept constant at 10 wt. %. The range of SiO_2/Al_2O_3 ratio explored varied from infinite (no alumina in NH_0_10) to 3.5 (20 % of alumina in NH_20_10). Chemical analyses by ICP-AES show that the experimental compositions compare well to nominal ones.

Table V-2: Chemical analysis (ICP-AES) and textural properties (N_2-physisorption) of the samples with variable Al_2O_3 content.

	Composition (wt. %) $SiO_2 : Al_2O_3 : MoO_3$	SSA ($m^2\ g^{-1}$)	Vp (ml g^{-1})	Dp (nm)[a]	SSAμ ($m^2\ g^{-1}$)[b]
NH_0_10	90.3 : 0.0 : 9.7	740	1.1	5.8	70
NH_5_10a	83.9 : 5.4 : 10.7	520	1.5	12.0	40
NH_10_10	79.9 : 10.0 : 10.1	330	0.6	7.8	30
NH_15_10	74.0 : 15.4 : 10.5	200	0.3	6.5	30
NH_20_10	68.8 : 19.4 : 11.8	190	0.3	6.7	30

[a] Average pore diameter ($4\ V_P/SSA_{BET}$)
[b] From *t*-plot analysis in the 0.35 – 0.5 nm range

All samples were mesoporous, with N_2 adsorption-desorption isotherms of type IV, according to the BDDT classification (Figure V-1). The specific surface area of the SiO_2-MoO_3 catalyst (NH_0_10) reaches 740 $m^2\ g^{-1}$. In alumina-containing samples the surface tends to decrease as the alumina content increases. Also, the pore volume and the mean pore size diameter of alumina-containing samples tend to decrease with increasing Al_2O_3 content. The NH_0_10 sample steps out of this trend with rather small mean pore size diameter and intermediate pore volume. *t*-Plot analysis indicated that the surface area developed by micropore walls (denoted SSAμ) was low.

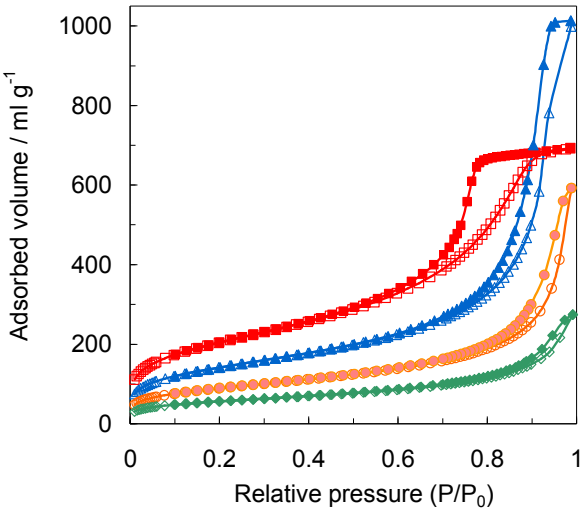

Figure V-1: N_2 adsorption-desorption isotherms of NH_Y_10 samples. Filled symbols are used for desorption isotherms: (■) NH_0_10, (▲) NH_5_10, (●) NH_10_10, (♦) NH_15_10 and the corresponding open symbols are used for adsorption isotherms. The isotherms of NH_20_10 catalyst are superimposed to those of NH_15_10 and are not shown for the sake of clarity of the figure.

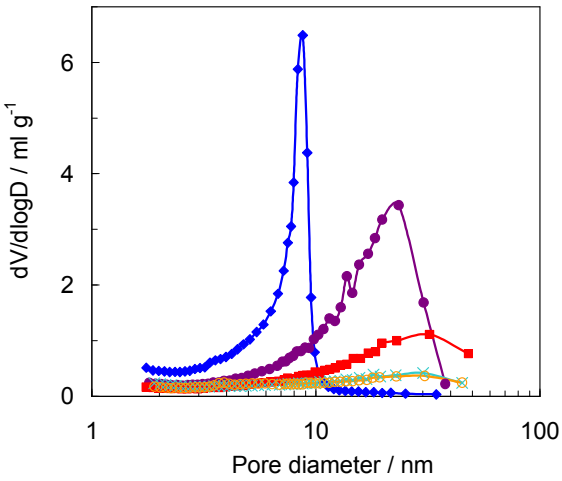

Figure V-2: Pore size distribution of (♦) NH_0_10, (●) NH_5_10, (■) NH_10_10, (×) NH_15_10 and (○) NH_20_10.

Transmission electron microscopy (TEM) of the NH_5_10 sample showed the presence of porous particles in the 200-1000 nm range, with mesopores in the 2-15 nm range (Figure V-3).

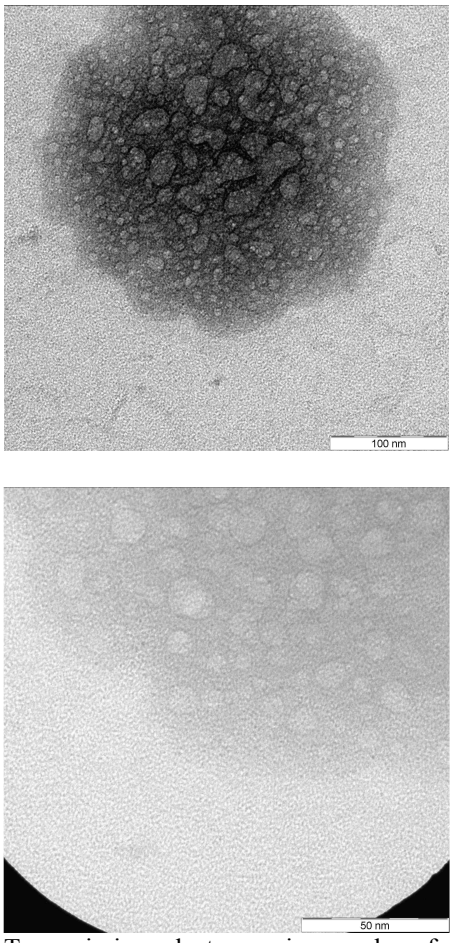

Figure V-3: Transmission electron micrographs of the NH_5_10 sample. Upper image: one microparticle (scale bar = 100 nm). Lower image: edge of one microparticle in inverted contrast mode (scale bar = 50 nm)

Temperature programmed desorption of ammonia (NH_3-TPD) was used to probe the acidity of the NH catalysts (Figure V-4). The thermogram obtained for NH_0_10 showed a broad desorption profile centered at 205°C and indicating the presence of weak acidic sites. The thermograms of all Al-containing samples showed that ammonia desorbed up to 500 °C, indicating the presence of acidic sites with higher strength. Their acidity is intermediate between the weakly acidic sites of silica and the highly acidic sites found in zeolites [235]. Following the method of Katada et al. [236] one Gaussian function was fitted to the peak centred at 205 °C and attributed to weak

acidic sites. The rest of the peak was attributed to medium and strong acidic sites (the further deconvolution of this high temperature peak appeared too delicate). Table V-3 gives the total amount of ammonia desorbed from each sample, as well as the density of acidic sites derived from this value and from the specific surface area of each catalyst. It appears that (i) the total acidity reaches a maximum for the sample with 10 % Al_2O_3 (NH_10_10), while the maximum in terms of surface density of acidic sites is reached for the NH_15_10 sample and (ii) the proportion of medium and strong acidic sites continuously increases as the alumina content increases.

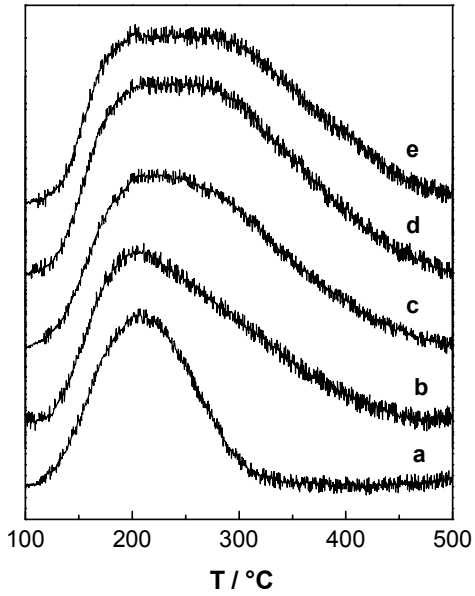

Figure V-4: NH_3-TPD thermograms obtained from (a) NH_0_10, (b) NH_5_10a, (c) NH_10_10, (d) NH_15_10 and (e) NH_20_10.

Table V-3: Acidity measured by NH_3-TPD.

	NH_3 desorbed (mmol g^{-1})	Density of acid site (nm^{-2})	Density of weak sites (nm^{-2})[a]	Density of medium + strong sites (nm^{-2})[a]
NH_0_10	0.9	0.7	0.7 (100 %)	0 (0 %)
NH_5_10a	1.0	1.2	0.8 (70 %)	0.4 (30 %)
NH_10_10	1.6	2.6	1.5 (59 %)	1.1 (41 %)
NH_15_10	1.5	4.2	2.3 (54 %)	1.9 (46 %)
NH_20_10	1.4	3.9	2.0 (52 %)	1.9 (48 %)

[a] under brackets is given the proportion of weak or medium + strong sites.

The XRD patterns of the NH samples presented in all cases a broad band around 20-25° typical of amorphous solids. There was no evidence of crystalline molybdenum oxide in the patterns of the sol-gel samples, showing that no MoO_3 crystallites larger than the detection limit – about 5 nm [203] – were present.

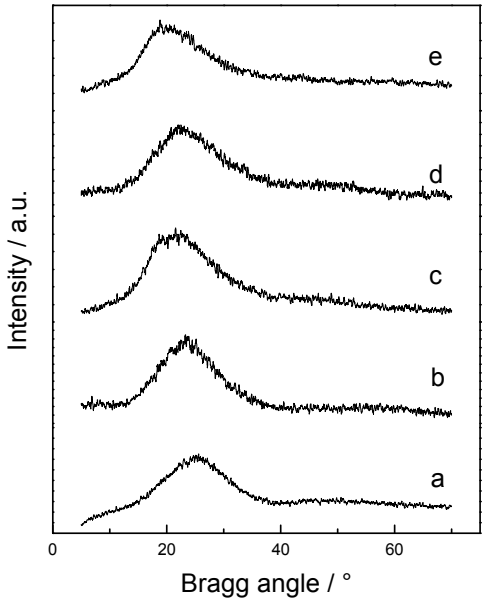

Figure V-5: XRD diffractograms of (a) NH_0_10, (b) NH_5_10a, (c) NH_10_10, (d) NH_15_10 and (e) NH_20_10.

From Raman spectroscopy the presence of MoO_3 crystallites is ruled out for all investigated NH catalysts (Figure V-6). The molybdenum species present in these samples are not easy to describe by Raman spectroscopy. In most cases, no band attributable to MoO_x species are detected on the background of the spectra, itself presumably originating from complex vibration modes of the silica-alumina matrix and of a broad and intense signal due to the fluorescence of impurities. It is noticeable that this background becomes increasingly intense as the alumina content in the catalyst increases, thereby supporting the idea of increasing amount of defects in the structure of the silica-alumina matrix as the Al content increases. The NH_0_10 catalyst is the only sample for which the

background was not too intense and for which two broad bands could be distinguished. Their maxima appear around 871-878 cm^{-1} and 945-950 cm^{-1}. The most intense peak is classically attributed to the terminal ν(Mo=O) vibration in amorphous polymeric MoO_x species [99, 162], while the other band is attributed to the vibration of Mo-O-Mo bonds in polymers of octahedral MoO_6 units [205] or to isolated tetrahedrally coordinated Mo atoms [99].

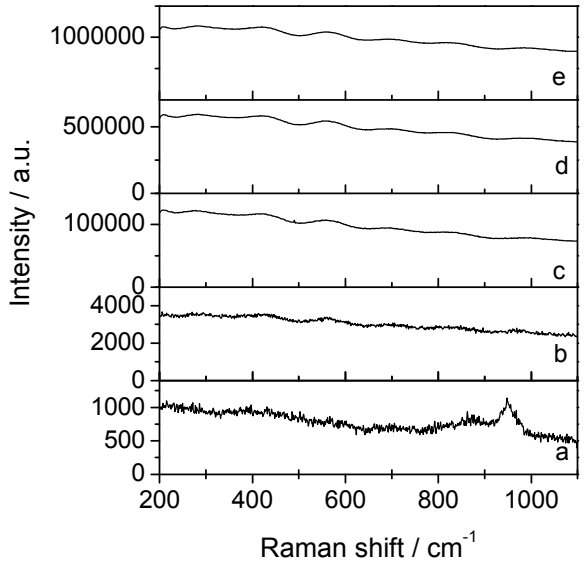

Figure V-6: Raman spectra of (a) NH_0_10, (b) NH_5_10a, (c) NH_10_10, (d) NH_15_10 and (e) NH_20_10.

The surface of the catalysts has been studied by XPS (Table V-4). Figure V-7 provides a convenient view of three important observations that can be done from XPS analysis. Firstly, the variation in the nominal Si/Al ratio is also detected at the surface: the Al surface concentration increases linearly with increasing Al_2O_3 content. Secondly, the Mo surface concentration tends to decrease with increasing Al_2O_3 content. Thirdly, C surface concentration tends to increase with increasing Al_2O_3 content. This has to be correlated with the fact that the acidity increases with the Al content. As the surface becomes more acidic, it tends to adsorb higher

amounts of volatile organic compounds (natural atmospheric compounds or oil vapours from the XPS vacuum pumps).

Table V-4: Surface composition analyzed by XPS

	Si (at. %)	Al (at. %)	Mo (at. %)	O (at. %)	C (at. %)	Surface composition SiO_2 : Al_2O_3 : MoO_3 (wt. %)
NH_0_10	31.06	0.00	1.16	65.18	2.60	91.8 : 0.0 : 8.2
NH_5_10a	27.12	2.26	0.98	64.56	5.09	86.4 : 6.1 : 7.5
NH_10_10	27.90	3.60	0.93	62.52	5.06	84.1 : 9.2 : 6.7
NH_15_10	25.42	5.48	0.91	62.37	5.81	78.8 : 14.4 : 6.8
NH_20_10	24.72	7.21	0.89	61.22	5.96	75.0 : 18.5 : 6.5

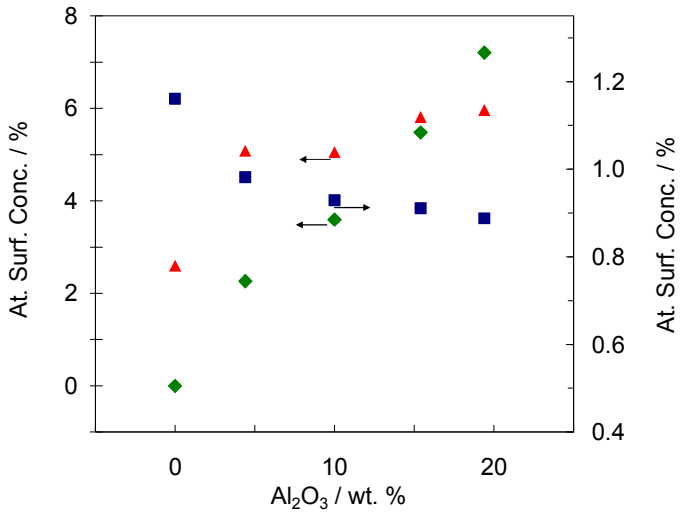

Figure V-7: Aluminium (♦), molybdenum (■) and carbon (▲) atomic surface concentration measured via XPS on NH_Y_10 samples.

The surface composition in terms of oxides has been calculated, under the approximation that every Si, Al and Mo atoms are in the oxide form and thus considering the stoichiometry of SiO_2, Al_2O_3 and MoO_3 respectively to calculate the values given in the last column of Table V-4. Carbon, water and other impurities are omitted. This surface composition is thus directly comparable to the bulk composition presented in Table V-2. It appears that the proportion of MoO_3 at the surface is slightly lower as

compared to the bulk. In other words, there is a tendency of Mo atoms to preferentially remain in the bulk of the solids. This tendency is more pronounced for catalysts with higher alumina content.

3.1.2. Metathesis activity

All NH samples were active in the self-metathesis of propene. The evolution of the metathesis activity with time on stream (Figure V-8) was very similar to those already reported in previous chapters for other MoO_3/SiO_2-Al_2O_3 catalysts. In most cases, the activity increases during the first 20 minutes of the test and then a slow deactivation occurs. The alumina-free sample is the noticeable exception. No activation period is observed and the activity – which is already the lowest initial activity measured for this set of catalysts – decreases readily. The rate of deactivation is evidently higher. Among Al-containing samples, the performances tend to increase as the Al_2O_3 content decreases. Remarkably, the NH_5_10 sample is much more active than the other Al-containing samples.

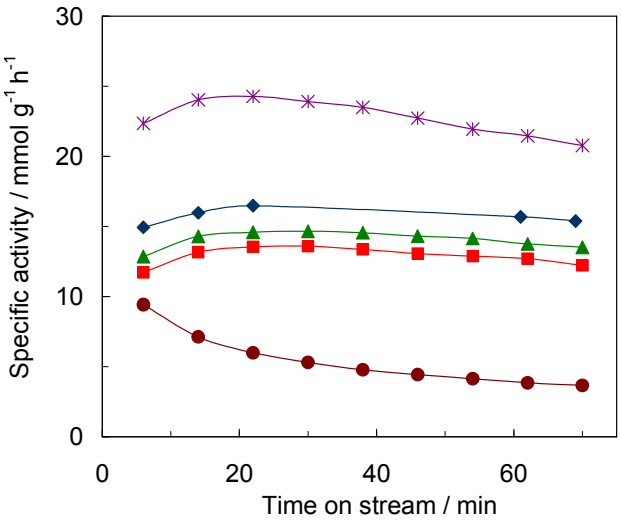

Figure V-8: Evolution of the specific metathesis activity with time on stream. (●) NH_0_10, (*) NH_5_10, (♦) NH_10_10, (▲) N_15_10 and (■) NH_20_10. Note: a technical problem occurred on the GC apparatus during the test of NH_10_10, interrupting the analysis for some minutes.

3.2. Discussion

3.2.1. Composition, texture and acidity of the catalysts

As far as light olefin metathesis is concerned, formulations involving three different oxides (Mo, Si and Al) are highly recommended (see ref. [86] and Chapter 1). The need for acidity of the metathesis catalysts is a well-known fact and we show here that introducing alumina in NH systems results in an increase in acidity (as further discussed below). The difficulty to design ternary mixed oxides including silica and a transition metal oxide with classical hydrolytic sol-gel technology (related to the very different reaction rates of silicon and metal precursors) is solved by using non-hydrolytic sol-gel chemistry. The good agreement between experimental and nominal compositions shows that the non-hydrolytic route used offers an excellent control over the composition of the materials. It shows that no metallic species was lost in the liquid phase or in the gas phase during the drying step. Moreover, non-hydrolytic sol-gel also provides materials with satisfactory textures: the catalysts are mesoporous with high surface areas and pore volumes. TEM images are consistent with N_2-physisorption measurements in showing highly porous materials. The porosity and the specific surface area developed by the samples were shown to decrease markedly upon Al introduction. This phenomenon seems to be intrinsic to silica-alumina based systems (see Chapter 2 and ref [132-133, 141]).

In the same way, the fact that the samples are totally amorphous (Figure V-5) is very encouraging, since MoO_3 crystals were identified as inactive species. Raman characterization allows going further in the description of the Mo species. In the NH_0_10 sample only amorphous MoO_x species are detected. These are present in the form of surface polymolybdates or isolated molybdates. The absence of MoO_3 crystals in this sample is noteworthy because it is well recognized that molybdenum oxide usually tends to form bulky crystals in MoO_3/SiO_2 catalysts prepared via classical techniques. The preferential formation of Mo-O-Mo bridges instead of Mo-O-Si bonds is driven by the acid-base nature of the interactions between silica and molybdena [237]. Both are acidic, so the interaction between both materials tends to be very weak and calcination usually leads to sintering of crystalline species. For comparison purpose, a

MoO_3/SiO_2 catalyst with exactly the same nominal composition as NH_0_10 was prepared via wet impregnation (WI) of a silicagel (Degussa Aerosil 200) with ammonium heptamolybdate, followed by evaporation, drying and calcination at 500 °C. The preparation procedure is identical to the one described for the preparation of AAx500 catalysts (Chapter 2). Figure V-9 shows a direct comparison of the Raman spectra of the non-hydrolytic sol-gel prepared catalyst and of the wet impregnated catalyst. The marked tendency of the MoO_3/SiO_2 catalyst obtained by WI to form bulk MoO_3 crystals (main sharp bands at 994, 819 and 666 cm^{-1} and smaller bands at 376, 335, 288 and 241 cm^{-1}) is evident. The opposite tendency is observed in NH_0_10: only two broad bands are detected, corresponding to amorphous MoO_x species.

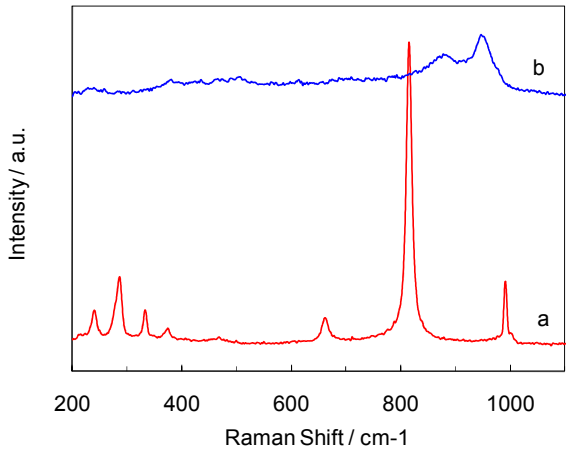

Figure V-9: Raman spectra of (a) MoO_3/SiO_2 catalyst prepared by wet impregnation of silica with AHM and calcined at 500 °C (same procedure as for AAx catalysts in Chapter 2) and (b) NH_0_10 catalyst.

Two reasonable arguments can be put forward to extrapolate the Raman results obtained on the NH_0_10 sample to the whole set of NH catalysts, namely, to affirm that only amorphous MoO_x species and no MoO_3 crystallites are found in NH catalysts. Firstly, the sensitivity of Raman spectroscopy for MoO_3 crystals is much higher than for amorphous MoO_x species [191]. The Raman cross section is much higher for crystals. Small

MoO_3 crystallites are usually very easily detected, as described in Chapter 4. Secondly, in Al-containing samples the fluorescence caused by defects in the materials would saturate any low intensity signals. Therefore, considering that no bands related to MoO_3 crystal species was detected, it is deduced that highly dispersed Mo species also occur in Al-containing samples. The higher affinity of molybdena for alumina (and for silica-alumina) than for silica is another argument that supports the idea of an excellent dispersion of Mo.

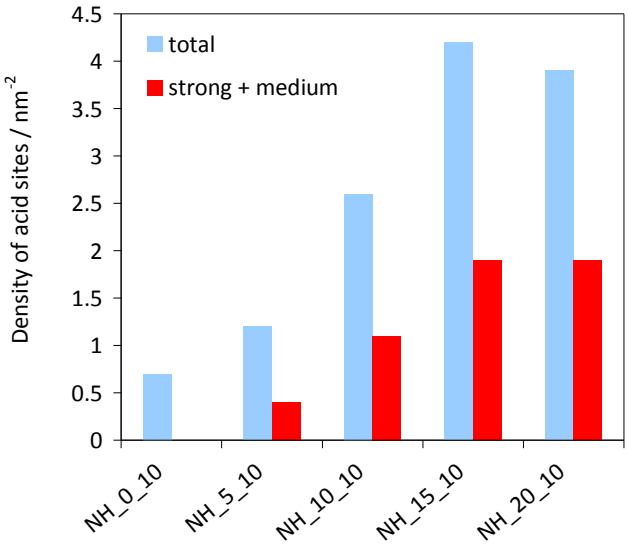

Figure V-10: Density of acidic sites in NH_Y_10 catalysts as determined by NH_3-chemisorption. Total acidity is shown in blue. Strong + medium acidity is shown in red. Weak acidity can be visualized as the difference between both columns.

Chapter 1, as well as studies from the literature, showed that the catalytic activity of supported molybdenum oxide metathesis catalysts was strongly influenced by the nature of the support. The high activity of catalysts supported on silica-alumina has been ascribed to the acidic character of the support [115, 145]. In the present study, the composition of the silica-alumina matrix also has a marked influence on the acidity of the samples. The Al-free catalyst is the less acidic both in terms of absolute amount of acidic sites and in terms of density of acid sites. Furthermore, it only exhibits weak acidity. In link with Figure I-4, the acidity of the NH

samples is shown in Figure V-10 to allow a direct comparison with the results described in Chapter 1. It is striking that the evolution of total, strong and medium acidity with the Al content is very similar in both systems. Thus from a qualitative point of view, the acidity of SAxMo catalysts evolves in the same way as the acidity of NH_Y_10 catalysts upon variation of the Si/Al ratio, even though their modes of preparation are very different.

3.2.2. Location of Mo atoms

XPS characterization gives further insights on the location of Mo oxide with respect to the other components of the catalyst. At first sight, the composition of the surface looks quite similar to the nominal composition, confirming that the solids appear relatively homogeneous. Such result cannot be obtained with classical hydrolytic sol-gel chemistry because in that case, the reactivity of Si alkoxide is much slower than that of Mo and Al precursors. The main advantage of the non-aqueous reactions used here is to partially level off these differences in reaction rates [121]. In fact, the reactions around silicon precursors are catalyzed by Lewis acids, like $AlCl_3$. As a consequence, in mixed silica-metal oxide systems the rates of reaction around silicon and metal precursors become similar which leads to homogeneous mixed Ti-Si, Si-Al, or Si-Zr oxides [123]. In the present case however, the Mo surface concentration was systematically slightly lower than expected in totally homogeneous materials. It must be admitted that the levelling of the kinetics was only partially achieved. Presumably, the Mo precursors reacted slightly faster than Si and Al precursors. As $MoCl_5$ is consumed faster than the other precursors during the formation of the gel, the reaction medium gets progressively Mo-poorer. It is thus reasonable to envisage the occurrence of a Mo concentration gradient in the solid.

An interesting observation is the increasing tendency of Mo atoms to remain in the bulk of the material as the Al content increases. This trend can possibly be interpreted in terms of a preferential reactivity of Mo precursors towards Al precursors (as opposed to Si precursors). Mo-O-Al bonds are indeed more stable than Mo-O-Si bonds. It should be noted at this stage that the dispersion of Mo atoms in the solid might be affected by the calcination step. The observations made here concern calcined samples, but it is not

ruled out at this stage that the dispersion of Mo atoms in the solid is actually different in the uncalcined xerogel. Indeed the Tammann temperature of MoO_3 is low (261°C), which means that the treatment at 500 °C can provoke phenomena as diffusion, sintering, migration, etc., during which the location of a given element with respect to the other components of the catalyst may change. This issue will be analyzed in details in section 4.

3.2.3. Correlation with metathesis activity

The metathesis activity of the Al-free catalyst is very poor. This correlates well with the conclusion of Chapter 1: the presence of Al is essential. Furthermore, the evolution of the activity of NH_0_10 with time on stream is also comparable to the case of SA100Mo. Fast deactivation takes place. All Al-containing catalysts perform significantly better. However, in the set of compositions studied here, the lower the Al content, the higher the activity. This observation is not in line with the conclusions of Chapter 1. Let us remember however that XRD and Raman experiments show the occurrence of highly dispersed Mo oxide species in the case of NH catalysts. The nature of the MoO_x species that are found on NH catalyst is thus very different from the nature of the species found on catalysts prepared by wet impregnation. So, direct comparisons are delicate. The two following paragraphs are attempts to correlate the metathesis activity with physico-chemical properties of NH catalysts.

A first trivial reason for the lower activity of the NH catalysts with high Al content (as compared to NH_5_10) is the observation that the Mo surface concentration in NH catalysts tends to be lower when the Al content is higher. This can presumably lead to lower amount of active sites at the surface of the catalysts with high Al content and in turn lead to lower activity. However, the differences in terms of Mo surface concentration are not pronounced. Only the NH_0_10 sample exhibit significantly higher amount of Mo at its surface.

In Chapter 1, the correspondence between the evolution of the total acidity of the samples as a function of the Al content and the evolution of their metathesis activity led us to conclude that the total acidity was the key parameter that dictates the activity. Here, such link can not be made directly.

The specific surface area is a decisive factor that must be taken into account. In Chapter 1, the specific surface area changes in the series of catalysts. However, if the activity is normalized by the specific surface area of each sample, the ranking of the catalysts does not change appreciably (not shown): the best supports are those with 15 or 20 wt. % of Al_2O_3. The activity of NH catalysts normalized by their specific surface area is presented in Figure V-11. Here, the specific surface area decreases steeply as the Al content increases (Table V-2). This normalization shows that the very active NH_5_10 actually exhibits roughly the same activity as NH_10_10 on a surface basis. So in this case, the higher specific activity of the 5 wt. % Al_2O_3 containing catalyst is explained by a textural effect. More interestingly, the catalysts with 15 and 20 wt. % of Al_2O_3 are significantly more active on a surface basis. These catalysts are more acidic. Overall, the activity normalized by the surface area is roughly linked to the acidity when it is also normalized by the surface area: higher density of acid sites leads leads to higher activity (Figure V-12).

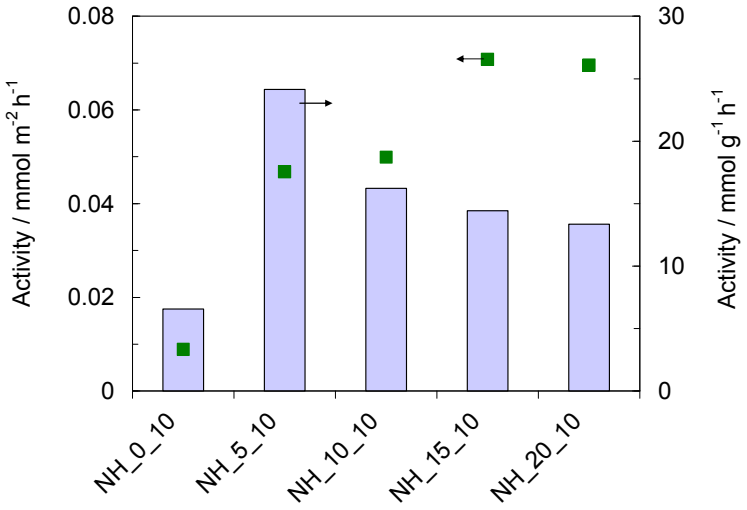

Figure V-11: Specific activity of NH_Y_10 samples (columns) and the same specific activity values normalized by the specific surface area (■).

In the end, even if a non negligible proportion of Mo atoms is probably dispersed into the bulk of the silica-alumina matrix and thus not

accessible to the reactant, NH systems perform well in the metathesis reaction. It is reasonable to state that the number of Mo atoms effectively available at the surface of the catalyst to perform the catalytic act is lower than in the case of catalysts prepared by wet impregnation. However, the specific activity is either in the same order as for classical MoO_3/SiO_2-Al_2O_3 catalysts (NH_10_10, NH_15_10, NH_20_10) or significantly higher (NH_5_10). This means either (i) that a much higher proportion of accessible Mo atoms yield active sites or (ii) that the active sites formed from the surface Mo species in NH samples are more active. Our results support the idea that very well-spread, presumably isolated, MoO_x species are the most active metathesis centre, like earlier suggested by Ono et al. [204].

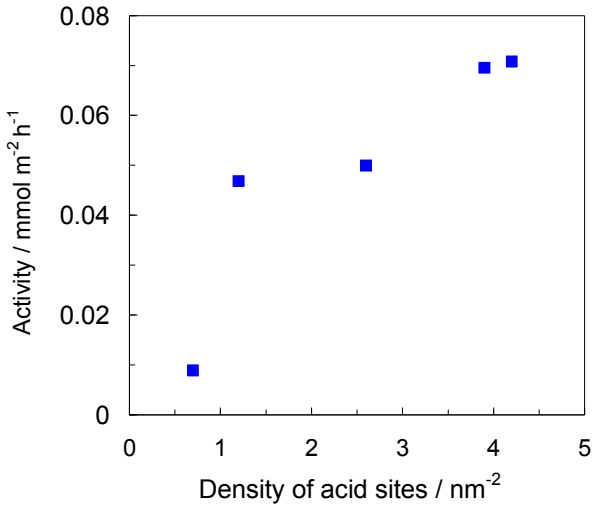

Figure V-12: Correlation between the activity (on a surface basis) and the density of acid sites in NH_Y_10 catalysts.

4. EFFECT OF MoO_3 LOADING IN SiO_2-Al_2O_3-MoO_3 CATALYSTS

4.1. Results

4.1.1. Catalysts characterization

In the second set of samples, the most favourable Si/Al ratio was selected and the MoO_3 loading was varied (Table V-5). Here also, the experimental compositions correlate well with nominal compositions. When the MoO_3 loading is varied in the 5-20 wt. % range, the texture is not significantly affected. The specific surface area remains approximately constant, in the 470-500 $m^2\ g^{-1}$ range, for the four compositions investigated. The pore volume and mean pore diameter are also very constant, except for NH_5_5 which exhibits a slightly lower porosity. The microporosity is very low for all samples. Note that the texture of the NH_5_10b sample is very similar to the texture of the NH_5_10a sample presented above, showing that the synthesis route is well reproducible.

Table V-5: Composition (ICP AES) and texture (N_2-physisorption) of catalysts.

	Experimental Composition (wt. %) SiO_2 : Al_2O_3 : MoO_3	SSA ($m^2\ g^{-1}$)	Vp (ml g^{-1})	Dp (nm)[a]	SSAμ ($m^2\ g^{-1}$)[b]
NH_5_5	90.3 : 5.2 : 4.6	500	0.9	7.2	40
NH_5_10b	86.4 : 4.1 : 9.5	480	1.6	13.1	20
NH_5_15	79.9 : 4.7 : 15.4	470	1.6	13.3	0
NH_5_20	77.0 : 4.2 : 18.8	490	1.6	13.3	10

[a] Average pore diameter ($4\ V_P/S_{BET}$)
[b] From *t*-plot analysis in the 0.35 – 0.5 nm range

In general, NH samples were amorphous (Figure V-13). The only exception concerned the sample with the highest MoO_3 loading (NH_5_20) for which a small diffraction line at 27.5° indicated the presence of traces of crystalline MoO_3 (JCPDS 05-0508). Raman measurements, like explained in the previous section did not allow the identification of specific MoO_x species but excluded the presence of MoO_3 crystals (not shown).

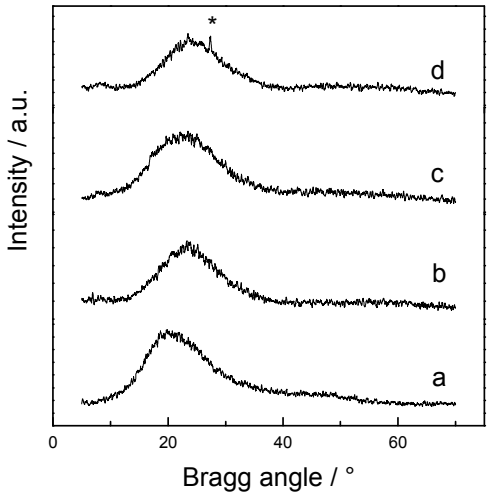

Figure V-13: XRD diffractograms of (a) NH_5_5, (b) NH_5_10, (c) NH_5_15 and (d) NH_5_20. The "*" symbol indicates the trace signal of the (021) crystallographic plane of orthorhombic MoO_3 at 27.3 ° (JCPDS 05-0508).

Table V-6: Surface characterisation by (XPS) on the fresh and calcined sol-gel samples.

	Si (at%)	Al (at%)	Mo (at%)	O (at%)	C (at%)	Cl (at%)	Mo $3d_{3/2}$ BE (eV)	Mo $3d_{3/2}$ FWHM (eV)
xNH_5_5[a]	26.4	1.3	0.3	57.4	14.2	0.4	232.8[b]	3.1[b]
xNH_5_10[a]	22.9	1.2	0.5	54.3	19.9	1.2	232.4[b]	2.5[b]
xNH_5_15[a]	22.9	1.5	1.0	52.0	19.9	2.7	232.3[b]	2.4[b]
xNH_5_20[a]	21.2	1.3	1.4	47.5	26.5	2.1	232.4[b]	2.7[b]
NH_5_5	29.7	1.6	0.4	62.9	5.4	<0.1	233.1	3.0
NH_5_10	27.1	2.3	1.0	64.6	5.1	<0.1	233.1	2.6
NH_5_15	27.2	1.6	1.6	64.1	5.4	<0.1	233.1	2.4
NH_5_20	26.4	1.6	2.0	64.4	5.6	<0.1	233.1	2.3

[a] "x" stands for "xerogel", namely the sample recovered after gelation and drying, but before calcination.
[b] data given for the most oxidized ($Mo^{(VI)}$) component of the Mo 3d peak

The surface composition of the samples was studied by XPS (Table V-6). In addition, the effect of calcination was investigated by analysing also the xerogels obtained after drying (before calcination at 500 °C). The high amount of carbon and the significant amount of chlorine found on the fresh xerogels have to be related to the presence of residual O^iPr and Cl groups

(inherent to the non-hydrolytic route used) at the surface of the xerogels. After calcination the carbon content decreased to about 5 at. %, and chlorine was no more detected. The residual carbon content was similar for all calcined samples (ca. 5 at. %). It is in the same range but slightly lower than the C contamination found on AAx catalysts (ca. 8 at. %). This shows that the residual organic groups originating from the non-hydrolytic sol-gel preparation were effectively removed during calcination and that the remaining carbon resulted from normal atmospheric carbon contamination. Importantly, Table V-6 also shows that the surface Mo content of the calcined samples was significantly higher than in the fresh xerogels.

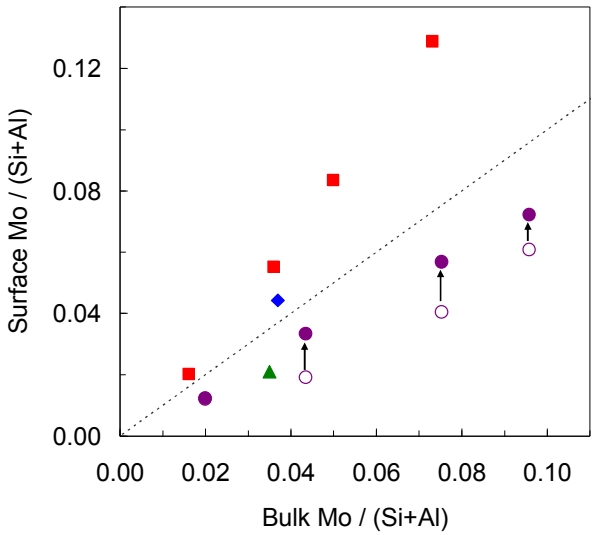

Figure V-14: Surface Mo / (Si+Al) atomic ratio determined by XPS as a function of the bulk Mo / (Si+Al) atomic ratio for (○) NH_5_X xerogels (before calcination), (●) NH_5_X catalysts, (▲) AA8300, (♦) AA8400 and (■) AAx500 catalysts. The bulk ratios are calculated from the composition determined by ICP-AES. The dotted line represents the ratio expected for totally homogeneous materials. The arrows indicate the increase in the Mo / (Si+Al) ratio after calcination of the xerogels.

To verify that this increase was not merely due to the decrease in C and Cl contents, the Mo / (Si+Al) atomic ratio was plotted as a function of the MoO_3 loading determined by ICP-AES (Figure V-14). This ratio was

significantly higher for the calcined samples than for the fresh xerogels (with an exception for the catalyst containing only 5% of MoO_3). Let us note that the Mo / (Si+Al) atomic ratios reported for NH samples are not very different from to those reported for AAx catalysts (Chapter 2, Figure II-11) calcined at 300 or 400 °C. The amount of Mo detected at the surface of AAx500 catalysts was clearly higher, but this was ascribed to the formation of MoO_3 crystallites at the outer surface of the particles, leading to much higher Mo / (Si+Al) ratios (Chapter 2).

Concerning the outermost surface of the catalysts, as characterized with time-of-flight secondary ion mass spectroscopy (TOF-SIMS) [234], Figure V-15 shows that the intensity of Mo^+ ions detected on NH catalysts increases linearly with the MoO_3 loading and that such ions are detected approximately at the same level in the AA8400, analysed as a reference.

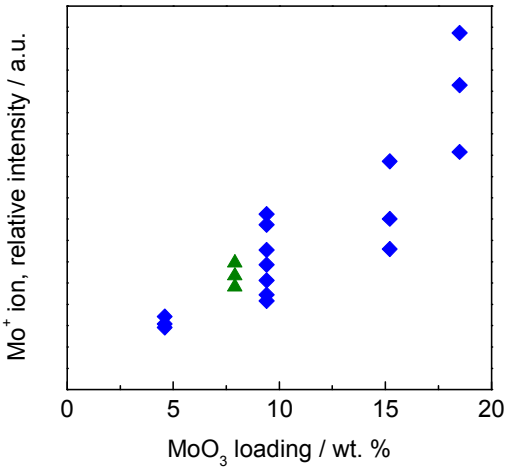

Figure V-15: Mo^+ ions relative intensity measured by TOF-SIMS on (♦) NH_5_X catalysts and (▲) on AA8400. At least three measurements have been performed on each catalyst. The poorer reproducibility of the measure on the SG sample was ascribed to the more open porosity and more irregular surface of these samples

Further insight on the Mo chemical environment might be gained from the observation of the position and width of the Mo 3d peak. The Mo 3d peak of fresh xerogels showed that two different oxidation states coexist: while the precursor ($MoCl_5$) is based on $Mo^{(V)}$ it is reasonable to think that

partial oxidation to $Mo^{(VI)}$ occurs when the xerogel is exposed to air. The calcination step results in the production of fully oxidized Mo species characterized by a well-defined doublet, with the Mo $3d_{3/2}$ component at 233.1 eV, as expected for $Mo^{(VI)}$ is molybdenum trioxide. The Mo 3d binding energy (BE) is systematically slightly higher in NH samples than in catalysts prepared by wet impregnation of heptamolybdate. Indeed AAx catalysts (Chapter 2) typically exhibit the Mo $3d_{3/2}$ peak at 232.6 – 232.8 eV. It is difficult to describe the Mo chemical environment from this shift because the silica-alumina matrix that interacts with Mo atoms is different in both cases (different Si/Al composition). This shift is however an indication that $Mo^{(VI)}$ cations in NH are more electronegative in NH samples than in impregnated catalysts. The full width at half maximum (FWHM) is relatively large for NH samples (Table V-6). For comparison, AAx samples had FWHM typically in the 1.9 – 2.0 range. This indicates that Mo atoms in NH catalysts undergo different surroundings while the environment of Mo atoms tends to be more definite in catalysts prepared by wet impregnation of AHM.

The negative TOF-SIMS general spectra of AAx and NH catalysts were different. In Figure V-16 the catalyst prepared by non-hydrolytic sol-gel with the highest loading is compared to the AA8400 catalyst. Typical patterns related to fragments containing one Mo atom are found for all samples regardless of the preparation method (peaks around 114, 129, 145 and 160 are attributed to MoO^-, MoO_2^-, MoO_3^- and MoO_4^- respectively). On the other hand, a clear difference appears regarding the detection of clusters containing more than one Mo atom (patterns around 288, 305 and 432 are identified as the $Mo_2O_6^-$, $Mo_2O_7^-$ and $Mo_3O_9^-$ ions respectively). These signals attributed to "poly-Mo clusters" were detected on samples prepared by wet impregnation but were never detected on NH samples, even at the highest loading. The detection of these clusters indicates the occurrence of Mo oxide oligomers or crystallites at the surface of the WI catalysts, while their absence in the case of SG samples suggests the occurrence of isolated Mo oxide surface species.

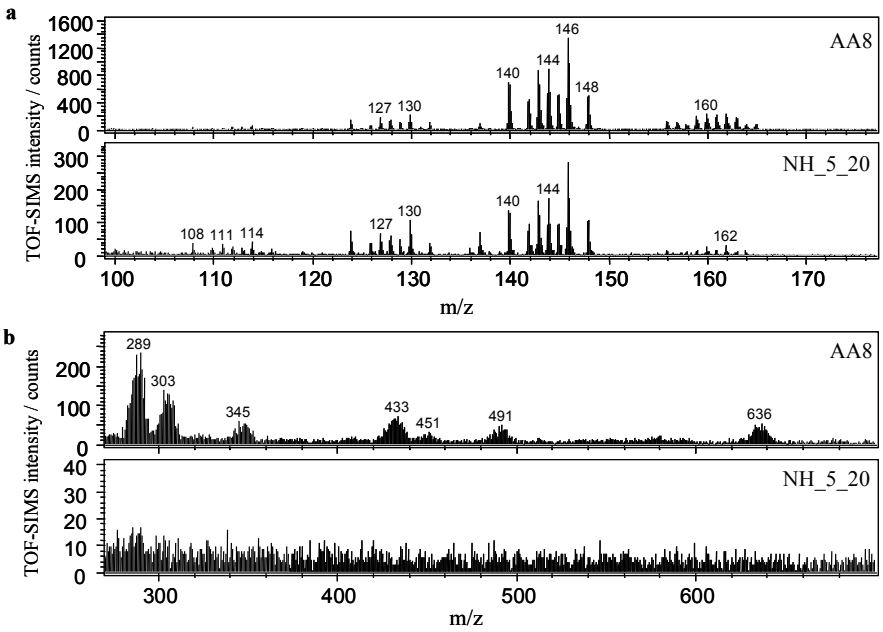

Figure V-16: Parts of the negative TOF-SIMS spectra obtained with AA8400 and NH_5_20 catalysts. (a) From 99 to 177 m/z. (b) From 270 to 700 m/z. Each spectrum has been recorded at least three times. The relative intensities of every peak were always in good agreement. The same results have also been obtained after a repeated experiment performed six months after the main data acquisition campaign.

4.1.2. Metathesis activity

The evolution of the conversion during catalytic tests with NH samples is very similar to all other Al-containing catalysts presented before. An induction period is again observed and the maximum specific activity is measured around 14-20 min. Increasing the MoO_3 loading from 5 to 10 wt. % leads to an important increase in activity. Further increments of loading provoke further activity increase but the extent of these improvements is progressively smaller as the loading gets higher.

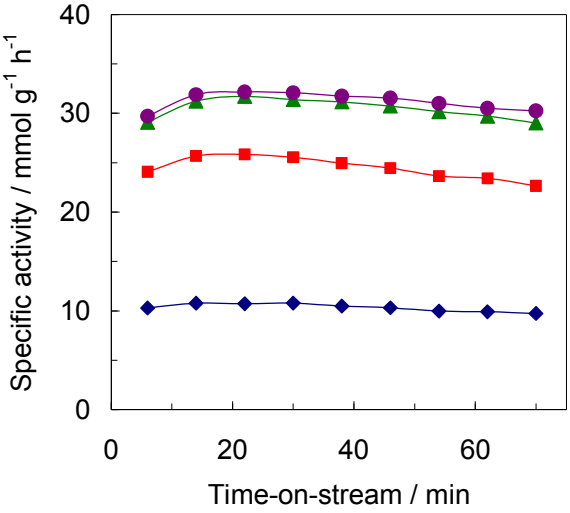

Figure V-17: Evolution of the specific metathesis activity with time on stream. (♦) NH_5_5, (■) NH_5_10, (▲) N_5_15 and (●) NH_5_20.

4.2. Discussion

4.2.1. Texture and structure of the catalysts

The texture of the NH catalysts is dictated mainly by the Si/Al ratio and the MoO_3 content has much less influence. In the set of catalysts investigated in this section, the available surface area can be considered as constant which allows proper comparison in terms of performances. XRD and Raman characterizations correlate to confirm that these catalysts are amorphous. Virtually no bulk MoO_3 was detected by XRD in the SG catalysts even at 20 % MoO_3 wt. loading, while in the classical impregnation preparation the formation of crystalline molybdenum oxide occurs at a loading as low as 8 wt. %. This was identified as a limitation of classical preparation methods which induced an obvious constraint: overloading of Mo should be avoided to prevent detrimental effect of bulk MoO_3 on the specific activity. As the dispersion of Mo species in the NH samples appeared excellent, non-hydrolytic sol-gel is perceived as very promising to overcome this limitation.

4.2.2. Location and nature of Mo species

The comparison of xerogels and calcined catalysts give valuable information on the preparation process. It appears clearly that the organic and chlorinated moieties originating from the reactants involved in the preparation are effectively removed during calcination.

Very interestingly, XPS results show that the calcination step modified the dispersion of Mo atoms in the solids. Surface characterization techniques attest of a significant Mo-enrichment of the catalyst surface after calcination. The increase in the Mo surface concentration is not linked to the cleaning of the surface from organic groups and chlorine atoms. Indeed, the Mo / (Si+Al) ratio increases significantly after calcination. This implies that Mo atoms migrate towards the surface of the catalyst during the treatment at 500 °C. This phenomenon was anticipated considering the low Tammann temperature of MoO_3 (261 °C). This temperature (defined as the melting temperature of the solid (in K) divided by two) is an empirical parameter corresponding roughly to the temperature at which solid defects are abundant enough to allow bulk mobility. As the temperature used in the calcination step is well above the Tammann temperature of Mo oxide, calcination can lead to the mobility of Mo species in the bulk of the material and at the surface. Such migration has already been observed for V oxide species with similar Tammann temperature (209 °C) during the calcination of V_2O_5-TiO_2 catalysts prepared by hydrolytic or non-hydrolytic sol-gel [122, 129, 238].

The remaining question is: are all Mo sites accessible (located at the surface of the solid) or homogeneously dispersed in the solid? The high surface area and the porosity of the materials seriously complicate the quantitative interpretation of XPS data. A first approach to answer this question is to compare the Mo / (Si+Al) atomic ratio determined by XPS on the NH samples to the same ratio obtained for catalysts prepared by wet impregnation (e.g. AA samples from Chapter 2). Indeed, in the latter case, all Mo atoms are brought onto the preformed support and it could be put forward that most Mo atoms are effectively detected by XPS. In fact, the line drawn for NH_5_X catalysts in Figure V-14 is close to the corresponding point for AA8400 catalysts, indicating a similar amount of Mo at the surface

of NH catalysts. The data point of the AA8300 sample is even lower. The AAx500 catalysts exhibit more Mo at their surface but this was ascribed to the formation of MoO_3 crystals at the outer surface of the particles. This shows that Mo atoms deposited onto the surface of a preformed support are not always probed to the same extent in impregnated catalysts, even if they are supposed to be located at the surface of the support. So such direct comparison can be misleading. The second approach would be to calculate an expected atomic Mo / (Si+Al) ratio from the bulk composition and to compare it to the surface ratio. This approach was successfully applied for V_2O_5/TiO_2 catalysts [122]. While the surface V/Ti ratio was equal to the expected bulk V/Ti ratio in the xerogel (indicating a very homogeneous solid) the surface V/Ti ratio increased significantly in the calcined catalyst (evidencing the migration of V towards the surface of the particles). In the present case (Figure V-14) the surface Mo / (Si+Al) ratio is lower both for the xerogels and for the calcined catalysts than the ratio expected for totally homogeneous materials. This would indicate that even after calcination, the Mo concentration is higher in the bulk than at the surface. However the same conclusion should then be drawn for the impregnated AA8400 catalysts. The data point is lower than the theoretical line even though all Mo are deposited at the surface. This discrepancy can also result from the fact that only the outer surface of the particles is probed, while Mo atoms can be dispersed down to the bottom of the pores. Additionally, the accuracy of each sensitivity factors is not assured and this can be misleading. In this study, the factors provided by the manufacturer were used, which do not necessarily apply to our materials. For example, the stoichiometric O/Mo atomic ratio in pure molybdenum trioxide is 3 but a ratio of 2.5 was determined experimentally by XPS. Similarly, the expected Mo/N ratio in ammonium heptamolybdate is 1.2 but a value of 1.5 was found experimentally. Verifying the exactitude of each sensitivity factor is not in the scope of the present research. Overall, comparing the Mo / (Si+Al) ratio of given materials with others is delicate.

In the present case, it is the relative increase in the Mo / (Si+Al) ratio after calcination that must be stressed. This increase is clear evidence of the migration phenomenon. Furthermore, the extent of the migration is presumably underestimated in the present case. One should not forget indeed

that the materials that are inspected here are porous, with high surface area. In such solids, the pore walls are very thin (in the order of a few nm). The explored depth is in the order of 10 nm with a large majority of the signal originating from the first nanometer (the efficiency of the production and detection of photoelectrons decrease exponentially with depth). Thus, the escape depth of the electrons is in the order of the thickness of the pore walls. As highlighted by Kerkhof and Moulijn [239], the assumption of a semi-infinite material depth is not valid in such case. The large majority of the available surface area is developed in pores of the solids. Therefore, if Mo migrates isotropically from the bulk of the solid toward its surface, most of the migration will concern the walls of the pores (arrows (1) in Scheme V-1) and only a minor part will concern the actual outer surface of the particles (arrows (2) in Scheme V-1). Any increase in Mo surface concentration at the outer surface of the particles will be detected in XPS as an increase in the Mo / (Si+Al) ratio (situation (b). On the other hand, segregation of Mo towards the walls of the pores will not be detected since the whole thickness of the wall is explored (situation (a)). Note that the above-mentioned example of the V_2O_5/TiO_2 catalysts concerned materials with much smaller surface area, for which the migration phenomenon was more clearly demonstrated.

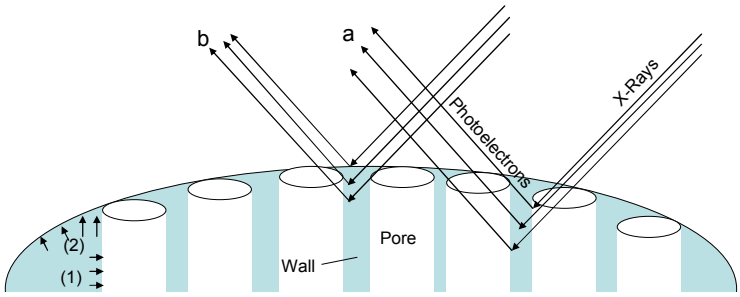

Scheme V-1: Schematic representation of the porous NH catalyst analyzed by XPS. On the left, arrows (1) indicate the migration of Mo atoms toward the surface of the pore walls as a result of calcination and arrows (2) indicate the same phenomenon directed toward the outer surface of the particle. Photoelectrons detected in situation (a) originate from the walls of the pores. Photoelectrons detected in situation (b) originate from the outer surface of the particle.

The Mo chemical environment is different in AA and in NH samples, as underlined by the different position and width of the XPS Mo 3d peaks. It is the interaction of Mo atoms with the other components of the catalysts that dictates such shift and broadening of the peaks. In the MoO_3 phase formed at the surface of the support after impregnation of AHM and calcination, $Mo^{(VI)}$ experiences mainly the interaction of neighbouring Mo atoms. Their environment is well defined and this translates into relatively narrow XPS peaks. In NH catalysts Mo atoms are dispersed into the silica-alumina matrix and at the surface. Their environment is more variable which translates into relatively broad XPS peaks.

Analysis of the surface by TOF-SIMS provides further insights on the nature of MoO_x species at the outermost border of the particles. In particular, TOF-SIMS gives strong indications that only isolated Mo species are present at the surface of SG catalysts. On the contrary, cluster ions containing more than one Mo atom are detected on WI samples. The occurrence of such species confirms the presence of agglomerated Mo oxide surface species (bulk crystals or polymeric species) in WI catalysts. In contrast the non-hydrolytic sol-gel route produces highly dispersed, isolated Mo oxide species.

4.2.3. Correlation with metathesis activity

The activity measurements in the self metathesis of propene can be understood in the light of the aforementioned characterization results. As the specific surface area of NH catalysts is relatively constant, the increase in catalytic activity can directly be correlated to an increase in the number or in the efficiency of the active centres at the surface of the catalysts when the MoO_3 loading rises. While the Mo surface concentration appears to increase linearly with the MoO_3 content, it is not the case for the specific activity. This suggests that the proportion of Mo surface species which yields active centres after activation is decreasing when the loading increases. However, the situation is different from the one encountered with AA catalysts for which a clear plateau was observed when the loading reached 8 wt. %. Here the activity of NH samples continues to rise which indicates that some of the

additional Mo atoms introduced in the preparation continue to yield additional active metathesis sites.

AA and NH catalysts are comparable in terms of composition and have textural properties in the same range. This chapter shows that the catalysts prepared by non-hydrolytic sol-gel clearly perform better than reference catalysts prepared by wet impregnation of AHM on the silica-alumina support. It should be recalled that the Mo surface concentration detected on AA samples had a marked influence in the metathesis activity of AAx catalysts. At the surface of NH catalysts, the Mo concentration is at best the same as in impregnated catalysts. Nevertheless, NH catalysts are much more active (up to two times more active than the best AAx500 catalysts). This shows that the nature of MoO_x surface species produced via the non-hydrolytic sol-gel route is more appropriate. A possible reason is the fact that Mo atoms are more electron deficient in NH sampes than in AA samples (the BE of the Mo 3d XPS peak is shifted upwards). More importantly, all characterization results indicate an excellent spreading of Mo atoms in the solid. The better performances of NH catalysts must be correlated to this improved dispersion. In particular, TOF-SIMS experiments suggest that mainly isolated Mo species are present at the surface of NH catalysts. Isolated Mo oxide species have already been proposed as the active metathesis sites [9, 88, 108, 156] but the debate is not closed because dimeric species [74] and dispersed polymolybdates are also frequently put forward [88]. The present study clearly supports the idea that isolated MoO_x species act as the active metathesis centres.

5. CONCLUSION

A new strategy for designing active metathesis catalysts was investigated. The method differs markedly from classical preparation methods: instead of depositing a catalytically active phase on a preformed support, the active phase is directly incorporated with the other components of the catalyst. Two main parameters of the composition were screened independently: the Si/Al ratio and the MoO_3 loading. Figure V-18 sums up the dependence of metathesis activity with catalyst composition.

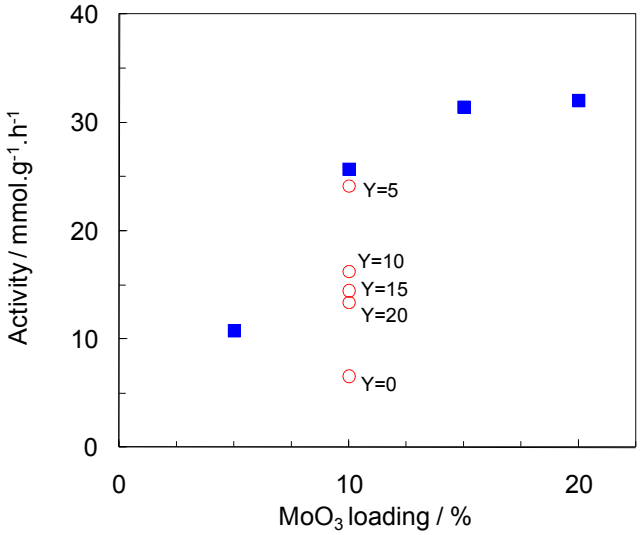

Figure V-18: Maximum specific activity (measured at 14 min time-on-stream) of NH catalysts as a function of the nominal MoO_3 loading (abscise) and of the Al_2O_3 content. (○) NH_Y_10 catalysts (the value of Y is given next to each data point) and (■) NH_5_X catalysts (Y is always very close to 5 wt. %; SiO_2/Al_2O_3 wt. ratio = 17). Note: The two results corresponding to NH_5_10a and NH_5_10b are very close to each other. This illustrates the good reproducibility of the preparation (and of the catalytic test, as already mentioned in the Experimental Section).

It is evident that the Si/Al ratio influences strongly the performances. The activity of the Al-free catalyst is very poor, which confirms previous finding from Chapter 1. Adding small amounts of Al_2O_3 in the formulation yields very active catalysts. The catalyst having the lowest Al_2O_3 loading (Y = 5 wt. %) was the most active in terms of specific activity. Further increase in the Al content lowers the specific surface area of the NH catalysts which decreases the specific activity. However, higher Al content also implies higher acidity, which is again identified as a positive effect in the genesis of active metathesis catalysts. When the activity is normalized by the surface area, the catalysts with 15 and 20 wt. % of Al_2O_3 are the most active ones.

Varying the MoO_3 loading but keeping the Si/Al ratio constant allowed maintaining the most favourable textural properties. The activity of the catalysts increases as the MoO_3 increases, even though a progressive levelling off is observed.

The best catalysts prepared via the non-hydrolytic route are much more active that the best catalysts prepared via other methods used in this study. To ensure the success of the strategy, three main challenges needed to be addressed: (i) all requirements related to the use of these materials as solid catalysts (good texture, control on the composition) should be met, (ii) the active component should be available for the reactants, at the surface of the catalyst and (iii) the active species should be present in their most active form.

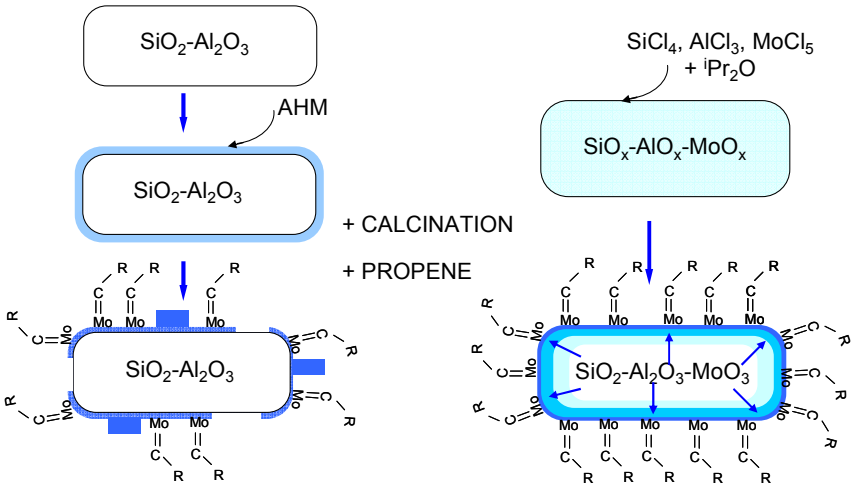

Scheme V-2: Schematic comparison of the classical and the new preparation routes. Left: a silica-alumina supported MoO_3-based catalyst is obtained via wet impregnation with AHM. As depicted in Chapter 2, the formation of bulky MoO_3 crystals can not be avoided when the loading and the calination temperature are high. With such uneven distribution of the Mo oxide phase, only a limited proportion of the Mo deposit can yield active sites upon contact with the olefin. Right: MoO_3-SiO_2-Al_2O_3 mixed oxide catalysts are obtained via the non-hydrolytic sol-gel route. Arrows indicate that the distribution of Mo in the solid changed after calcination (higher Mo surface concentration). As only very dispersed Mo species are stabilized at the surface, active metathesis sites are created in larger amount.

The first condition is met since solids with relatively high specific surface area and open porosity were produced. The marked influence of the Al_2O_3 content must however be stressed. The method is also very reliable as far as the control on the composition is concerned.

The active component of the formulation – Mo atoms – is initially dispersed into the solid matrix of the xerogel. XPS characterization even suggested the tendency of Mo atoms to build up in the core of the solid rather than at its surface. Slight differences in the kinetics of the non-hydrolytic condensation reactions of different precursors presumably explain this phenomenon. However, it is also demonstrated that the calcination step induces a partial redistribution of Mo atoms in the solid. Mo atoms migrate toward the surface of the catalyst. In the end, the concentration of Mo atoms at the surface of the catalyst is in the same order as (or a bit lower than) in reference catalysts prepared by wet impregnation of ammonium heptamolybdate.

The third challenge seems to be decisively met. Even if part of Mo atoms is probably "lost" in the bulk, the species that are actually exposed at the surface are very active. All characterization data indicate an excellent dispersion of Mo atoms with the predominance of isolated molybdate species. This is the key property of the catalysts prepared via non-hydrolytic sol-gel, which makes them excellent candidates for accomplishing the heterogeneous light olefin metathesis.

INTERMEDIATE CONCLUSION FOR PART III

In this last part of the thesis, an innovative preparation route has been investigated for the design of MoO_3-SiO_2-Al_2O_3 mixed oxides dedicated to the heterogeneous light olefin metathesis. The method, based on non-hydrolytic condensation of chloride precursors leads to materials with particular physico-chemical properties and high metathesis activity.

This success shows that strategies based on one-step synthesis of such ternary formulations are relevant and can be more indicated than methods in which the support is prepared first and then decorated with the active phase. In fact, the best catalysts prepared via non-hydrolytic sol-gel are two times more active than the best catalysts prepared in two steps from AHM.

The better performances of the mixed oxide catalysts are attributed to the excellent dispersion of Mo in the material. As expected, characterization tools indicate that a significant proportion of Mo atoms is "lost" in the bulk of the materials. The amount of Mo species actually accessible for the propene molecule at the surface of the catalyst is thus lower than in the case of impregnated catalysts. And despite this situation, the number of active sites (or their intrinsic activity) is higher. This shows that the nature of the Mo surface species has a marked impact on the metathesis activity.

GENERAL CONCLUSION

The heterogeneous metathesis of light olefins is a crucial reaction for the petro-chemical industry. It allows regulating the stocks of light alkenes as a function of the market and at low energy and environmental cost. MoO_3-based heterogeneous catalysts are highly regarded for that purpose as they are considered to be robust and cheap. Current challenges however, concern the mastering of the performances of these catalysts. It is known that only a small fraction of the Mo atoms present in the formulation actually turn out to be active. The nature and the genesis of active metathesis centres is still a matter of debate. As far as applied catalysis science is concerned, any better fundamental understanding of these systems could be helpfully implemented in the design of improved catalytic processes.

This thesis work proposes steps forward in the direction of a better understanding of the genesis of active MoO_3-based metathesis catalysts. This was done in two ways: (i) systematic investigations on decisive preparation parameters in conjunction with dedicated characterizations and (ii) exploration of new alternative methods for the preparation of MoO_3-based metathesis catalysts.

The impact of the composition of the support was investigated. The presence of Al in silica-rich silica-alumina support has a crucial effect on the metathesis activity of the Mo oxide phase. The effect of Al is studied on a systematic experimental base. The beneficial role of Al on the metathesis activity is linked to the increase in acidity brought about when the alumina content in the support increases from 0 to 15-20 wt. %. In this range of composition, a true mixed silica-alumina phase build up and exhibits interesting acidic Si-O(H)-Al bridges. At higher Al_2O_3 content, a pure alumina phase appears which is less adequate. An optimum was thus identified at ca. 15 wt. % of alumina in the support.

A systematic investigation on the most classical preparation method to MoO_3/SiO_2-Al_2O_3 catalysts gave new insights on the genesis of active and inactive species. In particular, the wet impregnation of heptamolybdate on a silica-alumina support often leads to the formation of bulky MoO_3 crystals as well as $Al_2(MoO_4)$. These species appears to have a negative effect on the performance of the catalysts. The formation of such species is linked to the preparation method (nominal Mo loading, calcination temperature). This part of the work identifies a threshold in terms of specific activity. It determines the limits of the classical preparation approach and highlights guidelines to overcome them. Precisely, the dispersion of the Mo deposit should be improved. To do this, the precipitation of Mo species at the outer surface of the particles of support must be impeded and the formation of the Anderson-type heteropolymolybdate $[Al(OH)_6Mo_6O_{18}]^{3-}$ during the impregnation should be avoided. The following sections of the thesis exploited these guidelines.

Using alternative precursors for the wet impregnation of silica-alumina was shown to be a possibly relevant strategy. The addition of oxalic acid in a heptamolybdate impregnation solution has a marked effect on the support and on the final catalysts properties. Oxalate ligands promote the partial dissolution of the aluminic domains of the support and impede the formation of complexes between dissolved Al^{3+} ions and polymolybdic anions in solution. Overall, the effect on the metathesis activity is modest but correlates well with physico-chemical properties of the catalysts: as no $Al_2(MoO_4)_3$ and no bulk MoO_3 crystals build up when the Mo loading increases, the specific activity rises linearly with the Mo loading. Using a molybdenum oxide hydrates solution allows improving the dispersion of the Mo deposit on the whole available support surface (including the inside of the pores). In such catalysts the formation of MoO_3 crystals is avoided and the genesis of $Al_2(MoO_4)_3$ is impeded. When the MoO_3 loading is in the 8-15 wt. % range, these catalysts noticeably outcompete the catalysts prepared via impregnation of ammonium heptamolybdate. However, when the Mo loading and the calcination temperature are high, a significant amount of $Al_2(MoO_4)_3$ finally builds up. As this observation was concomitant to a sudden drop in the metathesis activity, the aluminium molybdate phase was clearly identified as inactive and deleterious.

The direct thermal spreading of MoO_3 onto the silica-alumina support is a straightforward method to obtain active metathesis catalysts. The conversion of bulky MoO_3 crystals into amorphous Mo oxide dispersed at the surface of the support is demonstrated. This effect is however only partial and small MoO_3 crystallites (< 5 nm) remain in the materials, thereby limiting the activity of the catalysts to a moderate level.

The non-hydrolytic sol-gel technique was successfully implemented to prepare Mo-Si-Al mixed oxides that exhibited outstanding performances in the metathesis of propene. Via this route, very homogeneous mixed oxides with controlled composition and texture can be obtained. The dispersion of Mo atoms in the silica-alumina matrix appears excellent. The calcination of the xerogel is a crucial step: it provokes the migration of Mo atoms toward the surface of the catalysts. Here also, a correlation was established between the density of acidic sites and the metathesis activity of the catalysts. The surface area developed by the materials is also a determining factor. Upon optimization of the preparation, the best catalysts prepared via non-hydrolytic sol-gel are approximately two-times more active than the best catalysts prepared by classical wet impregnation. This part of the work highlights the superior activity of the isolated molybdate species that are stabilized at the surface of the materials.

In the end, this study has addressed some of the challenging issues that persist in the development of highly efficient heterogeneous catalysts for the metathesis of light alkenes. Answers and guidelines are proposed on systematic experimental bases.

It is striking however to realize that the thorough description of the actual active centres remains complicated. This is linked to the fact that a very low proportion of Mo atoms present in the catalyst actually turn out to be active. Mostly, physico-chemical characterizations allow probing the presence of the species that appear to be inactive (MoO_3 crystals or crystallites in XRD, TEM and Raman, $Al_2(MoO_4)_3$ in MAS NMR, “poly-Mo clusters” in TOF-SIMS, etc.). The actually active metathesis centres are then depicted by deduction, in opposition to the inactive species. It is easy to identify typical physico-chemical properties of the catalysts that correlate

with poor metathesis activity but it is very difficult to identify which characteristics correlate with good metathesis activity.

Even if the precise description of active sites should still be considered as a topical research objective, many valuable indirect insights are provided by this thesis work on the chemistry of MoO_3-based metathesis catalysts. Taking an overall look at the study, the conjunction of systematic investigations on given preparation parameters, of original preparation procedures and of detailed physico-chemical characterization surveys allows highlighting three essential guidelines. Firstly, the role of the support (or matrix) on the activity of the Mo phase is decisive. Our results suggest that the optimization of the support composition (e.g. Al content) and of the support texture is a relevant approach to reach improved performances. In addition, it is suggested that the intimacy of the contact between Mo species and the support – presumably Al atoms – is crucial too. Secondly, improving the Mo dispersion always has a positive impact the catalyst performances. That is, avoiding the formation of bulk MoO_3 crystals or even stabilizing monomeric MoO_x species are pertinent approaches. Thirdly, the preparation history of each sample has marked impacts on the final catalyst activity. This may appear surprising since all samples are activated in relatively harsh conditions before catalytic test. As thermal treatments (e.g.: calcination) were shown to have marked impacts on the physico-chemical properties of the active phase of the catalysts, the impact of the activation procedure could interestingly be studied in more details. Exploring smoother ways to pre-treat the sample might be a relevant strategy. All the results presented here indicate the importance of developing a firm know-how concerning the preparation parameters in the perspective of performance improvements.

REFERENCES

1. *Renewable Energy - Sustainable Energy Concepts for the Future*, ed. Roland Wengenmayr and Thomas Bührke. 2008, Berlin: Wiley-VCH.
2. N.T. Dintcheva and F.P. La Mantia, *Durability of a starch-based biodegradable polymer*, Polym. Degrad. Stab., 92 (2007) 630-634.
3. B. Zechendorf, *Sustainable development: how can biotechnology contribute?*, Trends Biotechnol., 17 (1999) 219-225.
4. J. García-Serna, L. Pérez-Barrigón, M.J. Cocero, *New trends for design towards sustainability in chemical engineering: Green engineering*, Chem. Eng. J., 133 (2007) 7-30.
5. P. Glavic and R. Lukman, *Review of sustainability terms and their definitions*, J. Clean. Prod., 15 (2007) 1875-1885.
6. J.N. Armor, *Energy efficiency and the environment: Opportunities for catalysis*, Appl. Catal. A, 194-195 (2000) 3-11.
7. X. Zhu, X. Li, S. Xie, S. Liu, G. Xu, W. Xin, S. Huang, L. Xu, *Two New On-Purpose Processes Enhancing Propene Production: Catalytic Cracking of C_4 Alkenes to Propene and Metathesis of Ethene and 2-Butene to Propene* Catal. Surv. Asia, 13 (2009) 1-8.
8. *Olefin Conversion Technology*. 2009, Lummus Technology, a CB&I Company.
9. K.J. Ivin and J.C. Mol, *Olefin Metathesis and Metathesis Polymerization*, ed. Academic Press. 1997, London.
10. *Olefins/Polyolefins Technologies, by Lummus Technology, a CB&I company*. Available from: http://www.cbi.com/lummus/process-technology/olefins.polyolefins.aspx, 2004-2010.
11. J.C. Mol, *Industrial applications of olefin metathesis*, J. Mol. Catal. A, 213 (2004) 39-45.
12. J.C. Mol, *Olefin metathesis over supported rhenium oxide catalysts*, Catal. Today, 51 (1999) 289-299.
13. R. Spronk, A. Andreini, J.C. Mol, *Deactivation of rhenium-based catalysts for the metathesis of propene*, J. Mol. Catal., 65 (1991) 219-235.
14. J. Aguado, J.M. Escola, M.C. Castro, S. Abdelhamid, J. Mietek, *Metathesis of 1-hexene over MoO_3 and Re_2O_7 supported on mesostructured [gamma]-Al_2O_3 prepared with cationic surfactants*, Stud. Surf. Sci. Catal., 156 (2005) 835-842.

15. J. Aguado, J.M. Escola, M.C. Castro, B. Paredes, *Metathesis of 1-hexene over rhenium oxide supported on ordered mesoporous aluminas: comparison with Re_2O_7/gamma -Al_2O_3*, Appl. Catal. A, 284 (2005) 47-57.
16. M. Stoyanova, U. Rodemerck, U. Bentrup, U. Dingerdissen, D. Linke, R.W. Mayer, H.G.J. Lansink Rotgerink, T. Tacke, *High-throughput preparation and screening of rhenium oxide-alumina catalysts in olefin metathesis*, Appl. Catal. A, 340 (2008) 242-249.
17. S.J. Huang, S.L. Liu, Q.J. Zhu, X.X. Zhu, W.J. Xin, H.J. Liu, Z.C. Feng, C. Li, S.J. Xie, Q.X. Wang, L.Y. Xu, *The effect of calcination time on the activity of WO_3/Al_2O_3/HY catalysts for the metathesis reaction between ethene and 2-butene*, Appl. Catal. A, 323 (2007) 94-103.
18. D. Lokhat, M. Starzak, M. Stelmachowski, *Gas-phase metathesis of 1-hexene over a WO_3/SiO_2 catalyst: Search for optimal reaction conditions*, Appl. Catal. A, 351 (2008) 137-147.
19. Y.D. Wang, Q.L. Chen, W.M. Yang, Z.K. Xie, X. Xu, D. Huang, *Effect of support nature on WO_3/SiO_2 structure and butene-1 metathesis*, Appl. Catal. A, 250 (2003) 25-37.
20. R.L. Banks and G.C. Bailey, *Olefin disproportionation. A new catalytic process*, Ind. Eng. Chem. Prod. Res. Dev., 3 (1964) 170-173.
21. W.L. Truett, D.R. Johnson, I.M. Robinson, B.A. Montague, *Polynorbornene by Coordination Polymerization*, J. Am. Chem. Soc., 82 (1960) 2337–2340.
22. J.L. Hérisson and Y. Chauvin, *Catalysis of olefin transformations by tungsten complexes. II. Telomerization of cyclic olefins in the presence of acyclic olefins*, Makromol. Chem., 141 (1971) 161-176.
23. R.R. Schrock, *Olefin metathesis by molybdenum imido alkylidene catalysts*, Tetrahedron, 55 (1999) 8141-8153.
24. R.R. Schrock, J.S. Murdzek, G.C. Bazan, J. Robbins, M. Dimare, M. Oregan, *Synthesis of molybdenum imido alkylidene complexes and some reactions involving acyclic olefins*, J. Am. Chem. Soc., 112 (1990) 3875-3886.
25. A. Poater, X. Solans-Monfort, E. Clot, C. Coperet, O. Eisenstein, *Understanding d^0-olefin metathesis catalysts: Which metal, which ligands?*, J. Am. Chem. Soc., 127 (2007) 8207-8216.
26. C. Pariya, K.N. Jayaprakash, A. Sarkar, *Alkene metathesis: new developments in catalyst design and application*, Coord. Chem. Rev., 168 (1998) 1-48.
27. R.H. Grubbs, P.L. Burk, D.D. Carr, *Mechanism of the olefin metathesis reaction*, J. Am. Chem. Soc., 97 (1975) 32653267.
28. R. Beumer, P. Bayón, P. Bugada, S. Ducki, N. Mongelli, F.R. Sirtori, J. Telser, C. Gennari, *Synthesis of novel simplified sarcodictyin/eleutherobin analogs with potent microtubule-stabilizing activity, using ring closing metathesis as the key-step*, Tetrahedron, 59 (2003) 8803-8820.
29. M. Colombo and I. Peretto, *Chemistry strategies in early drug discovery: an overview of recent trends*, Drug Discovery Today, 13 (2008) 677-684.

30. V.C. Edelsztein, P.H. Di Chenna, G. Burton, *Synthesis of C-C bonded dimeric steroids by olefin metathesis*, Tetrahedron, 65 (2009) 3615-3623.
31. P. Radha Krishna and G. Dayaker, *A stereoselective total synthesis of (-)-andrachcinidine via an olefin cross-metathesis protocol*, Tetrahedron Lett., 48 (2007) 7279-7282.
32. C.W. Bielawski and R.H. Grubbs, *Living ring-opening metathesis polymerization*, Progr. Polym. Science, 32 (2007) 1-29.
33. I. Czelusniak and T. Szymanska-Buzar, *Metathesis polymerization of norbornene and norbornadiene in the presence of tert-butylacetylene initiated by tungsten(II) and molybdenum(II) complexes*, Appl. Catal. A, 277 (2004) 173-182.
34. B. De Clercq and F. Verpoort, *Activity of a new class of ruthenium based ring-closing metathesis and ring-opening metathesis polymerization catalysts coordinated with a 1,3-dimesityl-4,5-dihydroimidazol-2-ylidene and a Schiff base ligand*, Tetrahedron Lett., 43 (2002) 9101-9104.
35. D.M. Haigh, A.M. Kenwright, E. Khosravi, *Ring opening metathesis polymerisations of norbornene and norbornadiene derivatives containing oxygen: a study on the regeneration of Grubbs catalyst*, Tetrahedron, 60 (2004) 7217-7224.
36. K.J. Ivin, A.M. Kenwright, E. Khosravi, J.G. Hamilton, *Ring-opening metathesis polymerization of 7-methylbicyclo[2.2.1]hepta-2,5-diene initiated by well-defined molybdenum and ruthenium carbene complexes*, J. Organomet. Chem., 606 (2000) 37-48.
37. Y. Yamaguchi, A. Fujita, N. Suzuki, T. Ito, *Metathesis polymerization of norbornene and terminal acetylenes catalyzed by bis(acetonitrile) complexes of molybdenum and tungsten*, J. Mol. Catal. A, 240 (2005) 226-232.
38. *The Nobel Prize in Chemistry 2005*. Available from: http://nobelprize.org/nobel_prizes/chemistry/laureates/2005/, 2005.
39. E.O. Fischer and A. Maasböl, *On the Existence of a Tungsten Carbonyl Carbene Complex*, Angew. Chem. Int. Ed., 3 (1964) 580-581.
40. R.R. Schrock, *Recent advances in olefin metathesis by molybdenum and tungsten imido alkylidene complexes*, J. Mol. Catal. A, 213 (2004) 21-30.
41. R.R. Schrock, *Multiple metal-carbon bonds for catalytic metathesis reactions (Nobel lecture)*, Angew. Chem. Int. Ed., 45 (2006) 3748-3759.
42. J. Feldman and R.R. Schrock, *Recent advances in the chemistry of d(0) alkylidene and metallacyclobutane complexes*, Prog. Inorg. Chem., 39 (1991) 1-74.
43. H.H. Brintzinger, D. Fischer, R. Mulhaupt, B. Rieger, R.M. Waymouth, *Stereospecific Olefin Polymerization with Chiral Metallocene Catalysts*, Angew. Chem. Int. Ed., 34 (1995) 1143-1170.
44. J.H. Oskam and R.R. Schrock, *Rate of interconversion of syn and antirotamers of Mo(CHCMe$_2$Ph)(NAr)(OR)$_2$ and relative reactivity toward 2,3-bis(trifluoromethyl)norbornadiene*, J. Am. Chem. Soc., 114 (1992) 7588-7590.

45. J.H. Oskam and R.R. Schrock, *Rotational isomers of $Mo^{(VI)}$ alkylidene complexes and cis-trans polymer structure investigation in ring-opening metathesis polymerization*, J. Am. Chem. Soc., 115 (1993) 11831-11845.

46. D.L. Wright, *Application of olefin metathesis to organic synthesis*, Curr. Org. Chem., 3 (1999) 211-240.

47. P.H. Deshmukh and S. Blechert, *Alkene metathesis: the search for better catalysts*, Dalton Trans., (2007) 2479-2491.

48. A.H. Hoveyda, P.J. Lombardi, R.V. O'Brien, A.R. Zhugralin, *H-Bonding as a Control Element in Stereoselective Ru-Catalyzed Olefin Metathesis*, J. Am. Chem. Soc., 131 (2009) 8378-+.

49. E.S. Sattely, S.J. Meek, S.J. Malcolmson, R.R. Schrock, A.H. Hoveyda, *Design and Stereoselective Preparation of a New Class of Chiral Olefin Metathesis Catalysts and Application to Enantioselective Synthesis of Quebrachamine: Catalyst Development Inspired by Natural Product Synthesis*, J. Am. Chem. Soc., 131 (2009) 943-953.

50. S.J. Malcolmson, S.J. Meek, E.S. Sattely, R.R. Schrock, A.H. Hoveyda, *Highly efficient molybdenum-based catalysts for enantioselective alkene metathesis*, Nature, 456 (2008) 933-937.

51. F. Blanc, A. Salameh, J. Thivolle-Cazat, J.-M. Basset, C. Copéret, A. Sinha, R.R. Schrock, *Grafting mechanism and olefin metathesis activity of well-defined silica-supported Mo imido alkyl alkylidene complexes*, C. R. Chim., 11 (2008) 137-146.

52. D.P. Allen, M.M. Van Wingerden, R.H. Grubbs, *Well-Defined Silica-Supported Olefin Metathesis Catalysts*, Org. Lett., 11 (2009) 1261-1264.

53. F. Blanc, C. Coperet, A. Lesage, L. Emsley, *High resolution solid state NMR spectroscopy in surface organometallic chemistry: access to molecular understanding of active sites of well-defined heterogeneous catalysts*, Chem. Soc. Rev., 37 (2008) 518-526.

54. F. Blanc, J. Thivolle-Cazat, J.M. Basset, C. Coperet, A.S. Hock, Z.J. Tonzetich, R.R. Schrock, *Highly active, stable, and selective well-defined silica supported Mo imido olefin metathesis catalysts*, J. Am. Chem. Soc., 129 (2007) 1044-1045.

55. C. Coperet, *Molecular design of heterogeneous catalysts: the case of olefin metathesis*, New J. Chem., 28 (2004) 1-10.

56. A. Hoveyda and A. Zhugralin, *The remarkable metal-catalysed olefin metathesis reaction*, Nature, 450 (2007) 243-251.

57. M. Mayr, M.R. Buchmeiser, K. Wurst, *Synthesis of a silica-based heterogeneous second generation Grubbs catalyst*, Adv. Synth. Catal., 344 (2002) 712-719.

58. M. Mayr, B. Mayr, M.R. Buchmeiser, *Novel well-defined heterogeneous metathesis catalysts*, Des. Monom. Polym., 5 (2002) 325-337.

59. N. Rendon, R. Berthoud, F. Blanc, D. Gajan, T. Maishal, J.M. Basset, C. Coperet, A. Lesage, L. Emsley, S.C. Marinescu, R. Singh, R.R. Schrock, *Well-Defined Silica-Supported Mo-Alkylidene Catalyst Precursors Containing One OR Substituent: Methods of Preparation and Structure-*

Reactivity Relationship in Alkene Metathesis, Chem. Eur. J., 15 (2009) 5083-5089.

60. N. Rendon, F. Blanc, C. Coperet, *Well-defined silica supported metallocarbenes: Formation and reactivity*, Coord. Chem. Rev., 253 (2009) 2015-2020.
61. J.M. Thomas and R. Raja, *Catalytic significance of organometallic compounds immobilized on mesoporous silica: economically and environmentally important examples*, J. Organomet. Chem., 689 (2004) 4110-4124.
62. X. Li, W. Zhang, S. Liu, S. Xie, X. Zhu, X. Bao, L. Xu, *Promoting effect of Mg in supported Mo/HBeta-Al_2O_3 catalyst for cross-metathesis of ethene and butene-2 to propene*, J. Mol. Catal. A, 313 (2009) 38-43.
63. H. Balcar, D. Mishra, E. Marceau, X. Carrier, N. Zilková, Z. Bastl, *Molybdenum oxide catalysts for metathesis of higher 1-alkenes via supporting MoO_2(acetylacetonate)$_2$ and MoO_2(glycolate)$_2$ on SBA-15 mesoporous molecular sieves*, Appl. Catal. A, 359 (2009) 129-135.
64. D.P. Debecker, K. Bouchmella, C. Poleunis, P. Eloy, P. Bertrand, E.M. Gaigneaux, P.H. Mutin, *Design of SiO_2-Al_2O_3-MoO_3 Metathesis Catalysts by Nonhydrolytic Sol-Gel*, Chem. Mater., 21 (2009) 2817-2824.
65. J. Handzlik and P. Sautet, *Active sites of olefin metathesis on molybdena-alumina system: A periodic DFT study*, J. Catal., 256 (2008) 1-14.
66. B.N. Shelimov, I.V. Elev, V.B. Kazansky, *Spectroscopic Study of Formation of Active Metal Carbene Species in Photoreduced Silica Molybdena Catalysts for Olefin Metathesis*, J. Mol. Catal., 46 (1988) 187-200.
67. Y. Iwasawa, H. Kubo, H. Hamamura, *Olefin metathesis over Al_2O_3 or SiO_2-attached molybdenum catalysts: active structures and mechanism for initial carbene formation*, J. Mol. Catal., 28 (1985) 191-208.
68. J.R. McCoy and M.F. Farona, *Olefin metathesis over a Re_2O_7/Al_2O_3 metathesis catalyst: Mechanism for initial metallacarbene formation*, J. Mol. Catal., 66 (1991) 51-58.
69. M.F. Farona and R.L. Tucker, *Studies on the mechanism of olefin metathesis promoted by a heterogeneous catalyst*, J. Mol. Catal., 8 (1980) 85-90.
70. R.H. Grubbs and S.J. Swetnick, *Mechanism of olefin metathesis over a supported molybdenum catalyst*, J. Mol. Catal., 8 (1980) 25-36.
71. J. Handzlik and J. Ogonowski, *Dynamic chemical counting of active centers of molybdena–alumina metathesis catalysts*, Catal. Lett., 88 (2003) 119-122.
72. J.R. Hardee and J.W. Hightower, *Propene metathesis over $CoMo/Al_2O_3$ - Poisoning by NO to determine active-site concentration*, J. Catal., 83 (1983) 182-191.
73. J. Guan, G. Yang, D.H. Zhou, W.P. Zhang, X.C. Liu, X.W. Han, X.H. Bao, *The formation mechanism of Mo-methylidene species over Mo/HBeta catalysts for heterogeneous olefin metathesis: A density functional theory study*, J. Mol. Catal. A, 300 (2009) 41-47.

74. J. Handzlik, *Properties and metathesis activity of monomeric and dimeric Mo centres variously located on [gamma]-alumina - A DFT study*, Surf. Sci., 601 (2007) 2054-2065.

75. J. Handzlik, *Computational study of the properties and metathesis activity of Mo methylidene species in HZSM-5 zeolite*, J. Mol. Catal. A, 316 (2010) 106-111.

76. J. Handzlik, *Theoretical study of propene metathesis proceeding on monomeric Mo centers of molybdena-alumina catalysts*, J. Catal., 220 (2003) 23-34.

77. J. Handzlik, *Degenerate propene metathesis on Mo-alkylidene centres of molybdena-alumina catalyst - a DFT study*, J. Mol. Catal. A, 218 (2004) 91-100.

78. J. Handzlik, *Metathesis activity of monomeric Mo-methylidene centres on (1 0 0) and (1 1 0)C surfaces of [gamma]-Al_2O_3 - a comparative DFT study*, Surf. Sci., 562 (2004) 101-112.

79. J. Handzlik, M. Gorski, T. Szymanska-Buzar, *A potential route to the formation of alkylidene ligand from two mutually cis alkene ligands: a DFT study*, J. Mol. Struct., 718 (2005) 191-201.

80. J. Handzlik and J. Ogonowski, *Theoretical study on ethene metathesis proceeding on Mo^{VI} and Mo^{IV} methylidene centres of heterogeneous molybdena-alumina catalyst*, J. Mol. Catal. A, 175 (2001) 215-225.

81. J. Handzlik and J. Ogonowski, *DFT study of ethene metathesis proceeding on monomeric Mo^{VI} centres of MoO_3/Al_2O_3 catalyst: the role of the molybdacyclobutane intermediate*, J. Mol. Catal. A, 184 (2002) 371-377.

82. J. Handzlik, J. Ogonowski, R. Tokarz-Sobieraj, *Dependence of metathesis activity of Mo-methylidene sites on their location on (1 0 0) [gamma]-Al_2O_3 - a theoretical study*, Catal. Today, 101 (2005) 163-173.

83. X. Li, J. Guan, D. Zhou, G. Li, X. Han, W. Zhang, X. Bao, *A DFT study of olefin metathesis over heterogeneous Mo/HBeta catalyst: The influence of Mo oxidation state*, J. Mol. Struct.: THEOCHEM, 913 (2009) 167-172.

84. J. Handzlik, J. Ogonowski, J. Stoch, M. Mikolajczyk, P. Michorczyk, *Properties and metathesis activity of molybdena-alumina, molybdena-silica-alumina and molybdena-silica catalysts - a comparative study*, Appl. Catal. A, 312 (2006) 213-219.

85. X. Li, W. Zhang, S. Liu, X. Han, L. Xu, X. Bao, *A high-resolution MAS NMR study on the potential catalysts Mo/HBeta for olefin metathesis: the interaction of Mo species with HBeta zeolite*, J. Mol. Catal. A, 250 (2006) 94-99.

86. X. Li, W. Zhang, S. Liu, L. Xu, X. Han, X. Bao, *Olefin metathesis over heterogeneous catalysts: interfacial interaction between Mo species and a Hbeta -Al_2O_3 composite support*, J. Phys. Chem. C, 112 (2008) 5955-5960.

87. X. Li, W. Zhang, S. Liu, L. Xu, X. Han, X. Bao, *The role of alumina in the supported Mo/HBeta–Al_2O_3 catalyst for olefin metathesis: a high-resolution solid-state NMR and electron microscopy study* J. Catal., 250 (2007) 55-66.

88. P. Topka, H. Balcar, J. Rathousky, N. Zilkova, F. Verpoort, J. Cejka, *Metathesis of 1-octene over MoO_3 supported on mesoporous molecular sieves: the influence of the support architecture*, Microporous Mesoporous Mater., 96 (2006) 44-54.

89. H. Balcar and J. Čejka, *Mesoporous molecular sieves as supports for metathesis catalysts*, in *Metathesis Chemistry: From Nanostructure Design to Synthesis of Advanced Materials*, Y. İmamoğlu and V. Dragutan, Editors. 2007, Springer. p. 151-166.

90. T. Ookoshi and M. Onaka, *A remarkable Mo catalyst for olefin metathesis: hexagonal mesoporous silica-supported molybdenum oxide (MoO_3/HMS)*, Chem. Commun., (1998) 2399-2400.

91. A. Gil and M. Montes, *Metathesis of propene on molybdenum-alumina-pillared montmorillonite*, Ind. Eng. Chem. Res., 36 (1997) 1431-1443.

92. J.C. Mol, *Activity and stability of laser-photoreduced supported molybdenum oxide metathesis catalysts* Catal. Lett., 23 (1994) 113-118.

93. H. Balcar, P. Topka, N. Zilkova, J. Perez-Pariente, J. Cejka, *Metathesis of linear alpha-olefins with MoO_3 supported on MCM-41 catalyst*, Stud. Surf. Sci. Catal., 156 (2005) 795-802.

94. S. Liu, S. Huang, W. Xin, J. Bai, S. Xie, L. Xu, *Metathesis of ethylene and butylene-2 to propylene with Mo on H[beta]-Al_2O_3 catalysts*, Catal. Today, 93-95 (2004) 471-476.

95. A.N. Startsev, O.V. Klimov, E.A. Khomyakova, *Mo/Al_2O_3 Catalysts Prepared Via Metal-Complex Precursors. 1. Synthesis of Catalysts and Their Activity in Propene Metathesis*, J. Catal., 139 (1993) 134-141.

96. B. Zhang, N. Liu, Q. Lin, D. Jin, *The effects of Mo oxidation states on olefin metathesis*, J. Mol. Catal., 65 (1991) 15-28.

97. P.C. Bakala, E. Briot, J.Y. Piquemal, J.M. Bregeault, P. Beaunier, *Comparison of the conventional impregnation method using ammonium heptamolybdate with a simple route to silica-supported molybdenum(VI) materials*, Catal. Commun., 8 (2007) 1447-1451.

98. J.A. Bergwerff, T. Visser, B.R.G. Leliveld, B.D. Rossenaar, K.P. de Jong, B.M. Weckhuysen, *Envisaging the physicochemical processes during the preparation of supported catalysts: Raman microscopy on the impregnation of Mo onto Al_2O_3 extrudates*, J. Am. Chem. Soc., 126 (2004) 14548-14556.

99. O. Collart, P. Van der Voort, E.F. Vansant, E. Gustin, A. Bouwen, D. Schoemaker, R.R. Rao, B.M. Weckhuysen, R.A. Schoonheydt, *Spectroscopic characterization of an MoO_x layer on the surface of silica. An evaluation of the molecular designed dispersion method*, Phys. Chem. Chem. Phys., 1 (1999) 4099-4104.

100. G. Plazenet, C. Martin, E. Payen, B. Rebours, J. Lynch, *Raman spectroscopic evidence for the formation of silicomolybdic entities on a Mo/HY zeolite catalyst*, Microporous Mesoporous Mater., 80 (2005) 275-278.

101. S. Braun, L.G. Appel, M. Schmal, *Effect of the nature of the support on molybdenum catalytic behavior in diesel particulate combustion*, Appl. Surf. Sci., 201 (2002) 227-235.

102. S. Braun, L.G. Appel, V.L. Camorim, M. Schmal, *Thermal spreading of MoO_3 onto silica supports*, J. Phys. Chem. B, 104 (2000) 6584-6590.

103. J. Handzlik, J. Ogonowski, J. Stoch, M. Mikolajczyk, *Anchored and impregnated molybdena-alumina metathesis catalysts - a comparative study*, Appl. Catal. A, 273 (2004) 99-104.

104. S. Jaenicke and W.L. Loh, *Preparation of highly dispersed molybdenum on alumina by thermal decomposition of $Mo(CO)_6$*, Catal. Today, 49 (1999) 123-130.

105. A.A. Olsthoorn and J.A. Moulijn, *An in situ infrared spectroscopic study of the activity of [gamma]-alumina supported $Mo(CO)_6$ for metathesis and ethene polymerization*, J. Mol. Catal., 8 (1980) 147-160.

106. J. Handzlik, J. Stoch, J. Ogonowski, M. Mikolajczyk, *Dependence of reactivity on pretreatment in molybdena-alumina catalysts for propene metathesis*, J. Mol. Catal. A, 157 (2000) 237-243.

107. K. Zama, Y. Imada, A. Fukuoka, M. Ichikawa, *Propene metathesis reaction on di- and trinuclear molybdenum complexes grafted on mesoporous FSM-16 and silica: Structural characterization and their catalytic performances*, Appl. Catal. A, 194-195 (2000) 285-296.

108. M. Anpa, M. Kondo, Y. Kubokawa, C. Louis, M. Che, *Dynamic studies of the photoinduced metathesis of C_3H_6 andphotoreduction of Mo with CO on anchored and inpregnated Mo/SiO_2 catalyst*, J. Chem. Soc., Faraday Trans. 1, 84 (1988) 2771-2782.

109. K.A. Vikulov, I.V. Elev, B.N. Shelimov, V.B. Kazansky, *IR and UV-VIS spectroscopic studies of the stable $Mo=CH_2$ carbene complexes over photoreduced silica-molybdena catalysts with chemisorbed cyclopropane, and thier role in olefin metathesis reactions*, J. Mol. Catal., 55 (1989) 126-145.

110. K.A. Vikulov, B.N. Shelimov, V.B. Kazansky, J.C. Mol, *Deactivation Mechanism of Photoreduced and Cyclopropane-Treated Molybdena Silica Catalysts for Olefin Metathesis*, J. Mol. Catal., 90 (1994) 61-67.

111. B.N. Shelimov, I.V. Elev, V.B. Kazansky, *Use of Photoreduction for Activation of Silica Molybdena Catalysts for Propylene Metathesis - Comparison with Thermal Reduction*, J. Catal., 98 (1986) 70-81.

112. M. Ichikawa, Q. Zhuang, G.J. Li, K. Tanaka, T. Fujimoto, A. Fukuoka, A.A. Tsyganenko, J.C. Mol, W. Grunert, W.K. Hall, J.C. Conesa, D.C. Koningsberger, J. Vedrine, J.J. Rooney, *SiO_2-Grafted Dinuclear Molybdenum Catalyst Derived from $Mo_2(OAc)_4$ Highly-Active for Olefin Metathesis Reaction*, Stud. Surf. Sci. Catal., 75 (1993) 529-541.

113. W. Grunert, A.Y. Stakheev, R. Feldhaus, K. Anders, E.S. Shpiro, K.M. Minachev, *Reduction and Metathesis Activity of MoO_3/Al_2O_3 Catalysts. 2. the Activation of MoO_3/Al_2O_3 Catalysts*, J. Catal., 135 (1992) 287-299.

114. I. Rodriguez-Ramos, A. Guerrero-Ruiz, N. Homs, P.R. Delapiscina, J.L.G. Fierro, *Reactions of Propene on Supported Molybdenum and Tungsten-Oxides*, J. Mol. Catal. A, 95 (1995) 147-154.

115. J. Handzlik, J. Ogonowski, J. Stoch, M. Mikolajczyk, *Comparison of metathesis activity of catalysts prepared by anchoring of $MoO_2(acac)_2$ on various supports*, Catal. Lett., 101 (2005) 65-69.

116. K. Tanaka, M. Sasaki, I. Toyoshima, *Activation of Encapsulation System MoO_3/SnO_2 for Olefin Metathesis by Snme4*, J. Phys. Chem., 92 (1988) 4730-4733.

117. K. Tanaka, *Intermediate Species of Terminal Alkene Metathesis on Molybdena-Titanias Activated with $SnMe_4$*, J. Mol. Catal., 46 (1988) 87-96.

118. J. Handzlik, J. Ogonowski, R. Dula, J. Stoch, E.M. Serwicka, *Pretreatment-induced redox processes in molybdena-alumina metathesis catalysts*, React. Kinet. Catal. Lett., 79 (2003) 135-141.

119. A. Vioux, *Nonhydrolytic sol-gel routes to oxides*, Chem. Mater., 9 (1997) 2292-2299.

120. A.M. Cojocariu, P.H. Mutin, E. Dumitriu, F.o. Fajula, A. Vioux, V. Hulea, *Non-hydrolytic synthesis of mesoporous silica-titania catalysts for the mild oxidation of sulphur compounds with hydrogen peroxide*, Chem. Commun., (2008).

121. P.H. Mutin and A. Vioux, *Nonhydrolytic Processing of Oxide-Based Materials: Simple Routes to Control Homogeneity, Morphology, and Nanostructure*, Chem. Mater., 21 (2009) 582-596.

122. D.P. Debecker, K. Bouchmella, R. Delaigle, P. Eloy, C. Poleunis, P. Bertrand, E.M. Gaigneaux, P.H. Mutin, *One-step nonhydrolytic sol-gel preparation of efficient V_2O_5-TiO_2 catalysts for VOC total oxidation*, Appl. Catal. B, 94 (2010) 38-45.

123. M. Andrianainarivelo, R. Corriu, D. Leclercq, P.H. Mutin, A. Vioux, *Mixed oxides SiO_2-ZrO_2 and SiO_2-TiO_2 by a non-hydrolytic sol-gel route*, J. Mater. Chem., 6 (1996) 1665-1671.

124. F. Barbieri, D. Cauzzi, F. De Smet, M. Devillers, P. Moggi, G. Predieri, P. Ruiz, *Mixed-oxide catalysts involving V, Nb and Si obtained by a non-hydrolytic sol-gel route: preparation and catalytic behavior in oxidative dehydrogenation of propane*, Catal. Today, 61 (2000) 353-360.

125. B.L. Caetano, L.A. Rocha, E. Molina, Z.N. Rocha, G. Ricci, P.S. Calefi, O.J. de Lima, C. Mello, E.J. Nassar, K.J. Ciuffi, *Cobalt aluminum silicate complexes prepared by the non-hydrolytic sol-gel route and their catalytic activity in hydrocarbon oxidation*, Appl. Catal. A, 311 (2006) 122-134.

126. V. Lafond, P.H. Mutin, A. Vioux, *Non-hydrolytic sol-gel routes based on alkyl halide elimination: toward better mixed oxide catalysts and new supports - application to the preparation of a SiO_2-TiO_2 epoxidation catalyst*, J. Mol. Catal. A, 182-183 (2002) 81-88.

127. V. Lafond, P.H. Mutin, A. Vioux, *Control of the texture of titania-silica mixed oxides prepared by nonhydrolytic sol-gel*, Chem. Mater., 16 (2004) 5380-5386.

128. P. Moggi, M. Devillers, P. Ruiz, G. Predieri, D. Cauzzi, S. Morselli, O. Ligabue, *Oxidative dehydrogenation of propane on pure and silica-dispersed multimetallic oxides based on vanadium and niobium prepared via hydrolytic and non-hydrolytic sol-gel methods*, Catal. Today, 81 (2003) 77-85.

129. P.H. Mutin, A.F. Popa, A. Vioux, G.r. Delahay, B. Coq, *Nonhydrolytic vanadia-titania xerogels: synthesis, characterization, and behavior in the selective catalytic reduction of NO by NH_3*, Appl. Catal. B, 69 (2006) 49-57.

130. A.F. Popa, P.H. Mutin, A. Vioux, G. Delahay, B. Coq, *Novel non-hydrolytic synthesis of a V_2O_5-TiO_2 xerogel for the selective catalytic reduction of NO_x by ammonia*, Chem. Commun., (2004) 2214-2215.

131. D.P. Debecker, R. Delaigle, K. Bouchmella, P. Eloy, E.M. Gaigneaux, P.H. Mutin, *Total oxidation of benzene and chlorobenzene with MoO_3- and WO_3-promoted V_2O_5/TiO_2 catalysts prepared by a nonhydrolytic sol-gel route.*, Catal. Today, (2010) In Press.

132. P.O. Scokart, F.D. Declerck, R.E. Sempels, P.G. Rouxhet, *Evolution of the acidic properties of silica-alumina gels as a function of chemical composition: infrared approach*, J. Chem. Soc., Faraday Trans., 1 (1977) 359-371.

133. R.E. Sempels and P.G. Rouxhet, *Infrared study of the adsorption of benzene and acetonitrile on silica-alumina gels: acidity properties and surface heterogeneity*, J. Colloid Interface Sci., 55 (1976) 263-273.

134. U. Rodemerck, P. Ignaszewski, M. Lucas, P. Claus, *Parallel synthesis and fast catalytic testing of catalyst libraries for oxidation reactions*, Chem. Eng. Technol., 23 (2000) 413-416.

135. M.M. Bettahar, G. Costentin, L. Savary, J.C. Lavalley, *On the partial oxidation of propane and propylene on mixed metal oxide catalysts*, Appl. Catal. A, 145 (1996) 1-48.

136. Z.X. Song, N. Mimura, J.J. Bravo-Suarez, T. Akita, S. Tsubota, S.T. Oyama, *Gas-phase epoxidation of propylene through radicals generated by silica-supported molybdenum oxide*, Appl. Catal. A, 316 (2007) 142-151.

137. M. Ruszel, B. Grzybowska, M. Gasior, K. Samson, I. Gressel, J. Stoch, *Effect of Au inV_2O_5/SiO_2 and MoO_3/SiO_2 catalysts on physicochemical and catalytic properties in oxidation of C-3 hydrocarbons and of CO*, Catal. Today, 99 (2005) 151-159.

138. G.E. Vrieland and C.B. Murchison, *Anaerobic oxidation of butane to butadiene over magnesium molybdate catalysts .1. Magnesia supported catalysts*, Appl. Catal. A, 134 (1996) 101-121.

139. M.C. Abello, M.F. Gomez, O. Ferretti, *Mo/gamma-Al_2O_3 catalysts for the oxidative dehydrogenation of propane. Effect of Mo loading*, Appl. Catal. A, 207 (2001) 421-431.

140. C.H. Bartholomew and R.J. Farrauto, *Fundamentals of industrial catalytic processes*. 2006, Hoboken, New Jersey: John Wiley &Sons, Inc.

141. S. Rajagopal, J.A. Marzari, R. Miranda, *Silica-Alumina-Supported Mo Oxide Catalysts - Genesis and Demise of Bronsted-Lewis Acidity*, J. Catal., 151 (1995) 192-203.

142. D. Martin and D. Duprez, *Evaluation of the acid-base surface properties of several oxides and supported metal catalysts by means of model reactions*, J. Mol. Catal. A, 118 (1997) 113-128.

143. D.D. Suresh, M.S. Friedrich, M.J. Seely, *Catalyst for the manufacture of acrylonitrile and methacrylonitrile*, US 5212137, 1993.

144. I.R. Subbotina, B.N. Shelimov, V.B. Kazansky, *Olefin metathesis over silica-supported molybdena catalysts activated by UV irradiation in the presence of alkanes*, Kinet. Catal., 38 (1997) 678-684.

145. H. Aritani, O. Fukuda, T. Yamamoto, T. Tanaka, S. Imamura, *Silica-alumina-supported molybdena catalyst for propene metathesis*, Chem. Lett., (2000) 66-67.

146. I. Rodriguezramos, A. Guerreroruiz, N. Homs, P.R. Delapiscina, J.L.G. Fierro, *Reactions of Propene on Supported Molybdenum and Tungsten-Oxides*, J. Mol. Catal. A, 95 (1995) 147-154.

147. K. Segawa, T. Soeya, D.S. Kim, *Supported Molybdena Catalysts - Characterization of Oxidized, Reduced, and Sulfided MoO_3 Prepared by an Adsorption Method*, Res. Chem. Intermed., 15 (1991) 129-151.

148. K. Tanaka, K. Miyahara, K. Tanaka, *Stereoselectivity in olefin metathesis over molybdenum oxide supported on titanium oxide*, J. Mol. Catal., 15 (1982) 133-46.

149. S. Hasegawa, T. Tanaka, M. Kudo, H. Mamada, H. Hattori, S. Yoshida, *Structure and reactivity of MoO_3-MgO catalysts*, Catal. Lett., 12 (1992) 255-266.

150. V. Indovina, A. Cimino, D. Cordischi, S. Dellabella, S. Derossi, G. Ferraris, D. Gazzoli, M. Occhiuzzi, M. Valigi, W. Grunert, M. Ichikawa, J. Goldwasser, C. Li, J.C. Mol, I.E. Wachs, W.K. Hall, *The Catalytic Activity of MoO_x/ZrO_2 in the Hydrogenation and Metathesis of Propene*, Stud. Surf. Sci. Catal., 75 (1993) 875-887.

151. Y. Iwasawa, H. Ichinose, S. Ogasawara, M. Soma, *Olefin metathesis over well-defined active fixed molybdenum catalysts - structure and oxidation state of the activesite abd reaction mechanism*, J. Chem. Soc.-Faraday Trans. I, 77 (1981) 1763-1777.

152. X.J. Li, W.P. Zhang, X. Li, S.L. Liu, H.J. Huang, X.W. Han, L.Y. Xu, X.H. Bao, *Insights into the Deactivation Mechanism of Heterogeneous Mo/H beta-Al_2O_3 Catalysts for Olefin Metathesis*, J. Phys. Chem. C, 113 (2009) 8228-8233.

153. C. Sarbu and B. Delmon, *Nanoscale composition inhomogeneity in silica-aluminas prepared by various methods*, Appl. Catal. A, 185 (1999) 85-97.

154. D.P. Debecker, F. Bertinchamps, N. Blangenois, P. Eloy, E.M. Gaigneaux, *On the impact of the choice of model VOC in the evaluation of V-based catalysts for the total oxidation of dioxins: Furan vs. chlorobenzene*, Appl. Catal. B, 74 (2007) 223-232.

155. F. Bertinchamps, C. Gregoire, E.M. Gaigneaux, *Systematic investigation of supported transition metal oxide based formulations for the catalytic oxidative elimination of (chloro)-aromatics - Part II: Influence of the nature and addition protocol of secondary phases to VO_x/TiO_2*, Appl. Catal. B, 66 (2006) 10-22.

156. J.L.G. Fierro and J.C. Mol, in *Metal Oxides: Chemistry and Applications*, J.L.G. Fierro, Editor. 2006, Taylor & Francis: Boca Raton. p. 517.

157. H. Aritani, O. Fukuda, A. Miyaji, S. Hasegawa, *Structural change of molybdenum on silica-alumina in contact with propene studied by ESR and Mo L-III-edge XANES*, Appl. Surf. Sci., 180 (2001) 261-269.

158. M.N. Kwini and J.M. Botha, *Influence of feed components on the activity and stability of cobalt molybdenum alumina metathesis catalyst*, Appl. Catal. A, 280 (2005) 199-208.

159. I.R. Subbotina, B.N. Shelimov, V.B. Kazansky, *Olefin metathesis over supported silica-molybdena catalysts activated by gamma-irradiation and mechanochemical treatment in the presence of alkanes*, Kinet. Catal., 39 (1998) 80-85.

160. D. Navez, G. Weinberg, G. Mestl, P. Ruiz, E.M. Gaigneaux, *Influence of the precursor (nature and amount) on the morphology of MoO_3 crystallites supported on silica*, Stud. Surf. Sci. Catal., 143 (2002) 609-617.

161. S. Knobl, G.A. Zenkovets, G.N. Kryukova, O. Ovsitser, D. Niemeyer, R. Schlögl, G. Mestl, *The synthesis and structure of a single-phase, nanocrystalline MoVW mixed-oxide catalyst of the Mo_5O_{14} type*, J. Catal., 215 (2003) 177-187.

162. G. Mestl and T.K.K. Srinivasan, *Raman spectroscopy of monolayer-type catalysts: Supported molybdenum oxides*, Cat. Rev. - Sci. Eng., 40 (1998) 451-570.

163. M. May, M. Asomoza, T. Lopez, R. Gomez, *Precursor aluminum effect in the synthesis of sol-gel Si-Al catalysts: FTIR and NMR characterization*, Chem. Mater., 9 (1997) 2395-2399.

164. E.J.M. Hensen, D.G. Poduval, P.C.M.M. Magusin, A.E. Coumans, J.A.R. van Veen, *Formation of acid sites in amorphous silica-alumina*, J. Catal., 269 (2010) 201-218.

165. C.L. Thomas, *Chemistry of Cracking Catalysts*, Ind. Eng. Chem., 41 (1949) 2564-2573.

166. M.W. Tamele, *Chemistry of the surface and the activity of alumina-silica cracking catalyst*, Disc. Faraday Trans., 8 (1950) 270-279.

167. R.C. Hansford, *Mechanism of Catalytic Cracking*, Ind. Eng. Chem., 39 (1947) 849–852.

168. K.J.D. MacKenzie, J. Temuujin, K. Okada, *Thermal decomposition of mechanically activated gibbsite*, Thermochim. Acta, 327 (1999) 103-108.

169. K.J.D. MacKenzie, J. Temuujin, M.E. Smith, P. Angerer, Y. Kameshima, *Effect of mechanochemical activation on the thermal reactions of boehmite ([gamma]-AlOOH) and [gamma]-Al_2O_3*, Thermochim. Acta, 359 (2000) 87-94.

170. T.-H. Chen, K. Houthoofd, P.J. Grobet, *Toward the aluminum coordination in dealuminated mordenite and amorphous silica-alumina: A high resolution ^{27}Al MAS and MQ MAS NMR study*, Microporous Mesoporous Mater., 86 (2005) 31-37.

171. P. Cloos, A.J. Leonard, J.P. Moreau, H. A., J.J. Fripiat, *Structural Organization in Amorphous Silico-Aluminas*, Clays Clay Miner., 17 (1969) 279-287.

172. A. Samoson, E. Lippmaa, G. Engelhardt, U. Lohse, H.G. Jerschkewitz, *Quantitative High-Resolution Al-27 NMR - Tetrahedral Nonframework Aluminum in Hydrothermally Treated Zeolites*, Chem. Phys. Lett., 134 (1987) 589-592.

173. P.J. Grobet, H. Geerts, M. Tielen, J.A. Martens, P.A. Jacobs, H.G.K.a.J. Weitkamp, *Framework and Non-Framework Al Species in Dealuminated Zeolite Y*, Stud. Surf. Sci. Catal., Volume 46 (1989) 721-734.

174. Z. Vít and O. Solcová, *Synthesis and properties of mesoporous silica-alumina with narrow pore size distribution obtained without use of pore-regulating agents*, Microporous Mesoporous Mater., 96 (2006) 197-204.

175. J.P. Gilson, G.C. Edwards, A.W. Peters, K. Rajagopalan, R.F. Wormsbecher, T.G. Roberie, M.P. Shatlock, *Pentacoordinated Aluminum in Zeolites and Aluminosilicates*, J. Chem. Soc.-Chem. Commun., (1987) 91-92.

176. L. Kellberg, M. Linsten, H.J. Jakobsen, *Al-27(H-1) Cross-Polarization and Ultrahigh-Speed Al-27 MAS NMR-Spectroscopy in the Characterization of USY Zeolites*, Chem. Phys. Lett., 182 (1991) 120-126.

177. M.F. Williams, B. Fonfé, C. Sievers, A. Abraham, J.A. van Bokhoven, A. Jentys, J.A.R. van Veen, J.A. Lercher, *Hydrogenation of tetralin on silica-alumina-supported Pt catalysts I. Physicochemical characterization of the catalytic materials*, J. Catal., 251 (2007) 485-496.

178. W.P. Zhang, D. Ma, X.W. Han, X.M. Liu, X.H. Bao, X.W. Guo, X.S. Wang, *Methane dehydro-aromatization over Mo/HZSM-5 in the absence of oxygen: A multinuclear solid-state NMR study of the interaction between supported Mo species and HZSM-5 zeolite with different crystal sizes*, J. Catal., 188 (1999) 393-402.

179. X. Carrier, J.F. Lambert, M. Che, *Ligand-promoted alumina dissolution in the preparation of MoO_x/gamma-Al_2O_3 catalysts: Evidence for the formation and deposition of an Anderson-type alumino heteropolymolybdate*, J. Am. Chem. Soc., 119 (1997) 10137-10146.

180. T. Klimova, J. Reyes, O. Gutiérrez, L. Lizama, *Novel bifunctional NiMo/Al-SBA-15 catalysts for deep hydrodesulfurization: Effect of support Si/Al ratio*, Appl. Catal. A, 335 (2008) 159-171.

181. J.A. Bergwerff, M. Jansen, B.G. Leliveld, T. Visser, K.P. de Jong, B.M. Weckhuysen, *Influence of the preparation method on the hydrotreating activity of MoS_2/Al_2O_3 extrudates: A Raman micro spectroscopy study on the genesis of the active phase*, J. Catal., 243 (2006) 292-302.

182. X. Carrier, J.F. Lambert, S. Kuba, H. Knozinger, M. Che, *Influence of ageing on MoO3 formation in the preparation of alumina-supported Mo catalysts*, J. Mol. Struct., 656 (2003) 231-238.

183. J.C. Edwards and E.C. Decanio, *Observation of $[Al(OH)_n(H_2O)_{6-n}]_n(MoO_4)$ in hydrotreating catalyst precursors by solid-state ^{27}Al NMR*, Catal. Lett., 19 (1993) 121-130.

184. G. Plazenet, E. Payen, J. Lynch, B. Rebours, *Study by EXAFS, Raman, and NMR spectroscopies of the genesis of oxidic precursors of zeolite-supported HDS catalysts*, J. Phys. Chem. B, 106 (2002) 7013-7028.

185. T. Klimova, M. Calderón, J. Ramírez, *Ni and Mo interaction with Al-containing MCM-41 support and its effect on the catalytic behavior in DBT hydrodesulfurization*, Appl. Catal. A, 240 (2003) 29-40.

186. T. Klimova, *Concerning the interpretation of ^{27}Al MAS-NMR spectra of Mo and NiMo catalysts on Al-containing MCM-41 supports: A reply to the comment by X. Carrier and M. Che on "Ni and Mo interaction with Al-containing MCM-41 support and its effect on the catalytic behavior in DBT hydrodesulfurization" [Appl. Catal. A 240 (2003) 29-40]*, Appl. Catal. A, 253 (2003) 321-325.

187. X. Carrier and M. Che, *Comment on "Ni and Mo interaction with Al-containing MCM-41 support and its effect on the catalytic behavior in DBT hydrodesulfurization" [Appl. Catal. A 240 (2003) 29-40]*, Appl. Catal. A, 253 (2003) 317-320.

188. A. Sampieri, S. Pronier, S. Brunet, X. Carrier, C. Louis, J. Blanchard, K. Fajerwerg, M. Breysse, *Formation of heteropolymolybdates during the preparation of Mo and NiMo HDS catalysts supported on SBA-15: Influence on the dispersion of the active phase and on the HDS activity*, Microporous Mesoporous Mater., 130 (2010) 130-141.

189. G. Macías, J. Ramírez, A. Gutiérrez-Alejandre, R. Cuevas, *Preparation of highly active NiMo/Al-SBA15 (x) HDS catalysts: Preservation of the support hexagonal porous arrangement*, Catalysis Today, 133-135 (2008) 261-266.

190. C. Sun, S. Yao, W. Shen, L. Lin, *Hydrothermal post-synthesis of HMCM-49 to enhance the catalytic performance of the Mo/HMCM-49 catalyst for methane dehydroaromatization*, Microporous and Mesoporous Materials, 122 (2009) 48-54.

191. X. Carrier, E. Marceau, M. Che, *Physical techniques and catalyst preparation: Determining the interactions of transition-metal complexes with oxide surfaces*, Pure Appl. Chem., 78 (2006) 1039-1055.

192. W. Grunert, A.Y. Stakheev, W. Morke, R. Feldhaus, K. Anders, E.S. Shpiro, K.M. Minachev, *Reduction and Metathesis Activity of MoO_3/Al_2O_3 Catalysts. 1. an Xps Investigation of MoO_3/Al_2O_3 Catalysts*, J. Catal., 135 (1992) 269-286.

193. A. Beltrán, F. Caturla, A. Cervilla, J. Beltrán, *Mo(VI) oxalate complexes*, J. Inorg. Nucl. Chem., 43 (1981) 3277-3282.

194. A. Klisinska, A.-S. Mamede, E.M. Gaigneaux, *Effect of the nature of the precursor on the morphology of MoO_3 thin films spin-coated on Si (100)*, Thin Solid Films, 516 (2008) 2904-2912.

195. T.N. Aridi and M.A. Al-Daous, *HDS of 4,6-dimethyldibenzothiophene over MoS_2 catalysts supported on macroporous carbon coated with aluminosilicate nanoparticles*, Appl. Catal. A, 359 (2009) 180-187.

196. A. Klisinska, A.S. Mamede, E.M. Gaigneaux, *Bismuth molybdates model catalysts with controlled crystallinities spin-coated on Si (100)*, Catal. Today, 128 (2007) 145-152.

197. A. Maione and M. Devillers, *Solid solutions of Ni and Co molybdates in silica-dispersed and bulk catalysts prepared by sol-gel and citrate methods*, J. Solid State Chem., 177 (2004) 2339-2349.

198. K. Hinokuma, K. Ogasawara, A. Kishimoto, S. Takano, T. Kudo, *Electrochromism of Spin-Coated $MoO_3.nH_2O$ Thin-Films from Peroxo-Polymolybdate*, Solid State Ionics, 53-6 (1992) 507-512.

199. E.M. Gaigneaux, K.-I. Fukui, Y. Iwasawa, *Morphology of crystalline [alpha]-MoO_3 thin films spin-coated on Si (100)*, Thin Solid Films, 374 (2000) 49-58.

200. E.R. Braithwaite and J. Haber, eds. *Molybdenum: An outline of its chemistry and uses*. Studies in Inorganic Chemistry. 1994, Elsevier: Amsterdam. 662.

201. P.C. Bakala, E. Briot, L. Salles, J.M. Bregeault, *Comparison of liquid-phase olefin epoxidation over MoO_x inserted within mesoporous silica (MCM-41, SBA-15) and grafted onto silica*, Appl. Catal. A, 300 (2006) 91-99.

202. J.-M. Brégeault, M. Vennat, S. Laurent, J.-Y. Piquemal, Y. Mahha, E. Briot, P.C. Bakala, A. Atlamsani, R. Thouvenot, *From polyoxometalates to polyoxoperoxometalates and back again; potential applications*, Journal of Molecular Catalysis A: Chemical, 250 (2006) 177-189.

203. A.N. Desikan, L. Huang, S.T. Oyama, *Oxygen-Chemisorption and Laser Raman-Spectroscopy of Unsupported and Silica-Supported Molybdenum Oxide*, J. Phys. Chem., 95 (1991) 10050-10056.

204. T. Ono, M. Anpo, Y. Kubokawa, *Catalytic Activity and Structure of MoO_3 Highly Dispersed on SiO_2*, J. Phys. Chem., 90 (1986) 4780-4784.

205. H. Jeziorowski, H. Knozinger, P. Grange, P. Gajardo, *Raman-Spectra of Cobalt Molybdenum Oxide Supported on Silica*, J. Phys. Chem., 84 (1980) 1825-1829.

206. S. Himeno, H. Niiya, T. Ueda, *Raman studies on the identification of isopolymolybdates in aqueous solution*, Bull. Chem. Soc. Jpn., 70 (1997) 631-637.

207. K.Y.S. Ng, X. Zhou, E. Gulari, *Spectroscopic characterization of molybdenum oxalate in solution and on alumina*, J. Phys. Chem., 89 (1985) 2477-2481.

208. J.P. Brunelle, *Preparation of catalysts by metallic complex adsorption on mineral oxides*, Pure Appl. Chem., 50 (1978) 1211-1229.

209. E. Baumgarten, F.O. Geldsetzer, U. Kirchhausen-Düsing, *Investigation and Modeling of the [gamma]-Al_2O_3/Water System*, J. Colloid Interface Sci., 173 (1995) 104-111.
210. W. Stumm, *Chemistry of the solid-water interface: Process at the mineral-water interface and particle-water interface in natural systems*, ed. J. Wiley & Sons. 1992, New York. 165-169.
211. R.W. Smith, *Kinetic aspects of aqueous aluminum chemistry: environmental implications*, Coord. Chem. Rev., 149 (1996) 81-93.
212. D. Bayot, M. Devillers, D. Peeters, *Vibrational spectra of eight-coordinate niobium and tantalum complexes with peroxo ligands: A theoretical simulation*, European Journal of Inorganic Chemistry, (2005) 4118-4123.
213. D. Bayot, B. Tinant, M. Devillers, *Spectroscopic and structural characterizations of ammonium peroxo-carboxylato molybdate(VI) complexes*, Inorganica Chimica Acta, 357 (2004) 809-816.
214. R.B. Watson, S.L. Lashbrook, U.S. Ozkan, *Chlorine modification of Mo/silica-titania mixed-oxide catalysts for the oxidative dehydrogenation of ethane*, J. Mol. Catal. A, 208 (2004) 233-244.
215. R.B. Watson and U.S. Ozkan, *K/Mo Catalysts Supported over Sol-Gel Silica-Titania Mixed Oxides in the Oxidative Dehydrogenation of Propane*, J. Catal., 191 (2000) 12-29.
216. F.C. Jentoft, H. Schmelz, H. Knözinger, *Preparation of selective catalytic reduction catalysts via milling and thermal spreading*, Appl. Catal. A, 161 (1997) 167-182.
217. S. Gunther, F. Esch, L. Gregoratti, A. Barinov, M. Kiskinova, E. Taglauer, H. Knozinger, *Gas-phase transport during the spreading of MoO_3 on Al_2O_3 support surfaces: Photoelectron spectromicroscopic study*, J. Phys. Chem. B, 108 (2004) 14223-14231.
218. S. Gunther, L. Gregoratti, M. Kiskinova, E. Taglauer, P. Grotz, U.A. Schubert, H. Knozinger, *Transport mechanisms during spreading of MoO_3 on Al_2O_3 supports investigated by photoelectron spectromicroscopy*, J. Chem. Phys., 112 (2000) 5440-5446.
219. A. Baiker, J.-D. Grunwaldt, C.A. Mueller, L. Schmid, *Catalytic materials by design*, Chimia, 52 (1998) 517-524.
220. R.D. Gonzalez, T. Lopez, R. Gomez, *Sol-gel preparation of supported metal catalysts*, Catal. Today, 35 (1997) 293-317.
221. J. Livage, *Sol-gel synthesis of heterogeneous catalysts from aqueous solutions*, Catal. Today, 41 (1998) 3-19.
222. V. Meille, *Review on methods to deposit catalysts on structured surfaces*, Appl. Catal. A, 315 (2006) 1-17.
223. J.A. Schwarz, C. Contescu, A. Contescu, *Methods for Preparation of Catalytic Materials*, Chem. Rev., 95 (1995) 477-510.
224. M. Schneider and A. Baiker, *Titania-based aerogels*, Catal. Today, 35 (1997) 339-365.
225. O. Lorret, V. Lafond, P.H. Mutin, A. Vioux, *One-step synthesis of mesoporous hybrid titania-silica xerogels for the epoxidation of alkenes*, Chem. Mater., 18 (2006) 4707-4709.

226. D.R. Cho, S.Y. Kim, D.W. Park, P.H. Mutin, *Selective catalytic oxidation of H_2S using nonhydrolytic vanadia-titania xerogels*, Korean J. Chem. Eng., 26 (2009) 377-381.

227. M.H. Dai, D.L. Tang, Z.J. Lin, H.W. Yang, Y.Z. Yuan, *Ti-Si mixed oxides by non-hydrolytic sol-gel synthesis as potential gold catalyst supports for gas-phase epoxidation of propylene in H_2 and O_2*, Chem. Lett., 35 (2006) 878-879.

228. M.H. Dai, D.L. Tang, Y.Z. Yuan, *Effect of Ti-Si mixed oxide support on gold catalysts for gas-phase epoxidation of propylene*, Chin. J. Catal., 27 (2006) 1063-1068.

229. A. Dolev, G.E. Shter, G.S. Grader, *Synthesis and structural characterization of Pt/amorphous Al_2O_3 catalyst*, J. Catal., 214 (2003) 146-152.

230. A.G. Fisch, N.S.M. Cardozo, A.R. Secchi, F.C. Stedile, P.R. Livotto, D.S. de Sa, Z.N. da Rocha, J.H.Z. dos Santos, *Immobilization of metallocene within silica-titania by a non-hydrolytic sol-gel method*, Appl. Catal. A, 354 (2009) 88-101.

231. Z. Jian, R. Jie, H. Yuning, B. Zhenfeng, L. Hexing, *Nanocrystalline Fe/TiCh visible photocatalyst with a mesoporous structure prepared via a nonhydrolytic Sol-Gel route*, J. Phys. Chem. C, (2007) 18965-9.

232. T.C.O. Mac Leod, D.F.C. Guedes, M.R. Lelo, R.A. Rocha, B.L. Caetano, K.J. Ciuffi, M.D. Assis, *Catalytic activity of Jacobsen catalyst encapsulated in an alumina matrix by the sol-gel process*, J. Mol. Catal. A, 259 (2006) 319-327.

233. J. Zhu, J. Yang, Z.F. Bian, H. Ren, Y.M. Liu, Y. Cao, H.X. Li, H.Y. He, K.N. Fan, *Nanocrystalline anatase TiO_2 photocatalysts prepared via a facile low temperature nonhydrolytic sol-gel reaction of $TiCl_4$ and benzyl alcohol*, Appl. Catal. B, 76 (2007) 82-91.

234. P. Bertrand and L.T. Weng, *Time-of-flight secondary ion mass spectrometry (ToF-SIMS)*, Mikrochim. Acta, 13 (1996) 167-182.

235. L. Rodriguez-Gonzalez, F. Hermes, M. Bertmer, E. Rodriguez-Castellon, A. Jimenez-Lopez, U. Simon, *The acid properties of H-ZSM-5 as studied by NH_3-TPD and ^{27}Al-MAS-NMR spectroscopy*, Appl. Catal. A, 328 (2007) 174-182.

236. N. Katada, H. Igi, J.H. Kim, M. Niwa, *Determination of the acidic properties of zeolite by theoretical analysis of temperature-programmed desorption of ammonia based on adsorption equilibrium*, J. Phys. Chem. B, 101 (1997) 5969-5977.

237. A.N. Desikan, W.M. Zhang, S.T. Oyama, *The effect of acid-base properties of supported molybdenum oxide in propylene oxidation*, J. Catal., 157 (1995) 740-748.

238. J.P. Balikdjian, A. Davidson, S. Launay, H. Eckert, M. Che, *Sintering and phase transformation of V-loaded anatase materials containing bulk and surface V species*, J. Phys. Chem. B, 104 (2000) 8931-8939.

239. F.P.J.M. Kerkhof and J.A. Moulijn, *Quantitative analysis of XPS Intensities for supported catalysts*, J. Phys. Chem., 83 (1979) 1612-1619.

References

PUBLICATION LIST

1. PUBLICATIONS

1.1. Published articles

1. *On the impact of the choice of model VOC in the evaluation of V-based catalysts for the total oxidation of dioxins: furan vs. chlorobenzene*
   D.P. Debecker, F. Bertinchamps, N. Blangenois, P. Eloy and E.M. Gaigneaux
   Applied Catalysis B: Environmental 74 (2007) 223–232

2. *Abatement of model molecules for dioxin total oxidation on V_2O_5-WO_3/TiO_2 catalysts: the case of substituted oxygen-containing VOC*
   D.P. Debecker, R. Delaigle, P. Eloy and E.M. Gaigneaux
   Journal of Molecular Catalysis A: Chemical 289 (2008) 38-43

3. *A New Bio-Inspired Route to Metal Nanoparticle-Based Heterogeneous Catalysts*
   D.P. Debecker, C. Faure, M.-E. Meyre, A. Derré and E.M. Gaigneaux
   Small 4(10) (2008) 1806-1812

4. *Recent advances in the understanding and development of titania supported vanadia catalysts for the oxidative abatement of (chloro-)aromatic air pollutants*
   R. Delaigle, **D.P. Debecker**, F. Bertinchamps and E.M. Gaigneaux
   Topics in Catalysis 52 (2009) 501-516

5. *Exploring, tuning and exploiting the basicity of hydrotalcites for applications in heterogeneous catalysis*
   D.P. Debecker, E.M. Gaigneaux and G. Busca
   Chemistry-A European journal, 15 (2009) 3920-3935

6. *Design of SiO_2-Al_2O_3-MoO_3 metathesis catalysts by nonhydrolytic sol-gel*
   D.P. Debecker, K. Bouchmella, C. Poleunis, P. Eloy, P. Bertrand, E. M. Gaigneaux and P. H. Mutin
   Chemistry of Materials 21 (2009) 2817-2824

7. *Nouvelle méthode de préparation de catalyseurs hétérogène à base de nanoparticules d'argent*
   D.P. Debecker and E.M. Gaigneaux
   Chimie Nouvelle 101 (2009) 1-3

8. *One-step non-hydrolytic sol–gel preparation of efficient V_2O_5-TiO_2 catalysts for VOC total oxidation*
   D.P. Debecker, K. Bouchmella, R. Delaigle, P. Eloy, E.M. Gaigneaux, P.H. Mutin
   Applied Catalysis B: Environmental, 93 (2010) 38-45.

1.2. Articles in press

9. *Total oxidation of benzene and chlorobenzene with MoO_3- and WO_3-promoted V_2O_5/TiO_2 catalysts prepared by a nonhydrolytic sol-gel route*
   D.P. Debecker, R. Delaigle, K. Bouchmella, P. Eloy, E.M. Gaigneaux, P.H. Mutin
   Catalysis Today. In Press.

10. *Flame-made vs. wet-impregnated vanadia/titania in the total oxidation of chlorobenzene: possible role of VOx species*
    B. Schimmoeller, R. Delaigle, **D.P. Debecker**, E.M. Gaigneaux
    Catalysis Today. In Press

1.3. Accepted articles

11. *Facile preparation of MoO_3/SiO_2-Al_2O_3 olefin metathesis catalysts by thermal spreading*
    D.P. Debecker, J. Siebenaler, M. Stoyanova, U. Rodemerck, E.M. Gaigneaux
    Studies in Surface Science and Catalysis. Accepted

12. *Ag-V_2O_5/TiO_2 total oxidation catalyst: autocatalytic removal of the surfactant and synergy between silver and vanadia*
    D.P. Debecker, R. Delaigle, M.M.F. Joseph, C. Faure, E.M. Gaigneaux
    Studies in Surface Science and Catalysis. Accepted.

1.4. Submitted articles

13. *Opposite effect of Al on the performances of MoO_3/SiO_2-Al_2O_3 catalysts in the metathesis and in the partial oxidation of propene*
    D.P. Debecker, D. Hauwaert, M. Stoyanova, A. Barkschat, U. Rodemerck, E.M. Gaigneaux
    Applied Catalysis A: General. Submitted.

14. *Genesis of active and inactive species during the preparation of MoO_3/SiO_2-Al_2O_3 metathesis catalysts via wet impregnation*
    D.P. Debecker, M. Stoyanova, U. Rodemerck, A. Léonard, B.-L. Su, E.M. Gaigneaux
    Journal of Physical Chemistry C. Submitted

15. *Dry preparation of MoO_3/SiO_2-Al_2O_3 metathesis catalysts as an alternative to the wet impregnation method: advantages and downsides*
    D.P. Debecker, M. Stoyanova, U. Rodemerk, P. Eloy, A. Léonard, B.-L Su, E.M. Gaigneaux
    Catalysis Today. Submitted.

2. CONFERENCE ABSTRACTS

2.1. Oral communications

1. *Onion-type multilamellar vesicles as an innovative tool for the preparation of metal-based heterogeneous catalysts*
   D.P. Debecker, M.-E. Meyre, E.M. Gaigneaux and C. Faure
   FAME Summer School. Madeira (Portugal). 30 September – 5 October 2007

2. *Relevance of oxygen-containing VOC as model molecule for the study of dioxin total oxidation on VOx/TiO2 catalysts*
   R. Delaigle, **D.P. Debecker** and E.M. Gaigneaux
   5th International Conference on Environmental Catalysis. Belfast (Ireland). 31 August - 3 September 2008.

3. *Onion-type vesicular microreactors for a new bio-inspired route to metal nanoparticle-based heterogeneous catalysts*
   D.P. Debecker, C. Faure, M.-E. Meyre, A. Derré, E.M. Gaigneaux
   European Material Research Society (eMRS) Fall Meeting, Warsaw, (Poland). 15 September 2008.

4. *Non-hydrolytic sol-gel chemistry for the design of Si-Al-Mo metathesis catalysts*
   D.P. Debecker, K. Bouchmella, C. Poleunis, P. Eloy, P. Bertrand, E.M. Gaigneaux, P.H. Mutin
   Outstanding Ph.D. formation day on Heterogeneous Catalysis and Nanostructures. Bruxelles (Belgium). 20 January 2009

5. *Onion-type vesicular microreactors for a new bio-inspired route to metal nanoparticle-based heterogeneous catalysts*
   C. Faure, **D.P. Debecker**, M.-E. Meyre, A. Derré, E.M. Gaigneaux
   First International Conference on Multifunctional, Hybrid and Nanomaterials. Tours (France). 15-19 March 2009

6. *Total oxidation of aromatic VOC on V_2O_5-(MoO_3)-(WO_3)/TiO_2 catalysts prepared by a non-hydrolytic sol-gel method*
   D.P. Debecker, R. Delaigle, K. Bouchmella, P. Eloy, E.M. Gaigneaux, P.H. Mutin
   6th World Congress on Oxidation Catalysis. Lille, France. 5-10 July 2009

7. *The role of VOx species in chlorobenzene oxidation by flame- and wet-made V2O5/TiO2*
   B. Schimmoeller, R. Delaigle, **D.P. Debecker**, E.M. Gaigneaux
   6th World Congres on Oxidation Catalysis, Lille, France. 5-10 July 2009

8. *Propene metathesis with Mo-Si-Al catalysts: why the non-hydrolytic sol-gel preparation offers unique opportunities*
   D.P. Debecker, K. Bouchmella, C. Poleunis, P. Eloy, P. Bertrand, E.M. Gaigneaux, P.H. Mutin
   EuropaCat IX, Salamanca, Spain. 30 August – 4 September 2009

9. *Surface characterization of wet impregnated and nonhydrolytic sol-gel prepared V2O5/TiO2 catalysts: the fate of the V active species*
   D.P. Debecker, K. Bouchmella, C. Poleunis, P. Eloy, P. Bertrand, E.M. Gaigneaux, P.H. Mutin
   13th European Conference on Applications of Surface and Interface Analysis, Antalya, Turkey. 18 October 2009

10. *A comparison of several types of carbon in 'de novo' dioxins formation: effects of time, doping with copper, water vapour, and suppression by sulphur dioxide*
    K. Shao, A. Buekens, **D.P. Debecker**, X. Li, S. Lu, J. Yan

2nd International Conference and Exhibition on Waste to Wealth & 6th International Conference On Combustion, Incineration Pyrolysis & Emission Control, Kuala Lumpur, Malaysia, 26-29 July 2010.

2.2. Poster communication

1. *Optimization of the operating conditions and of the formulation of VO_x/TiO_2 catalyst for the total oxidation of chlorinated-VOCs*
   F. Bertinchamps, **D.P. Debecker**, M. Treinen, M.A. Dos Santos, C. Grégoire, N. Blangenois, P. Eloy and E.M. Gaigneaux
   Europacat VIII, Turku/Abo (Finland). 26-31 August 2007

2. *Evaluation of VO_x/TiO_2 catalysts dedicated to dioxin abatement: on the role of an O-model in addition to Cl- models*
   D.P. Debecker, F. Bertinchamps, N. Blangenois, P. Eloy and E.M. Gaigneaux
   Europacat VIII, Turku/Abo (Finland). 26-31 August 2007

3. *An innovative preparation of heterogeneous metal nanoparticles catalysts for VOC abatement: the onion-type multilamellar vesicles route*
   D.P. Debecker, M.-E. Meyre, A. Derré, C. Faure and E.M. Gaigneaux
   5th International Conference on Environmental Catalysis. Belfast (Ireland). 31 August - 3 September 2008.

4. *Non hydrolytic Sol-Gel route for the design of Mo-based metathesis catalysts*
   D.P. Debecker, K. Bouchmella, E.M. Gaigneaux, H.P. Mutin
   European Material Research Society (eMRS) Fall Meeting, Cracovie (Poland). 15 September 2008

5. *Direct propene epoxidation with O_2: Homogeneous gas phase reactions initiated by heterogeneous MoO_3/SiO_2 catalyst*
   D.P. Debecker, B. Farin, E.M. Gaigneaux
   6th World Congress on Oxidation Catalysis. Lille, France. 5-10 July 2009

6. *Ammoxidation of ethylene to acetonitrile over chromium exchanged zeolite catalysts: Effect of the preparation method*
   F. Ayari, M. Mhamdi, **D. P. Debecker**, G. Delahay, E. M. Gaigneaux, A. Ghorbel
   6th World Congress on Oxidation Catalysis. Lille, France. 5-10 July 2009

7. *A novel route involving organic vesicles for the preparation of supported silver nanoparticle catalysts*
   D.P. Debecker, C. Faure, M.-E. Meyre, E.M. Gaigneaux
   EuropaCat IX, Salamanca, Spain, 30 August – 4 September 2009

3. MASTER THESIS

Le furane comme molécule modèle pour l'abattement catalytique des dioxines sur des formulations à base de VO_x/TiO_2
D.P. Debecker
Master in Bio-engineering in applied chemistry and bio-industries. Université catholique de Louvain, Louvain-la-Neuve (Belgium) 2006 pp. 94.

4. AWARDS

1. *"Prof. Albert De Vuyst Award"*
   Award for the best Master thesis by students from the Faculté d'Ingénierie biologique, agronomique et environnementale of the UCL.
   Faculté d'Ingénierie biologique, agronomique et environnementale (UCL). 29 June 2007.

2. *"AGC Award"*
   Award for the best presentation at the "Journées de Rencontres entre Jeunes Chimistes" of the "Société Royale de Chimie".
   Wépion (Namur). 20 March 2009